

2013

Characterising the deformation behaviour of human tooth enamel at the microscale

Simona O'Brien
Edith Cowan University

Follow this and additional works at: <https://ro.ecu.edu.au/theses>



Part of the [Dental Materials Commons](#), and the [Nanoscience and Nanotechnology Commons](#)

Recommended Citation

O'Brien, S. (2013). *Characterising the deformation behaviour of human tooth enamel at the microscale*.
<https://ro.ecu.edu.au/theses/566>

This Thesis is posted at Research Online.
<https://ro.ecu.edu.au/theses/566>

2013

Characterising the deformation behaviour of human tooth enamel at the microscale

Simona O'Brien
Edith Cowan University

Recommended Citation

O'Brien, S. (2013). *Characterising the deformation behaviour of human tooth enamel at the microscale*. Retrieved from <http://ro.ecu.edu.au/theses/566>

This Thesis is posted at Research Online.
<http://ro.ecu.edu.au/theses/566>

Edith Cowan University

Copyright Warning

You may print or download ONE copy of this document for the purpose of your own research or study.

The University does not authorize you to copy, communicate or otherwise make available electronically to any other person any copyright material contained on this site.

You are reminded of the following:

- Copyright owners are entitled to take legal action against persons who infringe their copyright.
- A reproduction of material that is protected by copyright may be a copyright infringement. Where the reproduction of such material is done without attribution of authorship, with false attribution of authorship or the authorship is treated in a derogatory manner, this may be a breach of the author's moral rights contained in Part IX of the Copyright Act 1968 (Cth).
- Courts have the power to impose a wide range of civil and criminal sanctions for infringement of copyright, infringement of moral rights and other offences under the Copyright Act 1968 (Cth). Higher penalties may apply, and higher damages may be awarded, for offences and infringements involving the conversion of material into digital or electronic form.

Characterising the Deformation Behaviour of Human Tooth Enamel at the Microscale

Simona O'Brien, MEng Sc, MIEI

A thesis presented for the degree of
Doctor of Philosophy

School of Engineering
Faculty of Computing, Health and Science
Edith Cowan University
Western Australia

14th May 2013

USE OF THESIS

The Use of Thesis statement is not included in this version of the thesis.

ABSTRACT

Enamel plays an important role in tooth function. Optimal combinations of composition and structure endow enamel with unique mechanical properties that remain largely unexplored. Specifically, more detailed understanding of the load-bearing ability of enamel is needed to mimic it synthetically and to design next generation biocomposite materials. This research investigates the variables that influence deformation behaviour of tooth enamel in relation to its hierarchical structure.

Initially, a new method was developed for preparing flat, finely polished tooth samples that were maintained in their normal hydrated state for nanoindentation testing. In contrast to conventional methods, which commonly utilise either inappropriate or excessive drying and/or chemically based embedding media (i.e., resins, glues), a novel embedding process was developed using an aqueous putty compound. Additionally, a custom-designed holder was manufactured for mounting wet tooth specimens on the nanoindentation stage that eliminated the need for hot wax or glue during testing. Considering that enamel is a functionally graded material that has different values of Young's modulus (E) and hardness (H) over the enamel thickness, a new approach of data analysis was developed for interpreting the mechanical properties of enamel at a range of fixed constant indentation depths. Resultant functions were used for predictive purposes. The values of E and H obtained from the nanoindentation instrument demonstrated a well-known decreasing gradient from the enamel occlusal surface towards the enamel-dentine junction (EDJ). In contrast to studies using conventional methods, this research showed that both properties also decreased with increasing depths at fixed locations. Furthermore, experimental results showed that resin embedding had detrimental effects on the E and H of enamel (i.e., both properties decreased with increasing depth), but had positive effects on both mild and severe wear resistance parameters (i.e., both parameters increased with increasing depth). When contrasted against the mechanical properties of enamel samples prepared using conventional protocols, this study postulates that the new

hydrated method has, for the first time, revealed the genuine E and H properties of this tissue.

The effects of sample preparation methods on tooth microstructure, especially along the EDJ, were investigated with optical microscopy and scanning electron microscopy (SEM). The new method of sample preparation combined with a careful dehydration process maintained the integrity of the EDJ interface even after applying multiple Berkovich indents up to maximum load of 400 mN. In contrast, the EDJ and the enamel surface were commonly separated and fractured in teeth that had been resin-embedded. Accordingly, the new method of sample preparation proved to be reliable for investigating the genuine microstructural characteristics of teeth.

The behaviour of the elastic region in tooth enamel was investigated with analytical and finite element models. The models were fitted into experimental values of E obtained from nanoindentation tests with a Berkovich indenter to identify a relationship between the mechanical responses of enamel under different loading conditions and microstructure. The decrease in E for enamel with increasing indentation depth was related to its enhanced load-bearing ability. The change of E was directly linked to the microstructural evolution (i.e., the rotation of mineral crystals) of enamel. The effective crystal orientation angle was found to be between 44° and 48° for indentation depths from 0.8 and 2.4 μm below according to the analytical model. The range of angles facilitated the shear sliding of mineral crystals and reduced the stress level as well as the volume of material under higher loads.

The behaviour of the plastic region in healthy enamel was investigated with finite element models fitted to nanoindentation data obtained with a Berkovich indenter to determine deformation mechanisms that result in excellent mechanical responses for tooth enamel during loading. When nanoindentation was conducted with increasingly applied loads but at a fixed location, the values of H decreased with increasing indentation depth. The decreasing trend in H was simulated by finite element models and showed a reduction in stress level and yield strength with increasing load. This key mechanism of the loading

dependence of mechanical properties resulted in remarkable enamel resilience and was related to the change of effective crystal orientation angle within the enamel microstructure.

The mechanical behaviour of enamel with respect to its microstructure was also investigated on teeth exposed to commercially available whitening treatments (tooth bleaching). Enamels exposed to a 6% bleaching treatment exhibited degraded mechanical properties (E and H) compared to unbleached controls. Furthermore, the creep and recovery responses of bleached enamel were also significantly reduced compared to controls. To determine the variables regulating tooth enamel deformation mechanisms during whitening treatments, analytical models were fitted to stress-strain curves. The effective crystal orientation angle of healthy enamel and the protein shear stress, τ_c , were identified as 50° and 2.5 % of the transverse stiffness of a staggered composite (E_2), respectively. After the bleaching treatment, the effective crystal orientation angle of enamel increased to 54° for $\tau_c = 1.5$ % of E_2 . Notably, bleaching reduced shear (τ_c) by 40 % compared to normal readings for unbleached controls. The changes in mechanical responses of bleached enamel were linked to the decrease of the shear bearing ability of protein components in the enamel microstructure. It is envisaged that these findings will provide new perspectives on applications of bleaching treatments and lead to the development of bleaching agents with less damaging effects to healthy enamel.

This work should stimulate new interest in understanding the deformation behaviour of tooth enamel at small scales, and offer new methods for the collection and analysis of data from samples prepared close to their native state, upon which novel and biologically relevant high-performance biocomposite materials can be engineered.

DECLARATION

I certify that this thesis does not, to the best of my knowledge and belief:

- (i) incorporate without acknowledgment any material previously submitted for a degree or diploma in any institution of higher education;
- (ii) contain any material previously published or written by another person except where due reference is made in the text; or
- (iii) contain any defamatory material

I also grant permission for the Library at Edith Cowan University to make duplicate copies of my thesis as required.

Simona O'Brien, 14th May 2013

ACKNOWLEDGEMENTS

Appreciation is expressed to those who have made contribution to this thesis and who have made my PhD study a wonderful journey.

I would like to acknowledge my supervisor, Dr Zonghan Xie, for his help and incredible support over the last three and a half years. I sincerely appreciate his scientific knowledge and invaluable expertise that has helped me to overcome many challenging problems. I would like to thank my supervisor, Dr Jeremy Shaw, for his guidance in sample preparation and optical & electron microscope imaging. I am grateful for his invaluable comments and patience in reading my drafts. I am also indebted to my supervisor, Winthrop Professor Paul V. Abbott, who kindly gave me his time and lent me some of his expertise from dentistry. I am thankful for his helpful ideas and professional advice. I would also like to acknowledge Dr Majid Tolouei-Rad for being my supervisor during the last few months of my study. I am thankful for his time and help during the submission process of my thesis.

I would like to acknowledge Professor Daryoush Habibi, head of the School of Engineering, for providing sound advice and moral support during my studies. I also sincerely recognise all of the School of Engineering staff at Edith Cowan University (ECU) who offered their kindness and professional competence during my study. Special recognition goes to: Dr Xiaoli Zhao for his unfailing help in finite element modelling and result presentations; Adrian Styles and Slavko Nikolic for their practical advice regarding the design and manufacture of a nanoindentation holder; Dr Johnny Lo and Associate Professor Ute Mueller for their mathematical/statistical software expertise inputs; Dr Greg Maguire for his writing support; and Clare Ashby of the Scholarship Office and Martine Hawkins of the Graduate Research School for their assistance during my studies.

I also wish to acknowledge my family who propped me up throughout my studies and provided tremendous support in good times and bad. I am indebted to

my father Milan Voňka who has looked after me since I was a child and who gave me so much love and support that helped me to achieve my goals. A big thank you for coming to Australia to mind Jacqueline and Kenneth during the kid's holidays despite your health problems. You have been a wonderful dad and granddad. No words can express the continuous support, love and patience of my husband Liam who has always been there for me when I was going through many emotional roller coasters. Thank you for being a great father to our children Jacqueline and Kenneth, taking care of all of the duties around the house and working so hard to support our family. Thank you Jacqueline and Kenneth for your love, hugs and kisses that helped me to stay encouraged right up to the end. I am sorry for not being with you or being around you as much as I would wish, but the completion of this work should change our life. To my aunt-in-law, Rose Walsh, for giving her love, help and time in watching over and taking care of the kids on many occasions. Thank you to my mother- and father-in-law, Ann and Dan, my sisters-in-law, Fiona and Susan, and my brothers-in-law, Brendan and Oliver, for their love and support while I was living in Ireland as well as in Australia. I miss you all.

I have been fortunate to meet Uday Farhan, my true friend and neighbour who became like family. It was a privilege to study for countless hours together at ECU. I am grateful to him for allowing me to share my doubts and worries and for helping me to release and conquer my stress. Thank you for your invaluable inputs and critical comments with all of the issues I had to deal with. Your generosity and caring for my family are greatly appreciated and will never be forgotten; my sincerest thanks and best wishes to you and your family. My profound thanks also go to my friends, Mahir Meghji, Dr Ainslie Denham and Jacqueline Ferreira, who I have been privileged to share time, guidance and support with during my time at ECU. Thank you so much for taking me out for a cuppa, cheering me up and being such wonderful people with positive minds. Huge thanks also go to my closed friends, Eva Blahova and Conrad Muhiga, who supported me during the final stage of my studies and looked after Jacqueline and Kenneth.

I acknowledge the facility and the scientific and technical assistance of the Australian Microscopy & Microanalysis Research Facility at the Centre for Microscopy, Characterisation & Analysis (CMCA), UWA, facility funded by the University, State and Commonwealth Government. Special thanks go to Peter Duncan, Dana Crisan and Lyn Kirilak, the CMCA personnel. I also thank the Australian Department of Education, Employment and Workplace Relations (DEEWR) for providing an Australian Postgraduate Award (APA) scholarship and ECU for offering a Research Excellence Award Scholarship during my PhD study. I greatly acknowledge the Australian Dental Research Foundation for the financial grant (6/2010) and the dental private practice, Sparkle Dental in Joondalup, for providing human teeth and dental products.

Last, but certainly not least, I am indebted and thankful to the rest of you, too numerous to mention, who have been a constant source of motivation, inspiration, support and guidance, and who helped me to remain positive and sane during my doctoral studies and encouraged me to achieve my goals. My sincerest thanks.

TABLE OF CONTENTS

TITLE PAGE	i
USE OF THESIS	ii
ABSTRACT	iii
DECLARATION	vi
ACKNOWLEDGEMENTS	vii
TABLE OF CONTENTS	x
LIST OF TABLES	xv
LIST OF FIGURES	xix
CONTRIBUTIONS	xxvi
1. INTRODUCTION	1
1.1 Problem statement	1
1.2 Primary objective	6
1.3 Secondary objectives	6
1.4 Research questions	6
1.5 Anticipated outcomes	7
1.6 Scope of thesis	8
2. LITERATURE REVIEW	10
2.1 Enamel	11
2.2 Chemical composition	12
2.3 Hierarchical structure	15
2.3.1 Characterisation of enamel hierarchy	15
2.3.2 Defects in tooth enamel structure	19
2.3.3 Techniques for observing enamel structure	20
2.4 Mechanical properties	21
2.4.1 Materials Science Fundamentals	21
2.4.2 The mechanical characteristics of enamel	23
2.5 Sample preparation	26

2.5.1	Methods of preparing teeth for nanoindentation testing	26
2.5.2	Microstructural observation of the enamel-dentine junction	29
2.6	Deformation behaviour of tooth enamel	30
2.6.1	Elastic behaviour	30
2.6.2	Elastic-plastic behaviour	32
2.6.3	Creep and recovery	36
2.7	Tooth whitening (bleaching)	38
2.8	Mechanistic models	42
2.8.1	Numerical models	42
2.8.2	Analytical models	48
3.	THEORY OF NANOINDENTATION	52
3.1.1	Projected area of contact, A_c	54
3.1.2	Young's modulus	57
3.1.3	Hardness	58
3.1.4	Stress-strain relationship	59
3.1.5	Creep – backcreep	60
3.1.6	Calibration	71
4.	METHODOLOGY	73
4.1	Sample preparation	73
4.1.1	Collection and storage	73
4.1.2	New method	73
4.1.3	Conventional method, A	76
4.1.4	Conventional method, B	77
4.1.5	Dehydration and drying procedure	78
4.1.6	Bleaching	78
4.2	Structural analysis	79
4.2.1	Optical microscopy	79
4.2.2	Focused ion beam milling/Transmission electron microscopy	79
4.2.3	Scanning electron microscopy	80
4.3	Nanoindentation test settings	80

4.3.1	Testing instrument.....	80
4.3.2	Sample holder design	80
4.3.3	Verification of indentation spacing	82
4.3.4	New method of data analysis to the constant indentation (Berkovich indenter)	83
4.3.5	Stress – strain test settings (Spherical indenter).....	84
4.3.6	Creep	86
4.4	Modelling of human tooth enamel	87
4.4.1	Numerical models	87
4.4.2	Analytical models.....	90
4.5	Mild and severe wear	91
5.	EFFECTS OF PREPARATION METHODS ON THE MECHANICAL BEHAVIOUR OF TOOTH ENAMEL	94
5.1	Summary	94
5.2	Introduction	94
5.3	Materials and methods.....	95
5.4	Results and discussion.....	97
5.4.1	E and H values.....	97
5.4.2	Dehydration and drying.....	104
5.4.3	Mild wear of enamel.....	107
5.4.4	Severe wear	110
5.5	Conclusion.....	114
6.	EFFECT OF PREPARATION METHODS ON ENAMEL MICROSTRUCTURE	116
6.1	Summary	116
6.2	Introduction	116
6.3	Materials and methods.....	117
6.4	Results and Discussion.....	117
6.5	Conclusion.....	121

7.	ELASTIC BEHAVIOUR OF TOOTH ENAMEL.....	122
7.1	Summary	122
7.2	Introduction	122
7.3	Materials and methods	123
7.4	Results and discussion.....	124
7.5	Conclusion.....	135
8.	EFFECT OF MICROSTRUCTURE ON PLASTIC BEHAVIOUR OF TOOTH ENAMEL.....	136
8.1	Summary	136
8.2	Introduction	136
8.3	Materials and methods	138
8.4	Results and discussion.....	139
8.5	Conclusion.....	147
9.	BLEACHING	149
9.1	Summary	149
9.2	Introduction	150
9.3	Materials and methods	151
9.4	Results and discussion.....	152
9.4.1	E and H.....	153
9.4.2	Creep and backcreep behaviour	156
9.4.3	Stress-strain analysis and modelling	163
9.5	Conclusion.....	165
10.	CONCLUSION.....	167
10.1	Findings.....	168
10.2	Future research directions	170
11.	REFERENCES	172
12.	APPENDICES	186
	Appendix A: SEM images of tooth sectioning	186

Appendix B: Nanoindentation holder – part 1	188
Appendix C: Nanoindentation holder – part 2	189
Appendix D: SEM images of Berkovich indents from different regions	190
Appendix E: E and H spatial distribution.....	192
Appendix F: E values - conventional methods A and B	193
Appendix G: H values - conventional methods A and B	196
Appendix H: E values - conventional method A and the new method	199
Appendix I: H values - conventional method A and the new method	202
Appendix J: E and H values for wet and dry samples	205
Appendix K: Indentation depths for occlusal surface and EDJ.....	207
Appendix L: Elastic behaviour of tooth enamel.....	208
Appendix M: E values for tooth enamel during whitening treatment	211
Appendix N: H values for tooth enamel during whitening treatment	212
Appendix O: Stress-strain properties of unbleached and bleached enamel	213

LIST OF TABLES

Table 2-1. Enamel mineral elements and their gradient from the enamel surface to the enamel-dentine junction (EDJ). Symbols \uparrow and \downarrow represent increasing gradient and decreasing gradients, respectively.	13
Table 2-2: Summary of hierarchical structural features of human enamel.	15
Table 2-3. Mechanical properties (E, H, K_c and σ_{fs}) of human tooth enamel and other materials. K_c	25
Table 4-1. Technical parameters of the new method of tooth preparation.....	75
Table 4-2. Sample preparation of enamel embedded in epoxy resin.	77
Table 4-3. Structural and mechanical properties of the enamel constituents used in the modelling analysis.	90
Table 5-1. Improvement and/or degradation of E (\pm standard error) in % as a positive or negative value, respectively.	100
Table 5-2. Improvement and/or degradation of H (\pm standard error) in % as positive or negative value, respectively.	101
Table 5-3. Mean values of E and H (\pm standard error) of “enamel samples 1 & 2”. The resulting values represent combined E and H values, respectively from the middle region of enamel for overall indentation depths from 0 to 2 μm	106
Table 5-4. Summary of the mild wear resistance of human tooth enamel for indentation depths ranging between 0 and 2 μm	108
Table 5-5. Mechanical properties of selective biological and dental materials used for mild wear comparison to human enamel [9, 115, 227, 229].	109
Table 5-6. Fracture toughness, K_c of enamel and other biological and dental materials.	110
Table 5-7. Summary of severe wear of tooth enamel for indentation depth ranging between 0 and 2 μm	111
Table 5-8. Severe wear of laminated biosilica and dental materials represented by proportional resistance parameter to micro-cracking from a sharp abrasive, $K_c^4/H.E^2$ [$\text{mN} \times 10^{-4}$].	113

Table 7-1. Mean indentation depth, h of five indents (from one indentation row) measured from the middle region (i.e., a normalised distance of 0.50) of enamel at various loads.	126
Table 7-2. Linear association between indentation load, P and depth, h_t	127
Table 7-3. Mean \pm standard deviation of E modulus at five indents (from one indentation row) measured from the middle region (i.e., a normalised distance of 0.5) of enamel.	127
Table 7-4. P -values for the comparisons of E moduli values measured at various loads against that obtained at the maximum indentation load of 400 mN. As previously shown, load is strongly correlated with indentation depth, thus these comparisons are also depth comparisons.	128
Table 7-5. The change of E in the middle region of enamel governed by the tilting of mineral crystals (angle $\theta \pm$ standard deviation) during deformation.	130
Table 8-1. Experimental results of mechanical properties of enamel obtained from extrapolation of nanoindentation results.	139
Table 8-2. Physical variables (\pm standard deviations) used in the FEM simulations.	140
Table 8-3. Mechanical properties of enamel and comparison materials used in FEM simulations.	143
Table 9-1. E and H values for unbleached and 7 days bleached enamel measured with a Berkovich indenter at the constant indentation depth ranging from 0 to 2 μm	155
Table 9-2. The absolute value of Δh_t (\pm standard error) [μm] for creep at 50, 100 and 130 mN loads and recovery at 5 mN of unbleached and 7 days bleached enamel specimens. The holding time of 900 s was applied for both, creep and recovery measurements.	159
Table 9-3. E_i^* and μ values from creep modelling at 50, 100 and 130 mN loads for unbleached and bleached enamel.	162
Table 12-1. E moduli values comparison between conventional methods A and B.	193
Table 12-2. P -values from t -tests for comparing E values between conventional methods A and B at 0 μm indentation depth.	193
Table 12-3. P -values from t -tests for comparing E values between conventional methods A and B at 0.5 μm indentation depth.	194
Table 12-4. P -values from t -tests for comparing E values between conventional methods A and B at 1.0 μm indentation depth.	194

Table 12-5. P-values from t-tests for comparing E values between conventional methods A and B at 1.5 μm indentation depth.	194
Table 12-6. P-values from t-tests for comparing E values between conventional methods A and B at 2.0 μm indentation depth.	195
Table 12-7. H values comparison between conventional methods A and B.	196
Table 12-8. P-values from t-tests employed for comparing H values between conventional methods A and B at the enamel surface (i.e., 0 μm indentation depth).....	196
Table 12-9. P-values from t-tests employed for comparing H values between conventional methods A and B at 0.5 μm indentation depth.	197
Table 12-10. P-values from t-tests employed for comparing H values between conventional methods A and B at 1.0 μm indentation depth.	197
Table 12-11. P-values from t-tests employed for comparing H values between conventional methods A and B at 1.5 μm indentation depth.....	197
Table 12-12. P-values from t-tests employed for comparing H values between conventional methods A and B at 2 μm indentation depth.	198
Table 12-13. E moduli values comparison between conventional method A and the new method.	199
Table 12-14. P-values from t-tests for comparing E values between conventional method A and the new method at the enamel surface (i.e., 0 μm indentation depth).	199
Table 12-15. P-values from t-tests for comparing E values between conventional method A and the new method at 0.5 μm indentation depth.....	200
Table 12-16. P-values from t-tests for comparing E values between conventional method A and the new method at 1.0 μm indentation depth.	200
Table 12-17. P-values from t-tests for comparing E values between conventional method A and the new method at 1.5 μm indentation depth.....	200
Table 12-18. P-values from t-tests for comparing E values between conventional method A and the new method at 2.0 μm indentation depth.	201
Table 12-19. H values comparison between conventional method A and the new method.	202
Table 12-20. P-values from t-tests for comparing H values between conventional method A and the new method at the enamel surface (i.e., 0 μm indentation depth).	202

Table 12-21. P-values from t-tests for comparing H values between conventional method A and the new method at 0.5 μm indentation depth.	203
Table 12-22. P-values from t-tests for comparing H values between conventional method A and the new method at 1.0 μm indentation depth.	203
Table 12-23. P-values from t-tests for comparing H values between conventional method A and the new method at 1.5 μm indentation depth.	203
Table 12-24. P-values from t-tests for comparing H values between conventional method A and the new method at 2.0 μm indentation depth.	204
Table 12-25. E and H values of “enamel sample 1” in dry and wet environments. The overall mean values denote the average of all E values for all indentation depths and regions.	205
Table 12-26. E and H values of “enamel sample 2” in dry and wet environments. The overall mean values denote the average of all E values for all indentation depths and regions.	206
Table 12-27. Values of indentation depths measured at the occlusal surface and near the EDJ.	207
Table 12-28. Resulting values of enamel model in its elastic region.	208
Table 12-29. Mean \pm standard deviation of E values at 5 indents (from one indentation row) measured from the middle region (i.e., a normalised distance of 0.5) used for the calculation of the effective crystal orientation angle, θ as a function of indentation depth, h for specimen 1.	209
Table 12-30. Mean \pm standard deviation of E values at 5 indents (from one indentation row) measured from the middle region (i.e., a normalised distance of 0.5) used for the calculation of the effective crystal orientation angle, θ as a function of indentation depth, h for specimen 2.	210
Table 12-31. E values of tooth enamel during 14 days bleaching treatment.	211
Table 12-32. H values of human tooth enamel during whitening treatment.	212
Table 12-33. Experimental stress-strain values of unbleached enamel in its elastic-plastic region.	213
Table 12-34. The best fit modelling values (i.e., $\tau_c = 2.5\%$ of E_2 and $\theta = 50^\circ$) of unbleached enamel in its elastic-plastic region.	214
Table 12-35. The best fit modelling values (i.e., $\tau_c = 2.0\%$ of E_2 and $\theta = 50^\circ$) of unbleached enamel in its elastic-plastic region.	215
Table 12-36. The best fit modelling values (i.e., $\tau_c = 1.5\%$ of E_2 and $\theta = 54^\circ$) of unbleached enamel in its elastic-plastic region.	216

LIST OF FIGURES

Figure 1-1. Hierarchical structure of human tooth enamel at (a) millimetre scale, (b-c) micron scale and (d) nanoscale.	1
Figure 2-1. A healthy human molar. In this image, the tooth is made up of a crown and four roots. Enamel, the most visible shiny part of dental tissue in the oral cavity, is in the crown region of the tooth. The root, the bottom part of the tooth below the gums, anchors the tooth in the alveolus bone socket in the jaw. Scale bar = 4 mm.	10
Figure 2-2. Cross sectional view of a human tooth, illustrating its major functional parts: enamel, dentine, cementum and pulp. Tooth enamel is a hard, brittle tissue that covers the outer part of the tooth in the crown region and encases the softer tougher dentine and pulp. Scale bar = 1 mm.	11
Figure 2-3. Crystal structure of hydroxyapatite and the relationship between the hexagonal and crystallographic unit cell. Adopted from [75].	16
Figure 2-4. Size and shape of enamel crystallites and growth [89].	16
Figure 2-5. Schematic illustration of a key-hole like enamel microstructure. Modified from [92]. Scale bar = 5 μm	17
Figure 2-6. Observation of the cross-sectional enamel surface in a hydrated environment using reflective light. The arrows indicate Hunter-Schreger bands. Scale bar = 1 mm.	18
Figure 2-7. Schematic stress-strain curve indicating the elastic and plastic behaviour of a material. The transition from the elastic to plastic region is identified as the yield point. Beyond this point, the material undergoes permanent deformation.	33
Figure 2-8. Deformation of tooth enamel at a crystalline level. E_{org} and E_{crys} denote Young's modulus of protein and mineral crystal, respectively. Adopted from [112].	43
Figure 2-9. Finite element model of enamel. (a) Dimensions of prisms and elements, (b) entire enamel block, (c) 14 elements from the front view and (d) differences in crystal orientation. Adopted from [107].	44
Figure 2-10. Deformation model of tooth enamel with schematic illustration of representative variables used for theoretical modelling of mineral crystal orientation angle, θ [7].	48

Figure 3-1. A schematic representation of load, P , versus displacement, h , obtained from nanoindentation experiments. The quantities shown are the maximum indentation load, P_{\max} , the contact depth after unloading, h_c , the contact stiffness during unloading, dP/dh . The h_c , and dP/dh determine Young's modulus and hardness of material. Modified from [203].....53

Figure 3-2. (a) A schematic representation of a Berkovich indenter with the projected area, A_c . The 65.27° semi-angle in (b), which represents the face angle with the central axis of the indenter, is used to calculate the A_c . The height of the dark-shaded triangle denotes the contact depth of penetration, h_c54

Figure 3-3. A Berkovich indenter at the full load and unload with indicated depth from the original specimen surface, h_t , at the maximum load, P_{\max} , and the contact depth, h_c , after unloading, respectively. Adopted from [25, 133, 138].....55

Figure 3-4. A schematic representation of the elastic indentation with a spherical indenter at full load, P at the indentation depth, h_t . R and $2a_c$ denote the nominal radius and the contact diameter of the indenter at the contact indentation depth, h_c , respectively. Adopted from [25, 133, 138].....56

Figure 3-5. A single Voigt model. The model represents the viscoelastic creep behaviour of a material under tensile forces, F . A spring with the storage modulus, E^* , and a dashpot with the viscous component of a material, η , are connected in parallel to simulate the creep behaviour.65

Figure 3-6. Three element Voigt model under tensile forces, F . The model illustrates the spring storage modulus, $E1^*$ and $E2^*$, with the dashpot loss modulus, η_2 . Modified from [214].67

Figure 3-7. Maxwell model under tensile forces, F . The model illustrates the spring storage modulus, $E1^*$, and the dashpot loss modulus, η_1 . Modified from [214].....69

Figure 3-8. Maxwell-Voigt model. The storage moduli, $E1^*$ and $E2^*$, denote springs in the model and represent the elastic responses of material. The loss moduli, η_1 and η_2 , are related to dashpots and determine the viscous responses of material. Modified from [214].....70

Figure 4-1. Preparation of the tooth specimen from a mandibular right third molar (M3) for nanoindentation tests. (a) Location of the first and second cuts in the tooth, relative to the mesial-distal plane. The polished surface is also indicated. Parallel black dashed lines show the approximate thickness of the sample. (b) Sectioned tooth embedded in the putty inside an epoxy cylinder. Specimens were kept hydrated to preserve their natural structure before indentation tests. Scale bar = 1 mm.74

Figure 4-2. An indentation device for probing mechanical properties of human tooth enamel in a hydrated environment.	81
Figure 4-3. (a) A specially designed holder for nanoindentation testing of human tooth enamel in a wet environment. (b) Stainless steel hexagonal socket set screws with flat points are driven into each slide towards the specimen. The bath is filled with Hank's Balanced Salt Solution. No mounting medium (i.e., glue or wax) is required for holding the samples in place during testing. Scale bar = 5 mm.	81
Figure 4-4. Indentation spacing of each array and each indent in distance of 20 μ m (a) and 50 μ m (b). In (a), indentation loads of 50, 200 and 400 mN were applied onto the enamel surface. The residual impression from previous indents of 20 μ m apart was unavoidable for 200 and 400 mN. In (b), partial loading-unloading was applied up to 400 mN with indentation arrays of 50 μ m apart from the enamel surface towards dentine. No overlaps of indents were found in the softer part of the tooth, the dentine (b). Scale bar = 100 μ m.	82
Figure 4-5. Typical calibration curve of a Berkovich indenter. The $A_{c,i}/A_c$ parameter denotes the ratio of an ideal contact area to a real contact area of a Berkovich indenter at the contact indentation depth, h_c	83
Figure 4-6. (a) Optical micrograph of the indentation layout on enamel. Residual impressions of Berkovich indents after partial loading-unloading was applied up to 400 mN with indentation arrays of 50 μ m apart across the enamel surface (b) Indentation load, P , as a function of displacement (i.e., penetration depth), h , of enamel measured by a Berkovich indenter. Scale bar = 100 μ m.	84
Figure 4-7. Typical calibration curve of a 5 μ m spherical indenter.	85
Figure 4-8. (a) Schematic representation of a spherical indenter of nominal radius R , contact radius, a_c and a flank angle, α , at the depth, h , that represents the transition between the sphere and cone. (b) Typical stress-strain ($H - a_c/R$) curve of tooth enamel with 30 incremental steps up to a load of 400 mN. The shaded area denotes 10 incremental steps and highlights the elastic-plastic region of tooth enamel before it softens and/or fractures.	85
Figure 4-9. FEM refined mesh used in the simulations.	88
Figure 4-10. (a) The force simulates the effect of a conical indenter, as a function of the distance from the axisymmetry, which is used to generate the desired deformation produced by the conical indenter, (b) the z displacement at the surface of the sample, generated by the force in (a).	89

Figure 5-1. Optical microscopic image of Berkovich indents across the EDJ. Berkovich indents in enamel and dentine exhibited larger sizes of imprints in the wet environment compared to the dry state. Scale bar = 50 μm .	97
Figure 5-2. Distributions of (a) E [GPa] and (b) H [GPa] data of healthy human molars prepared by the new method. These data were measured from the enamel occlusal surface (normalised distance = 0) towards dentine (normalised distance = 1). Standard error bars are derived from measurements on the three molars' specimens.	98
Figure 5-3. (a) E [GPa] and (b) H [GPa] of tooth enamel prepared by three different methods and measured at different indentation depths. This charts show that resin embedding significantly affects the E rather than the H values of tooth enamel. Notably, E values of tooth enamel are significantly different for all preparation methods and indentation depths, while only the H values of the conventional method B are significantly different to the conventional method A and the new method.	99
Figure 5-4. Typical distributions of (a) E [GPa] and (b) H [GPa] of tooth enamel at a normalised distance of between 0 and 1 and dentine at a normalised distance higher than 1 for the constant indentation depth 0.5 μm in the hydrated and dry state. The shaded region indicates the indentation area for which comparison analyses for wet and dry enamel were made. The standard error bars of two specimens at each location denote the combined value of experimental data, i.e. N = 80 of two enamel specimens.	104
Figure 5-5. Mild wear of enamel prepared by the new method and conventional methods A and B for indentation depths between 0 and 2 μm .	107
Figure 5-6. Ranking of tooth enamel with other biological and dental materials.	110
Figure 5-7. Severe wear of enamel prepared by the new method and by the conventional methods A and B for indentation depths between 0 and 2 μm .	111
Figure 5-8. Severe wear comparison of enamel prepared by the new method with other biological and dental filling materials.	113
Figure 6-1. SEM images of (a) mesial and (b) distal areas of human molar prepared by a conventional method, A. Detrimental effects of conventional method A on the enamel microstructure are evident. The tooth specimens exhibited artefacts in the form of fractures and cracks along the EDJ. Scale bar = 200 μm .	118
Figure 6-2. Morphological images of the EDJ prepared by the new method.	119

Figure 6-3. SEM images of Berkovich indents of 400 mN load across the EDJ region. Marked with a white arrow in a) and b), the images show no initiations of cracks from the edges of an indent along the EDJ boundary. Scale bar = 10 μm	120
Figure 7-1. A typical illustration of the indentation load, P , as a function of a displacement (i.e., indentation depth), h , of enamel produced by a Berkovich indenter in regions: (a) near the enamel occlusal surface, (b) in the middle and (c) close to the EDJ. The contact depth, h_c , was estimated to be $\sim 1.8 \mu\text{m}$, $\sim 1.9 \mu\text{m}$ and $\sim 2.1 \mu\text{m}$ in (a), (b) and (c), respectively.....	125
Figure 7-2. Transmission electron micrographs of (a) tooth enamel prepared parallel to the direction of the rods, (b) an enlarged view of circled area in (a). Courtesy of Dr. Z. Xie.	129
Figure 7-3. Schematic illustrations showing the responses of mineral crystals to increasing indentation loads from P_1 to P_3 (i.e., the increasing severity of deformation) by changing the effective crystal orientation angle from θ_1 to θ_3 , resulting in a change in E in the middle region of enamel.	131
Figure 7-4. Model of shear deformation between mineral crystallites. Note that A' is the projected area of a mineral platelet having a surface area of A_s onto the horizontal plane, τ is the shear stress, and α , β are the angles that the platelets make with the horizontal and vertical directions, respectively.	132
Figure 7-5. The shear stress distribution generated in enamel by indentation at a depth of $0.28 \mu\text{m}$: (a) perfect elastic model and (b) shear sliding enabled model.....	133
Figure 7-6. The size of regions under the influence of shear stresses greater than (s1) 3.0 GPa, (s2) 3.5 GPa, (s3) 4.0 GPa and (s4) 4.5 GPa, calculated from the FEM simulations. Note that 'PE' stands for the perfect elastic model and 'SS' for the shear-sliding model.....	134
Figure 8-1. Contour plots of stress distributions induced by a Berkovich indenter at $288.30 (\pm 4.17) \text{ mN}$ obtained via FEM simulations. (1) – (5) represent models 1-5 (see Table 8-2). FEM prediction of a) von Mises stress field σ_v , b) maximum in-plane shear stress σ_{max} , and c) contours of the vertical displacement h . Note that the σ_{max} is defined as $(\sigma_1 - \sigma_3)/2$, where σ_1 and σ_3 are the first and the third principal stresses, respectively, both of which are within the simulation plane.	141
Figure 8-2. Maximum equivalent strain in (a) enamel, indentation loading $288.30 (\pm 4.17) \text{ mN}$, (b) comparison material 1, the same indentation loading; and the h -displacement (c) enamel, indentation loading $288.30 (\pm 4.17) \text{ mN}$, (d) the comparison material, the same indentation loading.	142

Figure 8-3. FEM results of von Mises stress distribution, σ_v , induced by nanoindentation using the same load of 288.30 (\pm 4.17) mN, in a) comparison material 1, b) comparison material 2, c) comparison material 3 and d) enamel. (e) Normalised volume fraction with different stress levels enclosed – (1) $\sigma_v > 1.28$ GPa, (2) $\sigma_v > 1.47$ GPa, (3) $\sigma_v > 1.65$ GPa. 144

Figure 8-4. FEM simulations of plastic zones produced by nanoindentation using the same load of 285.35 mN in (a) enamel and (b) comparison material 1..... 144

Figure 9-1. E values of enamel undergoing a 2 week bleaching treatment and 7 days after bleaching treatment (recovery). 153

Figure 9-2. H values of enamel during a 2 week bleaching treatment and 7 days after bleaching treatment (recovery). 154

Figure 9-3. Representative load displacement curves of unbleached and 7 days bleached enamel with a calibrated 5 μ m spherical indenter showing a creep responses with 900 s holding time under maximum indentation load of 50 mN (a), 100 mN (b) and 130 mN (c) and backcreep (self-recovery) behaviour responses with 900 s holding time at minimum loads of 5 mN, respectively. The insets represent potential mechanical deformation of sacrificial bonds in proteins during loading (top image) and unloading (bottom image). It is expected that the damage to proteins (represented as a number of damaged/broken springs) gradually increases with increasing load for unbleached as well as bleached enamel..... 157

Figure 9-4. Typical creep and backcreep curves of unbleached and bleached enamel at (a,b) 50 and 5 mN, (c,d) 100 and 5 mN, (e,f) 130 and 5 mN with 900 s holding time at maximum and minimum load, respectively. 160

Figure 9-5. Creep responses for hold period of 900 s at 50 mN on unbleached and bleached enamel with a 5 μ m nominal radius spherical indenter. (a) Maxwell model, (b) Voigt model and (c) combined Maxwell-Voigt model were used to determine creep variables regulating deformation behaviour during bleaching treatment..... 161

Figure 9-6. Fitting curves obtained from stress-strain measurements for unbleached and 7 days bleached enamel. For each simulating procedure, the effective crystal orientation angle, θ , and the critical shear stress, τ_c , of the protein matrix were identified. 163

Figure 12-1. Backscattered electron images of the enamel-dentine junction after diamond saw sectioning. The images were taken on uncoated samples under the variable pressure of 9 Pa. Hard, brittle tooth enamel was found to be less resistant against severe damage than softer dentin with noticeable grooves from 30 μ m to 50 μ m. The arrowhead indicates the enamel-dentine junction. Scale bar = 20 μ m..... 186

Figure 12-2. Secondary electron images of the enamel-dentine junction after diamond saw sectioning under variable pressure of 10 Pa. The arrowhead indicates transition of grooves from harder enamel to softer dentin. Scale bar = 20 μm	187
Figure 12-3. Nanoindentation holder developed for UMIS nanoindentation instrument to test tooth enamel in its hydrated state.	188
Figure 12-4. Slides used for mechanical mounting of the enamel specimens.	189
Figure 12-5. Backscattered SEM image of Berkovich indents near the occlusal surface of tooth enamel after applying the load of 400 mN. The indents and arrays are 50 μm apart with no evident residual overlaps. Scale bar = 20 μm	190
Figure 12-6. Backscattered SEM image of Berkovich indents 50 μm apart in the middle region of tooth enamel. Notably, the applied load of 400 mN did not yield crack. Scale bar = 10 μm	190
Figure 12-7. Berkovich indents across the enamel-dentine junction. There were no radial cracks initiated from the edges of indents even after 400 mN load across the boundary between hard, brittle enamel and soft, tough dentin. Scale bar = 10 μm	191
Figure 12-8. Typical distributions of E and H of three healthy molars (a-c) from the enamel occlusal surface (normalised distance = 0) across the enamel-dentine junction (EDJ). The EDJ is indicated by a dashed line in the charts.	192

CONTRIBUTIONS

UPCOMING PUBLICATIONS

O'Brien S, Shaw J, Zhao X, Abbott PV, LO J, Munroe P, Hoffman M, Xie Z. Unlocking mechanistic links between the stiffness and structure of dental enamel; in preparation.

Zhao X, O'Brien S, Shaw J, Abbott PV, Swain MV, Xie Z. Dental enamel: a mechanically robust natural coating; in preparation.

O'Brien S, Shaw J, Lo J, Abbott PV, Munroe P, Zhao X, Xie Z. A new method of tooth enamel preparation for nanoindentation testing in the hydrated environment; in preparation.

O'Brien S, Shaw J, Lo J, Abbott PV, Munroe P, Zhao X, Xie Z. Elastic behaviour of human tooth enamel: experimental and modelling. Aust Dent J, Supp B, Abstract accepted, number: 0587; publication postponed to 2013.

Zhao X, Xie Z, O'Brien S, Shaw J, Abbott PV, Munroe P. Loading adaptive structure of tooth enamel: roles of yield strength and plasticity. Aust Dent J, Supp B, Abstract accepted, number: 0588; publication postponed to 2013.

SCIENTIFIC MEETINGS

O'Brien S, Shaw J, Abbott PV, Xie Z. Materials design principles of tooth enamel. 11th International Symposium on Biomineralisation, University of the Sunshine Coast, Queensland, Australia. July 2011, Oral presentation.

O'Brien S, Shaw J, Abbott PV, Xie Z. Modelling of tooth enamel: A combined SEM and mechanical testing approach. Electron Microscopy and Analysis Group Conference (EMAG), University of Birmingham, Birmingham, UK: September 2011, Poster presentation.

O'Brien S, Xie Z. Revealing the mechanical characteristic of tooth enamel. Materials Australia Meeting, Western Australia Branch, Cloverdale, Perth, Western Australia, Australia. July 2012, Oral presentation.

OTHER PUBLICATIONS

Farhan U, O'Brien S, Rad M. SolidWorks secondary development with visual basic 6 for an automated modular fixture assembly approach. Int J Eng 2012; 6 (6). Accepted in Nov 2012.

Farhan UH, Tolouei-Rad M, O'Brien S. An automated approach for assembling modular fixtures using SolidWorks. ICMET 2012. Proceedings of the International Conference on Manufacturing Engineering and Technology (ICMET); 2012 Dec, Perth, Australia. Accepted in Nov 2012.

1.Introduction

This chapter presents a description of the current literature on the deformation behaviour of tooth enamel and outlines the relevant problems that exist in the field of dental materials science. The objectives are given along with questions posed in this research. The aims and significance are also summarised. The last section of this chapter is devoted to the scope of the thesis.

1.1 Problem statement

The study of tooth enamel is a core aspect of dental research and has important applications in human health. Enamel, the outer exposed part of the tooth (**Figure 1-1(a)**), is a fascinating material owing to its inherently complex structural and functional properties. Enamel possesses remarkable mechanical properties stemming from its unique composition and hierarchical structure, which extend across multiple length scales (**Figure 1-1**) [1-4].

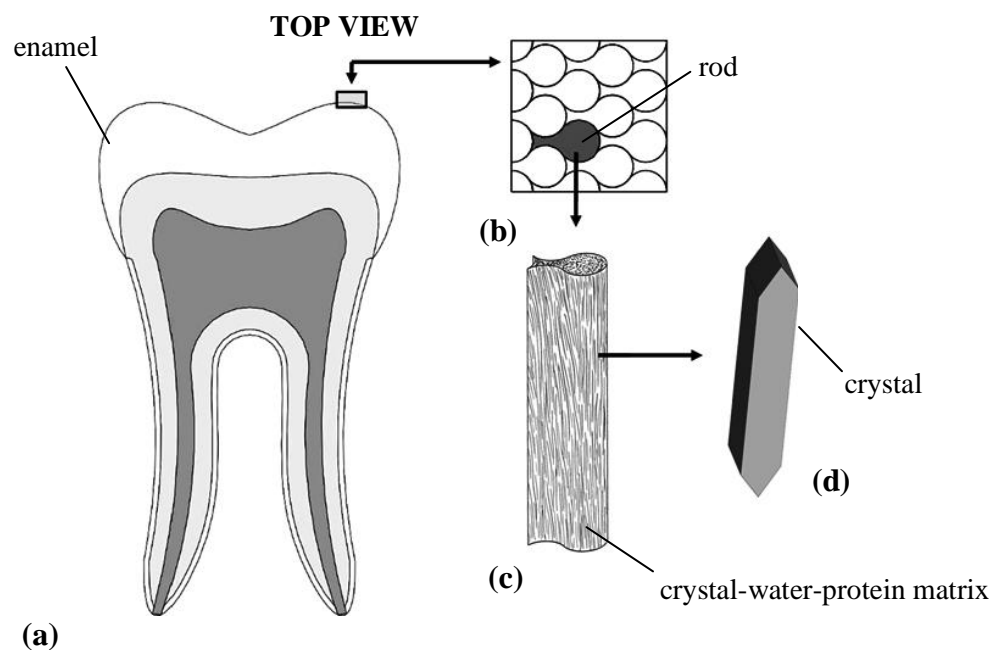


Figure 1-1. Hierarchical structure of human tooth enamel at (a) millimetre scale, (b-c) micron scale and (d) nanoscale.

At the nanoscale, enamel is composed of three distinct components: stiff inorganic flattened hexagonal apatite crystals (**Figure 1-1(d)**), soft organic proteins and water [5]. At greater length scales, these apatite crystals are glued together by proteins to form the basic building blocks of enamel, the rods (**Figure 1-1 (c)**). These rods are then joined by proteins making the keyhole-like shape of the enamel macrostructure (**Figure 1-1 (b)**). It has been shown that each level of hierarchy has distinct mechanical responses. However, the explanations of these responses and how they are interlinked to structure across each length scale (i.e., from nanoscale to macroscale) are still not well understood [3]. Notably, one of the important variables of the enamel microstructure that has been identified by analytical models is the effective orientation angle of the crystals [6, 7]. This angle was considered as the critical linking variable between the nanoscale deformation mechanism and mechanical responses of tooth enamel at the macroscale.

This angle may play a critical role in enamel ability to adjust its structure against an applied load, which is also called the “adaptive mechanical design” [8]. This mechanism is still not well identified and is an important, but missing, piece of information needed for the design of dental materials in restorative dentistry. Materials such as amalgam or composite fillings are used in dental treatments to repair the tooth. However, these materials commonly exhibit poor mechanical biocompatibility and are non-benign to the oral environment [9, 10]. These materials have a short longevity, a high tendency for microleakage and release chemical substances into the mouth (e.g. mercury, resins). This causes excessive wear to opposite teeth and as a result, numerous replacement procedures are required [9, 10].

The current understanding of the main mechanisms regulating deformation responses of tooth enamel against applied stresses during chewing, biting or grinding is also limited. It has been suggested that a key mechanism governing the renowned resilience of biomineralised tissues is the ability of proteins to

provide bridging and sacrificial bonding properties [11-13]. Other researchers have concluded that the unique deformation resilience of tooth enamel is related to a shear mechanism in the organic matrix [14]. Interestingly, enamel has been described as having metallic-like behaviour, where deformation resistance is achieved by shearing forces [15-17]. Although the excellent deformation mechanisms of tooth enamel are related to the toughening and shear mechanisms of proteins, there is no evidence to suggest how the organic component regulates these mechanisms when the loads change.

Methods of preparing and testing tooth enamel for nanoindentations are highly varied in the literature, as are the reported values for the mechanical properties of enamel. A broad range of protocols have been applied, with most relying on conventional resin-based embedding procedures for producing polished cross-sections of enamel [7, 15, 18-20]. Furthermore, few nanoindentation studies exist where enamel has been studied in its hydrated state [15, 21]. If biomimetic dental materials are to be fabricated that accurately emulate the tooth's functional properties, the genuine mechanical properties of tooth enamel must be known. Thus, potential artefacts arising from sample preparation procedures must be considered in dental research. To date, there are no studies reporting details on how to prepare tooth enamel for nanoindentation testing without using an embedding medium, or how to mount and test dental tissue in a wet environment without using glue or hot wax. Additionally, alterations of other factors such as different storage solutions, storage temperature, time, age and microarchitectural location are also known to result in changes to the measured nanomechanical properties of tooth enamel [18, 22-27].

Conventional methods for preparing enamel specimens commonly involve chemical dehydration and infiltration/encapsulation into mounting media (resins) followed by cutting, grinding and polishing prior to mechanical testing. Dehydration is a critical step in the process as any remaining water can impede the hardening and adhesion of the resin to the sample [28]. If done incorrectly,

the dehydration process can also change the enamel microstructure [29]. It has been shown that resin can infiltrate the surface of the tooth through pores and crevices and expand or contract during its transitional phase from liquid to solid. Resins used *in vivo* are also known to degrade due to enzymatic activity, saliva and water uptake, which can make resin more compliant and less stiff [30-35]. Given this evidence, resin embedding may significantly affect the mechanical properties of tooth enamel. However, the processes by which the sample preparation method alters enamel structure and composition, and the subsequent measured changes in its material properties, are poorly understood.

In addition to the sample preparation issues outlined above, variations in the way nanoindentation tests are undertaken and reported make inter-study comparisons difficult. For instance, Zhou and Hsiung [36] showed that Young's modulus of enamel varies, i.e. decreases with increasing indentation depth, even at a fixed location. Thus, given the dependence of Young's modulus of enamel on the penetration depth, it is essential to conduct measurements at constant depths when interrogating Young's modulus of enamel across its thickness. Unfortunately, most nanoindentation tests are performed under load control (i.e., constant loads), making it difficult to compare the modulus values obtained from different samples and regions, where indentation depths may differ [36-38]. Moreover, although the testing condition is known to affect the mechanical properties of enamel [23, 26], the majority of the tests are carried out either on dried samples or 'wet' specimens that were once dried during preparation [18, 39].

The mechanical properties of tooth enamel have been a topic of great scientific interest [40-51]. One of enamel most intriguing properties is its fracture toughness, which is comparable to that of glass, yet it is able to function under a wide range of loads and withstand forces up to 740 N with minimal fracture damage [52]. Recent results show that enamel is capable of recovery and even limited self-healing [53, 54]. Also, tooth enamel has the ability to absorb

considerable damage over time without catastrophic failure [53]. This ability has been explained by a microstructural mechanism of damage resistance, in conjunction with the capacity of the tooth to limit the generation of stresses under compressive loads. However, the load dependence and load carrying capability of tooth enamel with respect to its mechanical properties is not understood.

In addition to the need to repair damaged or diseased teeth, procedures based on cosmetic applications are also an important aspect of dentistry. Tooth whitening (bleaching) is considered a safe procedure by manufacturers and dentists and is increasing in popularity with the general public [55]. However, evidence is building that such treatments can result in adverse effects on tooth tissue and restorative materials [56, 57]. Furthermore, the mechanism by which teeth are whitened by oxidising materials such as hydrogen peroxide and carbamide peroxide is also currently under debate [58]. In a recent review it was shown that most bleaching products have no significant deleterious effects on the composition, structure and mechanical properties of enamel [59]. In contrast, another study demonstrated degradation of Young's modulus and hardness in bleached enamel, which was linked to an altered protein concentration within the tooth [60].

It has been argued that the alteration of properties and structure reported by these authors could be due to the methodologies used, which do not accurately reflect the *in vivo* situation [59]. With creep and recovery nanoindentation tests, the plastic deformation and recovery behaviour upon subsequent load release have been observed and related to the protein remnants within healthy enamel [15, 61, 62]. However, the creep-recovery deformation mechanism on bleached enamel in relation to its composition and structure, as well as variables that lead to the degrading properties of tooth enamel, are yet to be identified.

1.2 Primary objective

To close the gap in our understanding of the mechanical behaviour of tooth enamel, the main objective of this research was to measure the enamel nanomechanical properties in its hydrated environment and develop a basic understanding, especially at the nanostructural level, of the factors that contribute to the excellent deformation mechanisms of tooth enamel. The depth-sensing instrument (nanoindenter), optical microscope, scanning electron microscope and transmission electron microscope were used for this purpose.

1.3 Secondary objectives

- To develop a new method of sample preparation for testing tooth enamel in its hydrated state and identify the effects of resin embedding in the preparation process.
- To develop a new data analysis approach that probes the mechanical properties of tooth enamel at a constant indentation depth.
- To validate the effects of whitening treatments on enamel microstructure and determine variables controlling the mechanical responses of tooth enamel before and after bleaching treatments.

1.4 Research questions

1. Can the enamel specimen be prepared for nanoindentation testing with minimum surface and subsurface damage?
2. Can the embedding medium affect the mechanical properties of tooth enamel and its microstructure? And if so, how?

3. Can tooth enamel be mounted and tested in the nanoindenter (UMIS) in an environment approximating the enamel native state without using media such as glue or wax?
4. Can nanoindentation data be analysed at a constant indentation depth?
5. What are the mechanical properties of tooth enamel in its hydrated state and how do these values compare with conventional methods? For example: Young's modulus, hardness and wear resistance when tested with the new method and are these measurements a more accurate reflection of the tooth's properties?
6. Can the analytical models [6, 7] be used to justify mechanisms regulating deformation behaviour of tooth enamel in its elastic and plastic regions?
7. What is the relationship between composition, microstructure and mechanical properties?
 - What is the role of the organic component of enamel?
 - How does the structure of tooth enamel respond to a wide range of imposed loads?
 - Is there a relationship between protein – mineral crystal - water content, hierarchical structure and mechanical properties? Can the inelastic behaviour of tooth enamel be explained?
8. Can the deformation behaviour be modelled by considering compositional and micro-structural features in tooth enamel?

1.5 Anticipated outcomes

By addressing the primary and secondary objectives in Sections 1.2 and 1.3, the following research outcomes are anticipated:

- To offer a comprehensive understanding of the deformation mechanisms of tooth enamel and provide novel insights into mechanical function, protection and interrelation of the microstructural design of human teeth that will benefit the next generation of biocomposite materials.
- To present a picture of the genuine structure and mechanical properties of tooth enamel that will open the door to the design and application of new biomaterials in other fields, such as tissue engineering, restorative dentistry and dental material manufacturing.
- To offer scientists new opportunities to explore the unique microstructure and mechanical properties of other hydrated samples using innovative methods of sample preparation for nanoindentation.
- To advance the knowledge of why and to what extent whitening treatments change the mechanical properties of tooth enamel.

1.6 Scope of thesis

This thesis is made up of 12 main chapters. Starting with the introduction (Chapter 1) and ending with the list of references and appendices (Chapters 11 and 12, respectively), the chapters in between present a review on human tooth enamel, theories and methods used in this research and the five main research topics that were investigated.

Chapter 2 provides a review on the composition, structure and mechanical properties of tooth enamel. Sample preparation methods used in previous studies for nanoindentation testing and microscopic observations are discussed. Problems related to these methods are highlighted. Elastic/plastic deformation behaviour and creep – backcreep responses of human enamel are explained. The importance of these topics is summarised. Bleaching procedures and their effects on the

structure and mechanical properties of tooth enamel are also given. The chapter concludes with the application of numerical and analytical models that have been used in previous studies to investigate deformation behaviour of enamel.

The essential theoretical background of nanoindentation is summarised in Chapter 3. The fundamental concepts of E and H properties, stress-strain relationship and creep-backcreep nanoindentation tests are presented. Chapter 4 describes the materials and methods used in this research. Besides the newly developed method, conventional methods of tooth enamel preparation for nanoindentation testing are given. Steps of dehydration and drying procedures and whitening treatments are outlined. Variables and settings used for numerical and analytical models are also given.

In Chapter 5, a new method of sample preparation is presented, as are details of a new data analysis approach for nanoindentation, both of which were developed to investigate the effects of resin embedding in the sample preparation process. The effects of sample preparation methods on enamel microstructural integrity are presented in Chapter 6. Chapter 7 investigates load-dependent behaviour of tooth enamel in its elastic region and discusses the changes of Young's modulus across its thickness as well as at fixed locations and depths. Chapter 8 provides an explanation of the load-dependent plastic behaviour of tooth enamel by fitting the experimental results into finite element analysis models. In Chapter 9, the effects of whitening treatments on tooth enamel are presented.

Chapter 10 summarises the research presented in the thesis, and highlights the most significant findings that may stimulate further investigations on the deformation behaviour of both natural and synthetic composites.

2. Literature review

This chapter begins with a simple description of teeth before providing background information on the chemical, physical and mechanical properties of tooth enamel as a prelude to reviewing five particular topics that are closely related to this research. The key aim is to identify critical variables that influence deformation mechanisms of tooth enamel.

Dental health and overall health are directly linked. While an optimum nutritional intake through biting, grinding and chewing contributes to good dental health, strong healthy teeth are conducive to the overall health and wellbeing of humans and animals [40, 41, 51, 63]. Being the most outer layer of the tooth (**Figure 2-1**), enamel has evolved a unique composition and structure that provides direct protection against ensuing damage during dental function by retaining or adapting its shape [8, 17, 64].

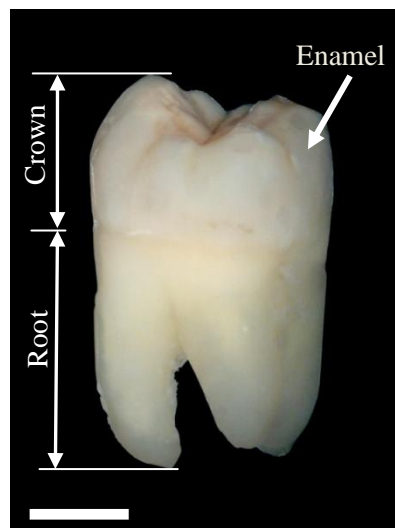


Figure 2-1. A healthy human molar. In this image, the tooth is made up of a crown and four roots. Enamel, the most visible shiny part of dental tissue in the oral cavity, is in the crown region of the tooth. The root, the bottom part of the tooth below the gums, anchors the tooth in the alveolus bone socket in the jaw. Scale bar = 4 mm.

2.1 Enamel

In dental anatomy, human teeth consist of three distinct calcified tissues: enamel, dentine and cementum (**Figure 2-2**). Enamel is the non-regenerative part that protects the tooth while dentine is the inner part of the tooth nourished by a layer of cells (odontoblasts) that are arranged along the wall of the pulp cavity. The pulp cavity is filled with pulp that is developed from the connective tissue. The pulp contains nerve fibres and blood vessels which are nervous tissue and epithelial tissue, respectively. Cementum surrounds the tooth root and helps to hold the tooth in place in the bone socket. The interface where enamel and dentine fuse is known as the enamel-dentine junction (EDJ).

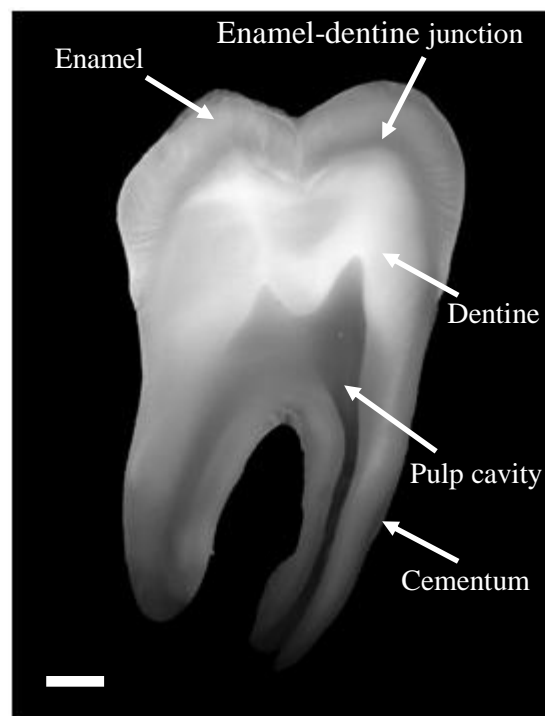


Figure 2-2. Cross sectional view of a human tooth, illustrating its major functional parts: enamel, dentine, cementum and pulp. Tooth enamel is a hard, brittle tissue that covers the outer part of the tooth in the crown region and encases the softer tougher dentine and pulp. Scale bar = 1 mm.

Enamel is finalised during the early stages of enamel development through numerous interactional processes occurring over time at various rates and durations between two adjacent tissues, the oral epithelium and neural crest-derived mesenchyme [65]. During development, mineral and organic phases undergo considerable changes which are controlled by the enamel forming cells, the ameloblasts [66]. The formation of these phases is dictated by the presence of Tomes' processes at the apical surface of ameloblasts cells [5].

In addition, the post-eruption maturation and remineralisation of enamel are affected by the existence of saliva, which has great importance in partially protecting teeth against early carious lesions [67]. However, enamel is not fully protected from the mechanical and chemical daily activity in the normal oral environment [40]. It is also important to mention that the thickness of the enamel layer varies considerably and that longer surviving enamel has a longer maturation process [68].

2.2 Chemical composition

Chemical composition plays an important role in terms of the overall understanding of mechanical responses of human tooth enamel. This composition can be better understood by taking into consideration the three main components of enamel: mineral, protein and water.

- *Mineral*

Enamel is considered a biocomposite material composed of 96 % mineral [69], which is made of crystalline calcium phosphate hydroxyl apatite (HAP), $\text{Ca}_{10}(\text{PO}_4)_6(\text{OH})_2$ [70, 71]. Alongside the major elements, calcium and phosphorus, traces of carbon, sodium, magnesium, chlorine, zinc, iron, strontium, fluoride and potassium are also found within the HAP crystals [72-74].

Notably, the density and chemical concentration of elements vary from the enamel surface towards the EDJ [75]. In general, the density of mineral crystals in healthy enamel decreases from the surface towards the EDJ. In terms of chemical concentration, calcium and phosphorus tend to decrease from the surface towards the dentine (**Table 2-1**).

Table 2-1. Enamel mineral elements and their gradient from the enamel surface to the enamel-dentine junction (EDJ). Symbols ↑ and ↓ represent increasing gradient and decreasing gradients, respectively.

Chemical elements of enamel mineral	Gradient concentration from the enamel surface to the EDJ
Ca	↓
P	↓
Na	↑
Mg	↑
Cl	↓

Conversely, distributions of minor elements in tooth enamel vary (**Table 2-1**). For instance, the average concentrations of magnesium and sodium in dry weight are higher near the EDJ than in the outer enamel layers, in contrast to chlorine, with its decreasing concentration gradient towards the EDJ [73, 76, 77].

It is important to introduce the role of fluoride as one of enamel chemical constituents in dental health. Human tooth enamel is exposed to fluoride in different ways, through food, toothpastes or drinking water. An optimal intake of fluoride is considered a key element in fortifying enamel against dental caries. However, fluoride intake must be used with caution. Excessive ingestion of fluoride is known to have negative effects on the tooth structure, such as increased porosity, pitting and corrosion, which can make enamel more prone to fracture and wear [78]. Some studies indicate a relationship between the solubility of enamel, its resistance to acid and the fluoride concentration [75, 79]. Fluoride concentration decreases from the surface towards the EDJ, making the

enamel surface less soluble and thus more resistant to acid attack from the oral environment compared to the subsurface.

- *Protein*

Tooth enamel contains approximately 1% protein [69]. Proteins cement the apatite crystals together. The density of proteins increases from the enamel surface towards the EDJ [75]. The protein function has not been fully clarified [75]. However, it is believed that this organic material allows limited differential movements between adjacent rods to reduce stresses without crack growth, thereby making enamel more flexible and resilient [14, 47].

- *Water*

Although mature enamel contains only 3% water [69], this still plays a significant structural role by supporting permeability, ion exchange, elasticity and reactivity of chemical elements within enamel [80]. Notably, no relationship has been demonstrated for permanent teeth between water content and the age or type of tooth [81].

Techniques such as vibrational spectroscopy, micro-Raman spectroscopy and scanning electron microscopy (SEM) equipped with the energy dispersive X-ray spectroscopy (EDS) have been shown to be useful tools for taking accurate measurements of chemical composition in dental hard tissues. The first detailed spectrographic analysis on human tooth enamel was presented by Lowater [82], who identified and qualitatively estimated the constituent chemical elements. With the development of more sensitive micro-Raman spectroscopy with high spatial resolution up to 1 μm , detailed mapping of organic and mineral compounds became popular for the analysis of human tooth enamel and other mineralised tissues [83]. By employing the latter technique, a monotonically decreasing gradient of mineral content from enamel to dentine with a concurrent monotonic increase in the organic component across the EDJ has been identified [83, 84]. Additionally, Raman spectrometry and SEM-EDS revealed that the

chemical composition of tooth enamel is altered by the presence of dental diseases [85, 86].

2.3 Hierarchical structure

2.3.1 Characterisation of enamel hierarchy

Tooth enamel is composed of many different hierarchical structural units at different scales, making enamel a robust natural biocomposite with great resilience against applied loads during dental function. The most important hierarchical structural units of enamel can be observed at both nanoscale and micron scale (**Table 2-2**).

Table 2-2: Summary of hierarchical structural features of human enamel.

Structural characteristics		Hierarchical features
Basic crystal unit	$\text{Ca}_{10}(\text{PO}_4)_6(\text{OH})_2$	Hexagonal unit
Crystal system	hexagonal	↓
Crystal shape	hexagon	Needle
Lattice variables	$a = 0.94 \text{ nm}$ $c = 0.68 \text{ nm}$	↓
Average crystal diameter	$d = 40 \text{ nm}$	Ribbon
Length of crystal	$L = 100 - 1000 \text{ nm}$	↓
Average length	$\bar{l} = 500\text{-}600 \text{ nm}$	Prism
Rod diameter (head)	$5 \mu\text{m}$	↓
Enamel boundary	$1 \mu\text{m}$	Rod

- *Nano-Scale Organisation*

Early in the enamel development, mineral crystals are commonly hexagonally shaped platelets in cross-section with average lattice variables $a = 0.94 \text{ nm}$ and $c = 0.68 \text{ nm}$ (**Figure 2-3**) [75, 87].

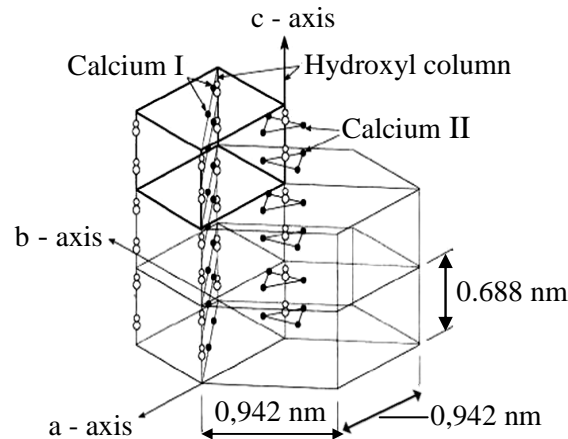


Figure 2-3. Crystal structure of hydroxyapatite and the relationship between the hexagonal and crystallographic unit cell. Adopted from [75].

As enamel matures, the mineral crystals can appear rectangular or as irregular polygonal shapes, with different lattice patterns as a result of density fluctuation, compositional variation, dislocations or other distortions [88-91]. In cross-section, the diameter of the dominant crystals in healthy, mature enamel is 40 to 50 nm, which corresponds to the combined average values of width and thickness of the mineral crystal 68.3 ± 13.4 nm and 26.3 ± 2.2 nm, respectively [89]. The long axis of the crystallite is parallel to the crystallographic c axis (**Figure 2-3**). The crystals grow in width, then in thickness (**Figure 2-4**) [89].

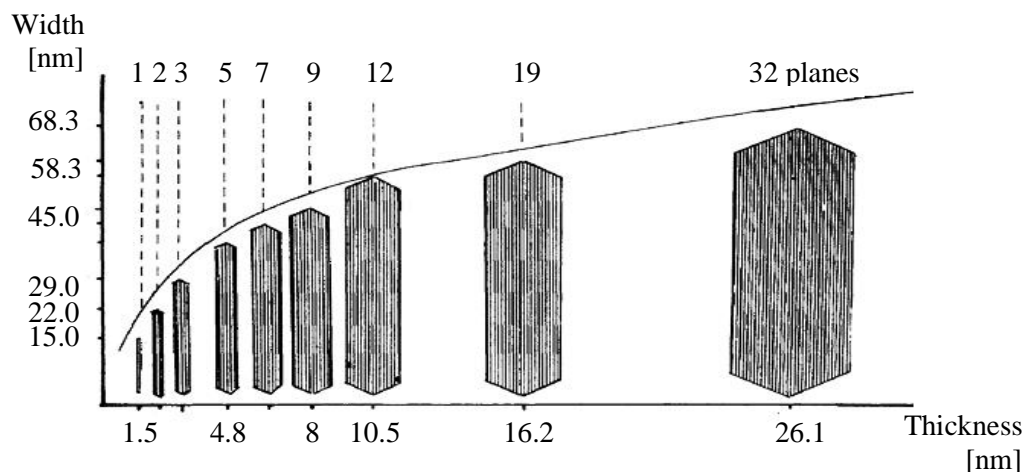


Figure 2-4. Size and shape of enamel crystallites and growth [89].

It has been suggested that the crystals may reach a total length of 100 to 1000 nm with an average crystalline length of 500 to 600 nm [91]. As the crystals develop, they pack together to adopt a ribbon-like shape with highly organised parallel arrays, which comprise the next order of hierarchical structure, the prisms (**Table 2-2**).

- *Micron Scale Organisation*

In mature enamel, the prisms, together with proteins and water, make up the next building blocks, the rods [5]. The keyhole-like rods with the “head” and “tail” regions are interlocked and bonded together by softer organic proteins (**Figure 2-5**), and these interspaces between adjacent rods of approximately 100 nm are very often described as the sheaths [40].

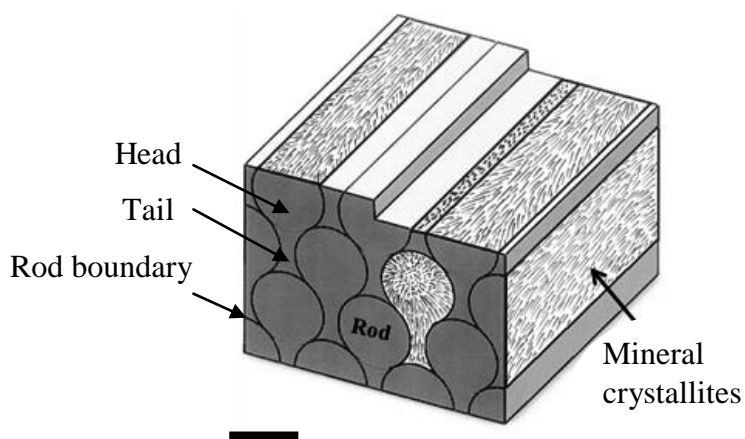


Figure 2-5. Schematic illustration of a key-hole like enamel microstructure. Modified from [92]. Scale bar = 5 μm .

In the central part of the rod, also called the “head”, HAP crystals run generally parallel to the rod axis, while those close to the edges of the rod slightly incline from the longitudinal axis. The diameter of the “head” region is about 5 μm . In the “tail” region, crystals are oriented in different directions (**Figure 2-5**). At the microscopic level, rods run from the EDJ nearing perpendicular direction to the enamel surface [40]. The orientation of the rods and how rod bundles cross

from the EDJ to the enamel surface (decussation) result in mechanically stiffer enamel with higher fracture resistance [17, 93].

- *Millimetre Scale*

There are structural features that can be observed in tooth enamel at the millimetre scale, including Retzius lines and the Hunter-Schreger bands (**Figure 2-6**), which result from the cross striated and interwoven rods [5]. Retzius lines form during alternating growth and rest periods over the course of the enamel development [94]. The Hunter-Schreger bands can be seen under reflective light as light and dark bands at the cross-sectional surface of enamel [95, 96]. It has been suggested that the appearance of Hunter Schreger bands is related to differences in the orientation and organisation of prisms [97]. This structural feature is preventing crack propagation within enamel making it harder and more resilient [98].



Figure 2-6. Observation of the cross-sectional enamel surface in a hydrated environment using reflective light. The arrows indicate Hunter-Schreger bands. Scale bar = 1 mm.

2.3.2 Defects in tooth enamel structure

Although tooth enamel is designed to last and function as it needs to, some nanoscale to millimetre scale defects have been identified in the tooth enamel structure.

- *Nano-Scale*

Enamel crystal structure at the atomic scale has a bearing on mechanical properties of the tooth. However, several crystalline defects have been reported; for instance fusion, dislocations and planar defects with central dark lines that may affect tooth properties and how the tooth functions. Kerebel et al. [90] and Daculsi et al. [89] reported that during enamel development, closely packed mineral crystallites induce mechanical stresses that result in dislocations, fusion and shrinkage in the crystallographic structure. Furthermore, Daculsi et al. and Kerebel et al. investigated the central dark line in the enamel crystals and postulated that this defect is only “a focal phenomenon, being no longer visible at high resolution magnifications” [89]. Later, Marshall et al. [99] argued that the central dark line can be seen using transmission electron microscopy and may exist due to variations in chemical composition or separation of crystalline phases in enamel. The authors emphasised that the occurrence of this dark line is of particular interest as it undergoes preferential dissolution and indicates the early initiation of caries.

- *Micron Scale to Millimetre Scale*

Tufts and lamellae have been reported as structural defects in tooth enamel from the micron to the millimetre scale. The tufts are closed cracks or defects filled with protein-rich matter that originate at the EDJ and run along tooth walls towards the occlusal surface of the tooth [40]. The tufts have been thought for a long time to represent weakened planes that lead to the onset of damage and the subsequent fracture as a result of the mechanical function of the tooth [100]. However, these defects have been shown to play an important role in the

mechanical responses of human teeth [53]. On the other hand, lamellae can be seen on the mature enamel surface and can also be defined as closed cracks filled with the organic matter [101] extending from tufts with progressing age [40, 53].

2.3.3 Techniques for observing enamel structure

Scanning electron microscopy (SEM) and transmission electron microscopy (TEM) have been commonly used for investigating many biological materials. While SEM can provide information about the material surface, TEM gives information from the projection of the thickness (~100 nm) of the internal structure of a material at the nanoscale level [102, 103].

The SEM is a widely used surface imaging tool that is suitable for structural observations of bio-mineralised materials. In SEM, two main signals are collected from the sample, including secondary electrons, which are emitted from atoms in the sample following excitation by the primary electron beam, and back-scattered electrons, which are primary beam electrons that have interacted with the sample. For this instrument, the specimen must be coated with gold or platinum (~2 nm) to minimise charging of the specimen in the vacuum chamber. Depending on the signal used and how the specimen is prepared, a conventional SEM image can show topographic and compositional contrast with high resolution. However, this method cannot physically reveal the material's subsurface structure. Dual beam techniques, combining a focused ion beam (FIB) with SEM, can facilitate the extraction of TEM sections from polished cross-sections of enamel and other hard tissues, thereby providing information on subsurface structure.

FIB is a traditional technique used by material scientists or geologists to cut thin sections of material. It is increasingly being used to study hard biological materials, i.e. biominerals [7, 104, 105]. This is because these materials cannot be cut with conventional apparatus such as microtomes. FIB-TEM sections can be produced in 2 to 3 hours by thinning the specimen at precise locations where

previous mechanical testing (nanoindentation, nanoscratching) has been conducted [7, 102, 103]. Because human tooth enamel is electrically non-conductive, a thin layer (≈ 2 nm) of gold, platinum or carbon is applied to the enamel surface before FIB milling.

2.4 Mechanical properties

In this section, the principles of materials testing are given along with how these are applied to studies investigating the mechanical properties of human tooth enamel.

2.4.1 Materials Science Fundamentals

In Materials Science, Young's modulus and hardness are key properties in engineering designs [106]. Young's modulus, E , is the property used to quantify the resistance of a material to elastic deformation [106]. The elastic deformation is reversible, which means that when an applied load is released, the material can return to its original shape. The E value is an important property defining the maximum limit of the materials' capability to function without failure. This value is commonly reported in [GPa] and expressed as the ratio of stress to strain, $E = \sigma/\epsilon$, where σ is the stress ratio of the applied force on the area and ϵ is the ratio of the deformation elongation to the original length. When the stress to strain ratio is proportional (i.e., linear), the deformation is elastic following Hooke's law, $\sigma = E \cdot \epsilon$. Thus, E can be expressed as $E = d\sigma/d\epsilon$. However, this equation can only be applied for isotropic material. If the applied stress is at some angle to one of the three principal axes of anisotropic material, the elastic modulus must be defined for each direction of the x , y and z axes, and is thus defined as E_x , E_y , and E_z .

The hardness, H , of a material is defined as the resistance of a material to plastic deformation, usually by penetration (indentation), bending, scratching, abrasion or cutting [106]. This property of a material is the result of a performed procedure. To obtain the H , the depth/area of an indentation left by an indenter is

measured while other variables are specified before experimental test: 1) shape of indenter, 2) applied force and 3) time. There are three traditional methods for expressing the relationship between hardness and the size of the impression: Brinell, Vickers, and Rockwell. While each of these methods is divided into a range of scales, defined by a combination of applied load and indenter geometry, they do not allow measurements of local properties of specimens that are relatively very small compared to indenter geometry.

Other properties, such as ductility, resilience, toughness and flexural strength, are also used for defining the mechanical behaviour of materials including tooth enamel (**Table 2-3**, pp. 25).

Ductility refers to the amount of plastic deformation that materials can sustain before they fracture and it can be expressed as a percentage of elongation, % LA, or reduction, % RA, of the material's cross-sectional area at the point of fracture [106]. Therefore, the ductility is a very important property in terms of designing and manufacturing materials, as it specifies the range of plastic deformation that the material can undergo before mechanical failure. Resilience of the material, U_r , is defined as the area under the stress-strain curve from the unloading state up to the state of yielding. The yielding point is determined by values of the yield stress and yield strain [106]. This property specifies the ability of a material to absorb energy during elastic deformation and then, upon unloading, to recover this energy. The area under the stress-strain curve can be measured from the state of unloading up to the point of fracture. The term toughness, K_c , is used to express the allowable amount of energy that the material can absorb upon fracture. The K_c of a material is determined by the ability of the material to resist the extension of pre-existing cracks, despite the build-up of stress concentration [106]. A property related to K_c is the flexural strength, σ_{fs} , which is defined as a force per unit area required to initiate and propagate a crack to fracture [106]. For brittle materials such as ceramics, three or four point transverse bending tests are commonly employed.

In contrast to the traditional methods that allow the measurement of microscale to macroscale properties of the bulk samples outlined above, nanoindentation instruments have been developed for measuring these properties down to the nanometre scale (Chapter 3).

2.4.2 The mechanical characteristics of enamel

Different mechanical testing methods are used to measure the mechanical responses of tooth enamel; these methods result in different approaches of data interpretation. Understanding the mechanical properties of human tooth enamel is essential for:

- evaluating mechanical properties and comparing enamel to other materials,
- assessing the suitability of dental materials (i.e. ceramics, veneer, alloy) and investigating the structure-properties relationship, and
- identifying the critical variables that regulate the structure properties-relationship, and theoretical modelling of enamel-like material.

Therefore, it is important that the methods used for measuring are comparable.

Enamel has unique mechanical properties related to its function of enabling the dental surface to concentrate stresses [17, 64, 107]. Furthermore, it has been shown that the E and H of enamel is related to its high mineral content [18], and yet it is a brittle material [53]. Numerous studies have been conducted to explore the mechanical properties of human tooth enamel; however, the deformation mechanisms of tooth enamel remain elusive. Understanding the relationships between the composition, structure and mechanical properties at the nanoscale is crucial for the future development of novel bio-mimic dental materials [25].

Human tooth enamel is a challenging material when trying to characterise and compare its mechanical properties, owing to its hierarchical structure [108]. At the macroscale, enamel appears as a homogenous bulk material, but at the microstructural level, enamel is a composite made of fibre-like rods embedded in a water-protein matrix. Its mechanical behaviour is similar to that of composite materials such as ceramics or columnar titanium nitride film [109-111].

Since mechanical properties change with the directions of crystallites as well as rods, enamel is considered as an anisotropic composite [107, 112]. Spears [112] evaluated the anisotropic behaviour of tooth enamel from two levels of hierarchy: the crystalline level, where the enamel is made up of straight parallel crystals held together by organic material, and the rod level, where structured enamel is composed of differently orientated crystals. With finite element models, Spears showed a strong dependency of E values with regard to prism orientations. In 1998, Xu et al. [39] determined that the E and K_c of tooth enamel is strongly dependent on the rod orientation and location of measurement (i.e., axial versus occlusal plane). Shimizu et al. [107] and Spears [112] showed that enamel properties vary as a function of prism orientation. However, results presented by Cuy et al. [18] and later by Braly et al. [113] contradict this. Both studies show only a weak correlation between mechanical properties and prism alignment. Moreover, Cuy et al. [18] have found a correlation between mechanical properties and chemical constituents of HAP in enamel. Notably, the authors reported a decreasing gradient of E and H values from the enamel surface to the EDJ and the same trend has been identified for the concentration of calcium and phosphate.

Averaged values of E , H , K_c and σ_{fs} for tooth enamel and other materials are summarised in **Table 2-3**.

Table 2-3. Mechanical properties (E, H, K_c and σ_{fs}) of human tooth enamel and other materials. K_c

Scale	Method	Specimen	Occlusal plane [GPa]	Axial plane [GPa]	Ref.
E of enamel					
Macro-	Compression testing	1 st molars	84.2 ± 6.2^a	78 ± 4.8^b	[114]
Micro-	Modified Vickers indentation	3 rd molars	94 ± 5	80 ± 4	[39]
Nano-	Nanoindentation	3 rd molars	87.5 ± 2.2	72.7 ± 4.5	[24]
E of other materials			[GPa]		
Micro-	Indentation	dentine	20 (average value)		[41]
Micro-	Vickers indentation	dental ceramics	65 ± 1.5 to 265 ± 10		[115]
Nano-	Nanoindentation	dental alloy	199.54 ± 12.5		[9]
H of enamel			[GPa]	[GPa]	
Micro-	Modified Vickers indentation	3 rd molars	3.62 ± 0.20	3.37 ± 0.15	[39]
Nano-	Nanoindentation	3 rd molars	3.9 ± 0.3	3.3 ± 0.3	[24]
H of other materials			[GPa]		
Micro-	Indentation	dentine	0.6 (average value)		[41]
Micro-	Vickers indentation	dental ceramics	5.3 ± 0.2 to 13 ± 0.3		[115]
Nano-	Nanoindentation	dental alloy	4.1 ± 0.17		[9]
K_c of enamel			[MPa \sqrt{m}]	[MPa \sqrt{m}]	
Micro-	Standard Vickers indentation	3 rd molars	0.77 ± 0.05	0.52 ± 0.06 1.30 ± 0.18	[39]
K_c of other materials					
Micro-	Indentation	dentine	3.1 (average value)		[41]
Micro-	Vickers indentation	dental ceramics	1.2 ± 0.14 to 7.4 ± 0.62		[115]
σ_{fs} of enamel			[MPa]		
Macro-	n/a	enamel	30 (average value for bulk sample)		[41]
Macro-	Three point bend test	enamel	49 ± 17 to 68 ± 16		[116]
Micro-	Micro-cantilever bend test	enamel-rod	750 ± 240 to 1420 ± 410	560 ± 160 to 412 ± 37	[116]
σ_{fs} of other materials			[MPa]		
Micro-	Indentation	dentine	-		[41]
Micro-	Three-point bending strength test	dental ceramics	106 ± 17 to 840 ± 140		[115]

^{a,b} Average values from Tables 1 and 2 [114] recalculated to GPa; 1 GPa = 145 000 psi.

When comparing tooth enamel to dental ceramics, enamel shows a higher stiffness than dental ceramics, while dental ceramics are harder than enamel. Furthermore, it has been shown that dental ceramic materials have the yield point that is three times higher than enamel [9]. This means that dental ceramics can

resist higher forces than enamel without sudden fracture. However, from a reliability point of view, the harder ceramic in contact with enamel can result in premature failure - i.e. excessive wear in the form of permanent plastic deformation or even surface damage of enamel [9].

To conclude, human tooth enamel is highly variable in shape, size, thickness, structure and properties. There are considerable variations in its composition, structure and mechanical properties between teeth or even within a single tooth.

2.5 Sample preparation

2.5.1 Methods of preparing teeth for nanoindentation testing

Nanomechanical properties of teeth are commonly measured with depth-sensing instruments. Because the scale of deformation during testing is very small, nanoindentation tests are considered as non-destructive and can be conducted on specimens of various sizes and types, including hard dental tissues, such as enamel [48, 117]. The sample preparation may be a simple process for most metallurgical samples; however, there are many caveats in the preparation methods of human teeth and other biological materials for nanoindentation tests [118, 119].

The sample is usually stored in aqueous solution, dried with tissue paper or in the air [1, 119, 120], then embedded in resin [18, 27, 36, 47, 121]; later the specimen is cut, ground, polished, and finally mechanically tested. Although the main purpose of resin embedding is to hold the specimen during preparation and testing, there are several problems associated with the use of resin during the preparation process.

One of these problems is related to the inappropriate dehydration or drying process. If this process is not followed carefully, trapped water in the specimen

can interfere with the medium [28]. Besides water uptake, enzymes, cholesterol esterase and saliva fluid also degrade exposed resin, making the resin more compliant and less stiff [31, 32, 34, 35, 122]. As a result, a poorly-polymerised resin may cause considerable contamination of the sample surface during cutting, grinding and polishing [123] and lead to fractured or cracked enamel surfaces [29].

Another problem may occur because of the dimensional changes and temperature of the resin during polymerisation. Contraction stresses may develop within resin due to polymerisation shrinkage and increasing temperature. Also, one may suspect that large scale shrinkage of resin may lead to considerable defects in the form of fractures within tooth enamel [124].

Depending on the viscosity of the embedding media, the use of resin can infiltrate pores and crevices in the tooth. Molecules of a smaller size will penetrate into tissue more easily and promote greater resin shrinkage than larger molecules [124]. As a result, the resin's ability of infiltration may lead to changes of the structure and near-surface properties of tooth enamel.

In order to ensure that nanoindentation measurements are consistent within and between samples, testing must be conducted on flat, level surfaces. In order to meet this requirement, samples are commonly polished in a consistent way using methods that minimise surface or subsurface damage. These methods are highly variable depending on the material concerned. To date, no studies have described the preparation of hydrated, flat, polished enamel surfaces for nanoindentation [48]. Furthermore, standard dry polishing protocols are highly varied in the literature, making it difficult to compare and contrast findings from different studies. Some of the artefacts and negative effects that can be generated by sample preparation include:

- *Inaccuracy in flatness.* This can occur due to uneven pressure while holding the sample during manual grinding and polishing procedures.

- *Contact area errors.* Since nanoindentation instrument measures mechanical properties indirectly from the contact area between the indenter and the tooth specimen at the specific indentation depth, the higher values of surface roughness may cause higher errors in measuring a contact area under the indenter at the specific depth [117].
- *Surface and subsurface damage.* As enamel is a brittle material, grinding and polishing may create some amount of surface and subsurface damage. This is because the quality of the finished surface depends on the microstructure and mechanical properties of the specimen material, the rate of material removal and how abrasion particles interact with surface of the specimen [125, 126]. For instance, it has been shown that grinding was encountered by residual surface cracks which affect strength and performance of the material [127]. Additionally, by investigating the relationship between the material removal rate and stress dependency on crystallographic orientations of brittle materials, previous studies showed that the primary deformation mechanism in lapping procedure is a brittle micro-cracking followed by plastic deformation mechanism in the polishing process [126, 128].
- *Errors in nanoindentation testing.* Mounting specimens in the nanoindenter is commonly achieved by adhering the sample to a flat stainless steel base with pre-heated wax [3, 54, 118] or cyanoacrylate glue [129]. Although only a thin layer is used, these gluing media may affect the samples' flatness or, if porous, its chemical properties, thereby affecting the microstructural or mechanical properties of the test specimen. A larger obstacle is testing the sample in a hydrated environment. Continuous spraying of the sample during experimentation has been used [21]; however, this can cause errors in

testing results due to changes in instrument temperature (thermal drift).

Apart from the artefacts and defects described above, it has been shown that different storage solutions, storage temperatures, times and testing in a hydrated or dried state have significant effects on the nanomechanical properties of tooth enamel [22, 23]. This is because the depth sensing instrument gathers properties from the near surface layer of the sample [22].

2.5.2 Microstructural observation of the enamel-dentine junction

The EDJ is a 15 to 25 μm -wide scalloped-like region that provides an interface between the hard, yet brittle enamel and the softer, tougher dentine and plays an important role in maintaining the biomechanical function of the tooth [21, 121, 130, 131]. Some authors reported that the EDJ acts to arrest cracks initiated from the enamel surface down to the EDJ [21], while others observed internal cracks extending from the EDJ into enamel [40].

Previous authors have investigated crack propagation across the EDJ with Vickers indents and reported that “the vacuum of conventional SEM sometimes led to cracking either along the line of indents or at/near the optical EDJ” [21]. However, it may be speculated that these defects resulted from drying procedures possibly due to different ratios of shrinkage of more hydrated dentine and less hydrated enamel. Although some authors used environmental SEM to confirm that “such spurious cracking did not compromise the results” [21], it has been demonstrated that the inappropriate drying process builds up tensions and is more likely to initiate a gap formation along the EDJ [29].

In order to overcome the disadvantages of the resin embedding process and potential degrading effects of sample preparation on structural and mechanical characteristics of tooth enamel, a new approach was followed in this research to:

1. develop a new method of tooth preparation that permits cutting, grinding and polishing human tooth enamel in a wet environment without chemical or liquid-based embedding media,
2. design and manufacture a new nanoindentation holder that provides testing of the tooth in a hydrated environment and avoids the application of a mounting media, such as wax, resin or glue during testing, and
3. provide high resolution morphological images of the EDJ.

2.6 Deformation behaviour of tooth enamel

A detailed understanding of the mechanical behaviour of tooth enamel is essential for improving the biocompatibility, functionality and longevity of current dental materials. A close bio-mimicking of tooth enamel elastic, plastic and viscous deformation responses could lead to enhanced longevity as well as the environmental sustainability of dental materials and restorative treatments. While the elastic responses of material can be assessed with E values acquired from nanoindentation load-displacement curves, plastic responses can be analysed with values of H and the yield point captured in stress-strain curves. By ascertaining elastic or plastic behaviour in this manner, it is assumed that deformations occurred instantaneously with no-time dependent effects. On the other hand, the time-dependent viscous behaviour can be analysed from indentation creep tests, by measuring depth as a function of time, and simulated with rheological models, such as Voigt, Maxwell and Voigt-Maxwell.

2.6.1 Elastic behaviour

Like many other rigid biomaterials, such as shells, bones or spicules [132], enamel exhibits a superior combination of mechanical properties emanating from a nanostructured assembly of a very hard crystalline phase enveloped by a

surpassingly soft, glutinous protein matter. However, enamel must maintain its functionality and endure high cyclic contact loads due to regular interactions with opposite teeth and return to its original shape [17].

The unique shape and functionality of enamel promote remarkable resistance to elastic deformation when applied loads are released. The E value is the property that quantifies this resistance and defines the maximum limit of enamel capability to function without failure. The E of enamel is frequently measured by depth-sensing indentation and is determined from the unloading part of the load displacement curve. It is therefore important to note that although there can be plastic deformation during unloading, it is assumed that these deformations are elastic [133]. In the nanoindentation theory, a known area of the contact is of great importance as the final calculations of properties are based on this variable [117]. The properties, derived from the contact area, are indirectly inferred from load-displacement curves; i.e., from the maximum depth of penetration and the slope of the unloading curve at the maximum load. Thus, the depth of penetration (the indentation depth) plays a critical role in data evaluation. If the E decreases from the enamel surface towards the EDJ, then it is anticipated that the penetration depth and analogous contact area increases under a constant load in this direction.

Generally, nanoindentation data are calculated and presented to the average depth of penetration. However, previous studies clearly demonstrate that the mechanical properties of enamel decrease with increasing depths of penetration [2, 37, 38, 54]. Therefore, each depth of penetration is critical in data interpretation and should not be averaged. Notwithstanding numerous amounts of nanoindentation studies, there are no reports on mapping of mechanical properties of human tooth enamel to the constant depths. Notably, the values of E vary as a result of many factors - such as: area of testing, testing environment and age of human enamel [18, 24-27]. In addition, the changes in indentation depth affect the E of enamel [36].

Thus, it is important to present E values at constant depths from the enamel occlusal surface towards the EDJ. However, constant loads are applied in most nanoindentation tests, which result in difficult E value comparisons when enamel is measured at different locations of the sample [36-38]. Another difficulty arises from drying specimens during sample preparation and nanoindentation testing [18, 23, 26, 39].

Thus, to provide guidance in the design of novel enamel-like nanomaterials [134] or in many other fields such as materials science, engineering, aeronautics and astronautics[135], it is essential to:

- conduct an in-depth investigation of the elastic region in tooth enamel under the influence of mechanical loads, and
- analyse the depth dependence of E in conjunction with a mechanistic based model and the enamel microstructure.

An elastic deformation model was used by Xie et al. [7] to identify a link between the E values of enamel, the thickness of proteins and the loading direction. The proposed nanoscopic model connected elastic responses of tooth enamel at the microscale by simulating E values from nanoindentation instrument. By doing so, the effective crystal orientation angle and the thickness of protein were identified. The authors demonstrated that these variables affect elastic responses of enamel during complex loadings. Accordingly, this well accepted model used for the investigation of elastic behaviour of tooth enamel [7] has been found essential to identify a relationship between the E values of enamel and the constant indentation depth in this study.

2.6.2 Elastic-plastic behaviour

The stress-strain curve provides important information on the elastic and plastic deformation of any material. To those who are unfamiliar with terms used in the field of materials science, a short explanatory introduction is given here.

As shown in **Figure 2-7**, the curve starts with a linear relationship between stress and strain (elastic region) and then generally deviates from this curve (plastic region).

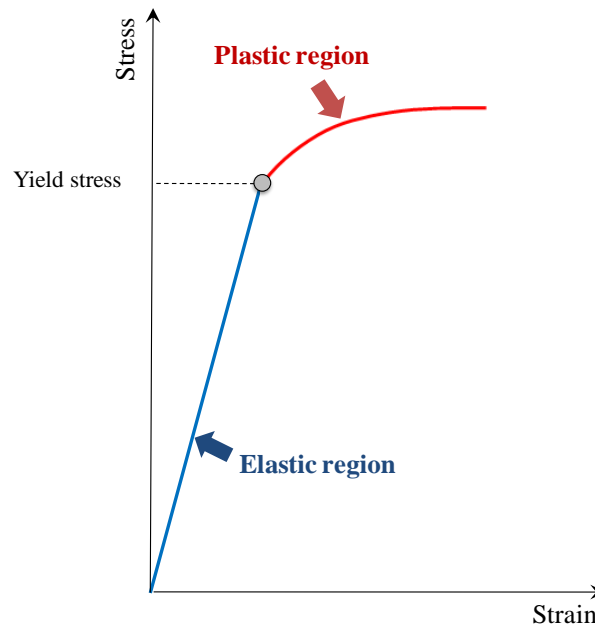


Figure 2-7. Schematic stress-strain curve indicating the elastic and plastic behaviour of a material. The transition from the elastic to plastic region is identified as the yield point. Beyond this point, the material undergoes permanent deformation.

The maximum stress on the linear portion of the curve represents the elastic limit, which is also called the yield or flow stress, beyond which the material undergoes plastic deformation. Once the material is plastically deformed, this deformation is irreversible, resulting in the permanent damage of the material. Berkovich and spherical indenters are commonly used in nanoindentation tests to investigate the mechanical properties of a material. In contrast to the Berkovich indenter, whose representative strain remains constant ($\approx 8\%$) for all indentation depths, the determination of stress-strain responses of materials can be performed with the spherical indenter whose strain gradually changes with the increasing

indentation depth/load and therefore, a gradual transition between the elastic and plastic region can be captured. This is because the start of the plastic deformation is delayed with a spherical indenter which is advantageous of the blunt tips while the plastic deformation occurs immediately even at small depths when the nanoindentation tests are performed with a Berkovich indenter [136, 137].

The early investigations of the elastic–plastic deformation behaviour of tooth enamel at a macroscale level was performed by Staines et al. in 1981 [26]. By using a spherical ball with a 6.32 mm diameter, the authors observed elastic deformation behaviour of tooth enamel on the initial loading curve to 1.6 μm indentation depth, the depth for which the reloading part of the curve matched the loading part. Based on this experimental observation and Timoshenko's & Goodier's theory of elasticity for ductile materials (metals), which assumes the start of the plastic deformation of material at 92 % of the mean pressure, Staines et al. reported the yield stress of 3.3 GPa for 2 μm indentation depth.

Although there has been a considerable amount of research carried out to investigate E and H of enamel at the nanoscale, no stress-strain properties of enamel had been reported in detail until the study by He et al. in 2006 [37]. That study extensively investigated the elastic-plastic responses of enamel. Interestingly, no transitional shifts from the elastic to plastic region of enamel were observed and only the plastic deformation of enamel was revealed, possibly due to the high range of applied loads used in this study (1 mN – 450 mN). The same study also introduced a new method of defining stress-strain properties in enamel by plotting the contact pressure, H, against $\tan\theta$, where H denotes the stress and $\tan\theta$ the strain property of the material. This method was based on a simple model for a spherical indentation for nanoindentation testing that was proposed in 1993 [138] and later refined in 2004 [139]. The advantage was to eliminate the radius of the indenter in all stress-strain calculations, and therefore, to decrease significant errors in measurements due to differences between the real and nominal tip of the spherical indenter. However, despite the high accuracy in

calculations of stress-strain responses of the material, this method did not determine a maximum load that could be used in defining elastic as well as plastic responses of enamel.

Given the importance of the maximum applied load in determining elastic to plastic regions of tooth enamel in respect to its hierarchical structure, in 2009, Ang et al. [118] investigated elastic-plastic behaviour at the intrarod level ($< 5 \mu\text{m}$) with a $8 \mu\text{m}$ diameter spherical indenter and much lower loads of 5 and 11 mN. The authors reported $1.6 \pm 0.1 \text{ GPa}$ for the yield stress and $0.6 \pm 0.05 \%$ for the yield strain at the indentation depth of 7 nm under a load of 280 μN . Notably, the value of the yield stress was halved when compared to Staines et al [26]. This was possibly due to the different testing method used in the stress-strain investigation of enamel. While Staines et al. investigated stress-strain properties at the macroscopic level as a whole tooth with a 6.32 mm diameter spherical indenter [26], Ang et al. reported these properties at the nanostructural level involving several hundreds of crystallites with a $8 \mu\text{m}$ diameter spherical indenter [118]. A more complex study was published by Ang et al. in 2010 revealing stress-strain properties of enamel over four different hierarchical length scales measured with three different spherical indents of radii: 8.3, 0.86 and 0.063 μm , respectively [3]. The authors identified the yield stress between 0.9 GPa for the multiple-rod level and 17 GPa for the single crystallite level in the range of applied loads between 32 and 1400 μN . The transitional phase from the elastic to plastic region was identified only for the crystallite level of enamel (nanoscale) possibly due to the lower loads and small volume involved in the deformation process. On the other hand, elastic deformation followed by the microcracking mechanism was identified for the macroscale level. Ang et al. suggested that different hierarchical structures and the role of proteins were critical in the deformation behaviour of enamel. Those findings were in agreement with results from earlier theoretical models proposed by He & Swain [111] and Xie et al. [7, 105]. In 2007, He & Swain introduced a simple nanoscopic model simulating a plastic deformation mechanism of tooth enamel in conjunction with the role of

proteins within its microstructure. Notably, this model showed that the shear deformation of proteins played a critical role in enamel resilience resulting in nonlinear plastic deformation. In 2008, Xie et al. developed more complex mechanical models for the elastic as well as plastic deformation mechanism of tooth enamel. As observed earlier by He & Swain [111], Xie et al. also identified protein properties such as the thickness and shear as the most critical variables influencing mechanical responses in enamel. Furthermore, the models determined the secondary variable, the effective crystal orientation angle of enamel crystallites between the indentation load and longitudinal axes of crystallites that affect the mechanical responses of tooth enamel.

Similar to enamel, biological materials such as spider silk also illustrate nonlinear deformation responses against contact-induced damage [2, 140]. The latter study showed that the key mechanisms of structural integrity to accommodate localised induced stresses were found in softening properties at the yield point and significant work hardening at large strains. In enamel, a work hardening has been previously observed without prior softening mechanism at the proportional limit. Because the stress-strain curves of tooth enamel are generally plotted in terms of scattered data and best fit functions, one may speculate that some softening mechanism in enamel may exist to promote the resistance against applied loads.

2.6.3 Creep and recovery

In the field of materials research, creep is defined as the time-dependent permanent deformation when a material is subjected to a constant load or stress [141].

Observed by several workers, tooth enamel has been found to have an exquisite time-dependent viscous behaviour that is believed to yield the superior ability of this biocomposite to function in the oral cavity over a person's lifetime [15, 16, 54, 62, 111].

Performing creep analysis on tooth enamel, He & Swain reported relatively stable creep responses under a 250 mN applied load over 900 s holding time and an even more striking extent of recovery up to 60 % at a load of 5 mN over a holding time of 900 s [15]. The authors related creep and backcreep mechanisms to structural and functional protein properties in enamel, i.e. to protein sheets and their sacrificial bonds, respectively. Furthermore, a greater creep-backcreep ability of enamel has been reported for the area near the EDJ than at the outer surface, possibly due to the higher organic content near the EDJ [54]. It was previously reported in the study by Ji & Gao, who investigated mechanical behaviour of nanostructured biocomposites with the use of mechanical models, that the higher volume concentration of proteins in biocomposite can be attributed to a material's capability to sustain extraordinary large plastic deformation over a longer period of time. This was found due to an inbuilt sacrificial bond mechanism that gives proteins the ability to undergo transition from entropic elasticity to metal plasticity [142]. Additionally, by investigating environmental conditions on mechanical responses of tooth enamel, the authors came to the conclusion that the decreasing content of proteins results in increasing brittleness of the material with decreasing ability of creep-backcreep behaviour [143]. Recently, Schneider et al. proposed a 3D creep model for two hierarchical levels of enamel that predicts viscous flow within enamel crystallites or rods [62]. For both the crystallite and rod level, the protein-water compound was treated as a viscous fluid whose flow represented shear stresses within the structure. In the model by Schneider et al., 4 % and 1 % indentation creep strains were determined for the crystalline and rod level, respectively. In contrast to the rod level, the authors suggested that the higher volume content of proteins at the crystalline level yielded a greater creep behaviour of tooth enamel.

Lastly, the process of self-healing mechanisms of damage resistance in brittle materials should be noted. For instance, in mica and silica, the process of self-healing occurs through a bridging mechanism in which the interfaces of cracks re-bond through the precipitation of fluid and chemical reactions of the crack

walls [144]. As a result, this bridging mechanism improves material properties such as strength and toughness [144]. A similar mechanism of self-healing has been found in tooth enamel [53]. In enamel, crack-like defects in the form of tufts are housed along the EDJ. Although these defects are unavoidable, they can be partially inhibited by replenishment of protein-rich material in those cracks [53]. Notably, one may investigate the self-healing mechanism in tooth enamel by performing a backcreep indentation test when the material endeavours to recover under minimum load after an unloading process over a time period.

2.7 Tooth whitening (bleaching)

Tooth whitening is a very popular procedure used by the public as well as by dental practitioners because of the aesthetics outcomes. The cosmetic improvement of tooth discoloration and the removal of various stains both increase self-esteem and confidence arising from having a “white bright smile”.

Although whitening procedures are more affordable and less destructive than restorative dental procedures, bleaching is not always guaranteed to be successful [145]. The efficiency of the whitening depends on the type, concentration and duration of application of the bleaching agent used [58]. The most common bleaching agents are hydrogen peroxide (HP) or carbamide peroxide (CP). CP, which is also called urea peroxide or urea hydrogen peroxide, is a compound product of urea ($\approx 64\%$) and hydrogen peroxide ($\approx 36\%$) [146]. Although the detailed mechanism of bleaching agents within the tooth structure remains elusive, it is understood that these agents act as oxidisers. They react with the organic matter within the tooth [147, 148] and they bleach extrinsic, intrinsic or internalised stains located within dental tissue through degradation of the organic compounds and oxidation of chromophores [57, 58, 149]. The extrinsic stains are of metallic (e. g., from intake of iron supplement tablets) or non-metallic origin (e. g., from intake of coffee, tea etc.) deposited on the surface of enamel, whereby intrinsic discolorations occur as a result of a change in the composition

or structure of dental hard tissue caused by, for instance dental fluorosis, tetracycline intake or ageing. On the other hand, the internalised stains originate from developmental effects (e. g., hypo- and hyper-mineralisation) and acquired effects (e. g., dental caries, some types of dental materials used in restorative treatment) [149]. While most extrinsic stains can be partially or completely removed mechanically (e. g., with whitening toothpastes), the intrinsic and internalised stains require chemical treatments. In general, the whitening treatments can be applied internally in root-filled teeth or externally on teeth with clinically normal pulps.

There are three main techniques for external whitening of teeth [145, 146, 150, 151]:

- a) dentist or dental personnel administered bleaching technique (also known as “in-office bleaching”, “power bleaching”, “in-surgery bleaching”, or “in-chair bleaching”),
- b) dentist-supervised, patient-administered nightguard bleaching technique (also known as “take-home bleaching”, or “at-home bleaching”), and
- c) patient-administered at home bleaching products sold over-the-counter (also known as “OTC” bleaching products).

The “in-office” bleaching treatment is a one-off procedure that uses bleaching agents for a shorter period of time (under 60 min). HP and CP are used with the following concentrations [146]: 25 % HP without a heat source, 35 % HP with or without a heat source, 35 % HP with a curing light, 70 % HP with a heat source and 35 % CP without a heat source. Depending on the level of HP concentration, the “at-home” bleaching treatment is a 2 to 6 week procedure. The HP concentrations vary from 1.5 % up to 10 %. The “OTC” whitening products include teeth whitening strips, mouthwashes, chewing gums and toothpastes. Because of their low concentrations of HP (less than 6 %) [58], these products

yield improved tooth whiteness over a longer period of time [152, 153]. However, their effects can be unpredictable and potentially dangerous [146].

Beside local adverse effects such as tooth cervical root resorption [154], non-reversible pulp damage [155], hypersensitivity and gingival irritation [156], the excessive usage of a high concentration of HP over longer periods of time may result in potential health hazards [57] such as genotoxicity, cytotoxicity and carcinogenicity [57, 157]. Furthermore, some investigators have indicated deleterious effects on mechanical properties of enamel and dentine [158-160], and restorative dental materials [56, 161] as well as tissue/material interfaces [162, 163]. Other adverse effects of whitening treatments include: alterations of the enamel surface and its inner structure [164, 165], increased porosity [166], a decreased Ca/P ratio [167, 168], denaturation of proteins [164, 169], a decreased fracture toughness [169], an increased surface roughness [170, 171] and an increase of mercury release from dental amalgam have been reported. On the contrary, other studies have claimed either no significant changes in surface morphology [172-174], chemical composition [173, 174], hardness [174, 175], surface roughness [176] or improvement in the enamel susceptibility to erosion [177].

It is clear that some of the studies investigating the whitening effects on dental hard tissues are conflicting, which may be attributable to differences in preparation methods, tooth samples, different bleaching agents (CP or HP) and their concentration and time of application, different testing methods (nanoscale vs. microscale testing), testing environment (dry vs. wet) or storage conditions (distilled water, artificial saliva, human saliva or no solution) [57, 58, 159, 173].

Although conclusions on dental hard tissue whitening treatments remain elusive, it is suggested that the degradation of enamel is more likely due to the alteration of the organic matter within the enamel microstructure under the chemical action of bleaching agents [164, 169]. Hegedüs et al. hypothesised that bleaching agents change the structural integrity of proteins, namely enamelin and

amelogenin [164]. HP, as the main bleaching agent or as one of the compounds of CP, oxidises organic components and chromophores in enamel. The second compound of CP is urea. Urea, also present in saliva, is a compound of carbon dioxide and ammonia [178, 179]. It has been reported earlier that urea has the capability to attack inter-prismatic regions inside enamel by destroying hydrogen bonds between carbon oxide and ammonia groups [164, 180-182]. Another study demonstrated increased porosity and an increased number of pits in the enamel surface which was exposed to urea for a week [181]. This is in agreement with the study by Goldberg et al., which identified tiny micro-channels in enamel after urea treatment [182]. Additionally, Arends et al. claimed that urea weakened or destroyed part of the peptide structure in the inter-prismatic region of enamel and that its interaction yielded protein removal [180]. However, the organic removal would have catastrophic effects on the mechanical responses of tooth enamel under applied loads. As discussed previously (Section 2.6), the organic matter plays a very important role in regulating the deformation mechanism of tooth enamel due to the ability of proteins to prevent catastrophic crack propagation within the enamel microstructure. Therefore, the potential organic removal during bleaching treatments would result in irreversible damage to the tooth. Enamel capability of self-healing and recovering during whitening treatment may be also hindered as a result of the tooth whitening process.

To the best of our knowledge, variables dictating the deformation mechanism of tooth enamel during whitening treatments have not been investigated. However, nanoindentation creep–recovery tests may provide new insights into self-healing and the recovery ability of unbleached (i.e., healthy) and bleached enamel, and they may help to determine variables controlling the mechanical responses of tooth enamel during whitening treatments.

2.8 Mechanistic models

2.8.1 Numerical models

Beside nanoindentation measurements, the biomechanical roles of tooth enamel can be explored with the use of finite element models (FEM). FEM can validate or disprove a hypothesis and theoretical assumption in conjunction with experimental results obtained from nanoindentation tests. In general, FEM simulate tooth function by dividing a virtual volume into a large number of cells and then applying virtual forces onto the surface. Distributions of ensuing stress are tracked by numerical iteration.

In previous studies investigating the deformation behaviour of tooth enamel, FEM were used to:

- predict deformation behaviour of tooth enamel at different levels of hierarchy under different loads [49, 107, 112],
- determine hoop stresses for axisymmetric, frictionless loading within the tooth crown and quantify initiation and evaluation of margin failure processes of cracks under critical loads within enamel [183-186], and
- investigate stress-strain behaviour of tooth enamel over its entire thickness [50].

A three-dimensional study by Spears [112] suggested that stresses remain confined to the region below the loaded area if the E value of tooth enamel is directionally-dependent at the crystalline and the microstructural level. For the crystalline level, Spears adopted the model from Katz [187] for a simple composite that illustrates enamel anisotropic behaviour (**Figure 2-8**).

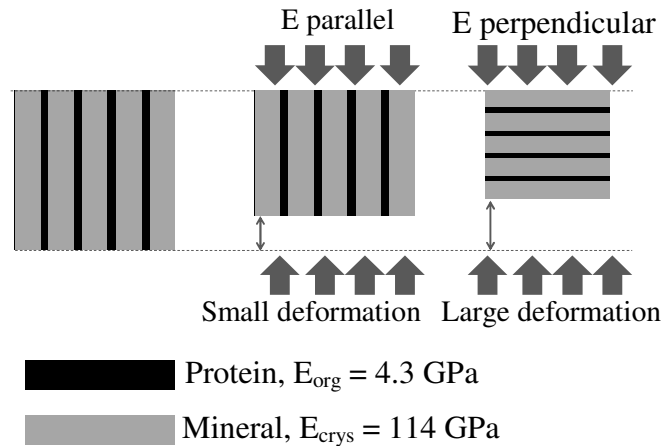


Figure 2-8. Deformation of tooth enamel at a crystalline level. E_{org} and E_{crys} denote Young's modulus of protein and mineral crystal, respectively. Adopted from [112].

In addition, by employing the model used by Ashby and Jones [188], the theoretical stiffness of the composite in a direction parallel (E_{para}) and perpendicular (E_{perp}) to the direction of crystal orientation was determined as $E_{\text{para}} = V_{\text{crys}}E_{\text{crys}} + (1-V_{\text{crys}})E_{\text{org}}$ and $E_{\text{perp}} = 1/[(V_{\text{crys}}/E_{\text{crys}}) + ((1-V_{\text{crys}})/E_{\text{org}})]$, where V_{crys} denotes the proportion of total enamel volume occupied by crystals, which is also known as volumetric fraction. For the crystalline level, Spears proposed to model enamel as a simple composite (based on the Katz's model) with the following prerequisites: 1) homogenous crystal orientation, and 2) V_{crys} between 0.81 and 0.99 [189], $E_{\text{crys}} = 114 \text{ GPa}$ and $E_{\text{org}} = 4.3 \text{ GPa}$ [112]. For the microstructural level, Spears modelled enamel as a hierarchical composite with anisotropic behaviour. For the modelling tooth enamel at the microstructural level, Spears used a cubic grid with 256 equally-spaced nodes and the Gantt model to reproduce the anisotropic behaviour of tooth enamel [112]. By assigning a Poisson's ratio of 0.3 to all elements in the rod, Spears was able to calculate the theoretical E value for each direction. Spears showed that enamel behaved anisotropically with respect to its stiffness. However, the shortcomings of this model were:

- assuming V_{crys} in a limited range and constant value for Poisson's ratio in all planes, and
- using ideal values of horizontal ($E_x = 20$ GPa) and vertical ($E_y = 30$ GPa) across-prism stiffness by omitting rod orientations in enamel.

In 2005, seven FEM were investigated by Shimizu et al. and modifications were made, resulting in the following advantages [107]:

- representing the geometry of the keyhole-shaped rod by reducing the number of elements to 14 (**Figure 2-9(a-d)**),

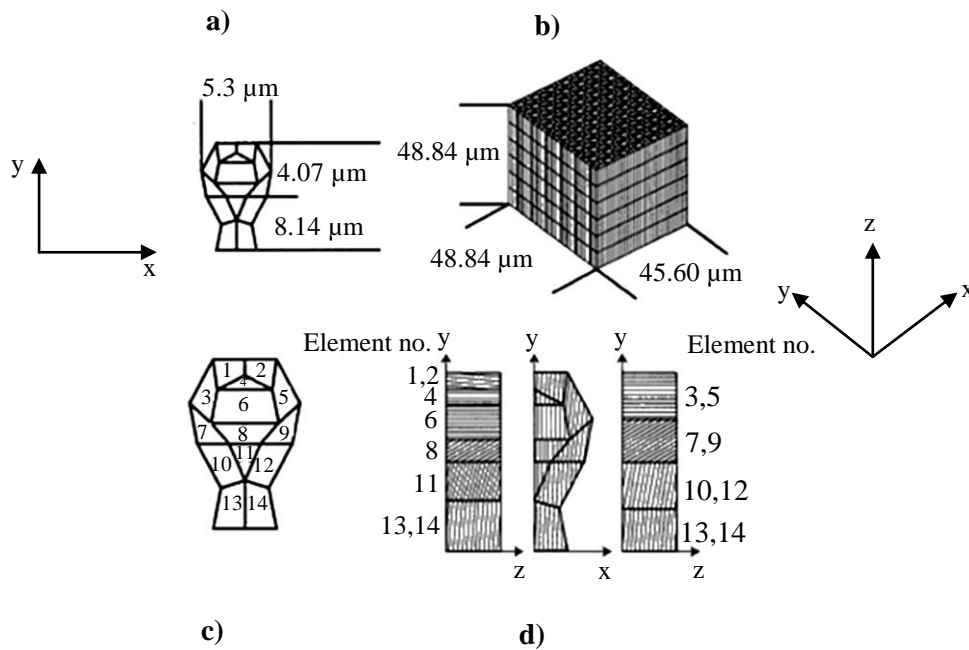


Figure 2-9. Finite element model of enamel. (a) Dimensions of prisms and elements, (b) entire enamel block, (c) 14 elements from the front view and (d) differences in crystal orientation. Adopted from [107].

- optimising time processing,

- investigating different orientations of rods in relation to the enamel wear, and
- assuming $E_z = 103 \text{ GPa}$ and $E_x = 32.1 \text{ GPa}$ (E values in two directions), $V_{\text{crys}} = 0.9$, $G_{yz} = 31 \text{ GPa}$ (shear modulus) and $\nu_{zx} = 0.313$ and $\nu_{xy} = 0.177$ (Poisson's ratios in two planes).

From the theoretical findings presented in the study by Shimizu et al., it could be inferred that the rod orientations affect the mechanical properties of tooth enamel. Although FEM are only based on theoretical assumptions, the latter results were found to be in accordance with anatomical and archaeological evidence.

Furthermore, FEM have been used for investigating deformation responses of intact teeth. Barak et al. used micro-CT scans to generate three dimensional FEM of human premolars for investigating deformation responses and stiffness of teeth before and after the initiation of defects [49]. By introducing a small cavity in the tooth, less than 10 % decrease of the relative tooth stiffness was observed. On the other hand, when the tooth was restored with composite resin, 98 % to 99 % of the tooth stiffness was recovered. With FEM, Barak et al. showed that a repaired tooth has lower fracture resistance against applied loads than an intact tooth. This study also demonstrated that restorative composite resin could not fully recover the tooth to its original state. However, despite a decreasing stiffness in the enamel cap due to the presence of a small cavity, enamel was still fully capable of resisting applied loads. This study provided clear evidence that the remarkable deformation resistance of the tooth stems from the shape of the tooth crown and morphology of the enamel cap. The authors concluded that while the enamel cap (i.e., the crown) protects dentine from accumulated detrimental strain concentrations, it also precisely controls tooth deformation resistance against applied loads [49].

Notably, dental crowns showed the ability to control the cracking mechanisms during masticatory function [183, 184]. A complete understanding of cracking modes within the dental crown when subjected to axial and off-axial loading is critical in the overall understanding of the deformation mechanism of teeth before they fracture. Although this topic has not been thoroughly investigated in this research, one should acquire knowledge of fracture modes to correctly interpret and therefore understand the overall deformation responses of tooth enamel under applied loads when they are simulated with FEM.

In 2007, Qasim et al. experimentally and numerically investigated margin crack mechanisms in strictly axial loaded brittle dome structures made of hemispherical glass shells filled with polymer resin [183]. To determine the initiation of crack propagation *in situ*, the dome structure representing a dental crown was subjected to a load of 2000 N with disk indenters of various compliances and was observed with a video camera. Later, the dome-like FEM were used to calculate hoop stress distributions within the structure and to validate experimental results. The experimental and numerical results showed that the behaviour of crack propagation was strongly dependent on the indenter that simulated chewing with food. The study showed that a protective mechanism of the tooth against catastrophic fracture under loads initiated with more compliant indenters representing a food bolus was to move the maximum tensile stresses away from the near contact area of the dome structure. Later, Ford et al. used FEM to validate the cracking mechanism of the dome structure when subjected to off-axial loading at 45 degrees to the axis of the dome [184]. The authors reported that dental crowns subjected to off-axial loading were more prone to fracture under low load due to increased deleterious tensile stresses in the dome side walls. In 2009, Chai et al. extended the FEM used previously by Qasim et al. and Ford et al. and reported another protective deformation mechanism of the tooth before its fracture [185]. By introducing loads between 250 and 600 N with a Teflon indenter representing food bolus of 0.48 GPa, the authors observed that cracks initiated first at the cervical margin of the tooth,

which longitudinally grew towards the occlusal surface with increasing loads. Although the FEM was simplified and did not include all of the variable elements in the calculation of stress dissipations in terms of the enamel shape, thickness etc., the model closely determined the fracture process within the dental tissues as an additional protective mechanism to survive a wide range of loads during masticatory function. The FEM proposed by Chai et al. [185] was later extended by Barani et al. [186], who used a three-dimensional FEM that included the dimensional and property characteristics of the tooth. Thickness, shape, and toughness, as well as crack propagation, have been identified as variables dictating fracture mechanisms within tooth tissue. Additionally, with the use of a combined nanoindentation and numerical approach, An et al. [50] identified a gradient in the mechanical properties as another variable having an effect on the fracture resistance of the tooth tissue.

The importance of a properties gradient in biological mineralised materials has been also highlighted by Bruet et al., who investigated dermal scales of armoured fish with the use of multi-layered FEM simulations [190]. The armoured fish scales are biocomposite materials made of mineral and protein with a quad-layered, interlocking structure. The first two outer layers of fish scales are ganoine and dentine, with E and H values ranging from 62 to 17 GPa and 4.5 to 0.54 GPa, respectively. Interestingly, the mechanical properties as well as gradients within each layer are similar to those of enamel and dentine in human teeth. The FEM showed that each layer of a fish scale exhibited its own unique deformation and fracture mechanism to maximise its survival. The knowledge of mechanical principles of fish scales structures and their gradients may provide a new, yet inspiring, approach to understanding composition–structure-property relationships within dental tissues.

To the best of our knowledge, a link between structural variables of tooth enamel (e. g., the effective crystal orientation angle and properties of proteins) within tooth enamel under applied loads in its elastic-plastic regions and

increasing indentation depths has not been investigated. Given the importance of gradient in properties and the structure-load adaptation of biological materials, FEM may prove/disprove variables that govern the mechanical responses of dental tissues.

2.8.2 Analytical models

Gradual changes of mechanical properties over the enamel thickness are well accepted and are related to the change of chemical composition and microstructure [54, 113].

These changes have been shown to be related to enamel microstructure, and more specifically to the effective crystal orientation angle of tooth enamel, θ , as illustrated in **Figure 2-10** [6, 38, 105]. The analytical model of human tooth enamel under applied load in its elastic and plastic region has been proposed by Xie et al. [105]. This model predicts the effective crystal orientation angle as the one of the critical variables influencing the deformation behaviour of tooth enamel regardless of loading direction.

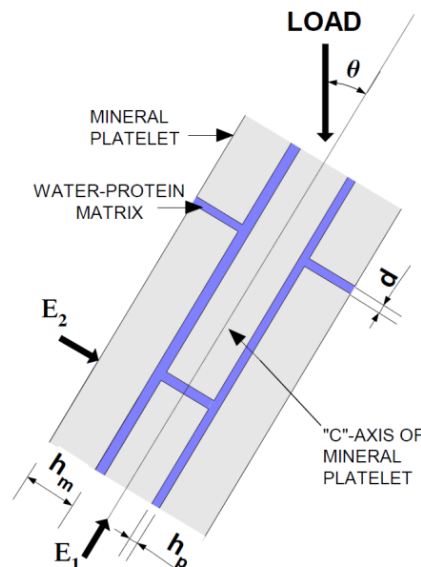


Figure 2-10. Deformation model of tooth enamel with schematic illustration of representative variables used for theoretical modelling of mineral crystal orientation angle, θ [7].

For the elastic behaviour of tooth enamel, the angle θ is derived from the modified mechanical model for wood tissues [191]. By considering enamel as a staggered mineral-protein composite [191, 192], Xie et al. proposed the elastic stress-strain behaviour of tooth enamel under compressive loads as [105]:

$$\sigma = E_e \varepsilon, \quad (2-1)$$

where σ , E_e and ε denote stress, elastic stiffness and strain of tooth enamel.

According to this model, the stiffness of enamel before the yield point, E_e , is defined as:

$$E_e = \frac{(\cos^2\theta - \sin^2\theta)^2}{\sin^4\theta} E_2 + 4 \frac{\cos^2\theta}{\sin^2\theta} G, \quad (2-2)$$

where θ is the angle between the mineral crystal and loading direction, E_2 the compression modulus of staggered, mineral-protein composite perpendicular to the c axis of the mineral crystal and G the shear modulus of staggered, mineral-protein composite.

According to a study by Liu et al. [193], the transverse stiffness of a staggered composite structure, E_2 , and the shear modulus of a staggered composite, G , are expressed as:

$$E_2 = \frac{1}{\frac{12K_p h_p (h_m + h_p)}{\alpha l^2 G_p (4G_p + 3K_p)} + \frac{1}{E_z}}, \quad (2-3)$$

$$G \approx \frac{h_p + h_m}{h_p} G_p, \quad (2-4)$$

where h_m and l are the thickness and the length of the mineral crystal, h_p and G_p the thickness and the shear modulus of protein layers between mineral platelets, α the non-uniformed shear strain factor of the composite, E_z the modulus of a

sandwich composite perpendicular to c axis of mineral platelet and K_p the bulk modulus of proteins.

The shear modulus of protein, G_p , the factor, α , the modulus of a sandwich composite perpendicular to c axis of mineral platelet, E_z , and the bulk modulus of protein, K_p , are determined as:

$$G_p = \frac{E_p}{2(1 + \nu_p)}, \quad (2-5)$$

$$\alpha = \left\{ 1 + \frac{4}{3} \left(\frac{(h_p + h_m)l}{h_p(l + d)} \right)^2 \right\} \left(\frac{l - d}{l + d} \right), \quad (2-6)$$

$$E_z = \frac{1}{\left(\frac{3h_p}{(h_p + h_m)(4G_p + 3K_p)} + \frac{1}{E_m} \frac{3K_p}{(4G_p + 3K_p)} \frac{(h_m^2 + 4\nu_m h_m h_p + 2h_p^2 - 2\nu_m h_p^2)}{h_m(h_p + h_m)} \right)}, \quad (2-7)$$

$$K_p = \frac{E_p}{3(1 - 2\nu_p)}, \quad (2-8)$$

Notably, the properties of proteins are important variables in the estimation of enamel stiffness perpendicular to the c-axis of mineral platelet (Eq. (2-3)) [105].

The stress-strain behaviour of tooth enamel beyond the yield point is defined as [105]:

$$\sigma = \left(\frac{(\cos^2 \theta - \sin^2 \theta)^2}{\sin^4 \theta} E_z \right) \cdot \varepsilon + 2 \frac{\cos \theta}{\sin \theta} \tau_c, \quad (2-9)$$

where the parenthesis in Eq. (2-9) indicates the elastic region of tooth enamel while remaining $2 \frac{\cos \theta}{\sin \theta} \tau_c$ represents the plastic region, ε is the compressive strain of enamel and τ_c denotes the shear strain of proteins in enamel and can be

predicted as a percentage of the E_2 value [105]. By employing the analytical model for investigating variables regulating the deformation behaviour of tooth enamel, Xie et al. reported the angle $\theta = 33^\circ$ for healthy enamel [105] and they concluded that the deformation behaviour of tooth enamel is affected by the thickness and properties of proteins. A latter study by Xie et al. suggested that enamel behaves rather isotropically at the nanoscale level [6]. This study showed that the angle θ of tooth enamel in its elastic-plastic region ranges between 33° and 34° and is independent to applied loads.

3. Theory of nanoindentation

Conventional tests, such as compressive, tensile, bending, shear strength and punch shear tests, have been used to investigate macroscale mechanical responses of bulk, biological materials such as teeth [48, 194]. At the microscale, properties of human teeth have also been very often explored by conventional indentation tests using Vickers or Knoop indenters in which optical measurements of residual indentation imprints were critical for determining the properties of materials [50, 109, 159, 175, 195-197].

However, these conventional tests have disadvantages. They do not measure submicron scale properties of materials, which is of importance for acquiring local properties of non-homogenous anisotropic structures such as human teeth [48, 198]. The nanoindentation instrument is an excellent tool for this purpose [24].

In general, Berkovich and spherical indenters are used to measure Young's modulus, E , and hardness, H , of human tooth enamel with indentation instruments [18, 27, 36, 105, 118, 129, 199, 200]. Depending on the type of indenter, the applied load and the enamel area of testing, the size of imprints can typically range from 5 to 20 μm . Notably, there are some other studies, in which authors used loads of 3, 5 and 10 mN to achieve residual imprints less than 1 μm [3, 201]. The accurate optical measurements of these imprints which are needed for determining the properties of a material are expected to be difficult and more likely inaccurate [202]. Therefore, in the nanoindentation instruments the contact area is not determined by direct measurements of imprints but by recording load as a function of indentation depth (**Figure 3-1**).

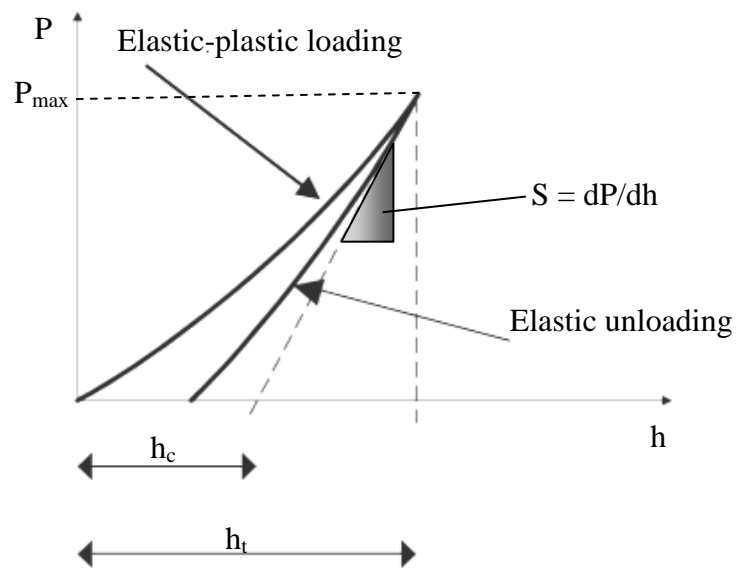


Figure 3-1. A schematic representation of load, P , versus displacement, h , obtained from nanoindentation experiments. The quantities shown are the maximum indentation load, P_{\max} , the contact depth after unloading, h_c , the contact stiffness during unloading, dP/dh . The h_c , and dP/dh determine Young's modulus and hardness of material. Modified from [203].

The maximum depth of penetration for a particular load, P , and the slope of the unloading curve yield E and H measurements of the specimen [117]. The unloading curve is assumed to be purely elastic with no occurrences of plastic deformations after load removal [117, 133].

Notably, measurements of material properties with a nanoindenter depend significantly on accurate measurements of the maximum load, P_{\max} , total displacement, h_t , at the P_{\max} , as well as the contact stiffness, S , during elastic unloading [139]. This indirect measurement of the contact area at the P_{\max} and the depth of penetration, h , are often generalised as a depth-sensing indentation technique (DSI) [204].

3.1.1 Projected area of contact, A_c

- *Berkovich indenter*

The projected contact area, A_c , at the P_{\max} for a Berkovich indenter is expressed as (**Figure 3-2(a)**):

$$A_c = \frac{a \cdot L}{2}, \quad (3-1)$$

where a and L represent the side and the length of the projected equilateral triangle, respectively.

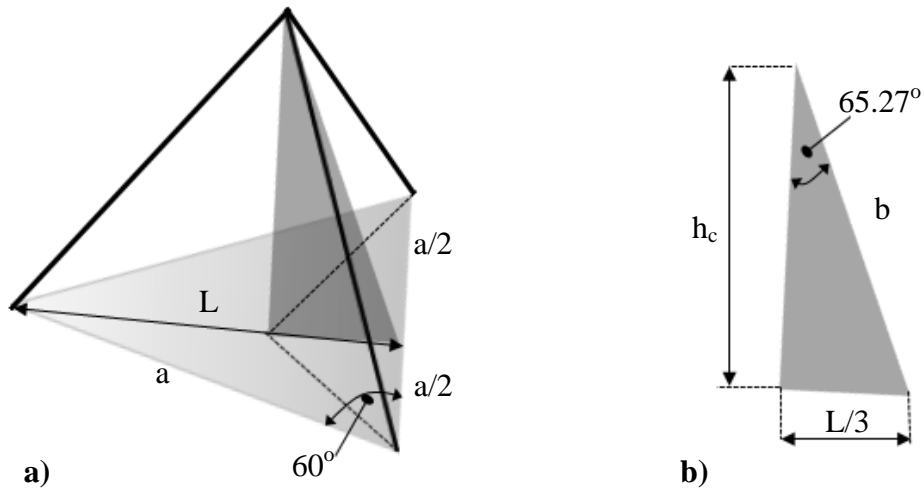


Figure 3-2. (a) A schematic representation of a Berkovich indenter with the projected area, A_c . The 65.27° semi-angle in (b), which represents the face angle with the central axis of the indenter, is used to calculate the A_c . The height of the dark-shaded triangle denotes the contact depth of penetration, h_c .

The L of the projected triangle in **Figure 3-2(a)**, and the hypotenuse, b , of a shaded triangle in **Figure 3-2(b)** are given by:

$$L = \frac{a}{2} \cdot \tan 60^\circ, \quad (3-2)$$

$$b = \frac{L/3}{\sin 65.27^\circ}. \quad (3-3)$$

Therefore, the contact indentation depth, h_c , of the Berkovich indenter is given by **(Figure 3-3)**:

$$h_c = b \cdot \cos 65.27^\circ. \quad (3-4)$$

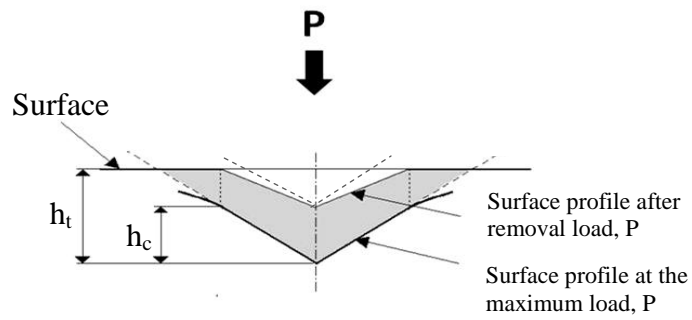


Figure 3-3. A Berkovich indenter at the full load and unload with indicated depth from the original specimen surface, h_t , at the maximum load, P_{\max} , and the contact depth, h_c , after unloading, respectively. Adopted from [25, 133, 138].

Substituting equations (3-2) and (3-3) into (3-4) gives:

$$h_c = \frac{a}{2 \tan 60^\circ \tan 65.27^\circ}. \quad (3-5)$$

From equation (3-5), the a of the projected equilateral triangle is:

$$a = 2 \tan 60^\circ \tan 65.27^\circ h_c. \quad (3-6)$$

The A_c at the P_{\max} for a Berkovich indenter is determined from the substitution of equation (3-6) with equation (3-1):

$$A_c = 3\sqrt{3} h_c^2 (\tan 65.27^\circ)^2 = 24.5 h_c^2. \quad (3-7)$$

- *Spherical indenter*

The A_c at the h_c of a spherical indenter is expressed as (**Figure 3-4**):

$$A_c = \pi a_c^2, \quad (3-8)$$

where a_c denote the radius of the indenter at the h_c .

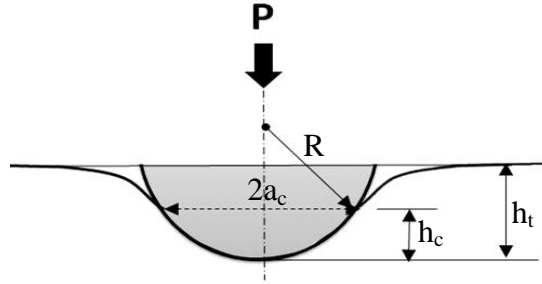


Figure 3-4. A schematic representation of the elastic indentation with a spherical indenter at full load, P at the indentation depth, h_t . R and $2a_c$ denote the nominal radius and the contact diameter of the indenter at the contact indentation depth, h_c , respectively. Adopted from [25, 133, 138].

From the known geometry of the spherical indenter under the P it is easy to see that:

$$(R - h_c)^2 = R^2 - a_c^2. \quad (3-9)$$

By rewriting equation (3-9) as:

$$R^2 - 2Rh_c + h_c^2 = R^2 - a_c^2, \quad (3-10)$$

the a_c can be expressed as:

$$a_c = \sqrt{2Rh_c - h_c^2}. \quad (3-11)$$

By substituting equation (3-11) into (3-8) and assuming $h_c^2 \ll 0$ when $h \ll R$, the A_c for the spherical indenter is given by:

$$A_c = 2\pi Rh_c. \quad (3-12)$$

3.1.2 Young's modulus

In nanoindentation instruments, E of a specimen is derived from the reduced modulus, E^* . Valid for any axisymmetric indenter, the value of E^* is determined from the slope of the unloading curve at P_{\max} as a function of the $S = dP/dh$ and the A_c at the h_c [139, 205, 206]:

$$E^* = \frac{1}{2} \left(\frac{dP}{dh} \right) \frac{\sqrt{\pi}}{\sqrt{A_c}} \frac{1}{\beta}. \quad (3-13)$$

In the equation (3-13), the geometry correction factor, β , is equal to 1.034 and 1.0 for a Berkovich and spherical indenter, respectively [117, 207].

The E^* combines E and Poisson's ratio, ν of the indenter (subscript i) and the specimen (subscript s), respectively:

$$\frac{1}{E^*} = \frac{1}{E_s'} + \frac{1}{E_i'}, \quad (3-14)$$

$$E' = \frac{E}{1 - \nu^2}. \quad (3-15)$$

With known values of E and ν for diamond tip indenter of 1050 GPa and 0.07, respectively, along with a reported value of ν for tooth enamel of 0.25, the E value of a specimen can be calculated from equation (3-14) [112, 193].

Notably, the A_c for the Berkovich and spherical indenters has been defined previously by equations (3-7) and (3-12).

- *Berkovich indenter*

The E^* for the Berkovich indenter is expressed as:

$$E^* = \frac{1}{2} \frac{dP}{dh} \frac{1}{h_c} \sqrt{\frac{\pi}{24.5}} \left(\frac{1}{1.034} \right). \quad (3-16)$$

- *Spherical indenter*

For the spherical indenter, the E^* value is derived as:

$$E^* = \frac{1}{2} \frac{dP}{dh} \sqrt{\frac{\pi}{A_c}} \left(\frac{1}{1.00} \right). \quad (3-17)$$

Substituting (3-8) into (3-17) or (3-12) into (3-17), the E^* is also given as:

$$E^* = \frac{1}{2a} \frac{dP}{dh}, \quad (3-18)$$

$$E^* = \frac{1}{2} \frac{dP}{dh} \frac{1}{\sqrt{2Rh_c}}. \quad (3-19)$$

3.1.3 Hardness

The H value is known as the indentation hardness or the mean pressure, p_m . In a nanoindenter test, the H is calculated as:

$$H = p_m = \frac{P}{A_c}, \quad (3-20)$$

where A_c is $24.5h_c^2$ and $2\pi Rh_c$ for the Berkovich and spherical indenters, respectively (Equations (3-7) and (3-12)).

3.1.4 Stress–strain relationship

As discussed in Section 2.6.2, the elastic–plastic deformation behaviour of a specimen can be analysed from the stress-strain curves with a spherical indenter whose strain varies with indentation load [117].

For a spherical indenter, the mean contact pressure, p_m , is expressed from equations (3-8) and (3-20) as:

$$p_m = \frac{P}{\pi a_c^2}. \quad (3-21)$$

The Hertzian equation in the elastic region for the a_c at the h_c is given by:

$$a_c^3 = \frac{3 PR}{4 E^*}. \quad (3-22)$$

Substituting equation (3-21) into (3-22) gives a relationship between p_m (stress) and a/R (strain):

$$p_m = \left(\frac{4E^*}{3\pi} \right) \frac{a_c}{R}. \quad (3-23)$$

The a_c of the spherical indenter used in equation (3-23) is determined from equation (3-11) when $h_c^2 \ll 0$ as:

$$a_c = \sqrt{2Rh_c}. \quad (3-24)$$

Notably, the h_c must be determined for the calculation of the a_c . The h_c is assumed to be half of the h_t in the region of elastic deformation during initial loading [117]:

$$h_c = \frac{1}{2} h_t. \quad (3-25)$$

Equation (3-25) is valid for the specimen surface that is frictionless and in the elastic contact with the spherical indenter. The h_t is expressed as:

$$h_t = \frac{1 - \nu^2}{E} \frac{3}{2} p_m \frac{\pi}{4a_c} (2a_c^2 - r^2), \quad (3-26)$$

where r denotes the semi-circle radius of the P, in which the stress is acting [208, 209]. The equation is valid when $r \leq a_c$. The value $\frac{1-\nu^2}{E}$ denotes the E^* .

Substituting (3-21) into (3-26), the h_t can be rewritten as [209]:

$$h_t = \frac{1}{E^*} \frac{3}{2} \frac{P}{4a_c} \left(2 - \frac{r^2}{a_c^2} \right), \quad (3-27)$$

Assuming $\frac{r^2}{a_c^2} \ll 1$ and substituting (3-22) into (3-27) gives:

$$h_t = \left(\frac{3P}{4E^*} \right)^{\frac{2}{3}} \left(\frac{1}{R} \right)^{\frac{1}{3}}, \quad (3-28)$$

where E^* is obtained from equation (3-14).

3.1.5 Creep – backcreep

3.1.5.1 Theory

The conventional nanoindentation tests provide values of E and H from load-displacement curves under a condition that enamel has no time-dependent behaviour under applied loads. However, recent studies have shown that enamel exhibits creep behaviour when loads are applied [16, 61, 62].

Creep can occur over a period of time under applied loads in the elastic or plastic region of a material and it can be quantitatively measured from indentation or uniaxial tests.

There are 4 potential mechanical responses that can be observed under applied loads within a material [117]:

- a) Elastic–plastic, where the material undergoes no time-dependent elastic deformation and no time-dependent plastic deformation,
- b) Viscoelastic–plastic, where the material undergoes time-dependent elastic deformation, but no time-dependent plastic deformation,
- c) Elastic–viscoplastic, where the material undergoes no time-dependent elastic deformation, but time-dependent plastic deformation, and
- d) Viscoelastic–viscoplastic, where the material undergoes time-dependent elastic deformation followed by time-dependent plastic deformation.

The creep properties of materials have been studied at the macro-scale with conventional uniaxial tests. For these kinds of tests, the specimen has to be of tens of millimetres in size to be able to fasten it at both ends for tensile testing. In the nanoindentation instruments, the specimen can be of a few millimetres size (i.e., less than 5 mm) and must be mounted flat to the nanoindentation stage for creep measurements. Although nanoindentation creep tests have the advantage of investigating creep responses of materials at the micron scale, tensile tests are different to compressive tests, i.e., the material may behave differently when subjected to the tensile or compressive loads. However, it has been shown that the nanoindenter, which uses compressive loads, provides to some extent information on the “elastic” and “viscous” properties of a material [117].

Although indentation instruments can also provide information on the indentation creep stress exponent, n , of a solid material, an important fact supported by the theoretical background should be noted. The value of n is derived from a power of law creep equation for a uniaxial test as [210]:

$$\dot{\epsilon}_u = A \cdot \sigma^n, \quad (3-29)$$

where $\dot{\epsilon}_u$ denotes the creep rate from the uniaxial test, A represents the material constant from the uni-axial test and σ denotes the uniaxial creep stress.

Based on the theory of Bower et al. [211], equation (3-29) can be generalised and rewritten in the form of:

$$\dot{\epsilon}_u = \left(\frac{\dot{\epsilon}_0}{\sigma_0^n} \right) \cdot \sigma^n, \quad (3-30)$$

where $\dot{\epsilon}_0$ and σ_0^n in the parentheses represent the material constant, A .

Substituting (3-20) into (3-29) and assuming B as the material constant obtained from the indentation tests gives:

$$\dot{\epsilon}_i = B \cdot (p_m)^n, \quad (3-31)$$

or alternatively:

$$\dot{\epsilon}_i = B \cdot (H)^n, \quad (3-32)$$

where $\dot{\epsilon}_i$ is the indentation creep rate of the material from indentation test.

The indentation creep rate is defined as the ratio of indenter displacement velocity, \dot{h} , to the indentation depth, h :

$$\dot{\epsilon}_i = \frac{\dot{h}}{h}, \quad (3-33)$$

where \dot{h} is defined as:

$$\dot{h} = \frac{dh}{dt}. \quad (3-34)$$

The dh/dt ratio is easily calculated from the indentation time–depth ($t - h$) curve.

Assuming the same value of n for equations (3-29), (3-31) and (3-32), and by knowing the relationship between A and B , the value n can be calculated from P - h - t values obtained from the indentation experiment.

In addition to equation (3-30), Bower et al. defined a link between the A and B for a viscous linear material tested with a conical indenter [211]:

$$A = \frac{8c}{3\pi \tan \beta} B, \quad (3-35)$$

where β and c represent the semi-angle of a conical indenter and the pile-up/sink parameter, respectively. However, LaManna et al. showed that the A obtained from indentation tests measured with a conical indenter is 30 % less than if it is measured with a uniaxial test [210].

Based on the theory by Tabor [212], the representative strain rates for conical indenter, ϵ_c and spherical indenter, ϵ_s can be expressed by:

$$\epsilon_c = 0.2 \tan \beta, \quad (3-36)$$

$$\epsilon_s = 0.2 \frac{a_c}{R}, \quad (3-37)$$

where β represents the angle between the face of the conical indenter and indented surface of the specimen.

By substituting differentiated equations (3-36) or (3-37) with respect to time into (3-32) and expressing the p_m , which is also known as H , from equation (3-20), He & Swain showed [61] that the n and the B can be calculated from logarithmic H - $\dot{\epsilon}$ curves for both a Berkovich and spherical indenter.

The creep indentation theory assumes that the strain rate sensitivity exponent, n , of a flow stress in (3-29) is the same as the strain rate sensitivity exponent, n ,

of hardness in (3-32) and that the square root of the project area of the contact, A_c , required in the equation (3-13) increases proportionally with increasing indentation depth, h_t , which enables extraction of the strain rate sensitivity parameter from a depth-time curve [213]. With the use of FEM, Stone showed that both assumptions are unfortunately invalid, except for low H/E materials [213].

Because the theoretical relationship between the uniaxial creep and the indentation creep remains unjustified [210, 213], this research was only motivated to report fundamental creep-backcreep responses of unbleached and bleached enamel.

3.1.5.2 Modelling

The indentation (h-t) curves can be fitted into rheological models consisting of a series of springs and dashpots to obtain the viscoelastic components of a material. The simulated responses of springs and dashpots provide information about stiffness and viscosity of the material in terms of the storage modulus, E^* , and the loss modulus, η , respectively.

There are three different kinds of models that can be analysed by IBIS software in the nanoindentation instrument, UMIS Australia [214]: a) three element Voigt model, b) two element Maxwell model and c) four element Voigt-Maxwell model.

The general theory used for the calculation of viscoelastic variables in spring-dashpots models can be explained by a single two element Voigt model (**Figure 3-5**).

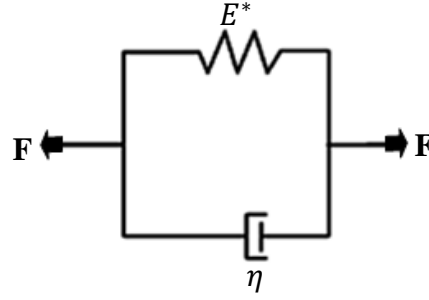


Figure 3-5. A single Voigt model. The model represents the viscoelastic creep behaviour of a material under tensile forces, F . A spring with the storage modulus, E^* , and a dashpot with the viscous component of a material, η , are connected in parallel to simulate the creep behaviour.

The spring force, F_1 , and dashpot force, F_2 , are given by:

$$F_1 = k \cdot x, \quad (3-38)$$

$$F_2 = c \cdot \frac{dx}{dt}, \quad (3-39)$$

where k and c represent the E^* of the spring and the η of the dashpot, respectively.

The equations (3-38) and (3-39) can be rewritten in the general form for the tensile stress of a spring, σ_1 , and a dashpot, σ_2 , as:

$$\sigma_1 = E^* \varepsilon, \quad (3-40)$$

$$\sigma_2 = \eta \frac{d\varepsilon}{dt}. \quad (3-41)$$

The total tensile stress under creep loading, σ , for time, $t > 0$, is:

$$\sigma = E^* \varepsilon + \eta \frac{d\varepsilon}{dt}. \quad (3-42)$$

Dividing both sides of the equation (3-42) by η and then multiplying it by $e^{\frac{E^*t}{\eta}}$, equation (3-42) becomes:

$$\left[e^{\frac{E^*t}{\eta}} \right] \cdot \frac{\sigma}{\eta} = \left[e^{\frac{E^*t}{\eta}} \right] \left(\frac{E^*\varepsilon}{\eta} + \frac{d\varepsilon}{dt} \right). \quad (3-43)$$

Integrating equation (3-43) according to the mathematical relationship $\int e^x dx = e^x + C$, where C is the constant, gives:

$$\frac{\sigma}{E^*} e^{\frac{E^*t}{\eta}} = \varepsilon \cdot e^{\frac{E^*t}{\eta}} + C. \quad (3-44)$$

For $t = 0$ and $\varepsilon = 0$, the constant C is expressed by:

$$C = \frac{\sigma}{E^*}. \quad (3-45)$$

The ε value can be calculated from equation (3-44) by substituting equation (3-45) into (3-44):

$$\varepsilon = \frac{\sigma}{E^*} \left(1 - e^{-\frac{E^*t}{\eta}} \right). \quad (3-46)$$

Hook's law is given by:

$$\sigma = E \cdot \varepsilon, \quad (3-47)$$

where σ , E and ε denote variables from tensile tests.

Dividing equation (3-47) by σ and E gives a general definition of the creep compliance, $J(t)$:

$$\frac{1}{E} = J(t) = \frac{\varepsilon}{\sigma}. \quad (3-48)$$

Equation (3-46) can be rewritten as:

$$\frac{1}{E} = J(t) = \frac{1}{E^*} \left(1 - e^{-\frac{E^*t}{\eta}} \right). \quad (3-49)$$

The equation (3-28) for a spherical indenter can be rearranged as:

$$h^{\frac{3}{2}} = \frac{3}{4} P \frac{1}{E^*} \left(\frac{1}{R} \right)^{\frac{1}{2}}. \quad (3-50)$$

Substituting equation (3-49) into equation (3-50) gives a t-h-P relationship (creep) of the material under load with a spherical indenter.

Similarly, the h_t for a Berkovich indenter is expressed from Sneddon's solution as [215]:

$$h_t^2 = \frac{\pi}{2} P \frac{1}{E^* \tan 70.3^\circ}. \quad (3-51)$$

Substituting equation (3-49) into equation (3-51) gives a t-h-P relationship (creep) of the material under load with the Berkovich indenter.

Notably, the E^* values in resulting creep equations represent only the E'_s values (refer to equation (3-14)).

- *J(t) of the three element Voigt model*

The total tensile force, F of the three element Voigt model is given by:

$$F = F_1 + F_2, \quad (3-52)$$

where F_1 represents a spring force with the storage modulus, E_1^* , that is in series with the force, F_2 , which denotes a parallel spring-dashpot elements with the storage modulus, E_2^* , and the viscosity, η_2 , respectively (**Figure 3-6**).

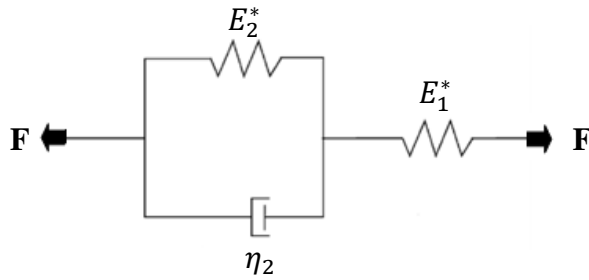


Figure 3-6. Three element Voigt model under tensile forces, F. The model illustrates the spring storage modulus, E_1^* and E_2^* , with the dashpot loss modulus, η_2 . Modified from [214].

The elements in series are subjected to the same force, whereas the parallel elements encounter the same incremental extension [216]. Therefore, equation (3-52) can be rewritten in terms of the total tensile stress acting on the system as:

$$\sigma = E_1^* \varepsilon + \left[E_2^* \varepsilon + \eta_2 \frac{d\varepsilon}{dt} \right]. \quad (3-53)$$

The combined system of viscous and non-viscous elements in series or parallel undergoes the same integration procedure as described previously for a single Voigt model.

The $J_1(t)$ of the spring with the E_1^* is:

$$J_1(t) = \frac{1}{E_1^*}. \quad (3-54)$$

The $J_2(t)$ of a parallel spring - dashpot element with the E_2^* and η_2 is given by:

$$J_2(t) = \frac{1}{E_2^*} \left(1 - e^{-\frac{E_2^* t}{\eta_2}} \right). \quad (3-55)$$

Summation of equations (3-54) and (3-55) gives the total $J(t)$ of the three element Voigt model in the form of:

$$J(t) = \frac{1}{E_1^*} + \frac{1}{E_2^*} \left(1 - e^{-\frac{E_2^* t}{\eta_2}} \right). \quad (3-56)$$

Substituting (3-56) in equations (3-50) and (3-51) gives a t-h-P relationship for a spherical and a Berkovich indenter, respectively:

$$h^{\frac{3}{2}} = \frac{3}{4} P \left[\frac{1}{E_1^*} + \frac{1}{E_2^*} \left(1 - e^{-\frac{E_2^* t}{\eta_2}} \right) \right] \left(\frac{1}{R} \right)^{\frac{1}{2}}, \quad (3-57)$$

$$h_t^2 = \frac{\pi}{2} P \left[\frac{1}{E_1^*} + \frac{1}{E_2^*} \left(1 - e^{-\frac{E_2^* t}{\eta_2}} \right) \right] \frac{1}{\tan 70.3^\circ}. \quad (3-58)$$

- *J(t) of the Maxwell model*

The total force, F, of the Maxwell model is:

$$F = F_1 + F_2, \quad (3-59)$$

where F_1 represents the force of a spring with the storage modulus, E_1^* , that is in series with force, F_2 , which denotes a dashpot element with viscosity, η (**Figure 3-7**).

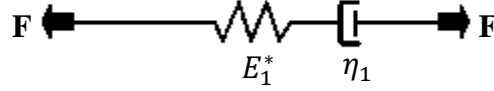


Figure 3-7. Maxwell model under tensile forces, F . The model illustrates the spring storage modulus, E_1^* , and the dashpot loss modulus, η_1 . Modified from [214].

Equation (3-59) can be rewritten in terms of the total tensile stress acting on the Maxwell system as:

$$\sigma = E_1^* \varepsilon + \left[\eta_1 \frac{d\varepsilon}{dt} \right], \quad (3-60)$$

where $\sigma_1 = E_1^* \varepsilon$ and $\sigma_2 = \eta_1 \frac{d\varepsilon}{dt}$.

The $J_1(t)$ of the spring with the storage modulus, E_1^* , is:

$$J_1(t) = \frac{1}{E_1^*}. \quad (3-61)$$

Dividing both sides of the σ_2 by η and integrating it, the $J_2(t)$ of a dashpot element is:

$$J_2(t) = \frac{1}{\eta_1} t. \quad (3-62)$$

Summation of equations (3-61) and (3-62) gives the total $J(t)$ of the Maxwell model:

$$J(t) = \frac{1}{E_1^*} + \frac{1}{\eta_1} t. \quad (3-63)$$

Substituting (3-63) in equations (3-50) and (3-51) gives a t-h-P relationship for a spherical and a Berkovich indenter, respectively:

$$h^{\frac{3}{2}} = \frac{3}{4} P \left[\frac{1}{E_1^*} + \frac{1}{\eta_1} t \right] \left(\frac{1}{R} \right)^{\frac{1}{2}}, \quad (3-64)$$

$$h_t^2 = \frac{\pi}{2} P \left[\frac{1}{E_1^*} + \frac{1}{\eta_1} t \right] \frac{1}{\tan 70.3^\circ}. \quad (3-65)$$

- *J(t) of the Maxwell-Voigt model*

The total J(t) of the Maxwell-Voigt model is obtained from the summation of equations (3-55) and (3-63) following the schematic representation given in **Figure 3-8**:

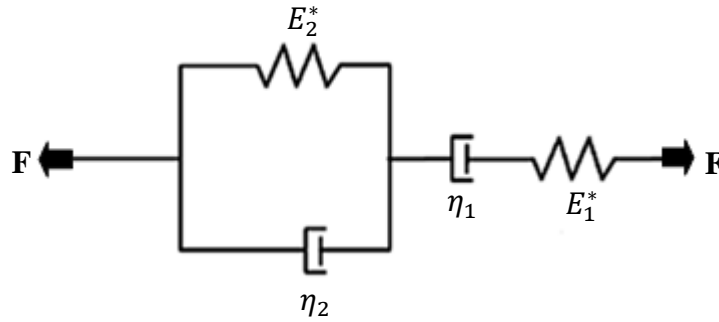


Figure 3-8. Maxwell-Voigt model. The storage moduli, E_1^* and E_2^* , denote springs in the model and represent the elastic responses of material. The loss moduli, η_1 and η_2 , are related to dashpots and determine the viscous responses of material. Modified from [214].

$$J(t) = \frac{1}{E_2^*} \left(1 - e^{\frac{-E_2^* t}{\eta_2}} \right) + \frac{1}{E_1^*} + \frac{1}{\eta_1} t. \quad (3-66)$$

Substituting (3-66) in equations (3-50) and (3-51) gives a t-h-P relationship for a spherical and Berkovich indenter, respectively:

$$h^{\frac{3}{2}} = \frac{3}{4} P \left[\frac{1}{E_2^*} \left(1 - e^{\frac{-E_2^* t}{\eta_2}} \right) + \frac{1}{E_1^*} + \frac{1}{\eta_1} t \right] \left(\frac{1}{R} \right)^{\frac{1}{2}}, \quad (3-67)$$

$$h_t^2 = \frac{\pi}{2} P \left[\frac{1}{E_2^*} \left(1 - e^{\frac{-E_2^* t}{\eta_2}} \right) + \frac{1}{E_1^*} + \frac{1}{\eta_1} t \right] \frac{1}{\tan 70.3^\circ}. \quad (3-68)$$

3.1.6 Calibration

During nanoindentation measurements, the actual geometry of a Berkovich or spherical indenter may be different to that of the ideal one. For instance, the change of the shape of the tip will inherently cause inaccuracy in the calculation of the A_c at the P_{\max} . As shown in equations (3-13) and (3-20), the A_c is a very important variable in the calculation of the E^* , and thus in the accurate estimation of E as well as H of a specimen.

In order to avoid incorrectness during tests due to any non-ideal shape of the indenters, the indenters must be calibrated against a standard calibration material. Fused silica, which has a constant E value, is often used for such calibration purposes. The aim of the calibration process is:

- to obtain a correction factor which represents a ratio between the actual projected area, A_c , and the ideal projected area, $A_{c,i}$, of the indenter at the h_c , and
- to apply the correction factor, $A_c/A_{c,i}$ in the calculation of E^* and H , respectively.

The $A_{c,i}$ of a Berkovich or spherical indenter is determined from equation (3-7) and (3-12), respectively, whereas the A_c is determined from the rewritten equation (3-13) as:

$$A_c = \frac{1}{4} \pi \left(\frac{dP}{dh} \frac{1}{E^*} \frac{1}{\beta} \right)^2, \quad (3-69)$$

where E^* is calculated directly from equation (3-14) for known values of E and ν for the diamond tip of the indenter, i.e., 1070 GPa and 0.07, respectively, along

with standard values of E and ν for fused silica, i.e., 72.5 GPa and 0.17, respectively [117].

Given the importance of the A_c value, the E^* and H of a specimen can be rewritten as:

$$E^* = \frac{1}{2} \left(\frac{dP}{dh} \right) \frac{\sqrt{\pi}}{\sqrt{A_c}} \frac{1}{\beta} \left(\frac{\sqrt{A_{c,i}}}{\sqrt{A_c}} \right), \quad (3-70)$$

$$H = \frac{P}{A_c} \left(\frac{A_{c,i}}{A_c} \right), \quad (3-71)$$

where $A_c/A_{c,i}$ denotes the correction factor.

4. Methodology

This chapter covers the laboratory protocols of the sample preparation methods, instruments and test settings used in this work. Besides standard materials and methods, a new method of tooth preparation, a new nanoindentation device allowing testing of human teeth in the wet environment, as well as a new approach to data analysis are given.

4.1 Sample preparation

4.1.1 Collection and storage

Ethical approval for human research was obtained from the Ethics Review Committee of Edith Cowan University with protocol number 4503. Healthy molars collected from private dental practices were extracted for orthodontic reasons and informed consent was obtained from the patients involved. Upon extraction, teeth were stored in Hanks' balanced salt solution (HBSS) (SIGMA - Aldrich Co., St. Louis, USA) with the addition of 0.02 % thymol crystals at 4 °C to prevent demineralisation and bacterial growth [22, 217]. Teeth were prepared and tested within less than four weeks from the extraction date.

4.1.2 New method

A new method of embedding was developed in order to maintain precise control over the tooth orientation and to conduct analyses of the teeth in their hydrated state. Epoxy resin and hardener (EpoFix, Struers A/C, Copenhagen, Denmark) were used at a ratio of 15 to 2 by volume to form 30 mm diameter by 10 mm high cylindrical blocks using plastic moulding cups (FixiForm, Struers). A ~15 mm diameter hole was drilled through the centreline of the block to form a hollow cylinder that was then partly filled at one end with aquatic putty (Selleys Knead-It Aqua, Selleys, Australia). This putty can polymerise in the presence of water and was chosen as a mounting medium to keep the tooth hydrated in

HBSS. The tooth was then inserted root first into the cylinder and pressed into the putty, leaving only the enamel occlusal surface exposed. The embedded tooth was placed back into HBSS with 0.02 % thymol crystals and stored at 4 °C for 60 minutes to ensure proper polymerisation of the putty. After an hour, the teeth were sectioned into two halves using a precision saw (Isomet 1000, Buehler Ltd., Lake Bluff, IL, USA) (**Figure 4-1(a,b)**).

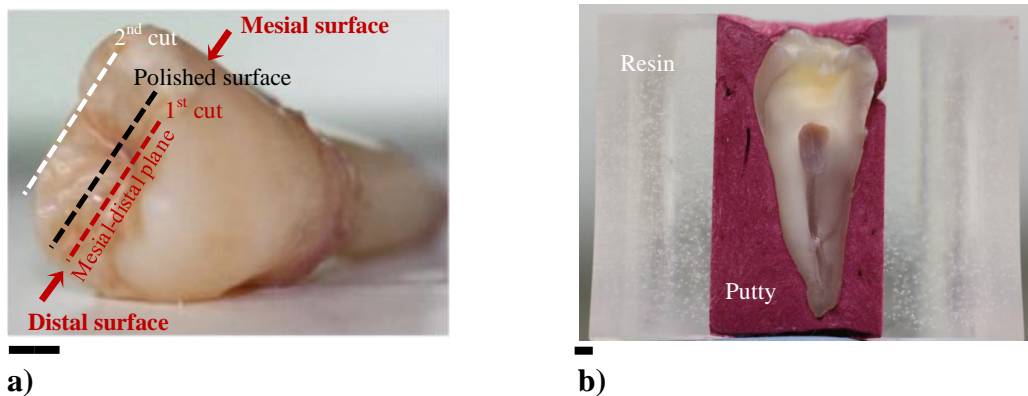
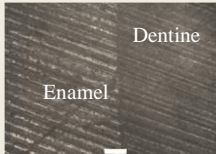
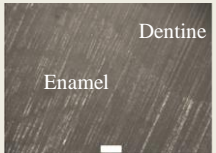
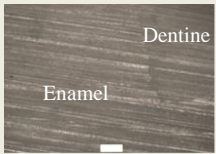


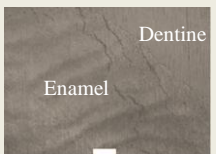


Figure 4-1. Preparation of the tooth specimen from a mandibular right third molar (M3) for nanoindentation tests. (a) Location of the first and second cuts in the tooth, relative to the mesial-distal plane. The polished surface is also indicated. Parallel black dashed lines show the approximate thickness of the sample. (b) Sectioned tooth embedded in the putty inside an epoxy cylinder. Specimens were kept hydrated to preserve their natural structure before indentation tests. Scale bar = 1 mm.

The cut surface was ground and polished following the key technical parameters given in **Table 4-1**. After each grinding and polishing step, the surface was examined under a light optical microscope (Trinocular Metallurgical Microscope, Brunel SP-200-XM, Brunel Microscopes Ltd, UK). A second cut, parallel to the first, was made at a distance of 5 mm from the polished surface. HBSS was used as a coolant during cutting. Once prepared, the specimen was immersed in HBSS with 0.02 % thymol crystals prior to nanoindentation tests. The enamel specimen was prepared in the hydrated environment within less than 2 hours.

Table 4-1. Technical parameters of the new method of tooth preparation.

Step	Consumables/Tools	Lubricant (Coolant)	Speed [rpm]	Time	Optical micrographs Scale bar = 100 μ m
Resin holder	15 ml resin 2 ml hardener	n/a	n/a	12 hrs	n/a
Blind hole	Φ 15mm twist drill bit	n/a	n/a	5 min	n/a
Embedding and curing	5-10 g putty	n/a	n/a	1 hr	n/a
1 st Cutting	Φ 152 mm diamond disk	HBSS	100	20 min	n/a
Grinding 1	SiC paper 320 (46 μ m)	Water	90	20 s	
Fine grinding	SiC paper 500 (30 μ m)	Water	90	20 s	
Polishing 1	SiC paper 1,200 (14 μ m)	Water	90	1 min	
Polishing 2	SiC paper 4,000 (5 μ m)	Water	90	1 min	
Final polishing	Nap cloth, MD NapR	Water	90	3 min	
2 nd Cutting	Φ 152 mm diamond disk	HBSS	100	20 min	

Optical micrographs of the enamel surface responses from severe damage after sectioning to defect-free surfaces after polishing are shown in **Table 4-1**.

During sectioning, uniformed, approximately 50 μm wide saw marks/grooves were produced in the enamel surface. High resolution scanning electron microscope images of the enamel resistance against severe damage can be also found in Appendix A.

Severe damage to the enamel surface was gradually removed during the grinding process, which involved suppressing the grinding grooves with successively finer grade silicon carbide papers. By applying 5 μm silicon carbide paper to the enamel surface, a matt ground surface of enamel with exposed interior microstructure was produced prior to final polishing. A defect-free surface of enamel was achieved with the synthetic napped cloth and water as the lubricant in the final process of polishing. The purpose of using water in this method was to avoid any chemically based lubricants which could affect mechanical properties of the tooth under investigation. Once prepared, the enamel surface was tested with a depth-sensing indentation system.

4.1.3 Conventional method, A

The intact human tooth sample was dried on the bench with tissue paper before resin embedding. A cold-curing epoxy resin mixture (EpoFix, Struers A/C, Copenhagen, Denmark) was poured into a plastic moulding cup (FixiForm, Struers) over the dried tooth specimen. Once the resin had cured, the tooth was sectioned following the protocol outlined above in Section 4.1.2, and then it was ground and polished following the procedure outlined in **Table 4-2**.

Notably, DiaPro Nap R and OP-U (Struers A/C, Copenhagen, Denmark) are mechanochemical polishing agents that were used during the final polishing process for good surface finish and they are part of the conventional protocol of the sample preparation. Specifically, DiaPro Nap R is a diamond polishing suspension while OP-U is a colloidal silica polishing suspension. These

suspensions have been developed by Struers A/C to reduce the time of preparation by 30 %, and at the same time improve the surface quality [218].

Table 4-2. Sample preparation of enamel embedded in epoxy resin.

Step	Consumables/Tools	Lubricant (Abrasive)	Speed [rpm]	Time
Resin embedding	15ml resin 2 ml hardener	n/a		12 hrs
1 st Cutting	Φ 152 mm diamond disk	HBSS	100	20min
Grinding 1	SiC paper 320 (46 µm)	Water	150	1min
Fine grinding	SiC paper 500 (30 µm)	Water	150	2min
Polishing 1	SiC paper 1,200 (14 µm)	Water	150	2min
Polishing 2	SiC paper 4,000 (5 µm)	Water	150	2min
Final polishing 1	Synthetic nap cloth, MD Nap	DiaPro Nap R	150	3 min
Final polishing 2	Porous neoprene cloth, MD Chem	OP-U	150	2 min
2 nd Cutting	Φ 152 mm diamond disk	HBSS	100	20min

4.1.4 Conventional method, B

The conventional method B was used to investigate the effect of resin embedding on the mechanical properties of the cut tooth surface. The intact human tooth sample was inserted with the root first into the resin cylinder hollow and pressed into the putty, leaving only the enamel occlusal surface exposed. The embedded tooth was placed back into HBSS with 0.02 % thymol crystals and stored at 4 °C for 60 minutes to ensure proper polymerisation of the putty. The tooth was sectioned in half with a precision saw (Isomet 1000, Buehler Ltd., Lake Bluff, IL, USA). One half of the tooth was dried on the bench with tissue and immediately embedded in cold-curing epoxy resin for 12 hours (EpoFix, Struers A/C, Copenhagen, Denmark). Once the resin had cured, the sample was

ground and polished following the key technical parameters outlined in **Table 4-2**.

Notably, the conventional method B differs from the new method by applying the resin embedding technique after cutting the tooth. This procedure was used to investigate how the surface properties may be affected by resin medium. To do so, the tooth was prepared by following the first four steps of the new method (refer to **Table 4-1**). The first four steps of the new method were required for the ease of handling the tooth during cutting.

4.1.5 Dehydration and drying procedure

Tooth samples were dehydrated and then dried following Janda's method [29]. In order to dehydrate the teeth, the specimens were submerged in water-ethanol mixtures with progressively increasing ethanol content of 70 %, 80 % and 96 % for 24 hr and 100 % for 72 hours; then, in water-acetone mixtures with increasing acetone content of 80% and 96% for 24 hours, and 100 % for 72 hours. Lastly, the specimens were dried in a vacuum desiccator for 2 hours.

4.1.6 Bleaching

Healthy human tooth samples were prepared by the new method (Section 4.1.2). Then, the specimens were submerged in HBSS leaving approximately 1 mm of polished surface above the solution level. The NiteWhite[®] ACP Turbo Take-Home Whitening Product (Discus Dental, LLC, CA, USA) in a 2.4 mL multi-dose syringe was applied on the tooth surface for a maximum period of 2 weeks following the recommended patient instructions for NiteWhite[®] ACP and DayWhite[®] ACP Take-Home Whitening Products. This whitening tooth gel, with 6 % hydrogen peroxide, was injected onto the fibre-free pad and placed gently on the exposed polished surface for 8 hours and stored at 4 °C in a fridge. After 8 hours, the tooth specimen was rinsed with HBSS and stored for 16 hours in HBSS at 4 °C in a fridge. This procedure was repeated every day for 14 days.

4.2 Structural analysis

4.2.1 Optical microscopy

The enamel surface responses, from severe damage after sectioning to defect-free surfaces after polishing during enamel preparation, were observed with a light optical microscope (Trinocular Metallurgical Microscope, Brunel SP-200-XM, Brunel Microscopes Ltd, UK).

4.2.2 Focused ion beam milling/Transmission electron microscopy

Ultra-thin sections of enamel, taken parallel to the direction of the rods, were prepared for transmission electron microscopy (TEM) using a dual-electron focused ion beam (FIB) workstation (Nova Nanolab 200, FEI Company, Hillsboro, OR, USA). The detailed procedure has been provided elsewhere [219]. Briefly, a layer of platinum ($\sim 1 \mu\text{m}$ in thickness) was first deposited to protect the surface area of interest from ion beam damage during the milling processes. A “rough” sectioning was then performed with a current of 10 nA, in which trenches were created on both sides of the platinum strip to obtain a cross-section of $\sim 3 \mu\text{m}$ in thickness. A number of “fine” mills were taken at reduced currents (from 5 to 1 nA) to thin the section to $\sim 1 \mu\text{m}$. Final mills were carried out at further reduced currents (from 300 to 100 pA) to decrease the thickness down to $\sim 100 \text{ nm}$ for electron transparency.

The transfer of the TEM specimen from the FIB sample holder to carbon coated copper TEM grids was conducted *ex-situ* using a high-precision micromanipulator (Kleindiek Nanotechnik GmbH, Reutlingen, Germany). TEM imaging was performed using a field emission gun-TEM (Philips CM200, Eindhoven, Netherlands).

4.2.3 Scanning electron microscopy

Tooth specimens were dehydrated and then dried following the protocol given in Section 4.1.5. The uncoated specimens were observed in a Zeiss 1555 environmental scanning electron microscope (SEM). Pressure between 9 and 10 Pa, high current beam signal, 120 μm apertures and 20 keV voltage were used for the variable pressure mode. The working distance was determined experimentally and was changed upon observation from 8 to 10 mm. Once aligned, secondary and backscattered electron images were obtained. The variable pressure mode has been used only for the observation of the enamel-dentine junction after diamond saw tooth sectioning. The images that show tooth enamel sections are attached to Appendix A. However, the variable pressure caused a lot of charging inside the SEM vacuum chamber during imaging and often resulted in blurry images.

In addition to the variable pressure, microscopic observation was conducted on coated specimens sputtered with a 3 nm layer of platinum. The alignments and focus were carried out with secondary electrons under accelerated voltage between 10 and 15 keV and 30 μm aperture. The working distance was set experimentally and was changed upon observation between 9 and 12 mm. Both secondary and backscattered images of the enamel surface have been collected.

4.3 Nanoindentation test settings

4.3.1 Testing instrument

A depth-sensing indentation system (Ultra-Micro Indentation System, UMIS-2000, CSIRO, Australia) with inbuilt IBIS2 software was used to investigate the near surface deformation behaviour of tooth enamel.

4.3.2 Sample holder design

The UMIS indentation stage was replaced with a custom designed stainless steel holder (**Figure 4-2**).

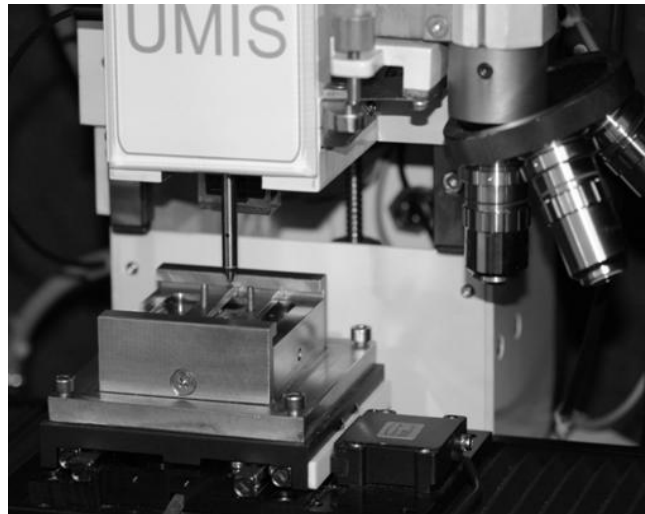


Figure 4-2. An indentation device for probing mechanical properties of human tooth enamel in a hydrated environment.

This holder, which was manufactured in the CNC Machining Centre (OKUMA, ACE Centre MB-46VAE, Japan) at the Edith Cowan University, clamped the tooth specimen onto the bottom of the bath using a slide-screw assembly (**Figure 4-3(a)**). In this way, the use of glue or wax was avoided.

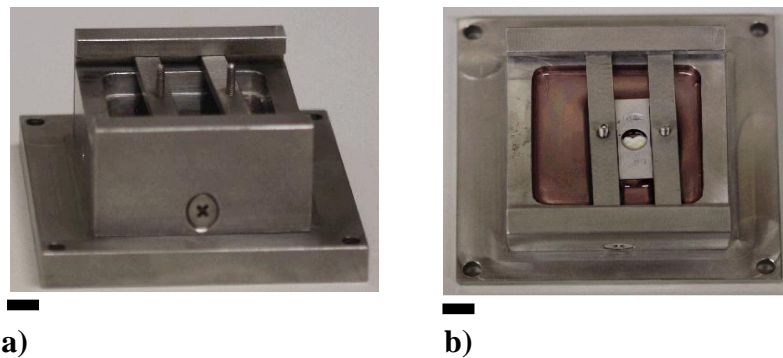


Figure 4-3. (a) A specially designed holder for nanoindentation testing of human tooth enamel in a wet environment. (b) Stainless steel hexagonal socket set screws with flat points are driven into each slide towards the specimen. The bath is filled with Hank's Balanced Salt Solution. No mounting medium (i.e., glue or wax) is required for holding the samples in place during testing. Scale bar = 5 mm.

The slides (**Figure 4-3(b)**) were inserted into the slotted recess of the holder. A 1 mm thick stainless steel plate was placed on top of the specimen to distribute the pressure evenly and to protect the specimen from damage during clamping. The holder allowed the tooth specimen to be submerged in HBSS and to test dental tissues in their hydrated state. The specifications of the holder and slides are attached to Appendix B and Appendix C.

4.3.3 Verification of indentation spacing

In order to verify the indentation spacing, arrays with 10 indents 20 μm apart were made under applied loads of 50, 200 and 400 mN, as depicted in **Figure 4-4(a)**. The 20 μm spacing between indents resulted in residual impressions from previous indents, mainly for 200 and 400 mN loads (**Figure 4-4(a)**).

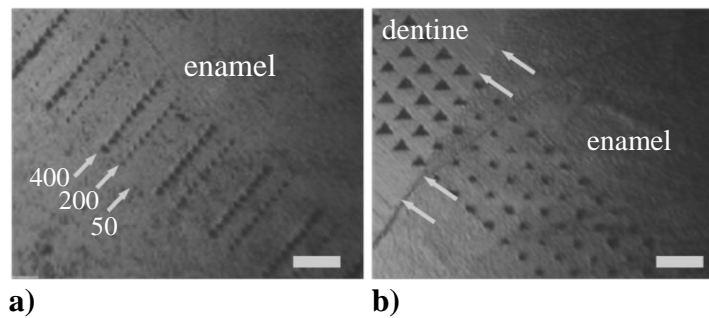


Figure 4-4. Indentation spacing of each array and each indent in distance of 20 μm (a) and 50 μm (b). In (a), indentation loads of 50, 200 and 400 mN were applied onto the enamel surface. The residual impression from previous indents of 20 μm apart was unavoidable for 200 and 400 mN. In (b), partial loading-unloading was applied up to 400 mN with indentation arrays of 50 μm apart from the enamel surface towards dentine. No overlaps of indents were found in the softer part of the tooth, the dentine (b). Scale bar = 100 μm .

For the three-sided Berkovich indenter, the contact area, A_c , is expressed as $24.56h_c^2$, where h_c is the contact indentation depth (Equation (3-7)). The relationship between the length, L , of an altitude of the triangle and h_c can be calculated from equations (3-2) and (3-6):

$$L = 3 \tan 65.27^\circ h_c. \quad (4-1)$$

Based on the current experimental work, the maximum h_c of enamel was found to be less than 3 μm . Therefore, it could be easily deduced that the L at the h_c of 3 μm is 19.5 μm . As shown in **Figure 4-4(b)**, a distance of 50 μm completely avoided any interferences of residual impressions from previous and/or neighbouring indents during nanoindentation testing from the enamel occlusal surface towards the dentine. SEM images of Berkovich indents from different regions of tooth enamel are given in Appendix D.

4.3.4 New method of data analysis to the constant indentation (Berkovich indenter)

Young's modulus, E , and hardness, H , of the polished surface of enamel was measured with a Berkovich indenter and determined to the constant indentation depth. The contact area of the tip as a function of penetration depth was calibrated on fused silica [139, 203]. A typical example of a calibration curve for the Berkovich indenter is shown in **Figure 4-5**.

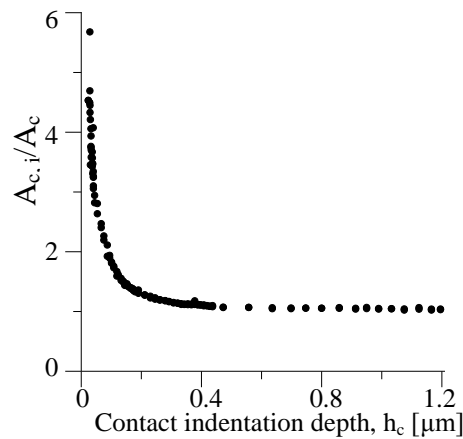


Figure 4-5. Typical calibration curve of a Berkovich indenter. The $A_{c,i}/A_c$ parameter denotes the ratio of an ideal contact area to a real contact area of a Berkovich indenter at the contact indentation depth, h_c .

The specimen was submerged in HBSS during testing. Each row contained 5 indents with an interval of 50 μm . The spacing between rows was 50 μm . Load-

partial unload tests were run in a closed-loop under load control. For the Berkovich indenter, the maximum 400 mN load was applied in eight increments. Following each increment were 10 decrements. Upon that, a function for E and H of enamel was derived for each indentation line [7, 8]. From this function, E and H were determined and plotted as a function of constant indentation depth (Figure 4-6(a,b)).

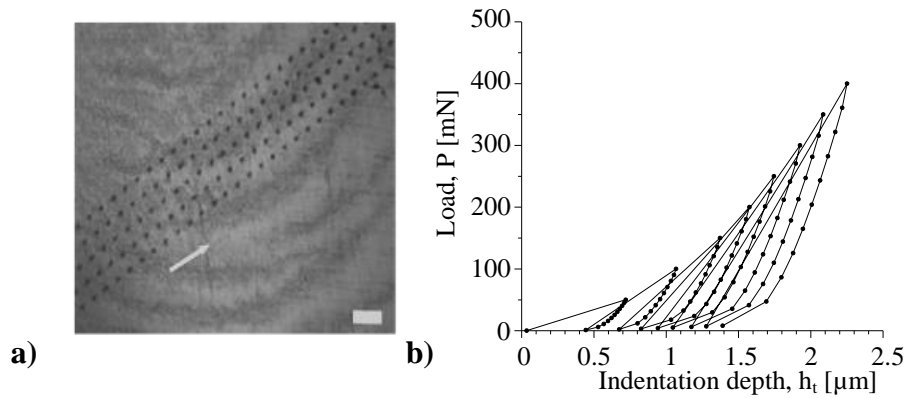


Figure 4-6. (a) Optical micrograph of the indentation layout on enamel. Residual impressions of Berkovich indents after partial loading-unloading was applied up to 400 mN with indentation arrays of 50 μm apart across the enamel surface (b) Indentation load, P , as a function of displacement (i.e., penetration depth), h_i , of enamel measured by a Berkovich indenter. Scale bar = 100 μm .

4.3.5 Stress – strain test settings (Spherical indenter)

The stress-strain properties from the middle region of tooth enamel were investigated with a spherical tipped indenter of a 5 μm nominal radius and 90° flank angle. The middle region of tooth enamel was located half of the distance between the occlusal surface of the tooth and the enamel-dentine junction (i.e., a normalised distance of 0.5). The specimen was submerged in HBSS during testing. The contact area of the tip was calibrated on fused silica [139, 203]. A typical example of a calibration curve for a 5 μm spherical indenter is shown in Figure 4-7.

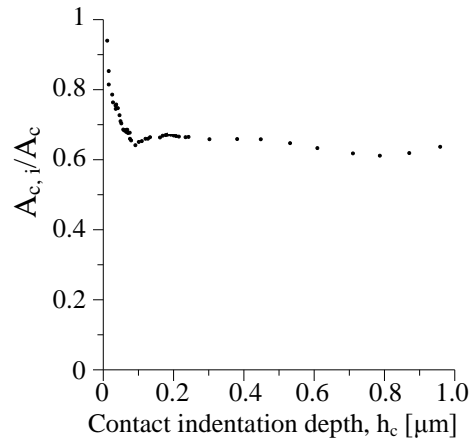


Figure 4-7. Typical calibration curve of a 5 μm spherical indenter.

For a conical indenter with a flank angle, α , of 90° and nominal radius, R , of 5 μm , the maximum strain (a/R) when the indentation depth is equal to the depth at the transition between a sphere and cone can be easily derived from the geometry shown in **Figure 4-8(a)**:

$$\frac{a_c}{R} = \frac{R \cos 45}{R} \approx 0.707 \quad (4-2)$$

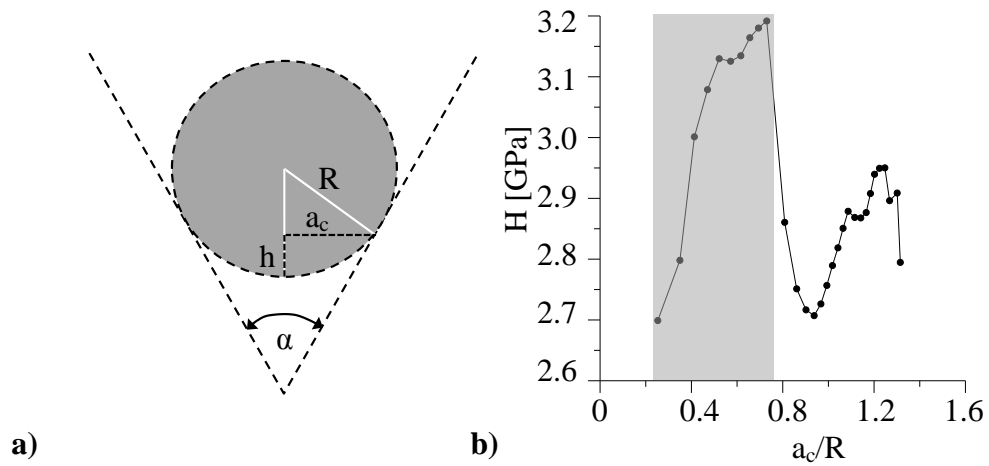


Figure 4-8. (a) Schematic representation of a spherical indenter of nominal radius R , contact radius, a_c and a flank angle, α , at the depth, h , that represents the transition between the sphere and cone. (b) Typical stress-strain ($H - a_c/R$) curve of tooth enamel with 30 incremental steps up to a load of 400 mN. The shaded area denotes 10 incremental steps and highlights the elastic-plastic region of tooth enamel before it softens and/or fractures.

(H-a/R) plots obtained from tests up to a maximum load of 400 mN shows that the first 10 incremental steps corresponded to the elastic–plastic region of enamel prior to the enamel softening and potentially fracturing. From **Figure 4-8(b)**, the maximum indentation load, $P = 130$ mN used for investigation of the stress-strain behaviour of tooth enamel was calculated from the relationship of the maximum load and the number of increments as:

$$P = \frac{P_{\max}}{\text{increments}_{\text{total}}} \cdot \text{increments}_{\text{shaded area}}, \quad (4-3)$$

where $P_{\max} = 400$ mN, $\text{increments}_{\text{total}} = 30$, $\text{increments}_{\text{shaded area}} = 10$.

The tests were run in two rows of indents; each row contained 5 indents with an interval of 50 μm . The spacing between rows was 50 μm . Load-partial unload tests were run in a closed-loop mode under load control. The indenter was loaded to a maximum load of 130 mN in thirty increments and unloaded to 2% of a maximum load in 10 decrements. The H values of enamel were derived as a function of h_c [7, 8]. H-a_c/R curves were generated with IBIS2 software according to the relationship given by equation (3-23).

4.3.6 Creep

In the creep indentation tests, the middle region of tooth enamel was tested with a spherical indenter of 5 μm (UMIS-2000, Australia). The specimens were submerged in HBSS during testing. The contact area of the spherical indenter was determined by calibration against fused silica. There were three separate creep-recovery tests that were run in a four-step loading mode on each sample. For creep measurements, the indenter was loaded to a maximum load of a) 50 mN, b) 100 mN and c) 130 mN within 10 s and held at a constant for 900 s and then unloaded to 5 mN within 15 s and held constant for 900 s. Each test commenced after a three hour thermal soak period in a closed laboratory environment. For each maximum load, the tests were run in a row of 5 indents with an interval of 50 μm . The distance between the indents was 50 μm to avoid

residual impressions from previous indents. After the completion of tests on healthy enamel, other creep measurements were repeated for tooth enamel that had been bleached for 7 days (Section 4.1.6).

4.4 Modelling of human tooth enamel

Two different approaches were used to investigate and theoretically predict the mechanical behaviour of human tooth enamel: numerical models and mechanistic models.

4.4.1 Numerical models

4.4.1.1 Elastic behaviour

It has been shown that mineral platelets of enamel start to slide against each other when the shear stress in the protein matrix exceeds a critical value [105]. Thus, finite element models (FEM) were constructed to clarify the effect of shear deformation on the magnitude and distribution of contact-induced stress in enamel. The simulations were performed using the COMSOL software. A two-dimensional axisymmetric model, with the axial coordinate z along the loading direction of the indenter, was built. The model consisted of an enamel block measuring $50\text{ }\mu\text{m} \times 50\text{ }\mu\text{m}$, loaded by a two-dimensional, conical-shaped axisymmetric indenter, with a tip angle of 70.30° , which approximated the three-dimensional Berkovich nanoindentation experiments. A refined mesh was used within an area of $10\text{ }\mu\text{m} \times 10\text{ }\mu\text{m}$ directly underneath the indenter, where the stress concentration was expected to rise during indentation in order to achieve high accuracy around the contact zone (**Figure 4-9**).

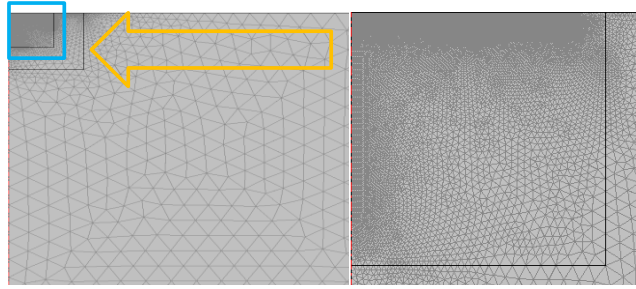


Figure 4-9. FEM refined mesh used in the simulations.

The total number of mesh elements was 17,631, which included the elements within the indenter. Further mesh refinements did not improve the simulation accuracy significantly. The contact between the indenter and the sample was assumed to be frictionless.

The details of the boundary conditions were as follows:

The bottom of the block ($z = 50 \mu\text{m}$) was fixed in the z direction, while the right edge ($x = 50 \mu\text{m}$) was fixed in the x direction. The axisymmetric axis coincided with the left edge of the block ($x = 0 \mu\text{m}$) to obtain full 3D simulation results. The tip of the indenter was located at $z = 0 \mu\text{m}$ (0 displacement) before the simulations. The indentation process was simulated as a downward displacement of the indenter from 0 to $0.4 \mu\text{m}$ at a step of $0.04 \mu\text{m}$.

4.4.1.2 Plastic behaviour

COMSOL Multiphysics software (Version 3.5a) was used in this work to evaluate the stress distributions within the samples under nanoindentations at different depths. A non-linear FEM of a two-dimensional, conical-shaped axisymmetric indenter, with a tip angle of 70.30° , was adapted to approximate the three-dimensional Berkovich nanoindentation experiments.

An independent study confirmed that, compared to full three dimensional modelling, the accuracy of such two-dimensional axisymmetric approximation was 2 to 3 %, a range within any experimental comparison significance [190].

The effect of the indenter tip was modelled by a distributed force (**Figure 4-10(a)**), which generated a deformation profile corresponding to the experimentally determined indenter cross-sectional tip-area function.

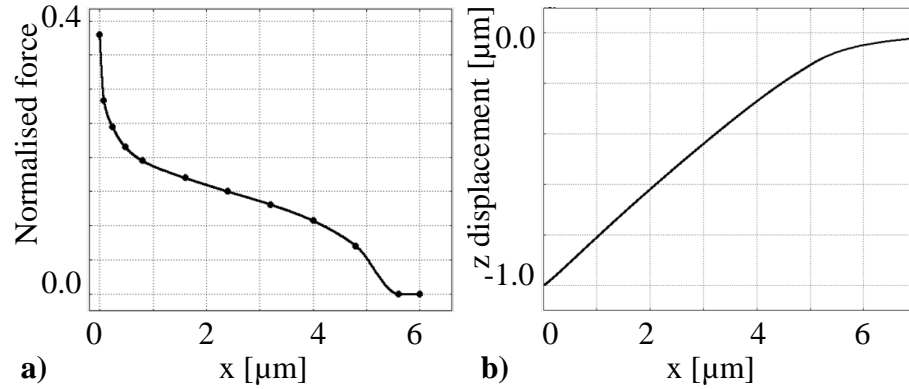


Figure 4-10. (a) The force simulates the effect of a conical indenter, as a function of the distance from the axisymmetry, which is used to generate the desired deformation produced by the conical indenter, (b) the z displacement at the surface of the sample, generated by the force in (a).

The linear relationship was confirmed by a cross sectional plot along the loading boundary, with a maximum error of less than 0.5 %. In order to avoid the unrealistic artefact of high stress around an idealised sharp tip, a curvature was introduced with a radius of ~ 20 nm. FEM meshes were generated in an interactive way to ensure that the mesh was denser in the regions where a large stress gradient was expected (**Figure 4-10 (b)**). Boundary conditions were set as follows: The left-hand side was the axial symmetry axis. The bottom and the right-hand side were fixed along the z and x directions, respectively, but were free to move in the other directions. For all models used, the overall dimension of the model was considerably larger than the coating thickness; thus, the edge effect due to boundary constraints was negligible.

4.4.2 Analytical models

4.4.2.1 Elastic behaviour

A mechanistic-based model given by equation (2-2) was used to simulate the elastic responses of tooth enamel under applied loads up to a maximum load of 400 mN with a Berkovich indenter. The structural and mechanical properties of the main constituents of enamel (i.e., the mineral and protein) used for the calculation of the transverse stiffness of a staggered composite, E_2 , and the effective crystal orientation angle, θ , are given in **Table 4-3** [3, 90, 91, 112, 142, 193, 220].

Table 4-3. Structural and mechanical properties of the enamel constituents used in the modelling analysis.

Property:	Mineral crystal			Protein		
	Symbol	Value	Ref.	Symbol	Value	Ref.
Thickness (nm)	h_m	50	[90]	h_p	1.5*	
Length (nm)	l	500	[91]			
Poisson ratio	ν_m	0.25	[193]	ν_p	0.45	[193]
Young's modulus [GPa]	E_m	129	[3]	E_p	2	[112, 142, 220]
Spacing of mineral crystals	d	1.5				

4.4.2.2 Stress–strain

The nanoindentation stress–strain responses of unbleached and bleached enamel (Section 4.3.5) were fitted into the mechanistic-based model expressed by equation (2-9) to determine variables regulating the deformation behaviour of tooth enamel during the whitening process.

Given that the organic matrix may denature during the bleaching (Section 2.7), it was hypothesised that if the hardness of enamel will decrease, the shear

modulus of proteins, τ_c , will also decrease for bleached enamel while the θ (i.e., the effective crystal orientation angle) of bleached enamel will increase due to the damaged functionality of proteins.

4.5 Mild and severe wear

Considerable efforts have been made in the field of Materials Science to increase materials' resistance against abrasion (i.e. wear) [221]. Scientists are often looking for answers and ideas regarding biological materials [222]. For instance, teeth in humans as well as in animals have been studied for their unique capability of being able to maintain their integrity as well as for their wear resistance. However, how tooth enamel is able to resist wear in the oral cavity over a person's lifetime remains unclear. Nevertheless, understanding of enamel wear resistance may provide key variables on how to strengthen other synthetic engineering materials and improve their resistance against abrasion. On the other hand, some factors could affect the wear resistance of the tooth, e. g., diet, the nature and preparation of the food, and cultural aspects in human population [223].

The resistance of tooth enamel can be ascertained theoretically with use of well-known ranking parameters and with data obtained from a nanoindentation instrument.

There are two types of wear of materials; mild and severe. While mild abrasion is considered as a multi-body process involving at least two materials with more likely dissimilar properties and the possible addition of some fluid. It also involves the material's removal at a scale of a grain or sub-grain size under low load and the action of polishing particles [224]. Severe abrasion is defined as a multiple-point multiple-pass body process in which the removal of particles is significantly larger than the grain size [128]. To ascertain wear resistance of a material, the H values have been used for a long time as the critical property of a

material for ranking. However, it has been shown that the E value is also an important in determining the wear behaviour of materials [221, 224, 225].

Parameters such as H/E and K_{IC}^4/H^*E^2 have been determined for ascertaining mild and severe wear resistance of materials, respectively. The H/E ratio is a well-known parameter in assessing the elastic limit of a material's wear resistance with surface contact [225]. As this parameter ranks a material's wear resistance in its elastic region before the material begins to be plastically deformed, this parameter can be used for measuring the tooth enamel resistance against mild wear. On the other hand, the K_{IC}^4/H^*E^2 ratio measures the resistance to micro-cracking; in other words resistance to the severe wear of a material. The theory of fracture mechanics underlying this parameter is summarised below.

The microcracking wear mechanism from sharp and stiff particles has been shown to be initiated at loads for which the predicted crack lengths are larger than the indent size [224, 226]. The threshold (i.e., the critical load for the initiation of cracks) is expressed as [226]:

$$c = \left(\frac{E}{H}\right)^{\frac{1}{2}} \left(\frac{\chi P}{K_c}\right)^{\frac{2}{3}}, \quad (4-4)$$

where c is the crack length measured from the centre of the indent, K_c is the fracture toughness and χ is 0.022 for the Berkovich indenter. Before the initiation of cracks at indent corners, the dimension of a plastic indent, a , is equal to the final crack, c , with both measured from the indent centre. Therefore, given $a = c$, the critical load, P_c , for the initiation of a microcrack against a sharp contact can be derived and rewritten as:

$$P_c = \frac{1}{\alpha^3 \chi^4} \frac{K_c^4}{E^2 H}, \quad (4-5)$$

where α is 1.30 for the three-sided Berkovich indenter.

Omitting constant values of α and χ in equation (4-5) yields the ratio of K_{IC}^4/H^*E^2 . This ratio may provide additional insights into the severe wear abrasion resistance of brittle biomineralised tissues such as teeth [227].

5. Effects of preparation methods on the mechanical behaviour of tooth enamel

5.1 Summary

A new method of tooth preparation was used to measure the mechanical properties of human tooth enamel in its wet environment. These properties were compared to the conventional methods, A and B. For the first time, experimental results obtained from the nanoindentation instrument were reported to the constant indentation depths from the enamel surface up to 2 μm . The overall data showed that the use of resin in the sample preparation of tooth enamel had detrimental effects on the Young's modulus, E, and hardness, H, but it had positive effects on mild and severe wear resistance. In addition, minimal changes of E and H from the enamel surface toward the enamel-dentine junction (EDJ) were found for dehydrated and later dried enamel compared to wet enamel.

5.2 Introduction

Tooth enamel is a highly brittle, yet resilient dental hard tissue [53], with characteristics of a woven fibre-reinforced composite [40], comprising on average 96% mineral, 1 % proteins and 3% water by weight [91]. Sustaining high loads of more than 1000 N [52, 228], enamel must withstand repeated contact damage while protecting the underlying softer dentine and pulp. In contrast to the self-healing ability of dentine, enamel cannot fracture during masticatory function, as the resultant damage of this hard tissue is non-reversible. Sample preparation plays an important role in determining the true mechanical properties of enamel. Different from testing of synthetic material, there is no standard approach established amongst researchers on how to prepare human teeth for nanoindentation testing in the wet environment [48] even though experimental results obtained from the nanoindentation instrument as well as structural

features of tooth enamel may be considerably affected by the preparation method [29].

Highlighting the evidence of sample preparation caveats in teeth and other biological materials (Section 2.5.1), the main aim of this study was to investigate the mechanical properties of tooth enamel prepared by three different methods: the new method and conventional methods A and B. In addition, the resulting mechanical properties of tooth enamel were analysed to constant indentation depths by employing a new approach of data analysis. The dehydration and drying process and its effect on the enamel properties were also investigated. In addition, mild and severe wear resistance of tooth enamel prepared by three different methods were ascertained according to the ratio's parameters of H to E and the resistance to micro-cracking, respectively (Section 4.5).

5.3 Materials and methods

Ten human molars were collected and stored following the protocol outlined in Section 4.1.1 and were tested within 4 weeks. The E and H values were reported in the range of constant indentation depths (i.e., from the enamel surface up to 2 μm). The values at 0 μm were extrapolated from experimental data to justify and compare the results with other studies.

- *Spatial distribution*

Three enamel specimens prepared by **the new method** were tested from the enamel surface to the EDJ with a Berkovich following the test settings given in Section 4.3.4.

- *E and H values of tooth enamel prepared by three different methods*

Five teeth were used for the comparison of sample preparation methods: two teeth were prepared by **conventional method A** (Section 4.1.3), three halves of

teeth were prepared by **conventional method B** (Section 4.1.4) and the remaining three halves of teeth were prepared by the **new method** (Section 4.1.2). The E and H results were obtained with the Berkovich indenter up to the maximum load of 400 mN in the wet environment using the test settings given in Section 4.3.4. On each specimen, 25 indents were made in the middle region of the enamel. Assuming a location area of indents being too small (i.e., $250 \mu\text{m}^2$), the values of E and H were analysed simultaneously and extrapolated to the constant indentation depths.

The E and H values of enamel specimens that were prepared by three different methods were analysed with t-tests to determine whether there were any statistically significant differences between the values/methods used. Since the methods were not dependent in any way, the first step was to employ the F-test two-sample for variances to ascertain whether there were significant differences in the variances between E and H values, respectively. The level of significance was set at $p = 0.05$ (i.e. 5 %). The null hypothesis (i.e., assuming equal variance between values) was accepted for $p > 0.05$. Upon analysing the resulting values of p values from the F-test, homoscedastic or heteroscedastic t-tests were employed at the significance level of 0.05 to determine whether E and H were deemed significant between different methods.

- *E and H values of wet and dehydrated – dried enamel*

For the dehydration and drying investigations, two molars, “enamel 1” and “enamel 2”, were prepared with the new method (Section 4.1.2) and tested with a Berkovich indenter up to a load of 400 mN in the wet environment from the occlusal surface towards the EDJ (Section 4.3.4). Later, enamel samples were dehydrated and dried following Janda’s approach (Section 4.1.5) and re-tested again alongside the previous indents following the test settings given in Section 4.3.4. Each line containing five indents was analysed individually to the constant indentation depth by extrapolating the average values of E and H, respectively. For more details about nanoindentation test settings, refer also to Sections 4.3.1,

4.3.2 and 4.3.3. Indentation imprints across the EDJ from nanoindentation tests in wet and dry environments are shown in **Figure 5-1**.

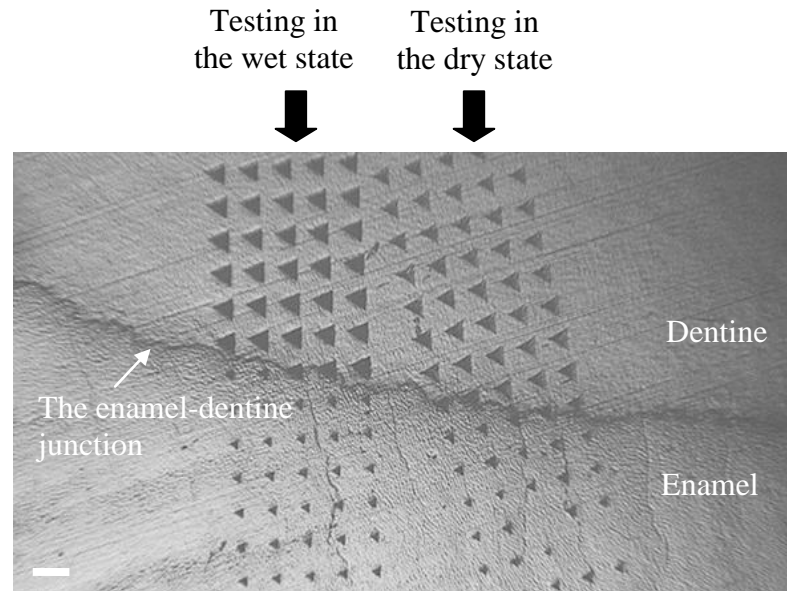


Figure 5-1. Optical microscopic image of Berkovich indents across the EDJ. Berkovich indents in enamel and dentine exhibited larger sizes of imprints in the wet environment compared to the dry state. Scale bar = 50 μm .

- *Wear resistance of tooth enamel prepared by three different methods*

The effects of resin embedding on the enamel wear resistance were investigated with ratios of a) H/E (mild wear), and b) K_{IC}^4/H^*E^2 (severe wear) at constant indentation depths up to 2 μm (Section 4.5).

5.4 Results and discussion

5.4.1 E and H values

Typical spatial distributions of E and H over the entire thickness of tooth enamel are shown in **Figure 5-2(a,b)**.

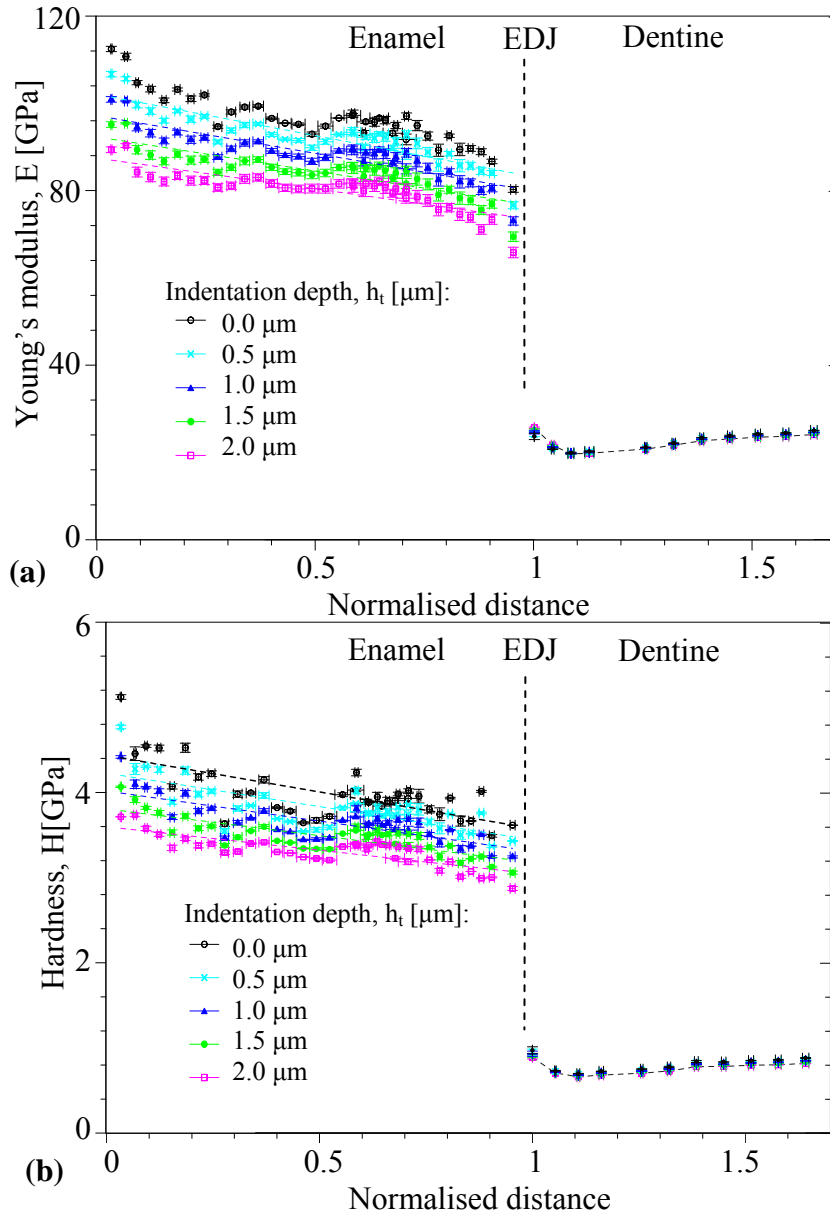


Figure 5-2. Distributions of (a) E [GPa] and (b) H [GPa] data of healthy human molars prepared by the new method. These data were measured from the enamel occlusal surface (normalised distance = 0) towards dentine (normalised distance = 1). Standard error bars are derived from measurements on the three molars' specimens.

By employing the new method of nanoindentation data analysis, the E and H plots show a decreasing gradient from the enamel occlusal surface towards the EDJ, yet interestingly a gradient with the increasing indentation depth up to 2 μm

at fixed locations. Varieties of spatial mappings of E and H of individual enamel specimens are also presented in **Figure 12-8** in Appendix E.

The E and H mean values (\pm standard errors) of healthy enamel prepared by three different preparation methods and plotted for selected indentation depths up to 2 μm are presented in **Figure 5-3(a,b)**.

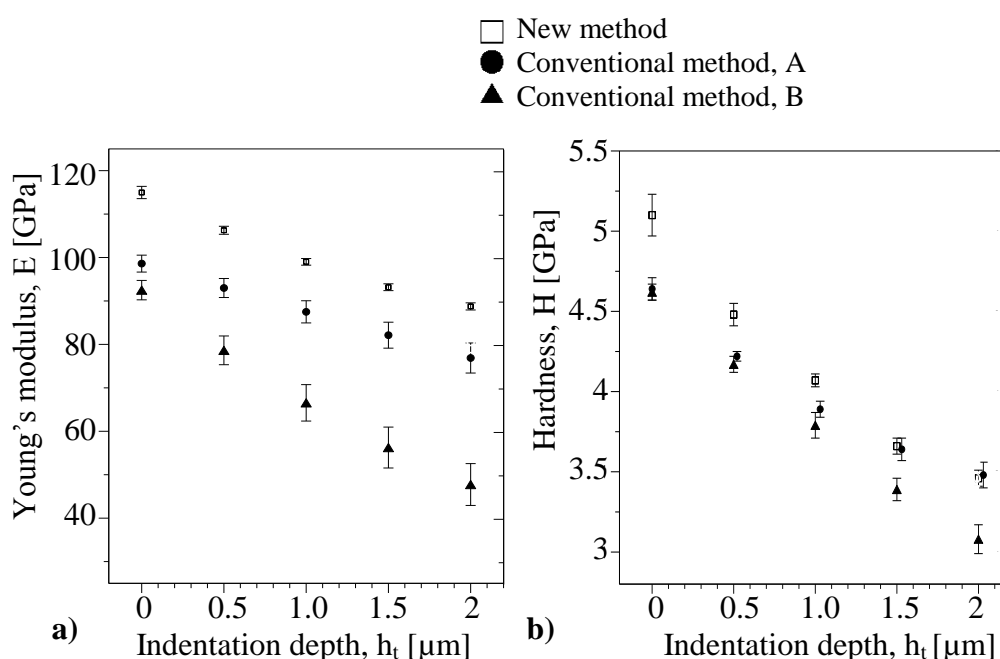


Figure 5-3. (a) E [GPa] and (b) H [GPa] of tooth enamel prepared by three different methods and measured at different indentation depths. This charts show that resin embedding significantly affects the E rather than the H values of tooth enamel. Notably, E values of tooth enamel are significantly different for all preparation methods and indentation depths, while only the H values of the conventional method B are significantly different to the conventional method A and the new method.

In general, E values decreased with increasing indentation depth for all of the preparation methods (**Figure 5-3(a)**). Comparing E values to conventional method A, the moduli of conventional method B were significantly different ($p < 0.05$) and lower for all indentation depths. For example, at 1 μm indentation depth, E values of conventional method B decreased by $23.94 (\pm 2.81) \%$ compared to conventional method A (**Table 5-1**).

Table 5-1. Improvement and/or degradation of E (\pm standard error) in % as a positive or negative value, respectively.

Comparison of E in %	Indentation depth [μm]					Overall mean
	0.0	0.5	1	1.5	2	
Conventional method, B to conventional method, A	-6.19 (± 0.42)	-15.44 (± 1.78)	-23.94 (± 2.81)	-31.50 (± 3.52)	-37.89 (± 3.77)	-22.99 (± 6.30)
New method to conventional method, A	16.60 (± 0.87)	14.29 (± 1.42)	13.16 (± 2.09)	13.45 (± 2.73)	15.45 (± 3.58)	14.59 (± 0.72)

The results summarised in **Table 5-1** clearly show that the use of resin on the sectioned tooth (conventional method B) during the sample preparation process had the most detrimental (i.e. negative) effects on the enamel stiffness. Statistical comparison of resulting E values for conventional methods A and B can be found in Appendix F.

On the other hand, E moduli of the new method were significantly higher than the values of conventional method A ($p < 0.05$). For instance, at 1 μm indentation depth, the value of E for the new method increased by 13.16 (± 2.09) compared to conventional method A. The new method resulted in higher values of E moduli for all indentation depths (**Table 5-1**). Comparison of the resulting values of E for conventional method A and the new method are given in Appendix H.

By analysing the results from both methods (**Table 5-1**), it is clear that the enamel stiffness is significantly higher in the new method while it is lower in the conventional methods. The higher value of the enamel stiffness was attributed to the sample preparation of the new method in which no chemically based substances were used that could degrade its properties. Therefore, the new method was adopted in this study to avoid any artefacts which could affect the nanoindentation testing results.

Decreasing trends of E moduli at different indentation depths have also been reported by other authors [36-38]. However, values reported in these studies were

much lower than the values obtained in this study with the new method. For example for 0.5 μm indentation depth, the reported values of E were between 60 and 70 GPa [38]. By comparing these values to the new method, the E modulus of the new method was $106.27 (\pm 0.92)$ GPa for the same indentation depth and region (**Table 12-13** in Appendix H), which corresponded to the decrease by 34.13 % to 43.54 % in the E of the new method. Interestingly, although Zhou & Hsiung used resin during the preparation process [36], their study showed the closest values of E moduli at representative depths for tooth enamel prepared by the new method.

Enamel H values of the three preparation methods decreased with increasing indentation depth for all three methods (**Figure 5-3(b)**). By comparing conventional method B to conventional method A, enamel at a depth of 0.5 μm was softer by $1.11 (\pm 0.44)$ % (**Table 5-2**).

Table 5-2. Improvement and/or degradation of H (\pm standard error) in % as positive or negative value, respectively.

Comparison of H in %	Indentation depth [μm]					Overall
	0.0	0.5	1	1.5	2	Mean
Conventional method, B to conventional method, A	-0.26 (± 0.53)	-1.11 (± 0.44)	-2.61 (± 0.67)	-6.94 (± 0.13)	-11.48 (± 0.37)	-4.48 (± 2.34)
New method to conventional method, A	9.85 (± 0.001)	6.17 (± 0.95)	4.59 (± 0.30)	0.46 (± 0.59)	-0.51 (± 0.79)	4.11 (± 2.12)

The H values of conventional methods A and B differed at lower depths, i.e. from 1.5 μm indentation depth. On the other hand, and by comparing the new method to conventional method A, the H obtained from the new method had higher values for all indentation depths with an overall mean of $4.11 (\pm 2.12)$ % (**Table 5-2**). For example, at 1 μm indentation depth, the H value of the new method was 4.07 ± 0.04 GPa (**Table 12-19** in Appendix I), while H values for conventional methods A and B were 3.89 ± 0.05 GPa and 3.79 ± 0.08 GPa (**Table 12-7** in Appendix G), respectively. Although the new method

demonstrated higher values of H for all indentation depths, the values between conventional method A and the new method significantly differed ($p < 0.05$) only for indentation depths ranging from the surface to 1 μm indentation depth. In contrast, differences of H values between conventional method A and the new method were not found to be significant ($p > 0.05$) for indentation depths between 1.5 and 2 μm . Resulting values of H comparisons (i.e., p-values) between conventional methods A and B and conventional method A and the new method can be found in Appendix G and Appendix I, respectively.

As previously published studies reported either constant load or average values of H, there was great difficulty in comparing H values to other studies in relation to the sample preparation process. Therefore, only as an example, a value from a chart for 0.5 μm indentation depth was extrapolated to represent enamel H prepared by resin-embedding. The H of the new method was 4.48 ± 0.07 GPa for 0.5 μm indentation depth, while previously published values of H for a given depth were between 4.00 GPa - 4.10 GPa [37], which corresponded to lower values of 8.48 % and ≈ 10.71 % in the H obtained with the new method.

Comparing conventional methods B to A and to the new method, the results of E and H for the sectioned tooth that was inappropriately dried (conventional method B) indicated the most negative effects of resin embedding on enamel mechanical responses. On the other hand, the new method which avoided resin embedding in the preparation process yielded the highest E and H values of enamel. Although previous studies showed several degradation mechanisms of resin embedding [31, 32, 34, 35, 122, 124], it could not be concluded whether the traces of water and the organic matter within inappropriately dried enamel affected resin polymerisation and thus compliance and stiffness of resin, or other well-known factors such as curing temperature, resin shrinkage and contraction stresses damaged the composition and/or structure of the dental tissue which resulted in a lower stiffness of enamel.

The detail of the resin infiltration through the tooth was outside of the scope of this study. Instead, this research focused on how the mechanical properties were affected by resin as an embedding medium. An important factor that may explain why E is more affected by resin is the measuring procedure in the nanoindentation test. From the nanoindentation measurements, the E value is estimated by analysing the unloading responses of the load-displacement curve while hardness is a less well defined term, changing with the load and the contact size (i.e., the contact area). An assumption is considered in the method of analysis of experimental values that the loading phase is elastic-plastic while unloading is elastic [117]. As the resin was used as an embedding medium in previously used conventional methods, the plastic deformation could more likely occur during the unloading phase. This deformation would affect the values of E during the nanoindentation test. Furthermore, as the E value is extracted from the combined value of a reduced modulus, E^* (Section 3.1.2), the H value is determined only as a load divided by a contact area A_c (Section 3.1.3). Notably, this could also lead to significant differences in reported E values compared to H values between the new method and conventional methods.

On the other hand, based on the results from the nanoindentation instrument, this study demonstrated that:

- resin embedding had significant degrading effects on the mechanical responses of tooth enamel that resulted in lower values of E and H ;
- conventional methods should be replaced by the new method for the investigation of enamel mechanical behaviour in its hydrated state.

5.4.2 Dehydration and drying

Typical spatial distributions of E and H values between dry and wet enamel are shown in **Figure 5-4(a,b)**.

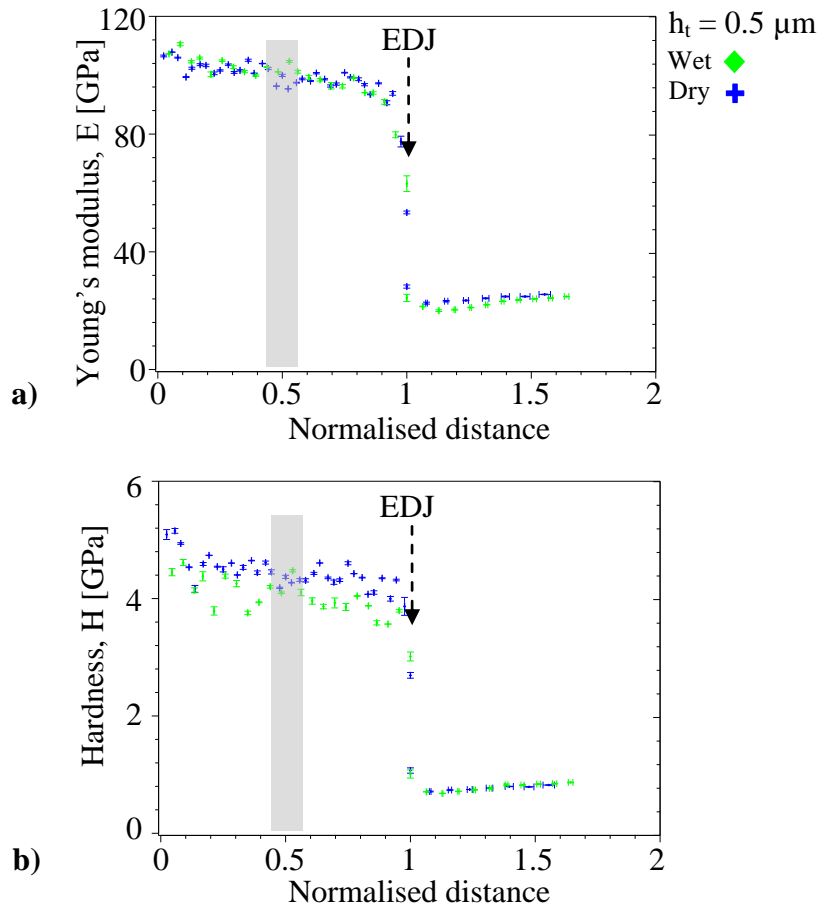


Figure 5-4. Typical distributions of (a) E [GPa] and (b) H [GPa] of tooth enamel at a normalised distance of between 0 and 1 and dentine at a normalised distance higher than 1 for the constant indentation depth $0.5 \mu\text{m}$ in the hydrated and dry state. The shaded region indicates the indentation area for which comparison analyses for wet and dry enamel were made. The standard error bars of two specimens at each location denote the combined value of experimental data, i.e. $N = 80$ of two enamel specimens.

By observing E and H values between wet and dry enamel over the entire thickness (**Figure 5-4(a,b)**), clear differences of E and H values were noticed

particularly near the EDJ. This could be explained by the gradual increase of water protein matrix and concurrently by the gradual decrease of mineral density in healthy enamel from the enamel occlusal surface towards the EDJ [189]. The increasing E and H differences between wet and dry enamel samples at the EDJ were possibly due to the existence of the organic phase that was affected by the dehydration and drying procedures. Since the enamel occlusal surface and the EDJ were not the main subject of this study, the comparisons between wet and dry samples were only pursued for the middle region of enamel, as indicated by the shaded region in **Figure 5-4(a,b)**.

Dry and wet E and H values of “**enamel sample 1**” measured in the middle region at selected indentation depths of up to 2 μm below the surface showed decreasing E and H trends with increasing loads/depths (**Table 12-25** in Appendix J). From this table, the average E values in the dry environment (95.04 ± 0.79 GPa) were higher than the values in the wet environment (92.28 ± 1.19 GPa), giving the overall ratio of 1.03 for all averaged indentation depths ($\approx 3\%$). E values of tooth enamel measured in the dry conditions decreased gradually from 100.39 ± 1.46 GPa at the enamel surface (i.e., 0 μm indentation depth) to 90.31 ± 0.40 GPa at 2 μm indentation depth. In contrast, the values of E in the wet environment declined from 99.37 ± 1.01 GPa to 84.57 ± 1.07 GPa. On the other hand, by comparing wet to dry H values of enamel (**Table 12-25** in Appendix J), the average H value of dry samples was higher (4.02 ± 0.05 GPa) than for the wet samples (3.72 ± 0.06 GPa) resulting in the overall ratio of 1.08 for all averaged indentation depths ($\approx 8\%$). In addition, “**enamel sample 2**” exhibited a similar trend to “enamel sample 1”, i.e., decreasing values of both E and H of enamel with increasing indentation depth. The ratios between wet and dry enamel samples of E and H were found to be 1.05 and 1.07, respectively, for the overall average indentation depths (**Table 12-26** in Appendix J).

The combined average values of E and H of enamel and their standard deviations, i.e., “enamel samples 1&2”, are represented in **Table 5-3**. A careful

dehydration and drying process increased E and H values by ≈ 4 and ≈ 7 %, respectively, compared to normal readings for wet samples (**Table 5-3**). In contrast, the differences of E and H values between dry and wet samples were much smaller than reported by other authors; for instance, it was postulated that samples were 15 % stiffer if they were tested in a dry environment [26]. In contrast to the results of the current experiments which both indicated E and H differences in the wet and dry environments, other authors have reported similar or identical E values between wet and dry samples and 100 % higher values for dry samples (ratio between dry and wet state 2:1) [23]. Additionally, 23 % higher values of microhardness were reported for protein-free enamel [47].

Table 5-3. Mean values of E and H (\pm standard error) of “enamel samples 1 & 2”. The resulting values represent combined E and H values, respectively from the middle region of enamel for overall indentation depths from 0 to 2 μm .

Enamel samples 1 & 2	Dry	Wet
E [GPa]	96.12(± 0.59)	92.42(± 0.72)
H [GPa]	4.09(± 0.04)	3.81(± 0.05)

Enamel is a composite of three different components: mineral, protein and water [189]. Although enamel contains only 1 % protein on the weight percent basis [91], this compound plays a pivotal role in enamel remarkable resistance against applied loads [45]. It optimises strength and maximises tolerance of flows within tissue by allowing limited differential movement between rods [14, 43, 47]. Furthermore, enamel comprises very little water content, i.e. 3 % by weight [91]. Although water itself plays a key role in the enamel structure [80], the water-protein matrix softens and plasticises human enamel [109]. In contrast, the dehydration media such as ethanol-water and acetone-water mixtures remove, either partially or completely, the water-protein phase from enamel [143]. As a result, enamel becomes harder and stiffer.

E and H data of enamel samples tested in the wet and dry state at the constant indentation depth between 0 and 2 μm were reported for the first time in this study (refer to Appendix J for more details). It was demonstrated that a careful dehydration and drying process had detrimental effects on enamel mechanical properties; however, this study showed that these effects were minimised when appropriate care was taken during sample preparation and dehydration-drying process.

From the above, it is proposed that the structure controls the mechanical responses of tooth enamel. Moreover, by protecting and preserving it, minimal differences between E and H can be achieved.

5.4.3 Mild wear of enamel

The elastic strain to failure ranking parameter H/E ratio, which is also called the plasticity index or the mild wear resistance parameter, was used to measure the limit of the elastic behaviour of tooth enamel at the surface contact (Section 4.5). The results of mild abrasion resistance of human tooth enamel prepared by the new and conventional methods A and B at the constant indentation depths are presented in **Figure 5-5**.

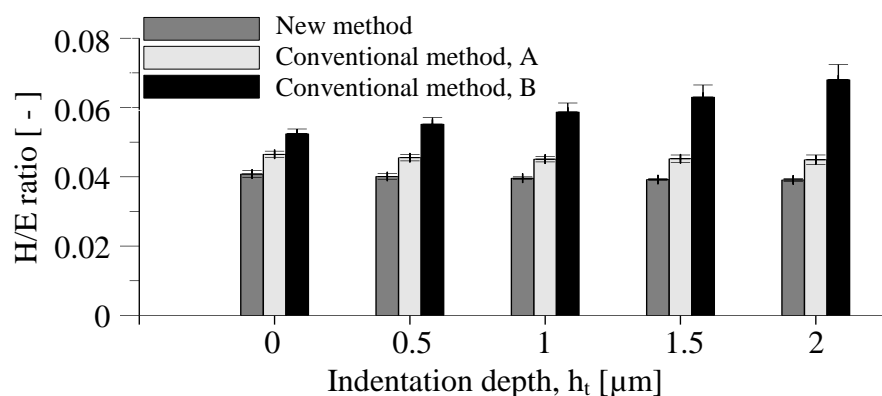


Figure 5-5. Mild wear of enamel prepared by the new method and conventional methods A and B for indentation depths between 0 and 2 μm .

Based on the experimental results, the mild wear ratio supports the hypothesis that resin used in the sample preparation process can significantly alter mechanical properties in nanoindentation tests. The H/E ratios of mild wear removal for enamel prepared by the conventional methods of A and B were significantly higher than for enamel prepared by the new method for all indentation depths. The overall values of mild wear resistance of enamel prepared with conventional methods, A and B, were 0.046 ± 0.001 and 0.057 ± 0.001 , respectively, in contrast to the ratio of enamel prepared by the new method, which was only 0.041 ± 0.003 (**Table 5-4**).

Table 5-4. Summary of the mild wear resistance of human tooth enamel for indentation depths ranging between 0 and 2 μm .

H/E ratio	Indentation depth [μm]					Overall H/E
	0	0.5	1	1.5	2	
New method	0.044 ± 0.001	0.042 ± 0.001	0.041 ± 0.001	0.039 ± 0.001	0.039 ± 0.001	0.041 ± 0.001
Conventional method, A	0.047 ± 0.001	0.046 ± 0.001	0.045 ± 0.001	0.045 ± 0.001	0.045 ± 0.001	0.046 ± 0.001
Conventional method, B	0.050 ± 0.001	0.053 ± 0.002	0.057 ± 0.003	0.060 ± 0.004	0.065 ± 0.004	0.057 ± 0.001

The overall ratio clearly indicates that a chemically based resin used during preparation had significant affirmative effects on the mild wear resistance of enamel with the increasing indentation depth. The highest value of mild wear resistance was found for enamel that was sectioned before resin embedding (conventional method B) possibly due to the greatest infiltration of the medium into the material, i.e. enamel. Although resin helped to improve mild wear resistance of enamel with depth, conventional methods A and B showed the largest detrimental effects on E and H (Section 5.4). Notably, there was an imperceptibly decreasing gradient of mild wear resistance with increasing indentation depth for enamel prepared by the new and conventional method A in contrast to conventional method B, which indicated an increasing gradient of H/E ratio with increasing indentation depth, as indicated in **Table 5-4**.

However, having higher values of the H/E ratio at the surface than at lower depths, as was shown for the new method and conventional method A, gives enamel a unique wear ability of being able to suppress abrasive removal material at the surface and therefore protect it from further mild abrasion. This study suggests that the significantly larger differences of the H/E ratio between enamel prepared by the new method and conventional method A and B were due to the resin infiltrated structure of enamel during the preparation process. Hence, it is apparent that resin drastically reduced E and H values while it enhanced tooth enamel mild wear resistance.

For ranking of enamel with other materials, the values of E and H reported in the literature are listed in **Table 5-5**.

Table 5-5. Mechanical properties of selective biological and dental materials used for mild wear comparison to human enamel [9, 115, 227, 229].

Biomaterials	E [GPa]	H [GPa]	Ref
Dry laminated biosilica, <i>M. chuni</i>	≈ 34	≈ 5	[229]
Dry radular teeth, <i>C. stelleri</i>	90-125	9-12	[227]

Dental materials	E [GPa]	H [GPa]	Ref
Zirconia-based ceramics (yttrium partially stabilised tetragonal zirconia polycrystal Y-TZP)	≈ 240.0	≈ 13.00	[115]
Glass-based feld spathic dental ceramics	≈ 78.90	≈ 10.64	[9]

Comparing the overall H/E ratio of tooth enamel prepared by the new method to other biomaterials, i.e., 0.041 ± 0.003 (**Table 5-4**), the ratio of mild abrasion wear of wet enamel is ≈ 2.39 and ≈ 3.59 times less than for radular teeth ($H/E \approx 0.098$) and biosilica ($H/E \approx 0.147$), respectively.

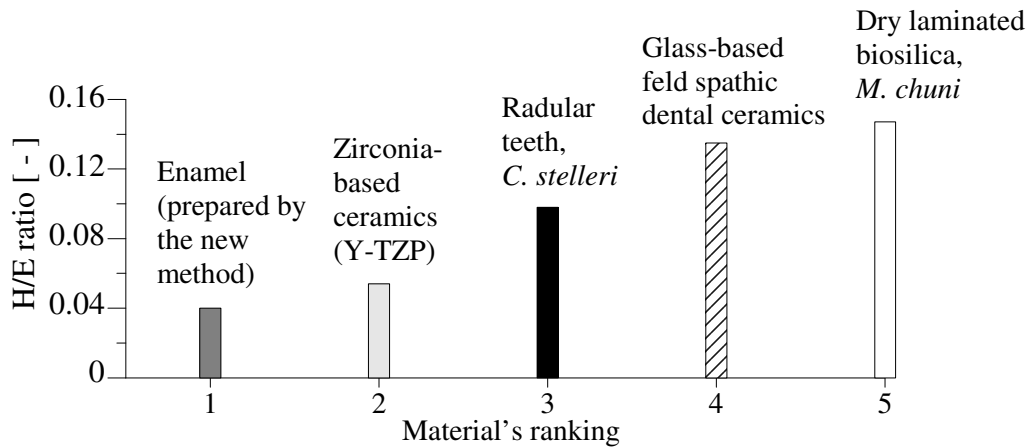


Figure 5-6. Ranking of tooth enamel with other biological and dental materials.

Biosilica and radular teeth have distinguished, yet superior mild abrasion capabilities compared to tooth enamel [11, 12]. Notably, the mild wear resistance of tooth enamel is similar to that of zirconia-based ceramics. In contrast, the glass-based ceramics exhibit similar wear behaviour as biosilica; however, they have ≈ 3.3 times higher mild wear ratio than enamel resulting in rather detrimental mild wear effects to opposing teeth (**Figure 5-6**).

5.4.4 Severe wear

Severe abrasive wear of enamel can be defined as a multiple-point multiple-pass body abrasive wear process that occurs in the oral cavity, for instance during grinding, biting or chewing of hard food, and can be ascertained by K_c^4/E^2H ratio (Section 4.5). The values of fracture toughness used in the calculations of this parameter for different materials are listed in **Table 5-6**.

Table 5-6. Fracture toughness, K_c of enamel and other biological and dental materials.

Fracture toughness, K_c	MPa.m ^{1/2}	Ref
Enamel in wet state	0.70	[230]
Dry laminated biosilica, <i>M. chuni</i>	0.84	[229]
Glass-based ceramics	1.36	[231]
Zirconia-based ceramics	5.5	[115]

While fracture toughness of radular teeth remains unknown [227], only laminated biosilica and the two most common dental ceramics were used in the present evaluations and comparisons of severe wear to human enamel prepared by the new method and conventional methods A and B. This study presents the results of threshold of ascertaining resistance to micro-cracking of enamel prepared by the new and conventional methods A and B at constant indentation depths between 0 and 2 μm , as shown in **Figure 5-7**.

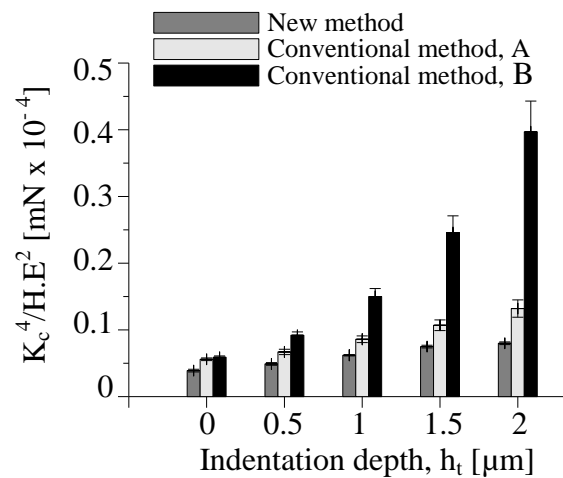


Figure 5-7. Severe wear of enamel prepared by the new method and by the conventional methods A and B for indentation depths between 0 and 2 μm .

In contrast to the mild wear of enamel prepared by the new method and conventional method A, which both demonstrated a diminutive decrease with increasing indentation depth, the resistance to micro-cracking indicated an opposite trend and increased with the indentation depth for all three preparation methods of enamel (**Table 5-7**).

Table 5-7. Summary of severe wear of tooth enamel for indentation depth ranging between 0 and 2 μm .

$K_{ic}^4/H.E^2$ [$\text{mN} \times 10^{-4}$]	Indentation depth [μm]					Overall $K_{ic}^4/H.E^2$ [$\text{mN} \times 10^{-4}$]
	0	0.5	1	1.5	2	
New method	0.036±0.001	0.048±0.001	0.060±0.001	0.076±0.002	0.088±0.003	0.062±0.003
Conventional method, A	0.053±0.002	0.067±0.004	0.083±0.005	0.102±0.009	0.124±0.016	0.086±0.005
Conventional method, B	0.060±0.002	0.092±0.008	0.147±0.016	0.241±0.033	0.390±0.074	0.186±0.023

In addition, tooth enamel performed better against severe wear damage in greater depths than at the surface level and even better when it was infiltrated with resin. Enamel sectioned before resin embedding (conventional method B) indicated significantly better overall averaged abrasion damage against sharp particles than enamel encapsulated in resin without cutting (conventional method A), 0.186 ± 0.023 (mN $\times 10^{-4}$) and 0.086 ± 0.005 (mN $\times 10^{-4}$), respectively.

Comparing enamel prepared by conventional methods, the overall severe wear of enamel prepared by the new method was only 0.062 ± 0.003 (mN $\times 10^{-4}$) for all indentation depths. Ascertaining enamel resistance to severe damage, enamel alone without infiltration of any media manifested higher vulnerability to the severe wear indicating that tooth enamel was more prone to cracks and fractures.

The experimental results suggested that environment and indentation depth strongly influenced the inhabitation and stabilisation of crack-like defects augmented by a mechanism of stress-shielding, prism-interweaving and self-healing [53]. Although resin embedding may reinforce enamel structure [49], the organic matter may be plasticised and this may result in enhanced severe wear abrasion resistance with increasing indentation depth. The very small volume of proteins in enamel plays a vital role in the crack resistance stability to tooth fracture by closing or gluing cracks within the material [53]. The enhanced toughness with increasing depth may be also due to the increasing interweaved prism-organic matter interplay that leads to enhanced crack shielding ability by subsequent sliding at the interfaces [229].

The resulting values of severe wear parameter for biosilica and dental ceramics are listed in **Table 5-8**.

Table 5-8. Severe wear of laminated biosilica and dental materials represented by proportional resistance parameter to micro-cracking from a sharp abrasive, $K_c^4/H.E^2$ [$\text{mN} \times 10^{-4}$].

Biomaterial	$K_c^4/H.E^2$ [$\text{mN} \times 10^{-4}$]
Dry laminated biosilica, <i>M. chuni</i>	0.86
Dental materials	
Glass-based feld spathic dental ceramics	0.52
Zirconia-based ceramics (yttrium partially stabilised tetragonal zirconia polycrystal Y-TZP)	12.22

The overall mean value of the severe wear parameter, $K_{ic}^4/H.E^2$ of tooth enamel prepared by the new method was found to be significantly lower (i.e., 0.062 ± 0.003 from **Table 5-7**) by a factor of 8, 14 and 200 compared to glass-based ceramics, biosilica and zirconia-based ceramics, respectively (**Figure 5-8**).

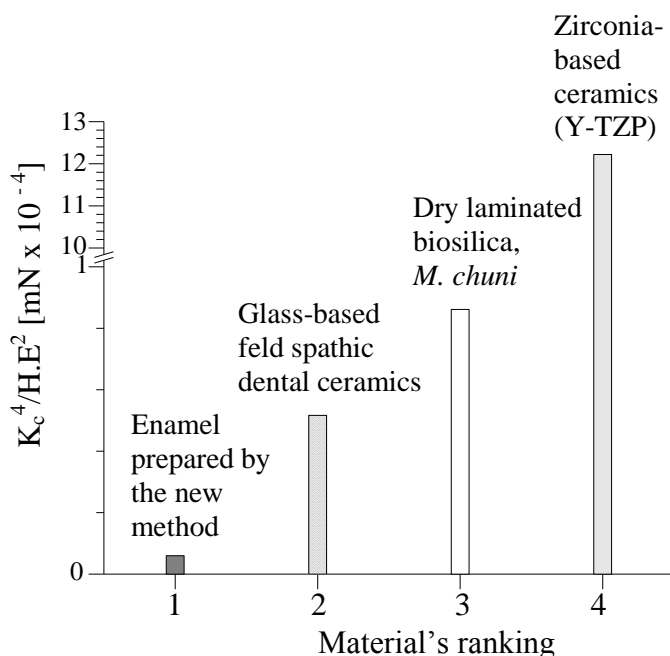


Figure 5-8. Severe wear comparison of enamel prepared by the new method with other biological and dental filling materials.

Notably, the severe wear parameter is strongly dependent on the value of fracture toughness of the material. For instance, for a value of fracture resistance, $K_{ic} = 0.57 \text{ MPa.m}^{1/2}$ [47] (instead of $0.7 \text{ MPa.m}^{1/2}$), the overall severe wear of enamel prepared by the new method decreased from $0.062 \pm 0.003 \text{ MPa.m}^{1/2}$ to $0.027 \pm 0.001 \text{ MPa.m}^{1/2}$.

While evaluating the results of mild and severe wear of tooth enamel to other materials, the mild wear properties of glass-based ceramics and severe wear properties of zirconia-based ceramics showed the most suitable wear characteristics to human tooth enamel. However, abrasion wear parameters are not the only factors that influence the wear between enamel and dental materials. Other variables such as ceramic microstructure, fracture toughness, and contact damage mechanism must also be considered in the overall evaluation and design of novel dental materials [9].

5.5 Conclusion

In conclusion, this chapter proposed a new method of tooth preparation for nanoindentation testing in the wet environment. The experimental E and H results from the new method at constant indentation depths were found to be higher by $14.59 \pm 0.72 \%$ and $4.11 \pm 2.12 \%$, respectively, compared to the conventional method A with a gradually decreasing gradient with increasing indentation depth at one location.

To the best of our knowledge, this is the first study which has attempted to report E and H values of wet and dry enamel at constant indentation depths between the enamel surface (i.e., $0 \text{ }\mu\text{m}$) and $2 \text{ }\mu\text{m}$. Although a careful dehydration and drying process increased E and H by $\approx 4 \%$ and $\approx 7 \%$, respectively, experimental data demonstrated that the E and H differences between dry and wet samples were diminished for tooth enamel prepared by the new method.

Mild wear resistance was analysed with elastic strain to failure ratio H/E to ascertain the effects of resin embedding in sample preparation process. The H/E ratios of mild wear removal for enamel prepared by conventional methods A and B were significantly higher than for enamel prepared by the new method for all indentation depths. The overall ratios showed that resin used during sample preparation had positive effects on the mild wear resistance of enamel with the increasing indentation depth. Notably, there was a decreasing gradient of mild wear resistance with the increasing depth for the new and conventional method A in contrast to conventional method B, which demonstrated an increasing gradient of H/E ratio with the increasing depth. Comparing enamel H/E ratio to other materials, the H/E ratio for enamel was 2.39, 3.59 and 3.3 times less than for radular teeth, laminated biosilica and glass-based ceramics. Zirconia-based ceramics exhibited similar mild wear behaviour to enamel.

This study presented for the first time the results of severe wear of enamel prepared by the new and conventional methods A and B at constant indentation depths between 0 and 2 μm . In contrast to the mild wear resistance of enamel prepared by the new method and conventional method A, which showed a diminutive decrease with increasing indentation depth, the resistance to micro-cracking indicated an opposite trend and increased with indentation depth for the new and conventional methods A and B. It was concluded that enamel performs better against severe wear damage at greater depths and when it is permeated with resin.

6. Effect of preparation methods on enamel microstructure

6.1 Summary

Two enamel specimens prepared by **the new method** and **conventional method A** were used to investigate the detrimental effects of preparation methods on the enamel microstructure. In addition, a tooth prepared by the new method was tested with a Berkovich indenter across the enamel-dentine junction (EDJ) in the wet state and later dehydrated and dried following an appropriate protocol. High resolution SEM images revealed the intact interface with no formation of cracks along or across the EDJ for a tooth prepared by the new method. On the other hand, a split boundary between enamel and dentine as well as a large amount of defects in the form of fissures on the enamel surface were observed for inappropriately dried enamel embedded in resin (conventional method A). This study showed that the new method of enamel preparation combined with Janda's dehydration and drying protocol yielded a preserved, genuine structure of dental tissue.

6.2 Introduction

Badly dehydrated and/or dried human teeth are hard, yet not compact, particularly near the EDJ [29]. Given the ratio of water-protein content for dentine and enamel 30 wt% and 4 wt%, respectively[48], these two distinctively hydrated tissues with very different biomechanical properties are expected to dry differently during dehydration and drying processes [130].

Once tooth specimens are dehydrated and all water replaced by ethanol and later on by acetone, both solvents must be removed in a controlled environment, for instance by using a vacuum desiccator to preserve the tooth structure.

Previous authors have investigated crack propagation across the EDJ with Vickers indents and reported that “the vacuum of conventional SEM sometimes led to cracking either along the line of indents or at/near the optical EDJ due to an inappropriate drying procedure” [21].

Given the unpreserved structure is a probable cause in abrupt changes along the EDJ region, the main objective of this investigation was to provide high resolution images of the EDJ interface for the enamel specimens prepared by the new method (Section 4.1.2) and the conventional method, A (Section 4.1.3).

6.3 Materials and methods

Two human molars were collected and stored following the protocol outlined in Section 4.1.1. One tooth was prepared by **conventional method A** (Section 4.1.3), dehydrated, and then dried following Janda’s approach (Section 4.1.5). The other tooth was prepared by the **new method** (Section 4.1.2) and tested with a Berkovich indenter up to maximum load of 400 mN in the wet environment near the EDJ. Later, this tooth sample was dehydrated, and then dried following Janda’s approach (Section 4.1.5).

The EDJ observation was conducted on coated specimens with 3 nm layer of platinum in a Zeiss SEM. For more details about the test setting apparatus, refer to Section 4.2.3.

6.4 Results and Discussion

SEM images of a human tooth prepared by the conventional method A are shown in **Figure 6-1(a,b)**. In this method, the tooth was dried on the bench before resin embedding. As a result, widespread sets of fractures over the tooth surface and crack formations along the EDJ (**Figure 6-1(a)**) and across the tooth (**Figure 6-1(b)**) were observed.

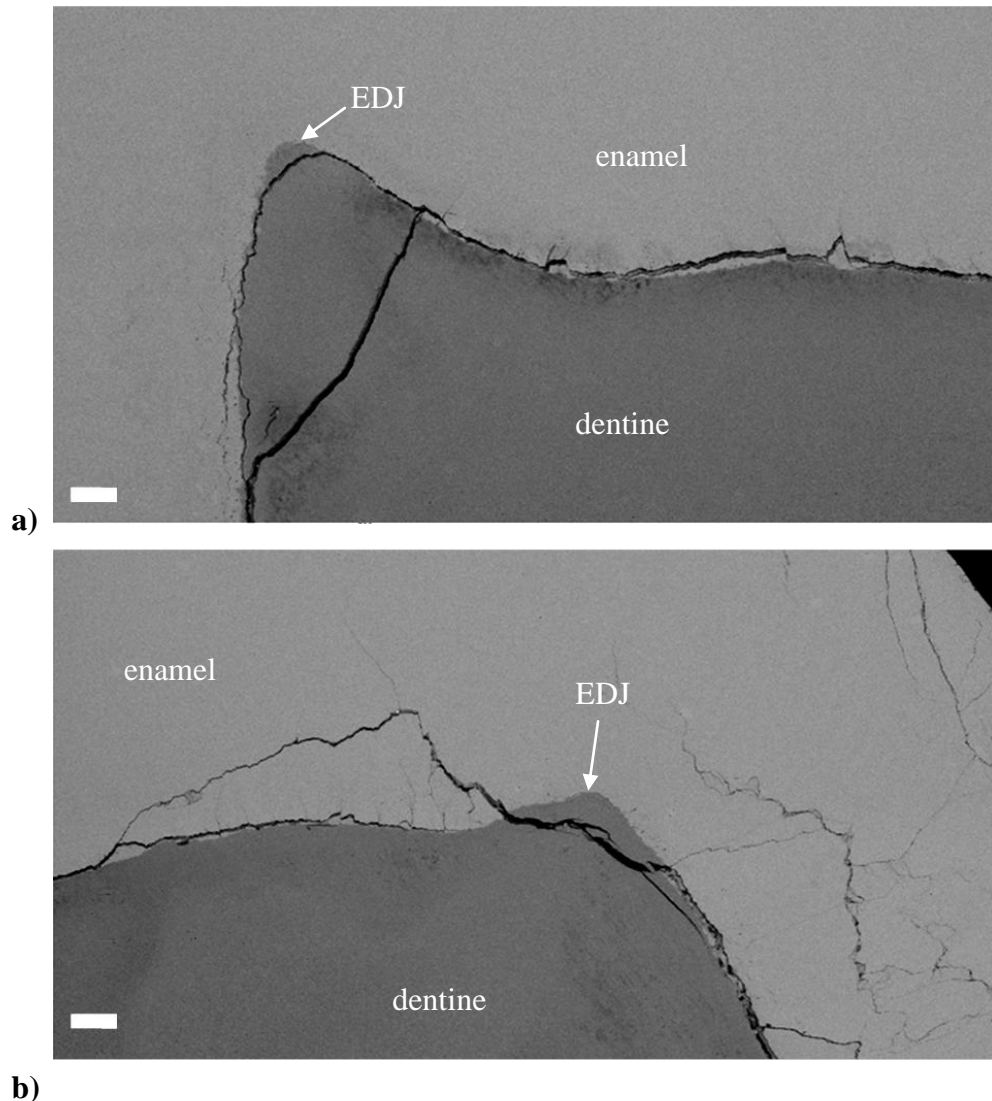


Figure 6-1. SEM images of (a) mesial and (b) distal areas of human molar prepared by a conventional method, A. Detrimental effects of conventional method A on the enamel microstructure are evident. The tooth specimens exhibited artefacts in the form of fractures and cracks along the EDJ. Scale bar = 200 μm .

A split EDJ boundary could be explained by the shrinkage of enamel and dentine due to uneven drying of the tooth during resin solidification. This leads to tension stresses along the EDJ that result in formation of cracks and fractures along the EDJ. By using conventional method A during the enamel preparation process, the EDJ appeared as a weak interface.

On the other hand, while preserving tooth microstructure under a careful dehydration and drying protocol, the genuine EDJ was observed (**Figure 6-2(a,b)**).

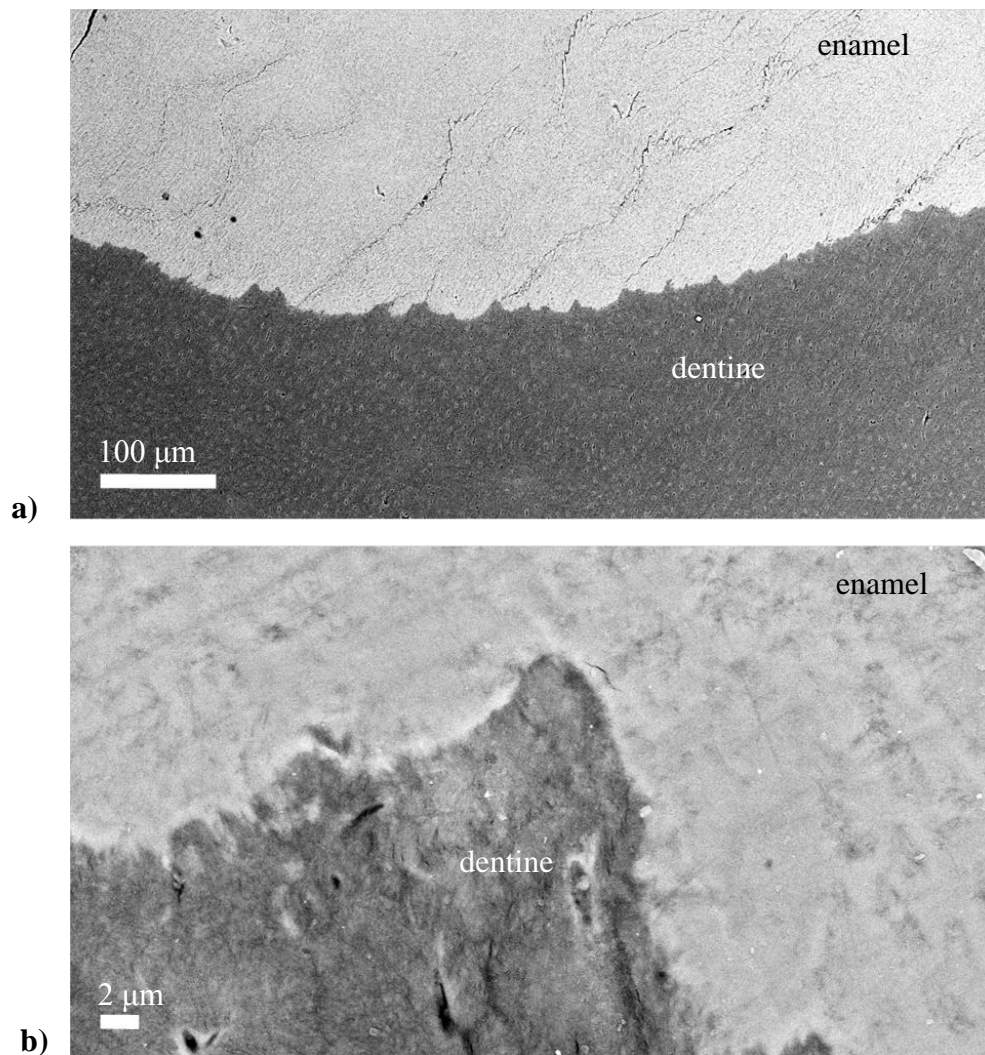


Figure 6-2. Morphological images of the EDJ prepared by the new method.

A scalloped pattern of the EDJ is shown in **Figure 6-2(a)**, with detailed focus in **Figure 6-2(b)**. In addition, the images show the intact EDJ even after multiple Berkovich indents up to a maximum load of 400 mN (**Figure 6-3(a,b)**).

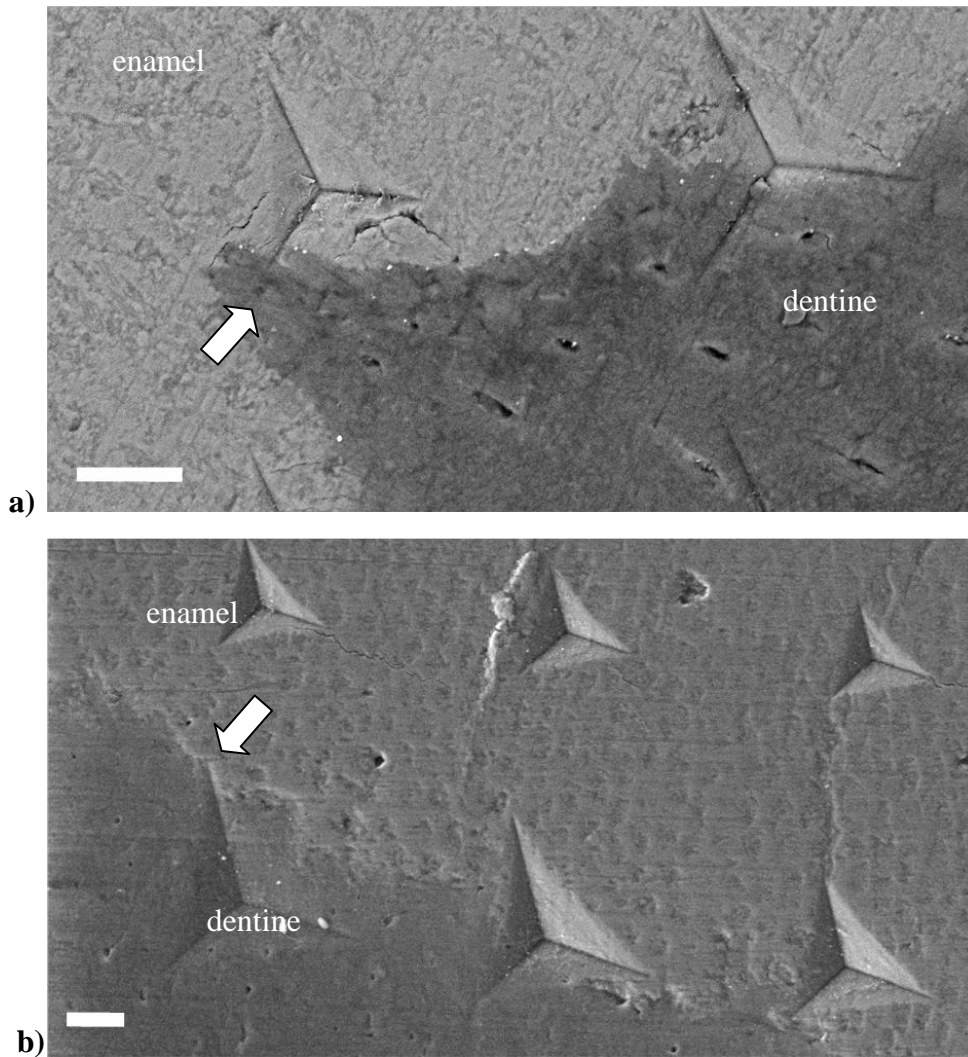


Figure 6-3. SEM images of Berkovich indents of 400 mN load across the EDJ region. Marked with a white arrow in a) and b), the images show no initiations of cracks from the edges of an indent along the EDJ boundary. Scale bar = 10 μm .

While the EDJ is considered as a weak interface due to mismatched properties between enamel and dentine [21], no propagating cracks along the indentation lines in enamel, dentine or at the EDJ were found after multiple indentation lines across the EDJ region up to maximum load of 400 mN (**Figure 6-3(a,b)**). The reason of using a Berkovich indenter was to probe the EDJ interface and see if corner cracks would emanate from the imprints under applied

loads. The absence of the corner cracks was in part associated with the benefits of the new method of the sample preparation.

Although it was previously shown that the role of the organic matrix may play an important role in preventing delamination of enamel and dentine [47], this study suggests that the preserved structure rather than the composition plays a more crucial role in maintaining the integrity of the EDJ. If the dehydration and drying procedure removes, partially or completely, the protein–water content of the tooth tissue [232], a weakened EDJ should be expected [47]. However, in this study, the EDJ remained intact and showed a strong physical interface that was revealed by SEM images.

6.5 Conclusion

This chapter demonstrated that an inappropriate dehydration and/or drying procedure followed by resin encapsulation during the sample preparation process resulted in the fractured EDJ and cracks across enamel. By following the protocol of the new method of tooth preparation, an intact boundary with a strong physical appearance was observed even after multiple indentations with Berkovich indents up to a load of 400 mN.

The features of the scalloped interface combined with gradual decreasing changes in mechanical properties are critical in designing novel hard coating materials in the field of nanotechnology where joining of two materials with two mismatched mechanical properties is of significant. A comprehensive modelling mechanism of the EDJ from the nano- to macro-scale is the topic of on-going investigation.

7. Elastic behaviour of tooth enamel

7.1 Summary

The relationship between the elastic behaviour and microstructure of enamel during loading was investigated under fully hydrated conditions. Young's modulus of enamel, E , was determined at constant depths according to the newly developed method of data analysis and simulated with a mechanical model. This model linked the depth-dependent modulus to the contact-induced microstructural evolution, i.e., to the change of the effective crystal orientation angle. The angle was found to be $\sim 45^\circ$ and could aided shear sliding in enamel by which the stress build-up was relieved.

7.2 Introduction

Being the hardest tissue in human body, tooth enamel is built to last [51]. The load-bearing capacity of enamel is governed by its unique ultrastructure that comprises well-organised hydroxyapatite (HAP) platelets glued together by protein matrix (**Figure 2-5**) [5]. The E value is commonly used to define the enamel resistance to deformation. Treated as a hybrid laminate at small scales [6, 111], enamel modulus is determined not only by the volume fraction and properties of its constituents, but also by the orientation of the mineral crystals [7].

The E of enamel is determined by depth-sensing indentation (DSI, often named nanoindentation) [139, 203]. Notably, E values of enamel reported in the literature vary considerably, where typical ranges from 50 to 120 GPa are found [18]. The observed variation in E stems from inconsistencies in measured location, testing environment (i.e., dry or hydrated) and sample condition (i.e., young or aged tooth) [18, 24-27]. Nevertheless, Zhou and Hsiung [36] showed

that the E of enamel decreases incessantly with increasing indentation depth even at a fixed location. They suggested that it is necessary to establish a direct link between the changing modulus and microstructural evolution of enamel during mechanical contact in order to better understand its function.

Given the dependence of E of enamel on the penetration depth, it is essential to conduct measurements at constant depths when interrogating the E of enamel across its thickness. Unfortunately, most DSI tests are performed under load control (i.e., constant loads), making it difficult to compare the modulus values obtained from different samples and regions, where indentation depths may differ [36-38]. Moreover, although the testing condition is known to affect the mechanical properties of enamel [23, 26], the majority of DSI tests are carried out on either dried samples or ‘wet’ specimens that were once dried during preparation [18, 39].

In the current study, an in-depth investigation of the elastic behaviour of enamel under the influence of mechanical loads was conducted. Enamel samples were prepared and tested in the fully hydrated state. E of enamel was measured in two different ways: from the surface to the enamel-dentine junction (EDJ) at constant depths and at a fixed location to different depths. The indentation size-dependence of E in the middle region of enamel was analysed using a mechanistic model with respect to its microstructure characteristics.

7.3 Materials and methods

- *Sample preparation and testing*

Two human molars were collected and stored according to the protocol given in Section 4.1.1. Teeth were prepared by the new method (Section 4.1.2) and tested with a Berkovich indenter from the occlusal surface towards the EDJ following the test settings given in Section 4.3.4. Later, the middle region of

tooth enamel was selected as the representative area for analysing E values with increasing depths.

- *Statistical analysis*

A one-way analysis of variance (ANOVA) was employed to verify whether there were any significant statistical differences between the E of enamel with increasing indentation depths. An ANOVA result was deemed significant if the p-value was less than 0.05, after which a Bonferroni post hoc test was implemented to determine the level of indentation load that results in a significant change in the E of enamel.

- *Microstructural observation*

Transmission electron microscope (TEM) images were taken according to the protocol described in Section 4.2.2.

- *Finite element analysis modelling*

Finite element models (FEM) were constructed to clarify the effect of shear deformation on the magnitude and distribution of contact-induced stress in enamel by using the COMSOL software. For more details, refer to Section 4.4.1.1.

7.4 Results and discussion

Load-displacement curves of enamel show that the resistance to deformation varies in enamel (**Figure 7-1(a-c)**). The contact indentation depth, h_c , measured at the enamel occlusal surface gradually increased towards the EDJ, suggesting that enamel becomes less stiff towards the inner region. This observation agrees with findings presented in Chapter 5. In addition, the overall indentation depth, h_t , increased from the occlusal surface towards the EDJ by 6.11 ± 1.42 % (Appendix K).

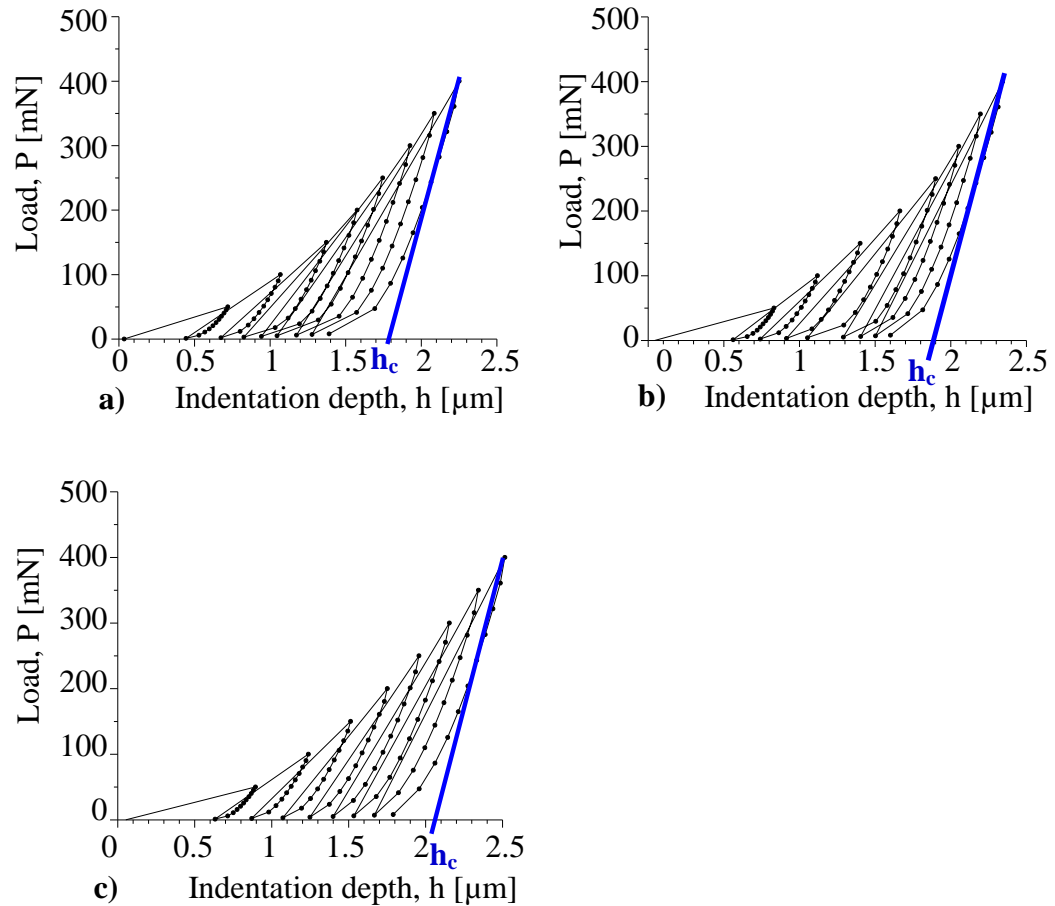


Figure 7-1. A typical illustration of the indentation load, P , as a function of a displacement (i.e., indentation depth), h , of enamel produced by a Berkovich indenter in regions: (a) near the enamel occlusal surface, (b) in the middle and (c) close to the EDJ. The contact depth, h_c , was estimated to be $\sim 1.8 \mu\text{m}$, $\sim 1.9 \mu\text{m}$ and $\sim 2.1 \mu\text{m}$ in (a), (b) and (c), respectively.

As discussed previously in Chapter 5, E decreased with the increasing distance from the enamel occlusal surface as well as with increasing indentation depths. The change of the elastic behaviour of enamel can, in part, be attributed to the variation in the concentration of calcium and phosphate from the surface towards dentine [18, 91]. Notably, a similar E decrease from the enamel occlusal surface towards the EDJ has been observed previously [36, 37], leading to the identification of enamel as a functionally graded material [54].

One of the objectives of this work was to illustrate that the E value varies with changing depths. However, it was extremely difficult to measure E exactly at a specified depth under controlled load, and hence, a direct comparison of E among the pre-determined depths was not a viable option. Alternatively, one could approach the problem by investigating whether there is a difference in E at various loads, which can then be translated to the corresponding depths. To begin with, the link between the indentation load and depth was explored for the middle region of enamel. As expected, larger loads led to greater depths (**Table 7-1**). On average, a load of 50 mN yielded an indentation depth of 0.80 μm , which steadily increased to 2.41 μm at a load of 400 mN.

Table 7-1. Mean indentation depth, h of five indents (from one indentation row) measured from the middle region (i.e., a normalised distance of 0.50) of enamel at various loads.

Load (mN)	Mean depth (μm)		
	Specimen 1	Specimen 2	Overall
50	0.81	0.79	0.80
100	1.17	1.15	1.16
150	1.44	1.42	1.43
200	1.68	1.67	1.68
250	1.91	1.87	1.89
300	2.10	2.07	2.09
350	2.26	2.24	2.25
400	2.42	2.40	2.41

The legitimacy of this approach was confirmed by a Pearson correlation analysis between the indentation load and depth (**Table 7-2**), which indicated that there was a strong linear and positive correlation ($r > 0.98$). Consequently, translating a load into a depth was a fairly straightforward process, which involved the linear interpolation of the mean depth values given in **Table 7-1**.

Table 7-2. Linear association between indentation load, P and depth, h_t .

Tooth	Pearson Correlation r
Specimen 1	0.987
Specimen 2	0.991

A simple exploratory analysis was initially carried out to provide the mean and standard deviation (**Table 7-3**) of E measurements at five indents taken from a single indentation row, which was located in the middle region of enamel.

Table 7-3. Mean \pm standard deviation of E modulus at five indents (from one indentation row) measured from the middle region (i.e., a normalised distance of 0.5) of enamel.

Load (mN)	Mean \pm St. Deviation	
	Specimen 1	Specimen 2
50	95.70 \pm 2.88	97.54 \pm 1.91
100	92.91 \pm 3.82	95.14 \pm 2.64
150	89.70 \pm 2.28	93.13 \pm 1.17
200	88.53 \pm 2.47	92.29 \pm 0.80
250	86.71 \pm 2.72	92.19 \pm 1.12
300	85.59 \pm 2.72	91.38 \pm 0.89
350	85.13 \pm 3.59	90.36 \pm 0.90
400	82.65 \pm 1.98	89.12 \pm 0.76

The middle region was defined by a normalised distance of 0.5 from the enamel occlusal surface. The preliminary results from **Table 7-3** indicated that there was a systematic reduction in E with increasing load (and hence, increasing depth). On average, the difference in E between loads of 50 and 400 mN was approximately 13 and 8 GPa, respectively, for tooth specimens 1 and 2. It must be noted here that the E values presented in **Table 7-3** for the middle region of tooth enamel are slightly higher than the values reported in **Figure 5-2(a)** for the same region. As there are great variations between and within human teeth, the

different E values could be explained by different samples used in this part of the study.

The results of the ANOVA indicated that there was a significant difference ($p < 0.001$) among the indentation loads in E values of enamel for the two tooth specimens. Subsequently, a Bonferroni post hoc test was implemented to determine the level of indentation load that resulted in a significant reduction in E of enamel. The results of the post hoc test are presented in **Table 7-4**.

Table 7-4. *P*-values for the comparisons of E moduli values measured at various loads against that obtained at the maximum indentation load of 400 mN. As previously shown, load is strongly correlated with indentation depth, thus these comparisons are also depth comparisons.

Load	<i>P</i> -value	
	Specimen 1	Specimen 2
50	< 0.001	< 0.001
100	< 0.001	< 0.001
150	0.007	0.002
200	0.040	0.018
250	0.452	0.024
300	> 0.500	0.468
350	> 0.500	> 0.500
400	> 0.500	> 0.500

The Bonferroni post hoc test revealed that, with the exception of specimen 2 at load 300 mN, there were no significant differences in E at loads 300 to 400 mN ($p > 0.05$), which translates to a ~2.09 to ~2.41 μm mean indentation depth. However, at lighter loads (i.e. < 250 mN or < 1.89 μm depth), the E of enamel began to significantly differentiate itself from that obtained at 400 mN ($p < 0.05$). With *p* values of less than 0.001, there was strong evidence to suggest that E at a load of 50 mN (0.80 μm overall mean depth) was substantially greater than that at a load of 400 mN (2.41 μm overall mean depth) for both tooth specimens. The results strongly agreed with Zhou et al. [36], who stated that the E values do

vary with changing depth. Additionally, the previous results showed (Chapter 5) that the E reduced with increasing depth in human tooth enamel over its entire thickness, i.e., from the occlusal surface toward the EDJ.

The changes of E with the indentation depth in a fixed location of enamel were analysed with a mechanical model. This model was built from the observation (**Figure 7-2(a,b)**) that enamel exhibits a staggered mineral-protein structure, in which the mineral crystals could rotate to accommodate the deformation [36].

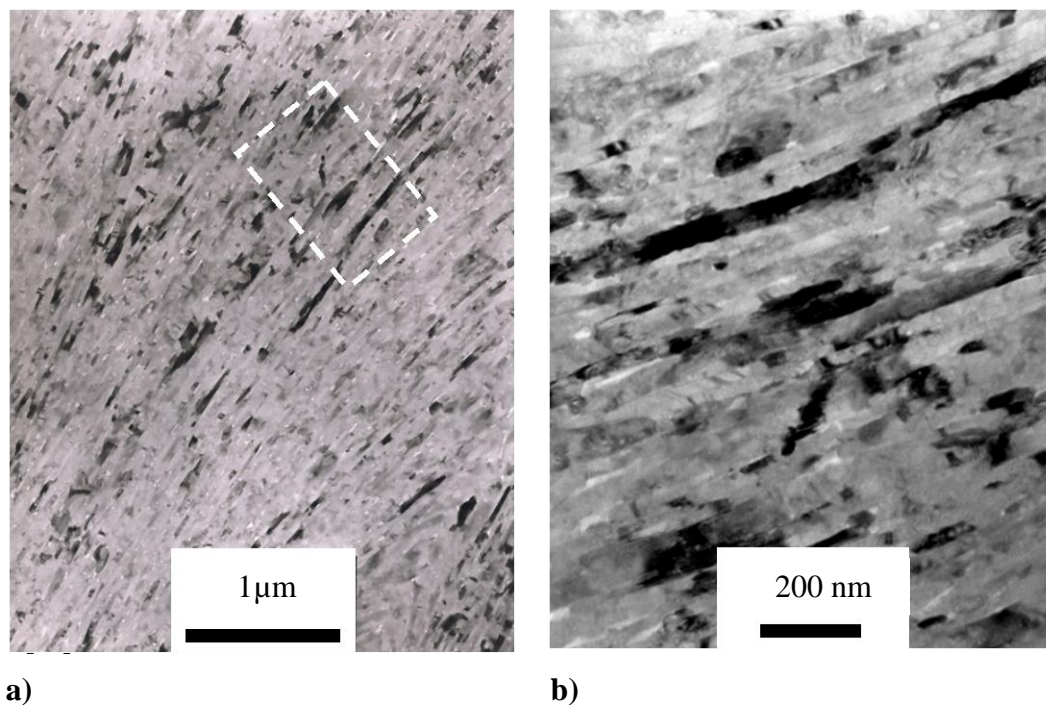


Figure 7-2. Transmission electron micrographs of (a) tooth enamel prepared parallel to the direction of the rods, (b) an enlarged view of circled area in (a). Courtesy of Dr. Z. Xie.

According to the analytical model (Sections 2.8.2 and 4.4.2.1), the E of enamel in its elastic region is calculated as $E_e = \frac{(\cos^2\theta - \sin^2\theta)^2}{\sin^4\theta} E_2 + 4 \frac{\cos^2\theta}{\sin^2\theta} G$. By using structural and mechanical properties of the main constituent of enamel, i.e., mineral and protein from **Table 4-3**, the shear modulus of the mineral-protein

component, G , and the modulus perpendicular to the c axis of mineral crystal, E_2 , were calculated (**Table 12-28** in Appendix L). Later, the effective crystal orientation angle was defined for the E moduli measured at different indentation depths at a location in the middle region of enamel for the loads between 50 and 400 mN (**Table 7-5**). The results showed that when the overall mean penetration depth increased from ~ 0.80 to ~ 2.41 μm (**Table 7-1**), the effective crystal orientation angle changed from ~ 44 to ~ 48 degrees (**Table 7-5**). The resulting values of the angle calculations for specimen 1 and specimen 2 can be found in Appendix L: **Table 12-29** and **Table 12-30**, respectively.

Table 7-5. The change of E in the middle region of enamel governed by the tilting of mineral crystals (angle $\theta \pm$ standard deviation) during deformation.

P [mN]	Specimen 1			Specimen 2		
	E [GPa]	θ°		E [GPa]	θ°	
50.00	95.70 \pm 2.88	44.59	+0.27 -0.26	97.54 \pm 1.91	44.85	+0.44 -0.41
100.00	92.91 \pm 3.82	44.94	+0.41 -0.38	95.14 \pm 2.64	45.28	+0.66 -0.58
150.00	89.70 \pm 2.28	45.25	+0.19 -0.18	93.13 \pm 1.17	45.83	+0.43 -0.39
200.00	88.53 \pm 2.47	45.38	+0.13 -0.13	92.29 \pm 0.08	46.04	+0.49 -0.44
250.00	86.71 \pm 2.72	45.40	+0.19 -0.18	92.19 \pm 1.12	46.40	+0.59 -0.52
300.00	85.59 \pm 2.72	45.53	+0.15 -0.15	91.38 \pm 0.89	46.63	+0.63 -0.55
350.00	85.13 \pm 3.59	45.71	+0.16 -0.16	90.36 \pm 0.90	46.74	+0.87 -0.73
400.00	82.65 \pm 1.98	45.93	+0.14 -0.14	89.12 \pm 0.76	47.32	+0.53 -0.47

Recently the effective crystal orientation angle has been identified as the critical variable, among others, that regulates the mechanical behaviour of enamel [105]. Using this concept, a deeper understanding of the elastic behaviour of enamel was developed in this work, that is, the decrease of E of enamel with

the increase of the indentation depth was governed by the rotation of the mineral-protein laminate assembly under the mechanical loading (**Figure 7-3**).

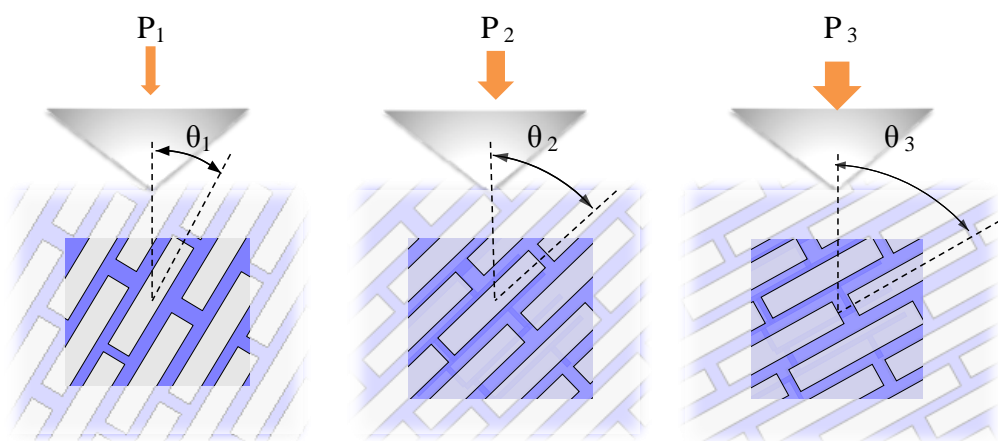


Figure 7-3. Schematic illustrations showing the responses of mineral crystals to increasing indentation loads from P_1 to P_3 (i.e., the increasing severity of deformation) by changing the effective crystal orientation angle from θ_1 to θ_3 , resulting in a change in E in the middle region of enamel.

The findings of a decreasing pattern of E from the occlusal surface of tooth enamel to the EDJ were previously related to the mineral and organic content or decussation. In general, the content of calcium and phosphorus decreases from the surface to the EDJ, while the protein content increases in this direction (Chapter 2). This reflects the decrease of E values from the surface to the EDJ (Chapter 5). In addition, this study revealed that the effective crystal orientation angle changes under applied loads with increasing depths. The relationship between E findings and the effective crystal orientation angle was also analysed by a physical model in this study for the middle region of tooth enamel. Note this nanoscale model simplified the prism decussation pattern of tooth enamel in order to observe the changes of E values and the effective crystal orientation angle for one region/one location.

According to the Hook's Law, a reduction in E would slow down or even reduce the rise of contact-induced stress in enamel, compared to the conventional material having a constant modulus. By doing so, the load-bearing ability would increase. In addition, it is interesting to note that the calculated values of the effective orientation angle are about 45° . A mechanistic model was used to rationalise the adoption of such an effective angle in the enamel structure (**Figure 7-4**).

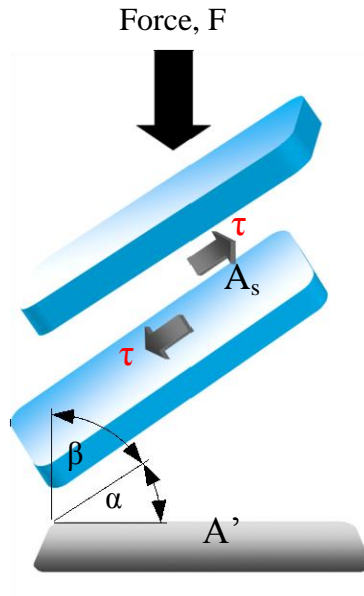


Figure 7-4. Model of shear deformation between mineral crystallites. Note that A' is the projected area of a mineral platelet having a surface area of A_s onto the horizontal plane, τ is the shear stress, and α , β are the angles that the platelets make with the horizontal and vertical directions, respectively.

According to the model, the shear stress, τ can be expressed as:

$$\tau = \frac{1}{2} \sigma \sin 2\alpha \quad (7-1)$$

where σ is the normal stress expressed as a force divided by an area. The shear deformation between mineral crystals is essential for the remarkable damage tolerance observed in enamel [6, 111]. To enable such shear process, the shear

stress developed between the mineral crystals should be maximised through the optimisation of the effective crystal orientation angle. Therefore, to meet this requirement, the effective crystal orientation angle should be close to 45° , which is consistent with what the model revealed (**Table 7-5**).

FEA simulations were performed to elucidate the benefit of shear deformation to enamel mechanical function. Compared to the ‘purely elastic’ model (i.e., without considering the shear process) (**Figure 7-5(a)**), a reduction in the maximum shear stress from 5.5 to 5.0 GPa, was observed, when the shear effect was taken into account (**Figure 7-5(b)**).

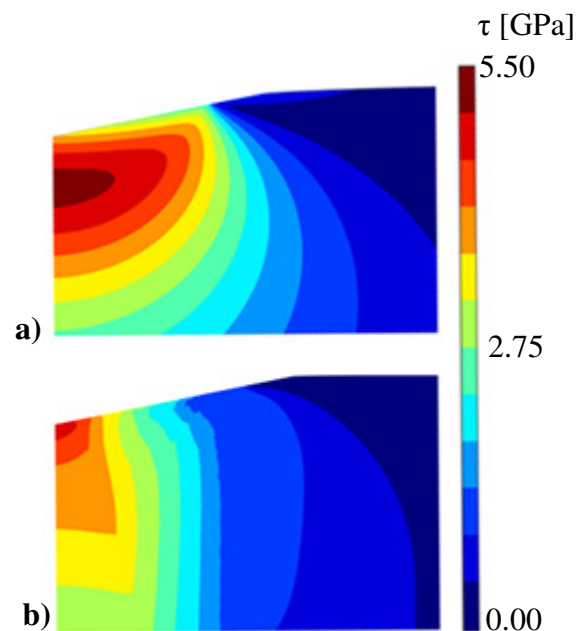


Figure 7-5. The shear stress distribution generated in enamel by indentation at a depth of $0.28\ \mu\text{m}$: (a) perfect elastic model and (b) shear sliding enabled model.

Additionally, the stress distribution pattern was also modified under shear deformation; the volume populated by larger stress was reduced significantly (**Figure 7-6**). For example, the volume acted by the stress level $> 3.5\ \text{GPa}$ was reduced by more than 70 % when the shear was enabled, and the volume influenced by the stress level $> 4.5\ \text{GPa}$ almost diminished when the shear was

considered. Consequently, the decrease of stress level and reduction of material volumes subjected to higher stresses, resulting from the shear deformation between mineral crystals, could further enhance the load-bearing ability of enamel.

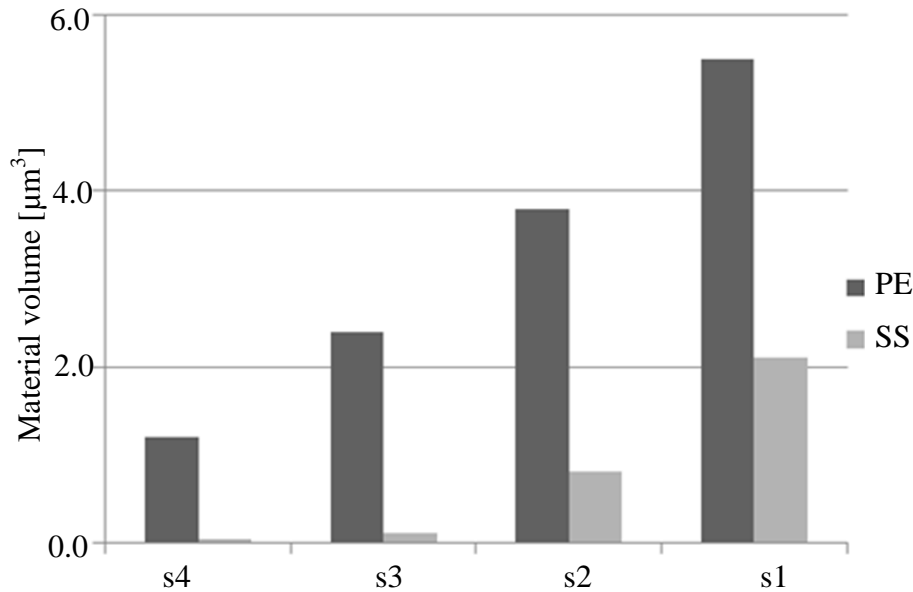


Figure 7-6. The size of regions under the influence of shear stresses greater than (s1) 3.0 GPa, (s2) 3.5 GPa, (s3) 4.0 GPa and (s4) 4.5 GPa, calculated from the FEM simulations. Note that ‘PE’ stands for the perfect elastic model and ‘SS’ for the shear-sliding model.

Notably, there are some shortcomings of this study that are important to discuss. The results of modelling showed that the crystal orientation is one of the important variables which could contribute to reduction of the enamel stiffness under indentation loading by the rotation; however, there are other factors involved that may contribute to the change of E with increasing depth, i.e., the level of observation, anisotropy of E moduli and orientation of mineral crystals [112], prism orientations [107], level of hierarchy [3], the shape of the tooth crown and morphology of the enamel cap [49], thickness and shape [186], gradient in mechanical properties [50], increasing organic content from the occlusal surface towards EDJ [5], as well as micro-cracking mechanism [50]. Although a micro-cracking mechanism could affect resulting values of the angle

θ due to loads higher than 200 mN [50, 105], no cracks or fractures have been observed under applied loads of 400 mN for the middle region of enamel (**Figure 12-6**). On the other hand, larger indents induced by higher loads could also be a concern as the indents may easily involve more than one crystal or prism, and thus greater organic content may lead to the decreased values of E moduli. Despite all limitation listed above, this study contributed to the identification of the effective crystal orientation angle as another variable that affect the remarkable resilience of tooth enamel in its elastic region. However, more investigations are needed to explore the application of this concept across the thickness of enamel when other factors are also involved.

7.5 Conclusion

By combining depth-sensing indentation tests and modelling, this study has shown that the change of E with increasing indentation depth was directly linked to the tilting of mineral crystals in the middle region of enamel. The results also showed that the effective crystal close to 45° facilitated the shear-sliding of mineral crystals during loading and was essential for the mechanical resilience of enamel. FEM revealed that the shear deformation not only lowered the stress level, but also reduced the size of material volumes subjected to larger stresses.

The present work is expected to renew interest towards understanding the mechanical characteristics of biological materials that often assume a laminate structure, through which additional design guidelines can be formulated for developing robust load-bearing materials.

8. Effect of microstructure on plastic behaviour of tooth enamel

8.1 Summary

Enamel, the outer layer of the tooth, has evolved over millions of years to perfect its mechanical function. The functionally gradient design of enamel has been extensively studied, which has been identified among other strategies to be crucial for its remarkable resilience during mechanical loading. However, another important mechanism through which the excellent mechanical properties of enamel is realised, the loading dependence of mechanical properties, has not yet been fully understood. Here experimental results which confirmed that the hardness, H , and yield strength, σ_y , of enamel decreased with increasing compressive loading are presented. Finite element models (FEM) revealed a significant reduction of stress level within enamel, resulted from the observed strain softening. This was attributed to the loading adaptive structure of enamel, i.e., through a change in the micro-fibril angle in enamel. Loading dependent σ_y was proved to play a key role in the observed stress reduction. It is envisaged that this work will stimulate in-depth investigations on the local mechanical behaviour of both natural and synthetic composites, and provide a fresh, important guide in the development of bio-inspired materials.

8.2 Introduction

The mechanical properties of tooth enamel, the outer layer of the tooth, have been a topic of great scientific and evolutionary interests [40, 41]. As one of the most inspiring properties, enamel only has a fracture toughness which is comparable with that of glass, yet it is designed to survive millions of functional contacts over a lifetime of the host individual. As such, it is often depicted as a smart biocomposite, which is highly resistant to cumulative deformation and

fracture [53]. The exceptional characteristic of damage tolerance of tooth enamel is also reflected by the substantial overloads required to drive any developing cracks to ultimate fracture, even though tooth enamel contains a multitude of microstructural defects that can act as sources of fracture [40]. The primary composition of enamel is hydroxyapatite (HAP). However, the indentation stress–strain curves and creep behaviour of enamel are totally different to HAP. Rather, enamel has mechanical properties similar to those of metals, not ceramics [54]. As one of the most durable natural materials, it has attracted increasing attention in the quest for advanced hard and tough composite materials [54, 233, 234].

Traditionally, tooth enamel was thought to be non-regenerative. However, strong experimental evidence from recent studies indicated that this material is capable of back-creeping, and even limited self-healing [53, 54]. Based on observations from the *ex situ* loading of human and sea otter molars, a microstructural mechanism of damage resistance was proposed. The ability of tooth enamel to absorb considerable damage over time without catastrophic failure was explained by a microstructural mechanism of damage resistance, in conjunction with the capacity of the tooth configuration to limit the generation of tensile stresses in largely compressive biting [53]. The microstructure of tooth enamel can be treated as a hybrid laminate that comprises long HAP mineral platelets held together by a thin layer of proteins [6, 111]. The mechanical properties of this structured biomaterial are determined not only by the volume fraction and properties of its components, but also by the orientation of its layered assembly [7].

It has been demonstrated previously in Chapter 5 and Chapter 7 that the H and elastic modulus, E , of human enamel were dependent on the indentation depth. This effect was attributed to the evolution within the microstructure during loading process (Chapter 7). However, the effect of loading dependence of E and

H on the stress distribution and load carrying capability of tooth enamel require further investigation.

This work aimed at investigating the implications of loading dependent mechanical variables. Experimental works were carried out using nanoindentation, and the results were analysed with the help of FEM. It has been found that the load-dependent variables play an important role in “loading adaptive structure”, which, in conjunction with the self-healing property, formed one of the key mechanisms which fulfilled the excellent property of exceptional resilience of tooth enamel.

8.3 Materials and methods

- Sample preparation and testing

Three teeth were used in this study. Teeth were collected and stored following the protocol in Section 4.1.1. The tooth samples were prepared by the new method (Section 4.1.2) and tested with a Berkovich indenter from the occlusal surface towards dentine according to the protocol given in Section 4.3.4. The occlusal surface was selected as the representative area in this study.

- FEM

COMSOL software was used in this work to evaluate deformation and stress distributions of tooth enamel under applied load. Physical variables of enamel, including E and σ_y at different indentation depths obtained from the experiment, are given in the Results section. More details about the simulation test settings can be found in Section 4.4.1.2.

8.4 Results and discussion

Nanoindentation experiments were carried out in order to obtain the mechanical variables for further FEM. Results obtained from extrapolation of load-depth-E-H results to the constant indentation depths indicated that E reduced with increasing indentation depth (**Table 8-1**), which was attributed to the changing fibre-angle in the enamel microstructure (Chapter 7).

Table 8-1. Experimental results of mechanical properties of enamel obtained from extrapolation of nanoindentation results.

Physical variables	Indentation depth [μm]		
	0.5	1.0	2.0
Indentation load (mN)	24.59 (± 5.05)	81.99 (± 1.37)	288.30 (± 4.17)
Young's modulus (GPa)	103.48 (± 0.26)	94.13 (± 0.44)	87.41 (± 0.80)
Hardness (GPa)	4.71 (± 0.03)	4.30 (± 0.05)	3.73 (± 0.04)
Yield strength (GPa)	1.57 (± 0.03)	1.43 (± 0.05)	1.24 (± 0.04)

Load-displacement curves of enamel showed that enamel becomes less stiff towards the inner region (**Figure 7-1**). The functionally graded properties of enamel were also observed in previous works [37, 54], and partly attributed to the variation in the chemical concentration of calcium and phosphate from the surface towards dentine [18, 54, 91].

For indentation depths of 0.5, 1 and 2 μm , the average H values were ~ 4.71 , ~ 4.30 and ~ 3.73 GPa, respectively (**Table 8-1**), which fall within one standard deviation of the corresponding measurements recorded previously [36]. This was in contrast to the E values which were found significantly higher for each indentation depth. The σ_y value at different indentation depths was derived as one third of the experimental H values. Notably, following the load dependence of the H, σ_y is also a function of the indentation depth (**Table 8-1**).

To clarify the effect of changes in E and σ_y as a function of indentation depth on the stress distribution within enamel, loading conditions at three different indentation depths, 0.5, 1.0 and 2.0 μm , labelled as model 1, 2 and 4, respectively (**Table 8-2**), were modelled using the corresponding E and σ_y values which were obtained from the current experiments.

Table 8-2. Physical variables (\pm standard deviations) used in the FEM simulations.

Variable	Model				
	1	2	3	4	5
Indentation load, L [mN]	24.59 (± 5.05)	81.99 (± 1.37)	81.99 (± 1.37)	288.30 (± 4.17)	288.30 (± 4.17)
Effective elastic modulus, E [GPa]	103.48 (± 0.26)	94.13 (± 0.44)	103.48 (± 0.26)	87.41 (± 0.80)	103.48 (± 0.26)
Yield strength, σ_y [GPa]	1.57 (± 0.03)	1.43 (± 0.05)	1.57 (± 0.03)	1.24 (± 0.04)	1.57 (± 0.03)

The loads to produce these three indentation depths in enamel were found to be 24.59 (± 5.05), 81.99 (± 1.37), and 288.30 (± 4.17) mN, respectively (**Table 8-1**). A bi-linear elastic-plastic model using von Mises criteria was assumed, and the isotropic tangent value used in the simulation was 2 GPa, which was obtained by calibrating the simulating results using experimental data.

For comparison purposes, simulations on two further models, model 3 and model 5, were also presented. For these two models, a hypothetical material, comparison material 1, was assigned. These had constant E and σ_y values being equal to those of model 1, which were the experimental values obtained at 0.5 μm indentation depth. The indentation loads for models 3 and 5 were identical to those used for the models 2 (81.99 (± 1.37)) and 4 (288.30 (± 4.17)), respectively (see **Table 8-2**).

Contour plots of different stress components are shown in **Figure 8-1(a-c)**.

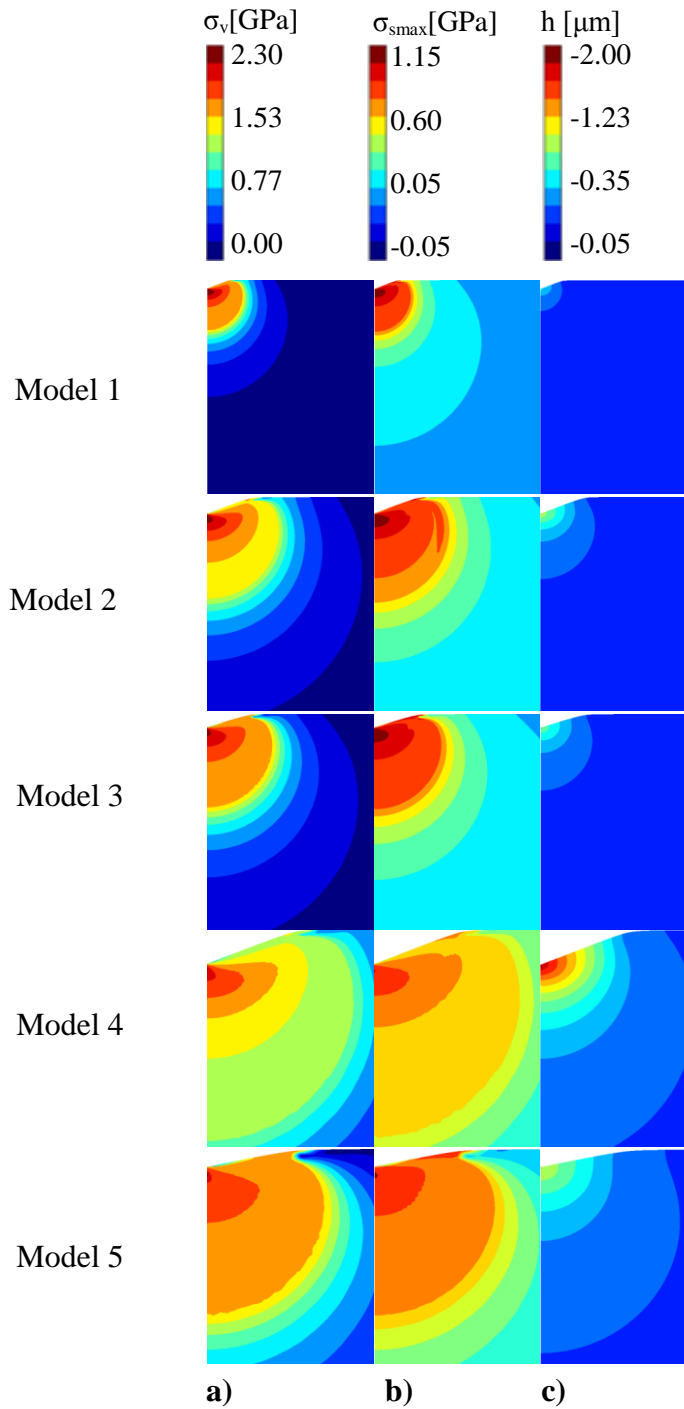


Figure 8-1. Contour plots of stress distributions induced by a Berkovich indenter at 288.30 (± 4.17) mN obtained via FEM simulations. (1) – (5) represent models 1-5 (see **Table 8-2**). FEM prediction of a) von Mises stress field σ_v , b) maximum in-plane shear stress σ_{smax} , and c) contours of the vertical displacement h . Note that the σ_{smax} is defined as $(\sigma_1 - \sigma_3)/2$, where σ_1 and σ_3 are the first and the third principal stresses, respectively, both of which are within the simulation plane.

A comparison between models 2 and 3, as well as between 4 and 5, revealed that under the same load, the real tooth material, enamel (models 2 and 4), had a larger deformation (**Figure 8-1(c)**), but with a substantially smaller stress level, compared to that within the comparison material (models 3 and 5), respectively. This was more evident for the von Mises stress (σ_v) (**Figure 8-1(a)**) and the maximum in plane shear stress (σ_{smax}) (**Figure 8-1(b)**), which more clearly indicated the degree of destructive level of the stress in the material. It is also interesting to note that, due to the reducing σ_y with the increasing indentation depth, reductions of the levels in σ_v and σ_{smax} were observed (comparing model 3 and 5 in **Figure 8-1(a,b)**), while the areas affected by these stresses increased. In other words, stress was more evenly distributed in tooth enamel than in the comparison material. As such, enamel showed less stress levels and better integrity over conventional materials under the same loading conditions, particularly when large deformations were induced. Furthermore, under the same 288.30 (± 4.17) mN load, the maximum strain within tooth enamel was $\sim 30\%$ higher, as compared to that in the comparison material 1 (**Figure 8-2(a,b)**), and the indentation depth (h-displacement) was also larger in enamel (**Figure 8-2(c,d)**).

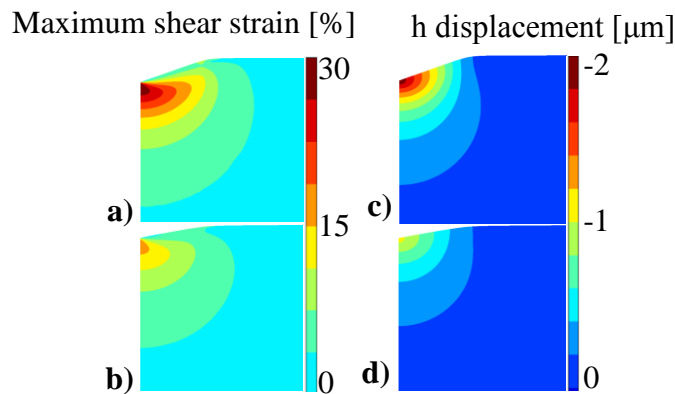


Figure 8-2. Maximum equivalent strain in (a) enamel, indentation loading 288.30 (± 4.17) mN, (b) comparison material 1, the same indentation loading; and the h-displacement (c) enamel, indentation loading 288.30 (± 4.17) mN, (d) the comparison material, the same indentation loading.

Although the elastic strain limit is only 0.1 for most materials, it has been shown that in tooth enamel the highest shear strain near the edge of the contact area could be as high as 0.48, since the initial inelastic deformation comes from the protein layer [111].

This study demonstrated that changes in two variables, E and σ_y , resulted in a “strain softening” mechanism in enamel which significantly reduced the stress level under the same loading condition. In order to determine which variable (i.e., E , or σ_y) played the more important role in this mechanism, models with two more comparison materials, comparison materials 2 and 3, were simulated. The former used the experimentally obtained E for different indentation depth and a constant σ_y , while the latter used a constant E , but the experimentally obtained σ_y (see **Table 8-3**).

Table 8-3. Mechanical properties of enamel and comparison materials used in FEM simulations.

Mechanical property:	Elastic modulus, E [GPa]	Yield strength, σ_y [GPa]
Enamel, 0.5 μm depth	103.48 (± 0.26)	1.57 (± 0.03)
Enamel, 1.0 μm depth	94.13 (± 0.44)	1.43 (± 0.05)
Enamel, 2.0 μm depth	87.41 (± 0.80)	1.24 (± 0.04)
Material 1	103.48 (± 0.26)	1.57 (± 0.03)
Material 2	87.41 (± 0.80)	1.57 (± 0.03)
Material 3	103.48 (± 0.26)	1.24 (± 0.04)

The simulation results are presented in **Figure 8-3(a-d)**. The models showed that the change in σ_y played a decisive role for inducing the observed strain softening effect, while the effect of E was insignificant. For example, a $\sim 17\%$ change in E only resulted in a change of $\sim 3\%$ in the equivalent stress, while a $\sim 20\%$ change in σ_y induced a change of $> 50\%$ in the equivalent stress (**Figure 8-3(e)**).

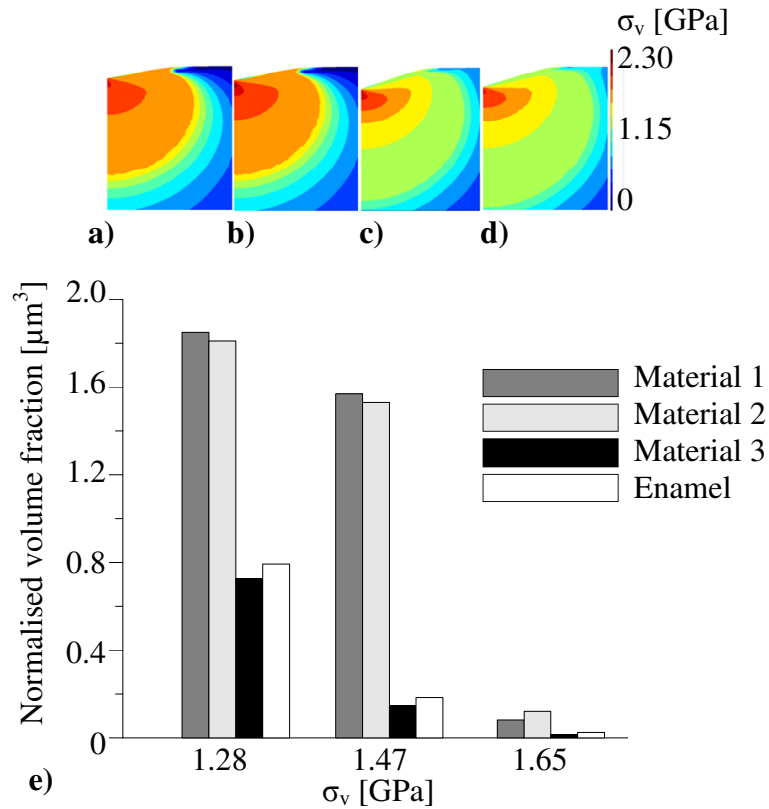


Figure 8-3. FEM results of von Mises stress distribution, σ_v , induced by nanoindentation using the same load of $288.30 (\pm 4.17)$ mN, in a) comparison material 1, b) comparison material 2, c) comparison material 3 and d) enamel. (e) Normalised volume fraction with different stress levels enclosed – (1) $\sigma_v > 1.28$ GPa, (2) $\sigma_v > 1.47$ GPa, (3) $\sigma_v > 1.65$ GPa.

In addition, the plastic zones were compared between model 4 (enamel) and 5 (comparison material 1) in **Figure 8-4(a,b)**.

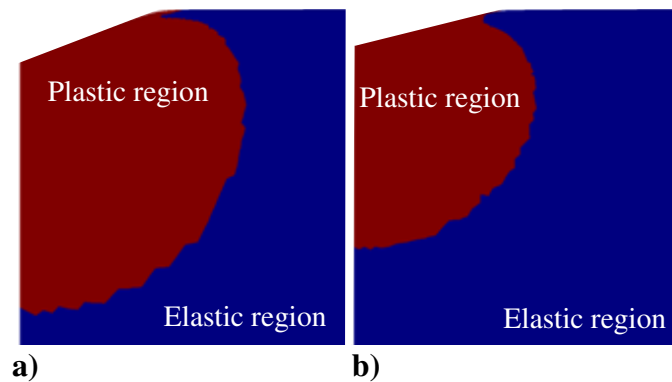


Figure 8-4. FEM simulations of plastic zones produced by nanoindentation using the same load of 285.35 mN in (a) enamel and (b) comparison material 1.

3D volumes of the plastic zones were estimated by using the sub-domain integration. Under the same load of 288.30 (± 4.17) mN the volume of the plastic zone was almost doubled ($\sim 192\%$) in the enamel sample, compared to that in comparison material 1. Strain energy in enamel was $\sim 171\%$ of that in the comparison material 1, i.e., tooth enamel was capable of absorbing much more energy than the conventional material, while incurring smaller stress. The experimental results in an independent study demonstrated that enamel showed much higher energy absorption capacity than a ceramic material with equivalent modulus [111].

Tooth enamel has a hybrid laminate microstructure [6, 111]. The effective modulus is determined not only by the volume fraction and E of its components, but also by the micro-fibril angle θ [7]. This micro-fibril angle will change during the loading process, inducing a change in the effective elastic modulus (Chapter 7). The experimental findings in this work indicated that, under compression loading conditions a similar change was also induced in H and σ_y .

Notably, loading induced changes in mechanical properties were observed in wood cells which also have a micro-fibril structure [192], with results obtained during tensile experiments. It was found that both E and σ_y of the wood specimen increased with the increase of tensile loading and decrease of micro-fibril angle, hence this effect was termed as strain stiffening. A model was developed based on a specific type of cell wall material, which is fully elastic up to a critical shear stress at which shear flow may occur in the matrix between cellulose fibrils and in a direction parallel to them. It has been reported that plants use the orientation of cellulose micro-fibrils to create cell walls with anisotropic properties, which enables organisms to control the shape and size of cells during growth, in order to adjust the mechanical performance of tissues, and to perform bending movements of organs [235]. In comparison, the indentation loading in the current experiment was compressive in nature. An increase in the compressive loading resulted in a micro-fibril angle increase and “strain softening”, with reduced E , H and σ_y . The

observed strain softening in enamel and strain stiffening wood cells have the same mechanism - the change in macroscopic properties of the material results from a change in micro-fibril angle. As such the observed micro-fibril structure can be termed as the “loading adaptive structure”, the significance and functionality of this to the integrity of tooth enamel will be discussed below.

Under a specific loading condition, the overall structural integrity of enamel in human tooth is dependent upon a number of factors, including its toughness, the degree of its strain softening, and its ability of self-healing. Remarkably, tooth enamel can sustain plastic deformation under moderate loading without catastrophic failure [41], and deform significantly during indentation with the potential for short-term [54] and long-term recovery [53]. This capability of self-healing and recovery enables the structure to absorb significant loading energy while maintaining structural integrity.

Therefore, sacrificial bonds [236] seem to play a key role in fulfilling the objective of adopting “loading adaptive structure” in tooth enamel. Smaller stress will induce smaller plastic deformation, which is repairable if the tooth is alive within a human body [54]. On the other hand, for a material with the constant E (conventional material), larger stress will be induced under the same loading conditions within the same region, which may result in larger deformation or fracture, which could be irrecoverable. As such, the design principal of the bio-material here is to sacrifice temporary plastic deformation in return for a smaller stress level within enamel, in order to avoid catastrophic permanent deformation or fracture. As such, a sacrificial bond is realised through loading adaptive structure which induces the observed strain softening.

Notably, the region-dependent plastic damage under indentation in the outer and inner part of tooth enamel has been explored in the recent study by An et al. [201]. This study attributed gradient distributions of enamel properties to a gradient in damage properties. The authors demonstrated on the Drucker Prager model, into which the chain density of proteins has been introduced, that the

region-dependent damage is dictated by the micro-crack propagation and the debonding and stretching of proteins in tooth enamel. Although this model closely matched the simulated plastic behaviour of tooth enamel under applied loads across the enamel thickness with experimental results and showed that enamel has higher capability to dissipate energy in the inner region due to the higher content of proteins in this area, the authors did not consider the effective crystal orientation angle that may significantly contribute to the region dependent gradient in properties. The combination of the modified Drucker Prager, which introduces the chain density of proteins, and the plastic model presented in this study, which incorporates the effective crystal orientation angle and properties of proteins, supported by Synchrotron micro-compression testing *in situ* in hydrated state have a great potential to reveal the genuine deformation mechanisms and variables regulating deformation responses of tooth enamel across different length scales. Further investigations are therefore essential to closely simulate, and therefore bio-mimic tooth enamel.

8.5 Conclusion

Nanoindentation experiments and FEM were carried out on human tooth enamel to investigate the effects of load-induced changes in mechanical properties. The E and H of human tooth enamel were confirmed to be load-dependent; the σ_y value, derived from hardness data, was also load-dependent. The same indentation load induced larger deformations but a lower stress level within enamel, compared to those induced in the comparison material with constant E and σ_y . The change in σ_y played a key role for inducing the observed strain softening. By contrast the contribution from the change in E was insignificant. The observed strain softening was partially attributed to the change in the micro-fibre angle under loading conditions. A sacrificial bond was realised through load-dependent plasticity within a loading adaptive structure.

In this study, tooth enamel was modelled as a homogenous and isotropic medium to clarify the impact of the load dependent variables on the stress and strain distributions within the material. Further investigations into the microstructural level are desirable to obtain a deeper understanding of the relationship between the localised change of the enamel microstructure and the mechanical variables under loading conditions.

9. Bleaching

9.1 Summary

Tooth enamel is considered a biocomposite material with a unique microstructure. The aim of this research was to investigate the mechanical responses of this material during a tooth whitening process. The mechanical effects of a bleaching agent containing 6% hydrogen peroxide were probed with nanoindentation testing. Three main measurements, Young's modulus, E , – hardness, H , with the Berkovich indenter, creep – backcreep and stress-strain with a 5 μm spherical indenter, were performed on unbleached (i.e., healthy) and bleached enamel. The results of these measurements were analysed to determine the key variables influencing mechanical responses during whitening treatments. Overall, the results indicated that the bleaching agent applied on the enamel surface for 7 days (i.e., standard treatment) compromised the structural integrity of mineral and proteins in tooth enamel. As a result, this study found that both E and H significantly decreased after whitening procedure. In terms of critical variables, this research showed that the critical shear stress of proteins, τ_c , decreased from 2.5 to 1 % of the transverse stiffness of a staggered composite, E_2 , which corresponded to a 40 % decrease of normal readings for the unbleached controls. Notably, θ angles with the Berkovich indenter were defined for the enamel in its elastic region in the range of $\sim 44^\circ$ to $\sim 48^\circ$ (Chapter 7). In this study, the θ increased when the 5 μm spherical indenter was used to investigate the elastic as well as plastic region of tooth enamel during whitening treatment, i.e., from 50° (healthy control) to 54° (bleached control). Given all of the above evidence, these findings may provide new perspectives on the use of bleaching agents. This may lead to development of new bleaching products with less harmful and damaging effects to healthy enamel.

9.2 Introduction

Bleaching has become a popular technique in restorative dentistry. This is because of the perceived improved aesthetics after the whitening procedures. However, there have been numerous studies reporting adverse effects of whitening treatments on tooth enamel composition and structure of. For instance, it has been shown that bleaching tooth enamel may alter or completely collapse hydrogen bonds in the protein structure. Furthermore, the bleaching agents can cause additional negative chemical reactions in the organic phase that can consequently result in the structural damage of proteins. Moreover, the urea (i.e., a component of the carbamide peroxide (CP) whitening agent) can potentially cause protein removal. Apart from affecting the enamel organic component, bleaching agents may significantly affect the enamel surface. Micro-channels, porosity and pits have been observed on the enamel surface following bleaching treatments.

The aim of this research was to determine the effects of a 6 % hydrogen peroxide whitening agent on enamel E and H properties at constant indentation depths ranging from 0 to 2 μm . Investigation of enamel self-healing and recovery ability during whitening treatments was also undertaken with creep and backcreep testing methods. Nanoindentation tests were performed to analyse stress-strain properties in healthy and bleached enamel. By fitting analytical models into stress-strain curves for healthy and bleached enamel, variables regulating deformation mechanism in the elastic–plastic region were determined. In Chapter 7, the θ of healthy enamel in its elastic region over constant indentation depths was identified with the Berkovich indenter from 44° to 48° . Here, a calibrated 5 μm spherical indenter was used to probe the elastic-plastic responses of tooth enamel during whitening treatments.

9.3 Materials and methods

Seven healthy molars were collected and stored following the protocol outlined in Section 4.1.1. Before initiation of the bleaching experiments, teeth were prepared by the new method (Section 4.1.2) and kept in HBSS in separate Petri dishes with the exposed polished surface facing upwards, and were stored at 4 °C in a fridge. The level of HBSS was adjusted to half the thickness of the tooth sample in the Petri dish. In this way, the bleaching product containing 6 % hydrogen peroxide was applied only to the polished tooth surface while the bottom part of the tooth was kept hydrated in HBSS. More details about the product and its application can be found in Section 4.1.6.

- *E and H properties*

The E and H properties were tested with a Berkovich indenter following the nanoindentation test settings and data analyses given in Section 4.3.4. These properties were measured by applying 15 indents in the middle region of each sample before and after the application of bleaching agent for 1 day, 3 days, 7 days and 14 days according to the bleaching protocol outlined in Section 4.1.6. Then, the enamel was submerged in HBSS for 7 days and re-tested according to the protocol outlined in Section 4.3.4. Three teeth were used for this experiment.

- *Creep and backcreep*

Nanoindentation tests with a 5 µm nominal radius spherical indenter were used to analyse the creep and backcreep behaviour of healthy and bleached enamel. First, healthy enamel prepared by the new method (Section 4.1.2) was tested according to the nanoindentation creep protocol given in Section 4.3.6. Then, the specimen was bleached for 7 days according to the bleaching protocol outlined in Section 4.1.6. After bleaching, enamel was re-tested by conducting a nanoindentation creep test (Section 4.3.6) and compared to the unbleached

controls. Three indentation lines in total of 15 indents were made on each enamel surface.

For modelling the viscoelastic behaviour of healthy and bleached enamel, the storage modulus, E^* , and viscous modulus, η , of the three-element Voigt model, two-element Maxwell model and four-element Maxwell-Voigt model were computed with the IBIS2 software by fitting creep curve functions into equations (3-57), (3-64) and (3-67). Two healthy molars were used for this experiment.

- *Stress and strain*

Two healthy molars prepared by the new method were tested with a calibrated 5 μm nominal radius spherical indenter to measure the stress-strain behaviour of tooth enamel in its middle region following the protocol given in Section 4.3.5. Another stress-strain experiment was conducted on enamel that was bleached for 7 days according to the protocol outlined in Section 4.1.6. The experiment was run in the middle region of tooth enamel following the test settings given in Section 4.3.5. An analytical model was used to determine the τ_c and θ values for healthy and bleached enamel (Section 4.4.2.2). In total, 10 indents were conducted in each experiment.

9.4 Results and discussion

Because of the nanoindentation instrument limitation in nanoindentation, flat, cross-sectional samples were prepared by the new method and tested by this instrument in the hydrated state. The same samples were also used for using the bleaching agent to investigate the effects of the whitening treatment on enamel properties. Therefore, this study assumed that the bleaching agent will affect tooth enamel from its occlusal surface towards the EDJ in a similar way as it would be applied to the enamel surface of the intact tooth in a real world scenario.

9.4.1 E and H

- *E and H values for 14 days whitening treatment and 7 days recovery*

The bleaching results of E values obtained from the nanoindentation tests with the Berkovich indenter are presented in **Figure 9-1**. The E values increased slightly after 3 days of bleaching at indentation depths between 0.5 and 2 μm . After that, the values decreased continuously to the end of the bleaching treatment. The E values near the surface of enamel ($\sim 0 \mu\text{m}$) fluctuated with no clear increasing or decreasing trend. The E mean values of tooth enamel that was retested 7 days after termination of the bleaching (refer to “7 days after bleaching” in **Figure 9-1**) dropped evidently compared to the bleached control (“14 days bleaching” in **Figure 9-1**) as well as to the unbleached control by 5 % (refer to “Before Bleaching” in **Figure 9-1**) for indentation depths between 0 and 1.5 μm . However, at 2 μm indentation depth, the mean E value also decreased by 4 % compared to unbleached enamel, while it remained unchanged compared to 14 days bleached enamel. Detailed results of E values during the whitening treatment can be found in Appendix M.

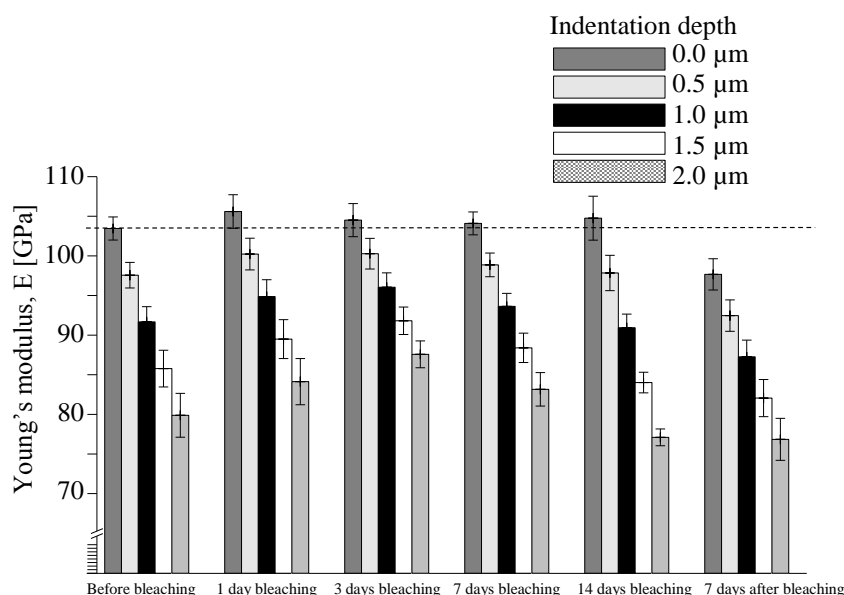


Figure 9-1. E values of enamel undergoing a 2 week bleaching treatment and 7 days after bleaching treatment (recovery).

The results of H values during the whitening process obtained from the nanoindentation tests with a Berkovich indenter are presented in **Figure 9-2**.

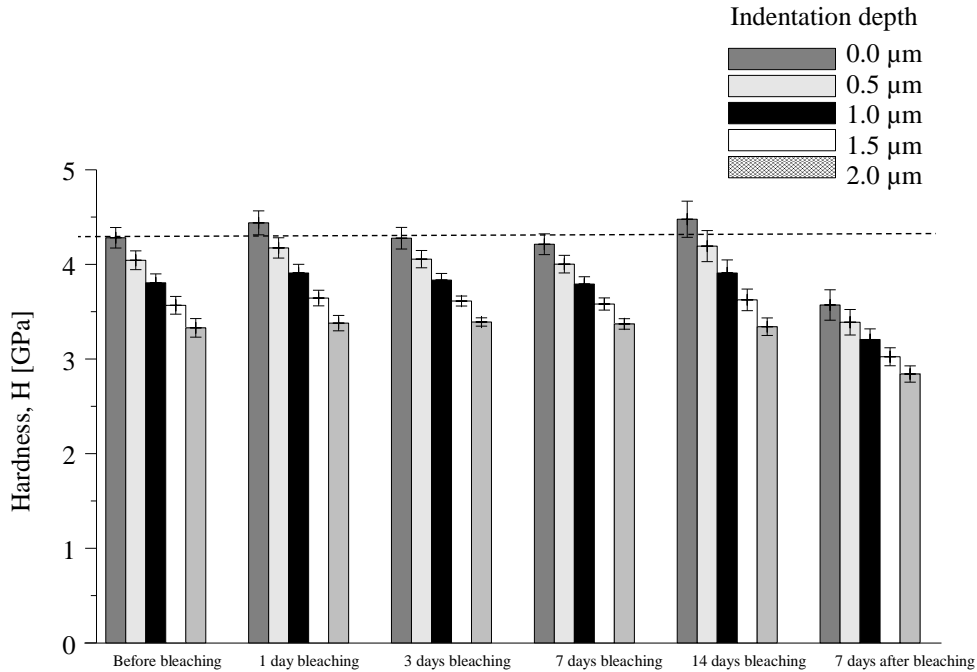


Figure 9-2. H values of enamel during a 2 week bleaching treatment and 7 days after bleaching treatment (recovery).

For H values (**Figure 9-2**), there was no change between the mean values during the bleaching procedure at indentation depths between 1.5 and 2.0 μm. In contrast, the values fluctuated at indentation depths from 0 to 1.0 μm. By re-testing bleached enamel 7 days after finishing the bleaching, the mean H values decreased by 18 % and 16 % compared to 14 days bleached and unbleached enamel, respectively, for all indentation depths. More details for H values during the whitening process can be found in Appendix N.

Overall, this study showed that the bleaching treatment for 14 days did not cause any significant changes in the mechanical properties of enamel for all indentation depths. However, compared to unbleached enamel, E and H values decreased after the 7 day recovery period following bleaching treatment at all indentation depths.

- *E and H values for 7 days bleaching*

For a 7 day bleaching treatment, the values of E and H were analysed in detail and then extrapolated as a function of a constant indentation depth in the range of 0 (i.e., the near surface value) and 2 μm . The general trend for both E and H values measured with the Berkovich indenter decreased with increasing indentation depths (**Table 9-1**) and agreed with previously reported trends shown in Section 5.4.1.

Table 9-1. E and H values for unbleached and 7 days bleached enamel measured with a Berkovich indenter at the constant indentation depth ranging from 0 to 2 μm .

Young's modulus [GPa]		Berkovich indenter			
Indentation depth [μm]	0.00	0.50	1.00	1.50	2.00
Unbleached enamel	103.94(1.46)	97.95 (1.62)	91.96 (1.92)	85.97 (2.32)	79.98 (2.77)
Bleached enamel	104.10(1.45)	98.87 (1.50)	93.63 (1.64)	88.39 (1.85)	83.16 (2.11)

Hardness [GPa]		Berkovich indenter			
Indentation depth [μm]	0.00	0.50	1.00	1.50	2.00
Unbleached enamel	4.28 (0.11)	4.04 (0.10)	3.81 (0.09)	3.58 (0.09)	3.37 (0.10)
Bleached enamel	4.21 (0.11)	4.00 (0.09)	3.79 (0.08)	3.57 (0.06)	3.33 (0.06)

From **Table 9-1**, the values of E for 7 days bleached enamel were higher compared to unbleached controls while the H values were found to be lower for all indentation depths. The results showed that E, and therefore the ability of bleached enamel to return to its original shape, increased marginally during bleaching treatment, while the H value and therefore the resistance to plastic deformation slightly decreased.

The mild wear resistance ratio, H/E was considered as a parameter to predict and rank the wear resistance of enamel to abrasive particles during whitening treatment (refer to Section 4.5). While the E values increased during bleaching treatment, which could be assessed as an improvement of enamel stiffness, the overall ratio H/E decreased for bleached enamel, i.e., by approximately 2.4 %.

As shown previously in **Figure 9-1** and **Figure 9-2**, the effects of a bleaching agent on the mechanical properties of unbleached enamel appeared within 7 days of finishing the bleaching procedure. As there is no clear information about the composition of bleaching agents, this study can only speculate that these whitening products may contain some enhancement ingredients that temporarily support the structural and mechanical integrity of enamel during bleaching. This assumption is based on the study by Thompson et al. [12], which demonstrated that by soaking the proteins in some solutions, such as calcium, sodium or phosphate, the energy dissipation improved within the protein matrix. As a result, the E and H of the material increased and the dissipated energy within the organic matrix also increased.

Therefore, this study suggests that when the bleaching agents with those added elements are applied to the enamel surface, the damage to the structural and mechanical properties of enamel are controlled by those agents. However, when the bleaching is terminated, the mechanical properties degrade even further. This indicates that potential alterations occurred inside the enamel structure. The retention of a whitening effect is an issue. As a result, it is challenging to maintain the mechanical properties.

The 7 day whitening treatment was further explored by investigating the creep-backcreep and stress-strain behaviours of tooth enamel.

9.4.2 Creep and backcreep behaviour

Typical creep-backcreep behaviour of unbleached and 7 days bleached enamel is shown in **Figure 9-3(a-c)**.

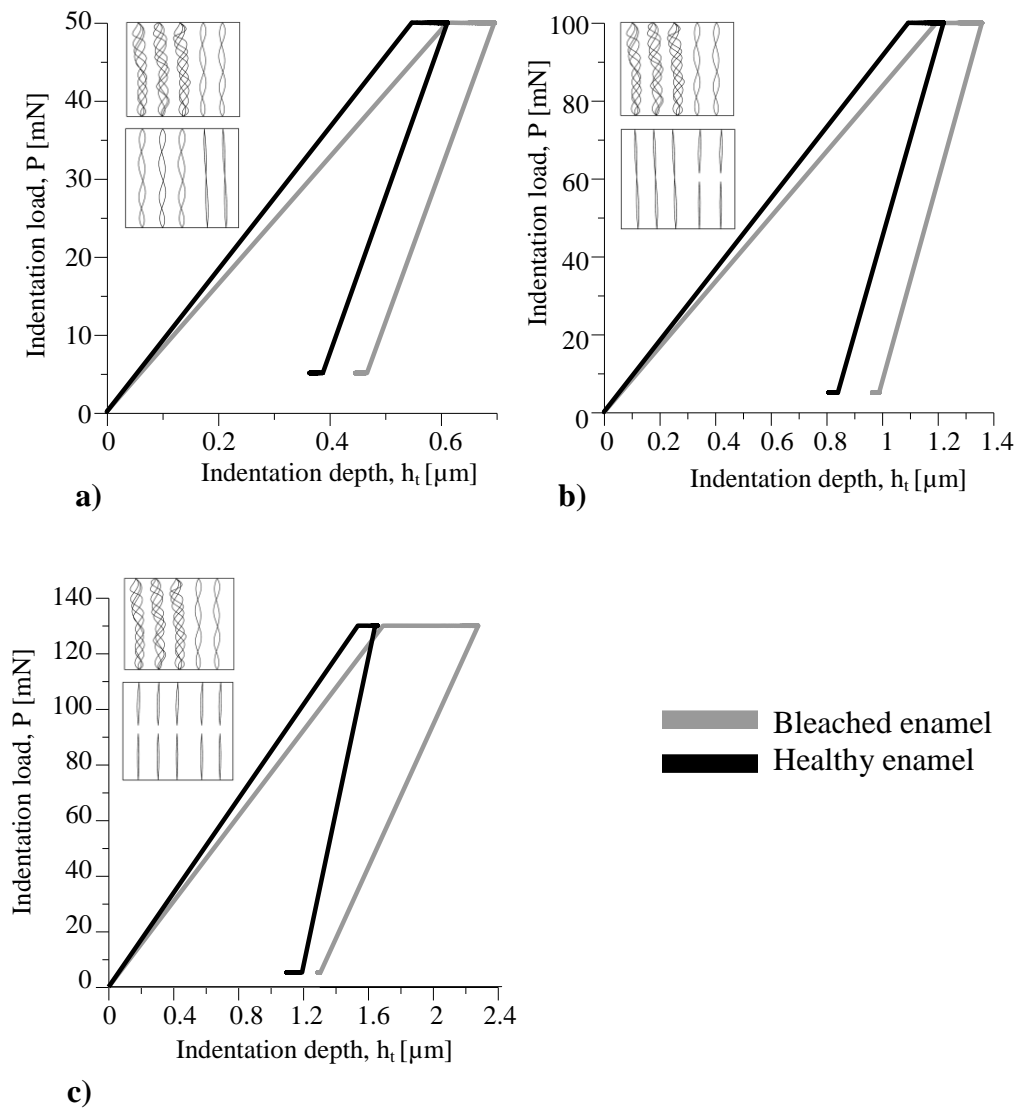


Figure 9-3. Representative load displacement curves of unbleached and 7 days bleached enamel with a calibrated 5 μm spherical indenter showing a creep responses with 900 s holding time under maximum indentation load of 50 mN (a), 100 mN (b) and 130 mN (c) and backcreep (self-recovery) behaviour responses with 900 s holding time at minimum loads of 5 mN, respectively. The insets represent potential mechanical deformation of sacrificial bonds in proteins during loading (top image) and unloading (bottom image). It is expected that the damage to proteins (represented as a number of damaged/broken springs) gradually increases with increasing load for unbleached as well as bleached enamel.

The figure illustrates two load displacement curves of unbleached and bleached enamel for three maximum loads of 50, 100 and 130 mN with a holding time of 900 s at maximum and minimum loads. These curves represent the creep mechanical responses of enamel at maximum load and the recovery behaviour at minimum load of 5 mN. These curves are typical for one specimen at one location and were obtained from the nanoindentation test with a calibrated 5 μm spherical indenter.

From **Figure 9-3(a,b)**, the indentation depth, h_t , of bleached enamel at creep stage slightly increased compared to unbleached enamel, while the recovery of the indentation depth diminished at minimum load. However, a 130 mN maximum load resulted in the significant increase of indentation depth, h_t , at creep stage and almost no recovery at minimum load (**Figure 9-3(c)**).

In recent years, investigations of protein functions have attracted more attention as their role still remains elusive and unclear. The protein is considered as a polymer, made of chains of different lengths that can fold and unfold, which contains sacrificial bonds that play a crucial role in providing superior toughening mechanisms and thus resistance against applied loads [12, 111]. As reported in pioneering studies [54, 61, 62], creep and more importantly self-healing (recovery) behaviour are of great importance for enamel to survive against applied loads in the oral cavity. It has been observed that the protein, acting as a gluing agent, prevents the separation of mineral crystals within biocomposite during applied loads and the material partially recovers as a result of the reformation of sacrificial bonds when the load is removed [13]. This could explain enamel behaviour, which could be associated with the important roles of the organic compounds within enamel in the creep and backcreep testing under maximum and minimum loads, respectively. Therefore, by assuming that the bleaching agent may affect the functionality of the organic matrix in terms of sacrificial bonds and remove, partially or completely, the protein compound, one may suspect that bleached enamel will be less recovered than unbleached enamel

after unloading. Overall, this agrees with the results showing that the bleaching agent used in this study had detrimental effects on creep and more importantly backcreep behaviour of tooth enamel.

It is clear that with increasing load the indentation depth, h_t , dramatically increased for bleached enamel due to the potential change of the protein's rigidity. The averaged values of indentation depth, h_t (\pm standard error), in μm measured during creep testing for healthy enamel were 0.66 (0.01), 1.30 (0.02) and 1.71 (0.06) μm , while for bleached enamel were 0.70 (0.01), 1.42 (0.03) and 1.84 (0.04) at maximum loads of 50, 100 and 130 mN, respectively. As mentioned earlier (Section 2.7), the bleaching agent may affect the structure and mechanical integrity of proteins. Based on these results, this study assumes that the low carrying capability of sacrificial bonds was more likely to yield serious damage within the protein matrix. This damage could be observed mainly in the recovery stage of enamel at the minimum load.

Table 9-2 summarises Δh_t values for unbleached and 7 days bleached enamel which correspond to the differences between the start and the end of the creep and recovery test, respectively.

Table 9-2. The absolute value of Δh_t (\pm standard error) [μm] for creep at 50, 100 and 130 mN loads and recovery at 5 mN of unbleached and 7 days bleached enamel specimens. The holding time of 900 s was applied for both, creep and recovery measurements.

Δh_t [μm]	50 mN	5 mN
Unbleached enamel	0.063 (0.008)	0.014 (0.004)
Bleached enamel	0.078 (0.001)	0.013 (0.004)
Δh_t [μm]	100 mN	5 mN
Unbleached enamel	0.159 (0.009)	0.025 (0.002)
Bleached enamel	0.199 (0.009)	0.020 (0.005)
Δh_t [μm]	130 mN	5 mN
Unbleached enamel	0.188 (0.046)	0.061 (0.014)
Bleached enamel	0.313 (0.045)	0.007 (0.005)

These Δh_t values are overall results and denote 20 indentation locations. From this table, Δh_t for bleached enamel increased by 23 %, 25% and 66 % under maximum loads of 50, 100 and 130 mN, respectively. On the other hand, there was a prominent decrease in the Δh_t values between unbleached and bleached enamel in the recovery stage at minimum load of 5 mN by 72 and 90 %, respectively, after applying maximum loads of 100 and 130 mN, yet only a decrease of 7 % after applying the maximum load of 50 mN.

The typical curves of creep and backcreep behaviour that were tested with a calibrated 5 μm spherical indenter at maximum loads of 50, 100 and 130 mN and minimum load of 5 mN are shown in **Figure 9-4(a-f)**.

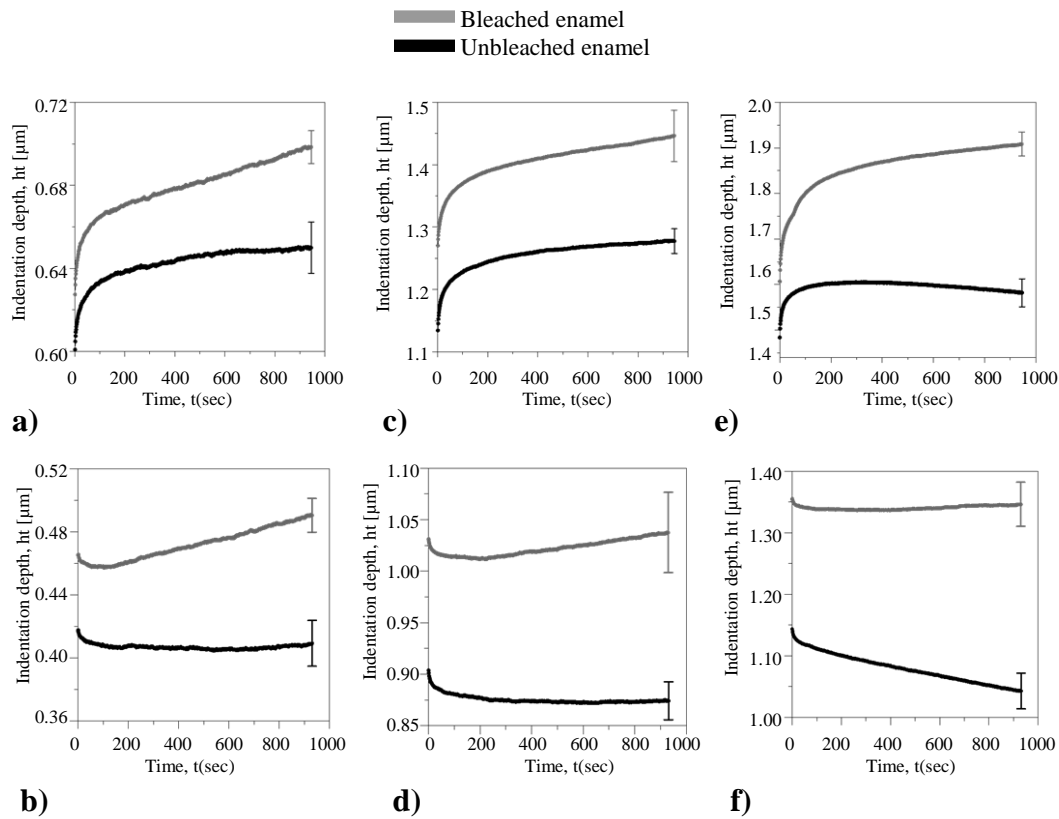


Figure 9-4. Typical creep and backcreep curves of unbleached and bleached enamel at (a,b) 50 and 5 mN, (c,d) 100 and 5 mN, (e,f) 130 and 5 mN with 900 s holding time at maximum and minimum load, respectively.

The creep and backcreep experiments can provide additional information about the mechanical responses of the organic compound in enamel. Therefore, to analyse the effects of a whitening treatment on the organic compound in enamel, rheological models were used to determine variables regulating creep behaviour within tooth enamel.

Typical creep responses for unbleached and bleached enamel at a 50 mN load by incorporating a hold period of time of 900 s are shown in **Figure 9-5(a-c)**.

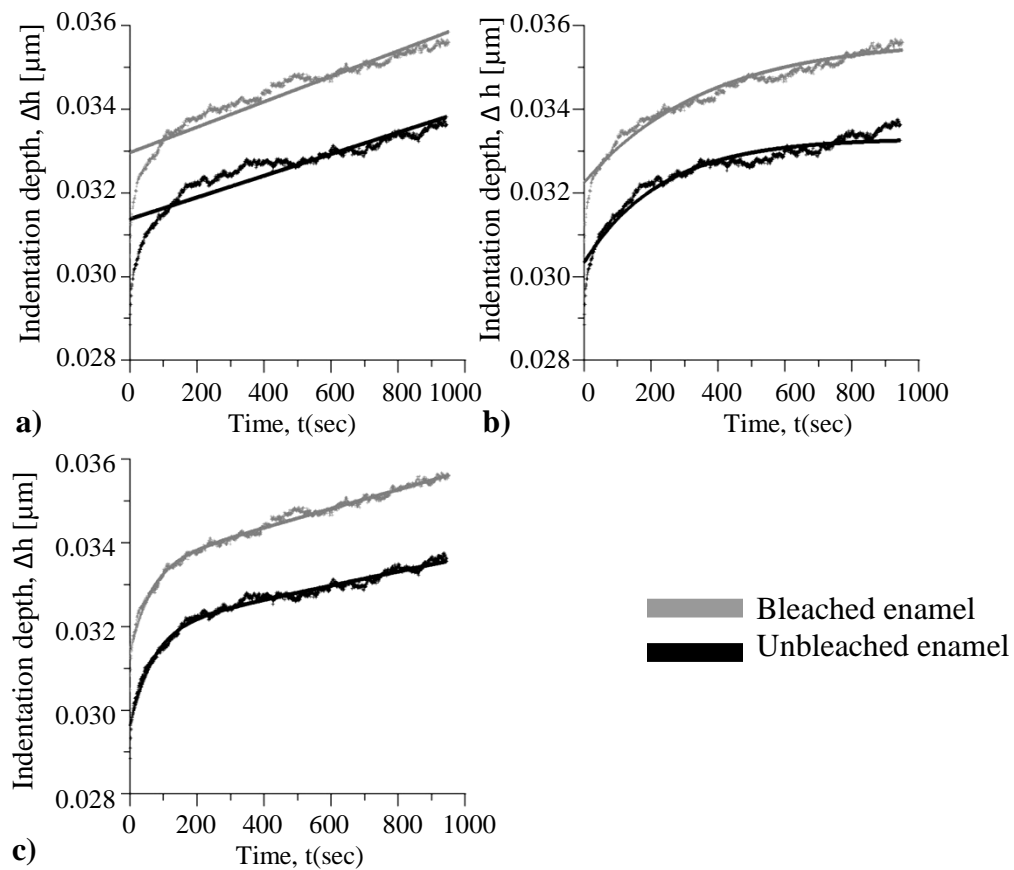


Figure 9-5. Creep responses for hold period of 900 s at 50 mN on unbleached and bleached enamel with a 5 μm nominal radius spherical indenter. (a) Maxwell model, (b) Voigt model and (c) combined Maxwell-Voigt model were used to determine creep variables regulating deformation behaviour during bleaching treatment.

Three models (Maxwell, Voigt and Maxwell-Voigt) were used to determine the storage moduli, E^* , and loss moduli, η , of enamel. To do so, the experimental data were fitted according to equations derived earlier in Section 3.1.5.2.

The Maxwell model did not show a reasonable fit for both unbleached and bleached enamel (**Figure 9-5(a)**). In comparison, the fitting procedure of creep responses curves into experimental data improved considerably in the Voigt model (**Figure 9-5(b)**). A nearly perfect fit between simulated and experimental data for unbleached and bleached enamel was found in the combined Maxwell-Voigt model (**Figure 9-5(c)**). The creep variables from these models are shown in **Table 9-3**.

Table 9-3. E_i^* and μ values from creep modelling at 50, 100 and 130 mN loads for unbleached and bleached enamel.

Model:	50 mN load		100 mN load		130 mN load	
Maxwell	Unbleached enamel	Bleached enamel	Unbleached enamel	Bleached enamel	Unbleached enamel	Bleached enamel
E_1^* [GPa]	33.41 (0.98)	30.51(0.61)	23.00(1.02)	21.12(0.60)	16.36 (0.43)	14.95 (0.69)
μ_1 [10^{12} Pa.s]	511.23 (46.83)	317.53 (14.65)	281.41(20.16)	186.61 (25.79)	205.52 (16.98)	115.16 (15.65)
Voigt						
E_1^* [GPa]	34.03(0.99)	31.59(0.69)	24.13(0.99)	22.19 (0.56)	17.70 (0.66)	15.94 (0.72)
E_2^* [GPa]	657.64 (85.29)	474.16 (30.56)	275.36(21.59)	208.77(16.63)	233.62 (4.68)	141.16 (3.06)
μ_2 [10^{12} Pa.s]	88.88 (7.55)	65.07 (8.67)	40.79(4.11)	34.84(3.16)	40.75 (1.85)	17.97 (1.43)
Maxwell - Voigt						
E_1^* [GPa]	35.26 (1.23)	31.89 (0.74)	24.56 (0.87)	22.91 (0.50)	18.13 (0.54)	16.40 (0.67)
E_2^* [GPa]	930.68 (100.96)	909.78 (80.86)	436.50(79.19)	275.66(22.29)	280.66 (15.48)	158.11 (10.89)
μ_1 [10^{12} Pa.s]	808.46 (121.37)	365.32(24.89)	582.43(74.50)	331.24(12.86)	407.91(10.77)	324.27(28.19)
μ_2 [10^{12} Pa.s]	30.01 (4.26)	19.33 (3.07)	20.97(2.28)	13.83 (1.37)	17.43 (3.24)	8.35 (0.81)

In general, the storage modulus, E_i^* , and viscosity, η , decreased with increasing applied loads from 50 to 130 mN for unbleached and bleached enamel. In addition, the modelling E_i^* and η values were lower for bleached enamel compared to unbleached enamel (**Table 9-3**).

The viscosity values, η , from **Table 9-3** were affected by two factors: the applied loads and the effects of application of the bleaching agent during creep experiments. Regarding the applied loads, the decreasing trend of viscosity could be explained by possible shear-thinning within the water-protein compound for unbleached and bleached enamel with increasing loads. On the other hand, the results showed that the viscosity dropped after the application of the bleaching agent on unbleached enamel for 7 days. The application of bleaching agents possibly yielded less sticky behaviour of this organic compound as shown on the decreasing trend of the viscosity for the bleached controls.

9.4.3 Stress-strain analysis and modelling

For a better understanding of the effects of 7 day whitening treatments, stress-strain analyses were conducted for unbleached and bleached enamel and fitted into analytical models. Raw data of stress, σ and strain, ϵ [0.2 a/R] (refer to Appendix O) from the nanoindenter were plotted into a chart to demonstrate transitional phase from the elastic to plastic region (**Figure 9-6**).

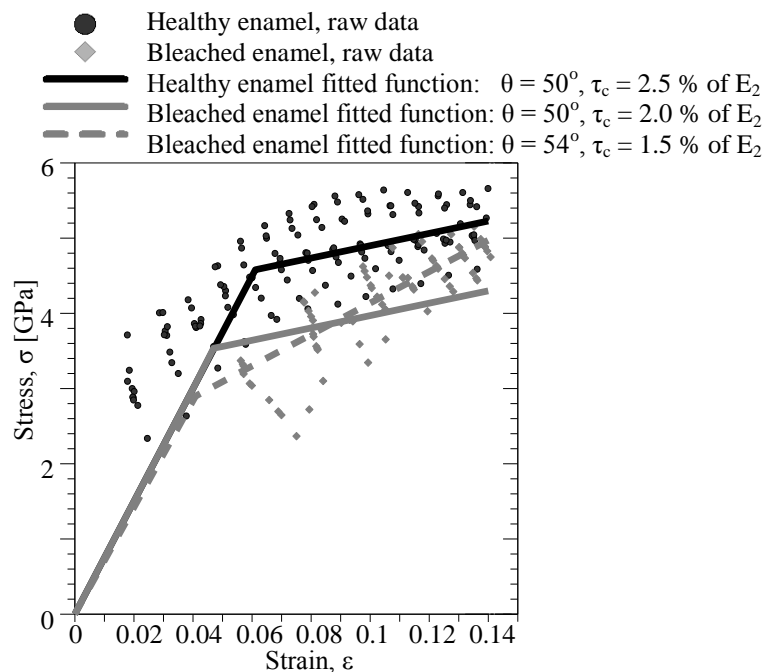


Figure 9-6. Fitting curves obtained from stress-strain measurements for unbleached and 7 days bleached enamel. For each simulating procedure, the effective crystal orientation angle, θ , and the critical shear stress, τ_c , of the protein matrix were identified.

As mentioned in Section 3.1.4, the reason for using a spherical indenter for these types of analyses was because the ε value increases under a spherical indenter with increasing applied loads, while it remains constant under a Berkovich indenter.

Furthermore, the analytical model defined by equations (2-1) and (2-9) for elastic and plastic regions, respectively, was used to determine variables regulating mechanical behaviour during bleaching treatment. This model was fitted first into stress-strain data for unbleached enamel. By using variables given in **Table 4-3** in equations (2-1) and (2-9), the effective crystal orientation angle, θ , and the critical shear stress, τ_c , of protein were found 50° and 2.5 % of E_2 , respectively, where E_2 denotes the transverse stiffness of a staggered composite structure. The yield point values, σ_y and ε_y , for unbleached enamel modelling curve were found to be 4.579 GPa and 0.061 (refer to Appendix O).

In the next step, the analytical model was applied to the raw data of bleached enamel. For this modelling, it was assumed that enamel microstructure, i.e., related to the angle θ , will not be affected and therefore will remain constant (50° degrees) during bleaching treatment, while the τ_c value within the organic matrix was expected to decrease. The iterative process was employed to determine the τ_c value for bleached enamel that closely fit to the stress-strain nanoindentation data. The generated curve revealed σ_y at 3.536 GPa and ε_y at 0.047 (refer to Appendix O). The closest fitted τ_c value of 2.0 % of E_2 for bleached enamel was identified from this process. However, for this value, the analytical modelling curve did not show a reasonable fit as presented in **Figure 9-6**. Therefore, another model was implemented for bleached enamel stress-strain data by changing both the θ and τ_c variables. As a result, the best fitted values of θ and τ_c for stress-strain data of bleached enamel were found to be 54° and 1.5 % of E_2 , respectively, with yield point values of $\sigma_y = 2.899$ GPa and $\varepsilon_y = 0.041$ (refer to Appendix O).

It is clear that the elastic region of unbleached enamel was reduced by the whitening treatment process. This was observed from a decrease of the σ_y and ε_y values from 4.579 to 2.899 GPa and from 0.061 to 0.041, respectively. Furthermore, the results of stress-strain analytical models in this study showed that shear properties of proteins were affected significantly. This can be seen from a decrease of τ_c value by 40 %, i.e., from 2.34 to 1.41 GPa (Appendix O). In addition, the rotational ability of mineral platelets increased after a whitening treatment yielding an increase of angle θ by 4° , i.e. from 50° to 54° . As a result, it was assumed that the structural integrity of mineral and proteins within unbleached enamel was compromised after bleaching.

In previous studies, shear properties and the angle θ values have been investigated for unbleached and hypomineralised enamel by using an analytical model [7, 105]. On the other hand, this study reports these variables for unbleached and bleached enamel for the first time by using the same analytical model. It was stated that shear properties of proteins affect the mechanical behaviour of enamel [105]. From this point of view, the authors demonstrated that the decrease of τ_c resulted in the reduction of enamel resistance to deformation which agrees with the findings in this research. Moreover, the authors demonstrated that the increase of angle θ resulted in more ductile enamel [105]. Hence, this study showed that enamel became less resistant to deformation with an increased θ angle after a whitening treatment.

9.5 Conclusion

This study demonstrated that bleaching agents containing 6% hydrogen peroxide have some control over the structural integrity of tooth enamel in terms of its mechanical responses during a whitening treatment. The termination of whitening treatment yields a significant decrease in stiffness and hardness of healthy enamel.

The creep and backcreep analysis showed that the bleached enamel recovered to a lesser extent than healthy enamel after unloading from maximum loads of 50, 100 and 130 mN, due to possible damage of the structural integrity of the organic matrix.

Moreover, this study showed that viscosity values, η , decreased due to applied loads as well as the whitening treatment. This study postulates that this was because of shear-thinning within the organic matrix. In addition, the organic matrix became less viscous as a result of bleaching agent application.

Regarding stress-strain measurements, the values of the yield point decreased after bleaching. Moreover, the analytical models elucidated variables regulating deformation behaviour of bleached enamel. Based on this modelling, the values of τ_c decreased significantly while the θ increased for bleached enamel. This gave evidence that the structural integrity of the mineral-protein compound in enamel was affected by the whitening treatment.

10. Conclusion

Understanding tooth function and structure is important for promoting and improving human health and wellbeing. Specifically, human tooth enamel, the outer part of the tooth, has been studied extensively in relation to its unique structural and compositional characteristics, which must withstand considerable forces during repeated daily use during the course of an individual's life. Unfortunately, the link between the microstructure, mechanical properties and function remain uncertain. A deep understanding of how they are linked is crucial for advancing dental health science but also for developing new biocomposite materials.

The main objective of this research was to understand the deformation behaviour of human tooth enamel in relation to its microstructure. To do so, a new preparation method was designed and applied to accurately determine mechanical properties of human tooth enamel in a hydrated state (Chapter 4, Section 4.1.2). The method included the use of a new embedding process (Chapter 4, Sections 4.1.3 and 4.1.4). Moreover, a steel holder was designed and manufactured to hold and test tooth specimens on the nanoindentation stage in a wet environment without the use of chemically based glues or hot waxes, as is the case for conventional methods (Chapter 4, Section 4.3.2).

A new analysis approach was developed to examine the mechanical properties of enamel at constant indentation depths (Chapter 4, Section 4.3.4). This is because the Young's modulus (E) and hardness (H) from nanoindentation tests are affected not only by samples and regions but also by indentation depths. In addition, the enamel-dentine junction (EDJ) was investigated using an optical and scanning electron microscopy (SEM) to identify the effects of preparation methods on the structural integrity of this region.

For a deeper understanding of the deformation behaviour of enamel, analytical and finite element models (FEM) were used to relate the elastic and plastic behaviour of tooth enamel to its microstructure.

Lastly, the effects of whitening treatments on the structure and mechanical properties of healthy enamel were explored. Both creep and recovery investigations were also included for healthy and bleached enamel to elucidate the effects of a bleaching agent on the structural integrity of enamel components (i.e., mineral and protein).

10.1 Findings

The following major findings can be drawn from this body of work:

- The E and H values of enamel prepared by the new method were higher compared to the properties obtained from conventional methods. While E values were significantly higher for all indentation depths, the H values only differed significantly from the enamel surface to 1 μm . This is because resin embedding during the sample preparation in the conventional methods had the most negative effects on E and H values. The elimination of the resin embedding in the new method resulted in the highest values of E and H (Chapter 5, Section 5.4.1).
- This study revealed that enamel is a functionally graded material measured at constant depths. In addition, there was a gradual decrease in these values with increasing indentation depth at one location over the entire thickness of tooth enamel (Chapter 5, Section 5.4.1).
- The differences of E and H values were reduced between hydrated enamel prepared by the new method and dried enamel prepared by a careful dehydration-drying process, suggesting that the microstructure

plays an important role in regulating the mechanical properties of enamel. Moreover, the values of E and H for hydrated and dried enamel samples were reported for the first time at constant indentation depths (Chapter 5, Section 5.4.2).

- Interestingly, while the use of resin decreased E and H, it had a positive effect in predicting mild wear (H/E) and severe wear ($K_c^4/H.E^2$) resistance of tooth enamel. The H/E parameter decreased with indentation depth for the new method and conventional method A, i.e., for the intact tooth embedded in resin prior to sectioning. However, the H/E parameter of the conventional method B increased with indentation depth, i.e., for the sectioned tooth prior to resin embedding. On the other hand, $K_c^4/H.E^2$ parameter increased with indentation depth for all preparation methods. Therefore, enamel is expected to resist severe wear damage, especially when the resin embedding process is used (Chapter 5, Sections 5.4.3 and 5.4.4).
- No cracks or fractured EDJ were observed for enamel prepared with the new method followed by a slow careful dehydration process even after multiple loads of 400 mN. The new method maintained a strong physical bond between enamel and dentine as revealed by SEM examination (Chapter 6).
- The changes of E values with indentation depth were linked to the effective orientation angle (θ) of the mineral crystals in enamel. This was quantified with a mechanistic model simulating enamel elastic behaviour. The range of angle θ was determined and found to change from 44 to 48 degrees when indentation depths increased from 0 to 2 μm . Such angles facilitated the shear-sliding of the mineral crystals and lowered stresses under applied loads (Chapter 7).

- The H values also had a decreasing trend with increasing indentation depth. From FEM analysis, the decreasing yield strength resulted in reduction of the stress level. The load- dependent hardness can also be linked to the change of the angle θ in tooth enamel (Chapter 8).
- Regarding the whitening treatment (bleaching), the nanoindentation tests showed that the bleached enamel 7 days after treatment was less stiff and softer than the unbleached control. In addition, the creep test showed that the bleached enamel recovered to a lesser extent after the load was released. It was inferred from the rheological creep models that the protein in bleached enamel was less viscous due to detrimental effects of the bleaching agent (Chapter 9).
- The values of the protein shear stress, τ_c , and the angle θ were affected significantly by bleaching. According to the analytical model, the τ_c value of proteins decreased, while the angle θ of mineral crystal increased for bleached enamel. The changes of these properties resulted presumably from the affected structural integrity of mineral and protein after whitening treatment (Chapter 9).

These findings not only bring new perspectives to the structure-property-function relationship of enamel, but should also help develop new robust load-bearing materials. In addition, the results of tooth bleaching experiments reported in this study support the need to conduct further research into the viability of current bleaching agents and the development of new, less damaging, methods for bleaching tooth enamel.

10.2 Future research directions

Even though significant advances in characterising the deformation behaviour of human tooth enamel at the microscale were achieved, future work is required

to cover the overall concepts of this behaviour under applied loads. This includes more investigations to:

- determine compositional and structural changes in enamel resulting from the sample preparation process. This includes, for instance, the use of scanning and transmission electron microscopy, spectroscopy, Micro-CT etc. to identify the effects of embedding medium on tooth enamel. In addition, investigations about how far the resin penetrates into the dental tissue and why H is less sensitive than E to the preparation technique are also required to identify the exact effects on mechanical properties of tooth enamel.
- conduct fine mapping of structural, compositional and mechanical properties across the EDJ in conjunction with more comprehensive mechanical models from the nano-scale to macro-scale. This includes the use of different type of indenters (e. g., Vickers) and loads in order to investigate the initiation and propagation of cracks from the indentation sites at the EDJ. These investigations will shed light on the EDJ interface, which remarkably combines two very distinct materials. This will lead to the design of new hard-coatings and dental materials where similarly fused disparate materials are of importance.
- explore the relationship between the enamel structural and mechanical variables under localised loads at different length scales. An in-depth understanding of the local mechanical behaviour will provide a new guide to develop enamel-like biomimetic materials with remarkable resilience and adaptive structure against applied loads.

11. References

- [1] Fu-Zhai C, Jun G. New observations of the hierarchical structure of human enamel, from nanoscale to microscale. *J Tissue Eng Regener Med* 2007;1:185-91.
- [2] He LH, Swain MV. Understanding the mechanical behaviour of human enamel from its structural and compositional characteristics. *J Mech Behav Biomed Mater* 2008;1:18-29.
- [3] Ang SF, Bortel EL, Swain MV, Klocke A, Schneider GA. Size - dependent elastic/inelastic behavior of enamel over millimeter and nanometer length scales. *Biomaterials* 2010;31:1955-63.
- [4] Bechtle S, Ang SF, Schneider GA. On the mechanical properties of hierarchically structured biological materials. *Biomaterials* 2010;31:6378-85.
- [5] Nanci A. Ten Cate's oral histology: development, structure, and function. 7th ed. St. Louis, Missouri, USA: Mosby Elsevier; 2008. Chapter 7, Enamel: composition, formation, and structure. pp. 141-90.
- [6] Xie Z, Swain MV, Hoffman MJ. Structural integrity of enamel: experimental and modeling. *J Dent Res* 2009;88:529-33.
- [7] Xie ZH, Swain MV, Swadener G, Munroe P, Hoffman M. Effect of microstructure upon elastic behaviour of human tooth enamel. *J Biomech* 2009;42:1075-80.
- [8] Meyers MA, Chen P-Y, Lin AY-M, Seki Y. Biological materials: structure and mechanical properties. *Prog Mater Sci* 2008;53:1-206.
- [9] He LH, Swain MV. Nanoindentation derived stress - strain properties of dental materials. *Dent Mater* 2007;23:814-21.
- [10] Petersen PE, Baez R, Kwan S, Ogawa H. Future use of materials for dental restoration: report of the meeting convened at WHO HQ, Geneva, Switzerland 16th to 17th November 2009 (in press). Geneva, Switzerland: WHO Press; 2009.
- [11] Peterlik H, Roschger P, Klaushofer K, Fratzl P. From brittle to ductile fracture of bone. *Nat Mater* 2006;5:52-5.
- [12] Thompson JB, Kindt JH, Drake B, Hansma HG, Morse DE, Hansma PK. Bone indentation recovery time correlates with bond reforming time. *Nature* 2001;414:773-6.
- [13] Fantner GE, Hassenkam T, Kindt JH, Weaver JC, Birkedal H, Pechenik L, et al. Sacrificial bonds and hidden length dissipate energy as mineralized fibrils separate during bone fracture. *Nat Mater* 2005;4:612-6.
- [14] Zhou JK, Hsiung LL. Biomolecular origin of the rate - dependent deformation of prismatic enamel. *Appl Phys Lett* 2006;89:3.
- [15] He L, Swain MV. Enamel - a "metallic-like" deformable biocomposite. *J Dent* 2007;35:431-7.
- [16] Menčík J, He LH, Swain MV. Determination of viscoelastic - plastic material parameters of biomaterials by instrumented indentation. *J Mech Behav Biomed Mater* 2009;2:318-25.

-
- [17] Rensbereger JM. Mechanical adaptation in enamel. In: Koenigswald WV, Sander PM, editors. Tooth enamel microstructure. Rotterdam, Brookfield, USA: A.A.Balkema; 1997.
- [18] Cuy JL, Mann AB, Livi KJ, Teaford MF, Weihs TP. Nanoindentation mapping of the mechanical properties of human molar tooth enamel. *Arch Oral Biol* 2002;47:281-91.
- [19] Myoung S, Lee J, Constantino P, Lucas P, Chai H, Lawn B. Morphology and fracture of enamel. *J Biomech* 2009;42:1947-51.
- [20] Mahoney E, Holt A, Swain M, Kilpatrick N. The hardness and modulus of elasticity of primary molar teeth: an ultra-micro-indentation study. *J Dent* 2000;28:589-94.
- [21] Imbeni V, Kruzic JJ, Marshall GW, Marshall SJ, Ritchie RO. The dentin - enamel junction and the fracture of human teeth. *Nat Mater* 2005;4:229-32.
- [22] Habelitz S, Marshall GW, Balooch M, Marshall SJ. Nanoindentation and storage of teeth. *J Biomech* 2002;35:995-8.
- [23] Guidoni G, Denkmayr J, Schoberl T, Jager I. Nanoindentation in teeth: influence of experimental conditions on local mechanical properties. *Philos Mag* 2006;86:5705-14.
- [24] Habelitz S, Marshall SJ, Marshall GW, Balooch M. Mechanical properties of human dental enamel on the nanometre scale. *Arch Oral Biol* 2001;46:173-83.
- [25] Lewis G, Nyman JS. The use of nanoindentation for characterizing the properties of mineralized hard tissues: state-of-the art review. *J Biomed Mater Res B Appl Biomater* 2008;87B:286-301.
- [26] Staines M, Robinson WH, Hood JAA. Spherical indentation of tooth enamel. *J Mater Sci* 1981;16:2551-6.
- [27] Park S, Wang DH, Dongsheng Z, Romberg E, Arola D. Mechanical properties of human enamel as a function of age and location in the tooth. *J Mater Sci: Mater Med* 2008;19:2317-24.
- [28] Jana D, editor. Sample preparation techniques in petrographic examinations of construction materials: a state-of-the-art review. Proceedings of the 28th International Conference on Cement Microscopy; 2006 Apr 30 - May 4; Denver, Colorado, USA: Curran Associates, Inc.; 2006 Oct. pp. 23-70
- [29] Janda R. Preparation of extracted natural human teeth for SEM investigations. *Biomaterials* 1995;16:209-17.
- [30] van Amerongen JP, van Amerongen WE, Watson TF, Opdam NJM, Roeters FJM, Bittermann D, et al. Restoring the tooth: 'the seal is the deal'. In: Fejerskov O, Kidd EAM, Nyvad B, Baelum V, editors. Dental caries: the diseases and its clinical management. Oxford, UK: Blackwell Publishing; 2009. p. 389.
- [31] Santerre JP, Shajii L, Tsang H. Biodegradation of commercial dental composites by cholesterol esterase. *J Dent Res* 1999;78:1459-68.
- [32] Soderholm KJ, Zigan M, Ragan M, Fischlschweiger W, Bergman M. Hydrolytic degradation of dental composites. *J Dent Res* 1984;63:1248-54.
- [33] Van Meerbeek B, De Munck J, Van Landuyt KL, Mine A, Lambrechts P, Sarr M, et al. Dental adhesives and adhesives performance. In: Curtis RV,

- Watson TF, editors. Dental biomaterials Imaging, testing and modelling. Boca Raton, FL: CRC Press; 2008.
- [34] Lin BA, Jaffer F, Duff MD, Tang YW, Santerre JP. Identifying enzyme activities within human saliva which are relevant to dental resin composite biodegradation. *Biomaterials* 2005;26:4259-64.
 - [35] Ito S, Hashimoto M, Wadgaonkar B, Svizero N, Carvalho RM, Yiu C, et al. Effects of resin hydrophilicity on water sorption and changes in modulus of elasticity. *Biomaterials* 2005;26:6449-59.
 - [36] Zhou J, Hsiung LL. Depth - dependent mechanical properties of enamel by nanoindentation. *J Biomed Mater Res A* 2007;81A:66-74.
 - [37] He LH, Fujisawa N, Swain MV. Elastic modulus and stress - strain response of human enamel by nanoindentation. *Biomaterials* 2006;27:4388-98.
 - [38] Xie ZH, Mahoney EK, Kilpatrick NM, Swain MV, Hoffman M. On the structure-property relationship of sound and hypomineralized enamel. *Acta Biomater* 2007;3:865-72.
 - [39] Xu HHK, Smith DT, Jahanmir S, Romberg E, Kelly JR, Thompson VP, et al. Indentation damage and mechanical properties of human enamel and dentin. *J Dent Res* 1998;77:472-80.
 - [40] Lawn BR, Lee JJW, Chai H. Teeth: among Nature's most durable biocomposites. *Annu Rev Mater Res* 2010;40:55-75.
 - [41] Lucas P, Constantino P, Wood B, Lawn B. Dental enamel as a dietary indicator in mammals. *BioEssays* 2008;30:374-85.
 - [42] Dunlop JWC, Fratzl P. Biological composites. *Annu Rev Mater Res* 2010;40:1-24.
 - [43] Gao HJ, Ji BH, Jager IL, Arzt E, Fratzl P. Materials become insensitive to flaws at nanoscale: lessons from Nature. *Proc Natl Acad Sci U S A* 2003;100:5597-600.
 - [44] Harjunmaa E, Kallonen A, Voutilainen M, Hamalainen K, Mikkola ML, Jernvall J. On the difficulty of increasing dental complexity. *Nature* 2012;483:324-7.
 - [45] Ji B, Gao H. Mechanical principles of biological nanocomposites. *Annu Rev Mater Res* 2010;40:77-100.
 - [46] Poolthong. Determination of the mechanical properties of enamel, dentine and cementum by an ultra micro - indentation system. Sydney: The University of Sydney; 1998.
 - [47] Baldassarri M, Margolis HC, Beniash E. Compositional determinants of mechanical properties of enamel. *J Dent Res* 2008;87:645-9.
 - [48] Angker L, Swain MV. Nanoindentation: Application to dental hard tissue investigations. *J Mater Res* 2006;21:1893-905.
 - [49] Barak MM, Geiger S, Chattah NLT, Shahar R, Weiner S. Enamel dictates whole tooth deformation: a finite element model study validated by a metrology method. *J Struct Biol* 2009;168:511-20.
 - [50] An B, Wang R, Arola D, Zhang D. The role of property gradients on the mechanical behavior of human enamel. *J Mech Behav Biomed Mater* 2012;9:63-72.

-
- [51] Lawn BR, Lee JJ-W, Constantino PJ, Lucas PW. Predicting failure in mammalian enamel. *J Mech Behav Biomed Mater* 2009;2:33-42.
- [52] Braun S, Bantleon HP, Hnat WP, Freudenthaler JW, Marcotte MR, Johnson BE. A study of bite force. 1. Relationship to various physical characteristics. *Angle Orthod* 1995;65:367-72.
- [53] Chai H, Lee JJW, Constantino PJ, Lucas PW, Lawn BR. Remarkable resilience of teeth. *Proc Natl Acad Sci U S A* 2009;106:7289-93.
- [54] He LH, Swain MV. Enamel - a functionally graded natural coating. *J Dent* 2009;37:596-603.
- [55] American Dental Association Council on Scientific Affairs. Tooth whitening/bleaching: treatment considerations for dentists and their patients. 2009 Sept. Revised 2010 Nov. Available from: http://www.ada.org/sections/about/pdfs/HOD_whitening_rpt.pdf.
- [56] Attin T, Hannig C, Wiegand A, Attin R. Effect of bleaching on restorative materials and restorations - a systematic review. *Dent Mater* 2004;20:852-61.
- [57] Goldberg M, Grootveld M, Lynch E. Undesirable and adverse effects of tooth-whitening products: a review. *Clin Oral Investig* 2010;14:1-10.
- [58] Joiner A. The bleaching of teeth: a review of the literature. *J Dent* 2006;34:412-9.
- [59] Joiner A. Review of the effects of peroxide on enamel and dentine properties. *J Dent* 2007;35:889-96.
- [60] Zimmerman B, Datko L, Cupelli M, Alapati S, Dean D, Kennedy M. Alteration of dentin - enamel mechanical properties due to dental whitening treatments. *J Mech Behav Biomed Mater* 2010;3:339-46.
- [61] He L-H, Swain MV. Nanoindentation creep behavior of human enamel. *J Biomed Mater Res A* 2009;91A:352-9.
- [62] Schneider GA, He LH, Swain MV. Viscous flow model of creep in enamel. *J Appl Phys* 2008;103.
- [63] Ungar P. Materials science: Strong teeth, strong seeds. *Nature* 2008;452:703-5.
- [64] Lanyon LE, Rubin CT. Functional adaptation in skeletal structures. In: Hildebrand M, Bramble DM, Liem KF, Wake DB, editors. *Functional vertebrate morphology*. Cambridge, Maas: Belknap Press; 1985. pp. 1-25.
- [65] Moss-Salentijn L, Moss ML, Yuan MS-T. The ontogeny of mammalian enamel. In: Koenigswald WV, Sander PM, editors. *Tooth enamel microstructure*. Rotterdam: Balkema; 1997.
- [66] Butler PM. The ontogeny of molar pattern. *Biol Rev* 1956;31:30-69.
- [67] Liebgott B. The anatomical basis of dentistry. 2nd ed. St. Louis, Missouri: Mosby, Inc.; 2001. Chapter 7, The head by regions. p. 355.
- [68] Boyde A. Microstructure of enamel. In: Chadwick DJ, Cardew G, editors. *Dental Enamel*. Chichester: John Wiley & Sons Ltd; 1997. pp. 18-31.
- [69] Driessens FCM, Verbeeck RMH. The mineral in tooth enamel and dental caries. In: Driessens FCM, Verbeeck RMH, editors. *Biominerals*. Boca Raton, Florida: CRC Press Inc.; 1990. p. 106.

-
- [70] Sakae T, Suzuki K, Kozawa Y. A short review of studies on chemical and physical properties of enamel crystallites. In: Koenigswald WV, Sander PM, editors. Tooth enamel microstructure. Rotterdam: Balkema; 1997.
- [71] Driessens FCM, Verbeeck RMH. The mineral in tooth enamel and dental caries. In: Driessens FCM, Verbeeck RMH, editors. Biominerals. Boca Raton, Florida: CRC Press; 1990. p. 118.
- [72] Drea WF. Spectrum analysis of dental tissues for "trace" elements. *J Dent Res* 1935;15:403-6.
- [73] Robinson C, Kirkham J, Brookes SJ, Shore RC. Chemistry of mature enamel. In: Robinson C, Kirkham J, Shore R, editors. Dental enamel: formation to destruction. Boca Raton, Florida: CRC Press; 1995.
- [74] Derise NL, Ritchey SJ. Mineral composition of normal human enamel and dentin and the relation of composition to dental caries: II. Microminerals. *J Dent Res* 1974;53:853-8.
- [75] Robinson C, Shore RC, Brookes SJ, Strafford S, Wood SR, Kirkham J. The chemistry of enamel caries. *Crit Rev Oral Biol Medicine* 2000;11:481-95.
- [76] Shaw JH, Yen PKJ. Sodium, potassium, and magnesium concentrations in the enamel and dentin of human and rhesus monkey teeth. *J Dent Res* 1972;51:95-101.
- [77] Legfros RZ, Sakae T, Bautista C, Retino M, Legeros JP. Magnesium and carbonate in enamel and synthetic apatites. *Adv Dent Res* 1996;10:225-31.
- [78] Cammack Smith M, Lantz E, Smith HV. The cause of mottled enamel. *J Dent Res* 1932;12:149-59.
- [79] Isaac S, Brudevold F, Smith FA, Gardner DE. Solubility rate and natural fluoride content of surface and subsurface enamel. *J Dent Res* 1958;37:254-63.
- [80] Legeros RZ, Bonel G, Legros R. Types of H₂O in human enamel and in precipitated apatites. *Calcif Tissue Res* 1978;26:111-8.
- [81] Bonte E, Deschamps N, Goldberg M, Vernois V. Quantification of free - water in human dental enamel. *J Dent Res* 1988;67:880-2.
- [82] Lowater F, Murray MM. Chemical composition of teeth. V. Spectrographic analysis. *Biochem J* 1937;31:837-41.
- [83] Schulze KA, Balooch M, Balooch G, Marshall GW, Marshall SJ. Micro - Raman spectroscopic investigation of dental calcified tissues. *J Biomed Mater Res A* 2004;69A:286-93.
- [84] Xu CQ, Yao XM, Walker MP, Wang Y. Chemical/molecular structure of the dentin - enamel junction is dependent on the intratooth location. *Calcif Tissue Int* 2009;84:221-8.
- [85] Tiznado-Orozco GE, Garcia-Garcia R, Reyes-Gasga J. Structural and thermal behaviour of carious and sound powders of human tooth enamel and dentine. *J Phys D: Appl Phys* 2009;42.
- [86] Kinoshita H, Miyoshi N, Fukunaga Y, Ogawa T, Ogasawara T, Sano K. Functional mapping of carious enamel in human teeth with Raman microspectroscopy. *J Raman Spectrosc* 2008;39:655-60.

-
- [87] Legeros RZ, Miravite MA, Quirolgico GB, Curzon MEJ. Effect of some trace elements on lattice parameters of human and synthetic apatites. *Calcif Tissue Res* 1977;22:362-7.
- [88] Warshawsky H. Organization of crystals in enamel. *Anat Rec* 1989;224:242-62.
- [89] Daculsi G, Kerebel B. High - resolution electron microscope study of human enamel crystallites: size, shape, and growth. *J Ultrastruct Res* 1978;65:163-72.
- [90] Kerebel B, Daculsi G, Kerebel LM. Ultrastructural studies of enamel crystallites. *J Dent Res* 1979;58:844-51.
- [91] Driessens FCM, Verbeeck RMH. The mineral in tooth enamel and dental caries. In: Driessens FCM, Verbeeck RMH, editors. *Biomaterials*. Boca Raton, Florida: CRC Press Inc.; 1990. p. 115.
- [92] Nanci A. Ten Cate's oral histology: development, structure, and function. 7th ed. St. Louis, Missouri, USA: Mosby Elsevier; 2008. p. 143.
- [93] Popowics TE, Rensberger JM, Herring SW. Enamel microstructure and microstrain in the fracture of human and pig molar cusps. *Arch Oral Biol* 2004;49:595-605.
- [94] Radlanski RJ, Renz H. A possible interdependency between the wavy path of enamel rods, distances of Retzius lines, and mitotic activity at the cervical loop in human teeth: a hypothesis. *Med Hypotheses* 2004;62:945-9.
- [95] Hunter J. The natural history of the human teeth: explaining their structure, use, formation, growth, and diseases ; A practical treatise on the diseases of the teeth : intended as a supplement to the natural history of those parts. Birmingham, Ala: Classics of Dentistry Library; 1979.
- [96] Schreger D. Beitrag zur Geschichte der Zähne. *Beitr Zergliederungskunst* 1800;1:1-7.
- [97] Osborn JW. A 3-dimensional model to describe the relation between prism directions, parazonal and diazonal, and the Hunter - Schreger bands in human tooth enamel. *Arch Oral Biol* 1990;35:869-78.
- [98] Martin T. On the systematic position of *Chaetomys subspinosus* (Rodentia: Caviomorpha) based on evidence from the incisor enamel microstructure. *J Mamm Evol* 1994;2:117-31.
- [99] Marshall AF, Lawless KR. TEM study of the central dark line in enamel crystallites. *J Dent Res* 1981;60:1773-82.
- [100] Lee JJ-W, Kwon J-Y, Chai H, Lucas PW, Thompson VP, Lawn BR. Fracture modes in human teeth. *J Dent Res* 2009;88:224-8.
- [101] Sognnaes RF. The organic elements of the enamel. *J Dent Res* 1950;29:260-9.
- [102] Xie ZH, Munroe PR, Moon RJ, Hoffman M. Characterization of surface contact - induced fracture in ceramics using a focused ion beam miller. *Wear* 2003;255:651-6.
- [103] Cairney JM, Munroe PR, Hoffman M. The application of focused ion beam technology to the characterization of coatings. *Surf Coat Technol* 2005;198:165-8.

-
- [104] Saunders M, Kong C, Shaw JA, Clode PL. Matrix - mediated biomineralization in marine mollusks: a combined transmission electron microscopy and focused ion beam approach. *Microsc Microanal* 2011;17:220-5.
- [105] Xie ZH, Swain M, Munroe P, Hoffman M. On the critical parameters that regulate the deformation behaviour of tooth enamel. *Biomaterials* 2008;29:2697-703.
- [106] Callister W.D.Jr, Rethwisch DG. Fundamentals of material science and engineering. An integrated approach. 3rd ed. Danvers, MA, USA: John Wiley and Sons; 2008. Chapter 7, Mechanical properties. pp. 186-235.
- [107] Shimizu D, Macho G, Spears I. Effect of prism orientation and loading direction on contact stresses in prismatic enamel of primates: implications for interpreting wear patterns. *Am J Phys Anthropol* 2005;126:427-34.
- [108] Katz JL, Misra A, Spencer P, Wang Y, Bumrerraj S, Nomura T, et al., editors. Multiscale mechanics of hierarchical structure/property relationships in calcified tissues and tissue/material interfaces. Symposium on Next Generation Biomaterials; 2005 Sep 25-28; Pittsburgh, PA.
- [109] White SN, Luo W, Paine ML, Fong H, Sarikaya M, Snead ML. Biological organization of hydroxyapatite crystallites into a fibrous continuum toughens and controls anisotropy in human enamel. *J Dent Res* 2001;80:321-6.
- [110] Bhowmick S, Jayaram V, Biswas SK. Deconvolution of fracture properties of TiN films on steels from nanoindentation load - displacement curves. *Acta Mater* 2005;53:2459-67.
- [111] He LH, Swain MV. Contact induced deformation of enamel. *Appl Phys Lett* 2007;90:3.
- [112] Spears IR. A three-dimensional finite element model of prismatic enamel: a re-appraisal of the data on the Young's modulus of enamel. *J Dent Res* 1997;76:1690-7.
- [113] Braly A, Darnell LA, Mann AB, Teaford MF, Weihs TP. The effect of prism orientation on the indentation testing of human molar enamel. *Arch Oral Biol* 2007;52:856-60.
- [114] Craig RG, Peyton FA, Johnson DW. Compressive properties of enamel, dental cements, and gold. *J Dent Res* 1961;40:936-45.
- [115] Guazzato M, Albakry M, Ringer SP, Swain MV. Strength, fracture toughness and microstructure of a selection of all-ceramic materials. Part II. Zirconia-based dental ceramics. *Dent Mater* 2004;20:449-56.
- [116] Chan YL, Ngan AHW, King NM. Use of focused ion beam milling for investigating the mechanical properties of biological tissues: a study of human primary molars. *J Mech Behav Biomed Mater* 2009;2:375-83.
- [117] Fischer-Cripps AC. Nanoindentation. 2nd ed. Ling FF, editor. New York: Springer Science + Business Media, LLC; 2004.
- [118] Ang SF, Scholz T, Klocke A, Schneider GA. Determination of the elastic/plastic transition of human enamel by nanoindentation. *Dent Mater* 2009;25:1403-10.
- [119] Whitenack LB, Simkins DC, Motta PJ, Hirai M, Kumar A. Young's modulus and hardness of shark tooth biomaterials. *Arch Oral Biol* 2010;55:203-9.

-
- [120] Ge J, Cui FZ, Wang XM, Feng HL. Property variations in the prism and the organic sheath within enamel by nanoindentation. *Biomaterials* 2005;26:3333-9.
- [121] Fong H, Sarikaya M, White SN, Snead ML. Nano - mechanical properties across dentin - enamel junction of adult human incisors. In: Li PJ, Calvert P, Kokubo T, Levy R, Scheid C, editors. *Mineralization in Natural and Synthetic Biomaterials*. Warrendale: Materials Research Society; 2000. pp. 85-90.
- [122] Dental biomaterials. Imaging, testing and modelling. Curtis RV, Watson TF, editors. Boca Raton, FL: CRC Press; 2008.
- [123] Li C, Risnes S. A comparison of resins for embedding teeth, with special emphasis on adaptation to enamel surface as evaluated by scanning electron microscopy. *Arch Oral Biol* 2004;49:77-83.
- [124] Kidd EAM, van Amerongen JP, van Amerongen WE. The role of operative treatment in caries control. In: Fejerskov O, Kidd EAM, Nyvad B, Baelum V, editors. *Dental caries: the diseases and its clinical management*. 2nd ed. Oxford, UK: Blackwell Munksgaard; 2009. pp. 363-64.
- [125] Samsonov GV, Gaevskaya LA, Adamovskii AA. Mechanism of abrasive polishing of refractory transition metals. *Powder Metall Met Ceram* 1976;15:71-4.
- [126] Guzzo PL, De Mello JDB. Effect of crystal orientation on lapping and polishing processes of natural quartz. *IEEE Trans Ultrason Ferroelectr Freq Control* 2000;47:1217-27.
- [127] Quinn GD, Ives LK, Jahanmir S. Machining cracks in finished ceramics. *Key Eng Mater* 2005;290:1-13.
- [128] Xie ZH, Moon RJ, Hoffman M, Munroe P, Cheng YB. Role of microstructure in the grinding and polishing of alpha - sialon ceramics. *J Eur Ceram Soc* 2003;23:2351-60.
- [129] Guidoni GM, He LH, Schoeberl T, Jaeger I, Dehm G, Swain MV. Influence of the indenter tip geometry and environment on the indentation modulus of enamel. *J Mater Res* 2009;24:616-25.
- [130] Lin CP, Douglas WH, Erlandsen SL. Scanning electron microscopy of type I collagen at the dentin-enamel junction of human teeth. *J Histochem Cytochem* 1993;41:381-8.
- [131] Rywkind AW. So-called scalloped appearance of the dentino - enamel junction. *J Am Dent Assoc* 1931:1103.
- [132] Mayer G. Rigid biological systems as models for synthetic composites. *Science* 2005;310:1144-7.
- [133] Fischer-Cripps AC. Critical review of analysis and interpretation of nanoindentation test data. *Surf Coat Technol* 2006;200:4153-65.
- [134] Hannig M, Hannig C. Nanomaterials in preventive dentistry. *Nat Nanotechnol* 2010;5:565-9.
- [135] Ortiz C, Boyce MC. Materials science - bioinspired structural materials. *Science* 2008;319:1053-4.
- [136] Fischer-Cripps A.C. *Nanoindentation*: Springer Science + Business media, LLC; 2004. pp 7, 25.

-
- [137] Oyen ML. Mechanics of indentation. In: OYEN ML, editor. Handbooks of nanoindentation with biological applications. Singapore: Pan Stanford Publishing; 2011. pp.123.
- [138] Field JS, Swain MV. A simple predictive model for spherical indentation. *J Mater Res* 1993;8:297-306.
- [139] Oliver WC, Pharr GM. Measurement of hardness and elastic modulus by instrumented indentation: advances in understanding and refinements to methodology. *J Mater Res* 2004;19:3-20.
- [140] Cranford SW, Tarakanova A, Pugno NM, Buehler MJ. Nonlinear material behaviour of spider silk yields robust webs. *Nature* 2012;482:72-U91.
- [141] Callister W.D.Jr, Rethwisch DG. Fundamentals of material science and engineering. An integrated approach. 3rd ed. Danvers, MA, USA: John Wiley and Sons; 2008. p. 326.
- [142] Ji B, Gao H. Mechanical properties of nanostructure of biological materials. *J Mech Phys Solids* 2004;52:1963-90.
- [143] He LH, Swain MV. Influence of environment on the mechanical behaviour of mature human enamel. *Biomaterials* 2007;28:4512-20.
- [144] Roach DH, Lathabai S, Lawn BR. Interfacial layers in brittle cracks. *J Am Ceram Soc* 1988;71:97-105.
- [145] Haywood VB, Heymann HO. Nightguard vital bleaching. *Quintessence Int* 1989;20:173-6.
- [146] Fasanaro TS. Bleaching teeth: history, chemicals, and methods used for common tooth discolorations. *J Esthet Dent* 1992;4:71-8.
- [147] Goldstein GR, Kiremidjianschumacher L. Bleaching: is it safe and effective? *J Prosthet Dent* 1993;69:325-8.
- [148] Sulieman MAM. An overview of tooth-bleaching techniques: chemistry, safety and efficacy. *Periodontol* 2000 2008;48:148-69.
- [149] Watts A, Addy M. Tooth discolouration and staining: a review of the literature. *Br Dent J* 2001;190:309-16.
- [150] Kelleher M. Dental bleaching: QuintEssentials of dental practice Vol. 38. Bremen: Quintessenz Verlag; 2010. Available from: <http://ECU.ebilib.com.au/patron/FullRecord.aspx?p=693907>.
- [151] Auschill TM, Hellwig E, Schmidale S, Sculean A, Arweiler NB. Efficacy, side-effects and patients' acceptance of different bleaching techniques (OTC, in-office, at-home). *Oper Dent* 2005;30:156-63.
- [152] Collins LZ, Maggio B, Liebman J, Blanck M, Lefort S, Waterfield P, et al. Clinical evaluation of a novel whitening gel, containing 6% hydrogen peroxide and a standard fluoride toothpaste. *J Dent* 2004;32:13-7.
- [153] Joiner A. Whitening toothpastes: a review of the literature. *J Dent* 2010;38:E17-E24.
- [154] Friedman S, Rotstein I, Libfeld H, Stabholz A, Heling I. Incidence of external root resorption and esthetic results in 58 bleached pulpless teeth. *Endod Dent Traumatol* 1988;4:23-6.
- [155] Buchalla W, Attin T. External bleaching therapy with activation by heat, light or laser - a systematic review. *Dent Mater* 2007;23:586-96.

- [156] Leonard RH, Jr., Haywood VB, Phillips C. Risk factors for developing tooth sensitivity and gingival irritation associated with nightguard vital bleaching. *Quintessence Int* 1997;28:527-34.
- [157] Tredwin CJ, Naik S, Lewis NJ, Scully C. Hydrogen peroxide tooth - whitening (bleaching) products: review of adverse effects and safety issues. *Br Dent J* 2006;200:371-6.
- [158] Hairul Nizam BR, Lim CT, Chng HK, Yap AUJ. Nanoindentation study of human premolars subjected to bleaching agent. *J Biomech* 2005;38:2204-11.
- [159] Attin T, Schmidlin PR, Weyhaupt F, Wiegand A. Influence of study design on the impact of bleaching agents on dental enamel microhardness: a review. *Dent Mater* 2009;25:143-57.
- [160] Magalhaes JG, Marimoto ARK, Torres CRG, Pagani C, Teixeira SC, Barcellos DC. Microhardness change of enamel due to bleaching with in-office bleaching gels of different acidity. *Acta Odontol Scand* 2012;70:122-6.
- [161] Kwon YH, Shin DH, Yun DI, Heo YJ, Seol HJ, Kim HI. Effect of hydrogen peroxide on microhardness and color change of resin nanocomposites. *Am J Dent* 2010;23:19-22.
- [162] Vieira C, Silva-Sousa YTC, Pessarello NM, Rached-Junior FAJ, Souza-Gabriel AE. Effect of high-concentrated bleaching agents on the bond strength at dentin/resin interface and flexural strength of dentin. *Braz Dent J* 2012;23:28-35.
- [163] Ellias E, Sajjan G. Effect of bleaching on microleakage of resin composite restorations in non-vital teeth: an *in-vitro* study. *Endod* 2002;14:9-14.
- [164] Hegedüs C, Bistey T, Flóra-Nagy E, Keszthelyi G, Jenei A. An atomic force microscopy study on the effect of bleaching agents on enamel surface. *J Dent* 1999;27:509-15.
- [165] Kaur D, Vishwanath, Jayalakshmi KB. Effect of various night guard vital bleaching agents on surface morphology of enamel - a SEM study. *Endod* 2003;15:2-7.
- [166] Bitter NC. A scanning electron microscopy study of the effect of bleaching agents on enamel: a preliminary report. *J Prosthet Dent* 1992;67:852-5.
- [167] Rotstein I, Dankner E, Goldman A, Heling I, Stabholz A, Zalkind M. Histochemical analysis of dental hard tissues following bleaching. *J Endod* 1996;22:23-6.
- [168] McCracken MS, Haywood VB. Demineralization effects of 10 percent carbamide peroxide. *J Dent* 1996;24:395-8.
- [169] Seghi RR, Denry I. Effects of external bleaching on indentation and abrasion characteristics of human enamel *in vitro*. *J Dent Res* 1992;71:1340-4.
- [170] McGuckin RS, Babin JF, Meyer BJ. Alterations in human enamel surface morphology following vital bleaching. *J Prosthet Dent* 1992;68:754-60.
- [171] Titley K, Torneck CD, Smith D. The effect of concentrated hydrogen peroxide solutions on the surface morphology of human tooth enamel. *J Endod* 1988;14:69-74.
- [172] Haywood VB, Leech T, Heymann HO, Crumpler D, Bruggers K. Nightguard vital bleaching: effects on enamel surface texture and diffusion. *Quintessence Int* 1990;21:801-4.

-
- [173] Wang X, Klocke A, Mihailova B, Stosch R, Guttler B, Bismayer U. Effect of bleaching on dental hard tissues: a Raman and IR spectroscopic study. *Key Eng Mater* 2007;330-332:1405-8.
- [174] Duschner H, Gotz H, White DJ, Kozak KM, Zoladz JR. Effects of hydrogen peroxide bleaching strips on tooth surface color, surface microhardness, surface and subsurface ultrastructure, and microchemical (Raman spectroscopic) composition. *J Clin Dent* 2006;17:72-8.
- [175] Smidt A, Feuerstein O, Topel M. Mechanical, morphologic, and chemical effects of carbamide peroxide bleaching agents on human enamel in situ. *Quintessence Int* 2011;42:407-12.
- [176] De Freitas ACP, Botta SB, Teixeira FD, Salvadori M, Garone-Netto N. Effects of fluoride or nanohydroxiapatite on roughness and gloss of bleached teeth. *Microsc Res Tech* 2011;74:1069-75.
- [177] Pretty IA, Edgar WM, Higham SM. The effect of bleaching on enamel susceptibility to acid erosion and demineralisation. *Br Dent J* 2005;198:285.
- [178] Khaustova SA, Shkurnikov MU, Grebenyuk ES, Artyushenko VG, Tonevitsky AG. Assessment of biochemical characteristics of the saliva using Fourier transform mid-infrared spectroscopy. *Bull Exp Biol Med* 2009;148:841-4.
- [179] Biswas SD, Kleinber.I. Effect of urea concentration on its utilization, on pH and formation of ammonia and carbon dioxide in a human salivary sediment system. *Arch Oral Biol* 1971;16:759-&.
- [180] Arends J, Jongebloed WL, Goldberg M, Schuthof J. Interaction of urea and human enamel. *Caries Res* 1984;18:17-24.
- [181] Jongebloed W, Arends J, Goldberg M, Schuthof J. A SEM study of urea interaction with human enamel. *J Dent Res* 1983;62:454.
- [182] Goldberg M, Arends J, Jongebloed WL, Schuthof J, Septier D. Action of urea solutions on human enamel surface. *Caries Res* 1983;17:106-12.
- [183] Qasim T, Ford C, Bush MB, Hu XZ, Malament KA, Lawn BR. Margin failures in brittle dome structures: Relevance to failure of dental crowns. *J Biomed Mater Res B Appl Biomater* 2007;80B:78-85.
- [184] Ford C, Qasim T, Bush MB, Hu X, Shah MM, Saxena VP, et al. Margin failures in crown-like brittle structures: off-axis loading. *J Biomed Mater Res B Appl Biomater* 2008;85B:23-8.
- [185] Chai H, Lee JJW, Kwon J-Y, Lucas PW, Lawn BR. A simple model for enamel fracture from margin cracks. *Acta Biomater* 2009;5:1663-7.
- [186] Barani A, Keown AJ, Bush MB, Lee JJW, Chai H, Lawn BR. Mechanics of longitudinal cracks in tooth enamel. *Acta Biomater* 2011;7:2285-92.
- [187] Katz JL. Hard tissue as a composite material. 1. Bounds on elastic behavior. *J Biomech* 1971;4:455-73.
- [188] Ashby MF, Jones DR. *Engineering materials*. 1st ed. Oxford, England: Pergamon Press; 1980.
- [189] *Dental enamel: formation to destruction*. Edited by Colin Robinson, Jennifer Kirkham, Roger Shore: Boca Raton: CRC Press; 1995.
- [190] Bruet BJF, Song JH, Boyce MC, Ortiz C. Materials design principles of ancient fish armour. *Nat Mater* 2008;7:748-56.

-
- [191] Keckes J, Burgert I, Fruhmenn K, Muller M, Kolln K, Hamilton M, et al. Cell - wall recovery after irreversible deformation of wood. *Nat Mater* 2003;2:810-4.
- [192] Fratzl P, Burgert I, Keckes J. Mechanical model for the deformation of the wood cell wall. *Z Metallkd* 2004;95:579-84.
- [193] Liu B, Zhang L, Gao H. Poisson ratio can play a crucial role in mechanical properties of biocomposites. *Mech Mater* 2006;38:1128-42.
- [194] Waters NE. Some mechanical and physical properties of teeth. In: Vincent JFV, Currey JD, editors. *The mechanical properties of biological materials*. Cambridge, UK: Cambridge University Press; 1980. pp. 99-135.
- [195] Low IM. Depth - profiling of crystal structure, texture, and microhardness in a functionally graded tooth enamel. *J Am Ceram Soc* 2004;87:2125-31.
- [196] White SN, Paine ML, Luo W, Sarikaya M, Fong H, Yu ZK, et al. The dentino - enamel junction is a broad transitional zone uniting dissimilar bioceramic composites. *J Am Ceram Soc* 2000;83:238-40.
- [197] Zantner C, Beheim-Schwarzbach N, Neumann K, Kielbassa AM. Surface microhardness of enamel after different home bleaching procedures. *Dent Mater* 2007;23:243-50.
- [198] Ebenstein DM, Pruitt LA. Nanoindentation of biological materials. *Nano Today* 2006;1:26-33.
- [199] He L-H, Carter E, Swain M. Characterization of nanoindentation - induced residual stresses in human enamel by Raman microspectroscopy. *Anal Bioanal Chem* 2007;389:1185-92.
- [200] Poolthong S, Swain MV, Mori T. Ultra micro - indentation of tooth using spherical and triangular indenters. *J Dent Res* 1998;77:1129-29.
- [201] An B-B, Wang R-R, Zhang D-S. Region-dependent micro damage of enamel under indentation. *Acta Mech Sin* 2012;28:1651-8.
- [202] Fischer-Cripps AC. A review of analysis methods for sub-micron indentation testing. *Vacuum* 2000;58:569-85.
- [203] Oliver WC, Pharr GM. An improved technique for determining hardness and elastic modulus using load and displacement sensing indentation experiments. *J Mater Res* 1992;7:1564-83.
- [204] Van Landingham MR. Review of instrumented indentation. *J Res Natl Inst Stand Technol* 2003;108:249-65.
- [205] Cheng CM, Cheng YT. On the initial unloading slope in indentation of elastic - plastic solids by an indenter with an axisymmetric smooth profile. *Appl Phys Lett* 1997;71:2623-5.
- [206] Pharr GM, Oliver WC, Brotzen FR. On the generality of the relationship among contact stiffness, contact area, and elastic modulus during indentation. *J Mater Res* 1992;7:613-7.
- [207] King RB. Elastic analysis of some punch problems for a layered medium. *Int J Solids Struct* 1987;23:1657-64.
- [208] Johnson KL. *Contact mechanics*. Cambridge: Cambridge University Press; 1985.
- [209] Fischer-Cripps AC. The hertzian contact surface. *J Mater Sci* 1999;34:129-37.

-
- [210] LaManna JA, Oliver WC, Pharr GM, editors. On the measurement of material creep parameters by nanoindentation. Symposium on Fundamentals of Nanoindentation and Nanotribology III held at the 2004 MRS Fall Meeting; 2005; Boston, MA.
- [211] Bower AF, Fleck NA, Needleman A, Ogbonna N. Indentation of a power law creeping solid. *Proc R Soc London Ser A-Math Phys Eng Sci* 1993;441:97-124.
- [212] Tabor D. The hardness of metals. Oxford: Clarendon Press; New York: Oxford University Press; 2000, c1951.
- [213] Stone DS, Jakes JE, Puthoff J, Elmustafa AA. Analysis of indentation creep. *J Mater Res* 2010;25:611-21.
- [214] Fischer-Cripps AC. A simple phenomenological approach to nanoindentation creep. *Mater Sci Eng, A* 2004;385:74-82.
- [215] Sneddon IN. Boussinesq's problem for a rigid cone. *Math Proc Cambridge Philos Soc* 1948;44:492-507.
- [216] Viscoelastic behaviour. In: Mills N, editor. *Plastics: Microstructure and engineering applications*. 3rd ed. Oxford, UK: Butterworth-Heinemann; 2005. pp. 205-8.
- [217] White JM, Goodis HE, Marshall SJ, Marshall GW. Sterilization of teeth by gamma radiation *J Dent Res* 1994;73:1560-7.
- [218] Struers 2013 Consumables Catalogue. Struers; 2013. Available from: http://www.struers.com/default.asp?top_id=3&main_id=155&doc_id=937&target=self&admin_language=2.
- [219] Xie ZH, Hoffman M, Munroe P, Singh R, Bendavid A, Martin PJ. Microstructural response of TiN monolithic and multilayer coatings during microscratch testing. *J Mater Res* 2007;22:2312-8.
- [220] Oyen ML, Ferguson VL. Bone as a composite material. In: Ochsner A, Ahmed W, editors. *Biomechanics of hard tissues*. Weinheim: Wiley-VCH Verlag GmbH & Co. KGaA; 2010.
- [221] Oberle TL. Properties influencing wear of metals. *J Met* 1951;3:438-39.
- [222] Gordon JE. Biomechanics: the last stronghold of vitalism. In: Vincent JFV, Currey JD, editors. *The mechanical properties of biological materials*. Cambridge, UK: Cambridge University Press; 1980. pp. 1-11.
- [223] Molnar S, Barrett MJ, Brian L, Brace CL, Brose DS, Dewey JR, et al. Tooth wear and culture: a survey of tooth functions among some prehistoric populations. *Curr Anthropol* 1972;13:511-26.
- [224] Zok FW, Miserez A. Property maps for abrasion resistance of materials. *Acta Mater* 2007;55:6365-71.
- [225] Leyland A, Matthews A. On the significance of the H/E ratio in wear control: a nanocomposite coating approach to optimised tribological behaviour. *Wear* 2000;246:1-11.
- [226] Lawn BR. Fracture of brittle solids. 2nd ed. New York: Cambridge University Press; 1993.
- [227] Weaver JC, Wang Q, Miserez A, Tantuccio A, Stromberg R, Bozhilov KN, et al. Analysis of an ultra hard magnetic biomineral in chiton radular teeth. *Mater Today* 2010;13:42-52.

-
- [228] Waltimo A, Kononen M. Maximal bite force and its association with signs and symptoms of craniomandibular disorders in young Finnish non-patients. *Acta Odontol Scand* 1995;53:254-8.
 - [229] Miserez A, Weaver JC, Thurner PJ, Aizenberg J, Dauphin Y, Fratzl P, et al. Effects of laminate architecture on fracture resistance of sponge biosilica: lessons from Nature. *Adv Funct Mater* 2008;18:1241-8.
 - [230] Bajaj D, Arola DD. On the R - curve behavior of human tooth enamel. *Biomaterials* 2009;30:4037-46.
 - [231] Fischer H, Marx R. Fracture toughness of dental ceramics: comparison of bending and indentation method. *Dent Mater* 2002;18:12-9.
 - [232] He L. Human enamel - elegantly designed natural biocomposite. Germany: VDM Verlag; 2009.
 - [233] Barthelat F. Biomimetics for next generation materials. *Philos Trans R Soc, A* 2007;365:2907.
 - [234] Sanchez C, Arribart H, Guille MMG. Biomimetism and bioinspiration as tools for the design of innovative materials and systems. *Nat Mater* 2005;4:277-88.
 - [235] Burgert I, Fratzl P. Plants control the properties and actuation of their organs through the orientation of cellulose fibrils in their cell walls. *Integr Comp Biol* 2009;49:69.
 - [236] Rief M, Gautel M, Oesterhelt F, Fernandez JM, Gaub HE. Reversible unfolding of individual titin immunoglobulin domains by AFM. *Science* 1997;276:1109.

12. Appendices

Appendix A: SEM images of tooth sectioning

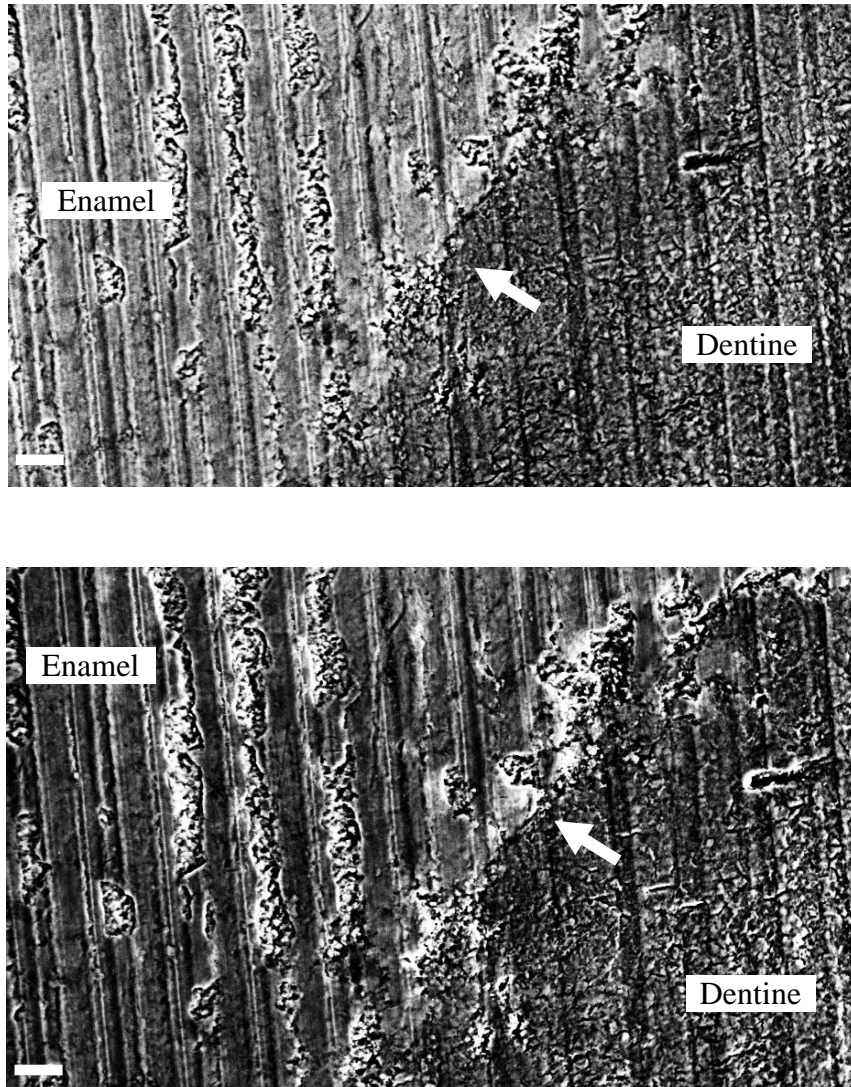


Figure 12-1. Backscattered electron images of the enamel-dentine junction after diamond saw sectioning. The images were taken on uncoated samples under the variable pressure of 9 Pa. Hard, brittle tooth enamel was found to be less resistant against severe damage than softer dentin with noticeable grooves from 30 μm to 50 μm . The arrowhead indicates the enamel-dentine junction. Scale bar = 20 μm .

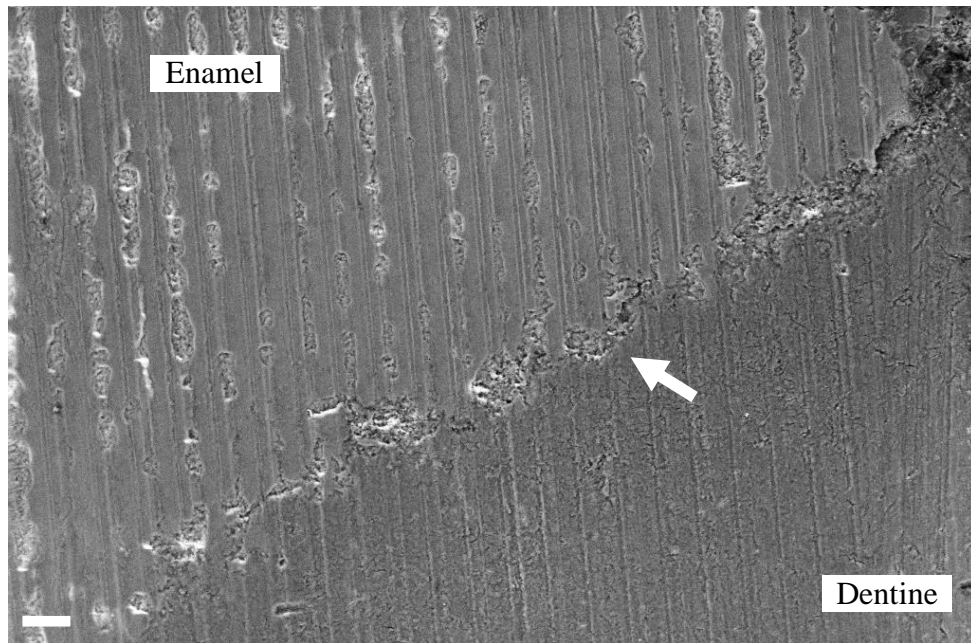


Figure 12-2. Secondary electron images of the enamel-dentine junction after diamond saw sectioning under variable pressure of 10 Pa. The arrowhead indicates transition of grooves from harder enamel to softer dentin. Scale bar = 20 μm .

Appendix B: Nanoindentation holder – part 1

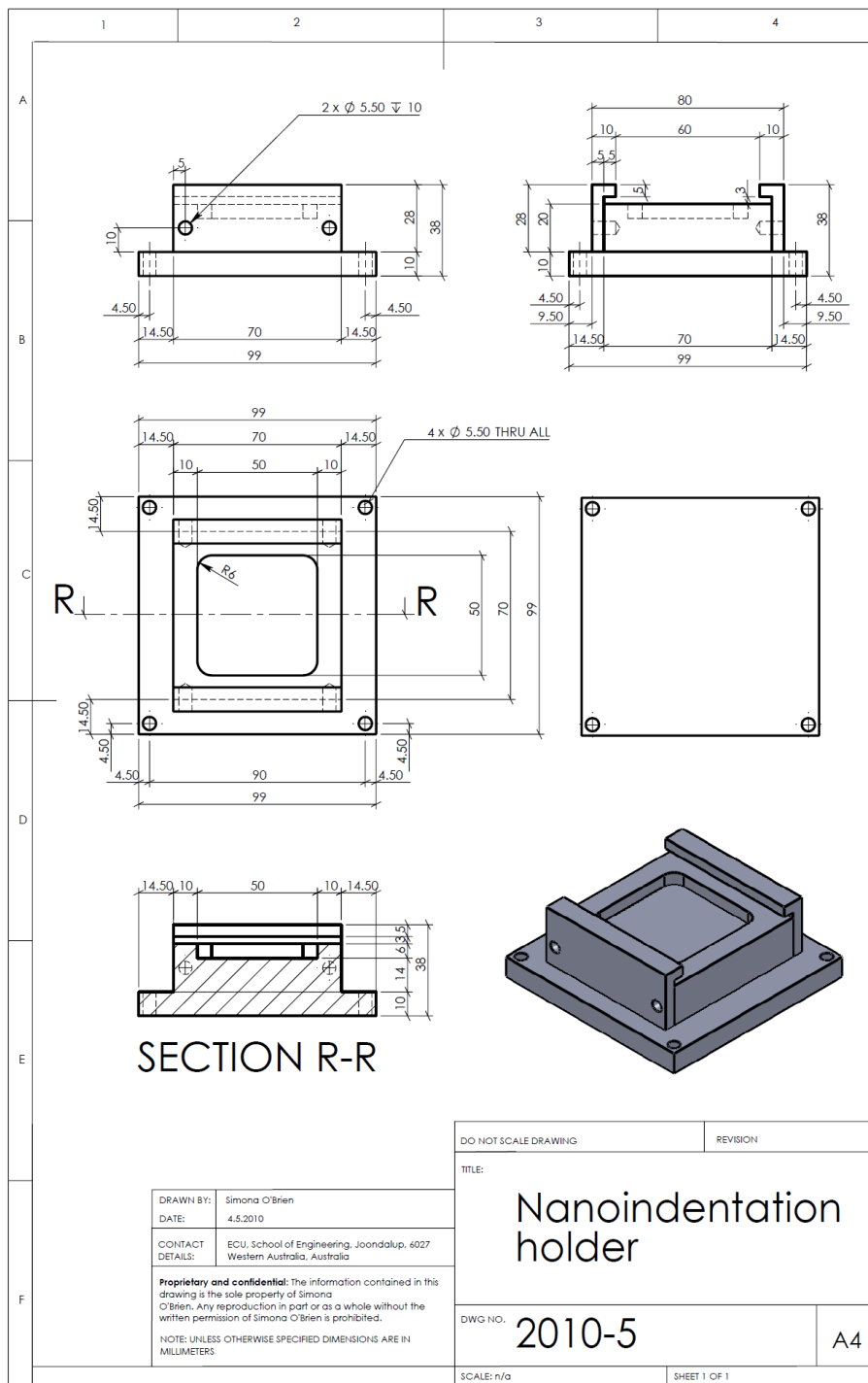


Figure 12-3. Nanoindentation holder developed for UMIS nanoindentation instrument to test tooth enamel in its hydrated state.

Appendix C: Nanoindentation holder – part 2

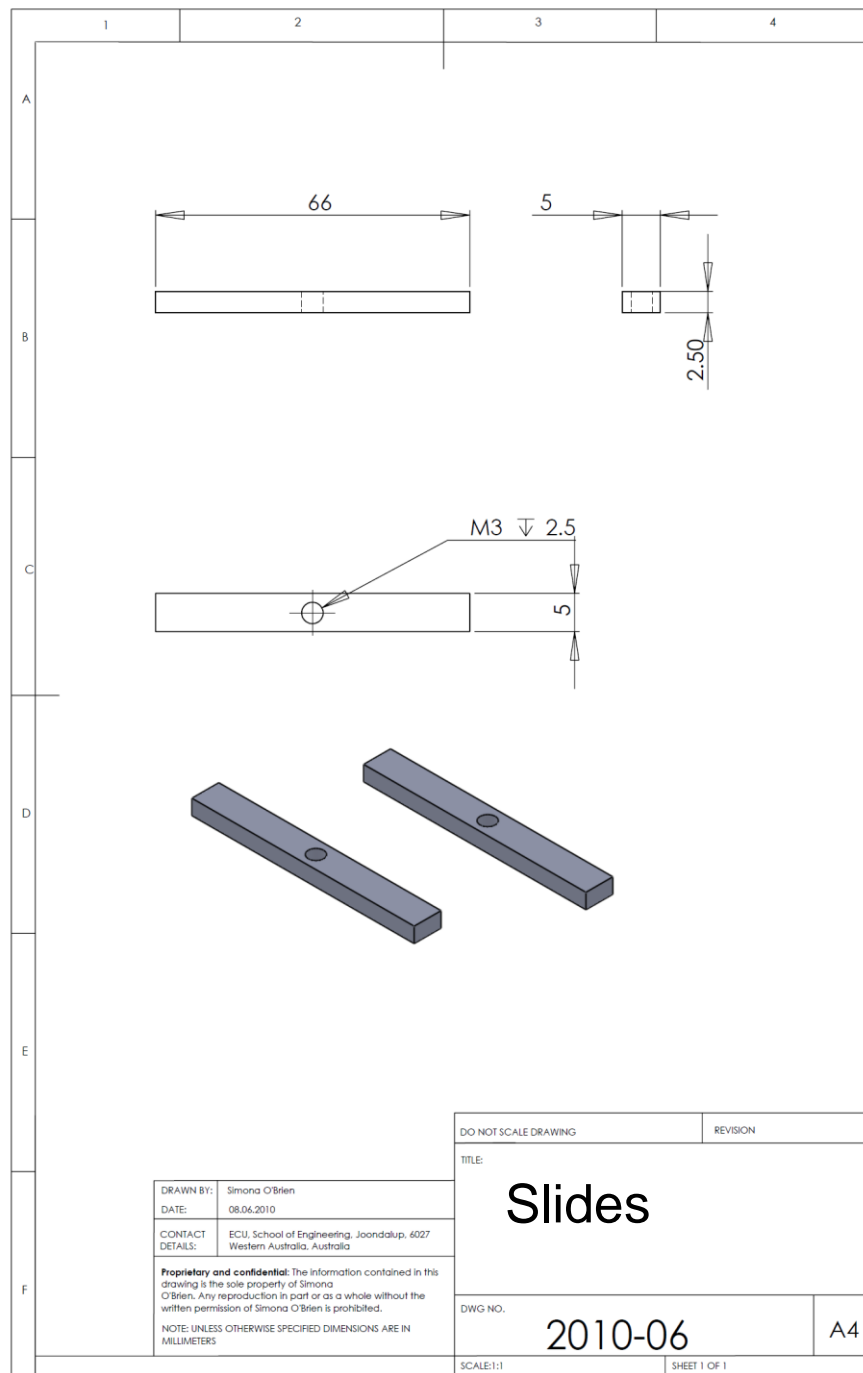


Figure 12-4. Slides used for mechanical mounting of the enamel specimens.

Appendix D: SEM images of Berkovich indents from different regions

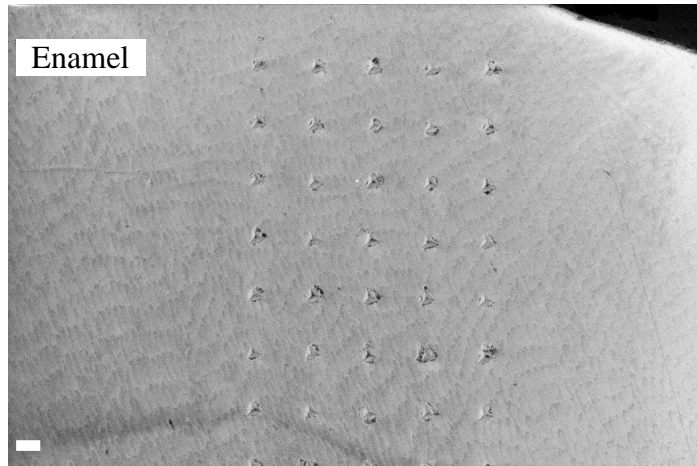


Figure 12-5. Backscattered SEM image of Berkovich indents near the occlusal surface of tooth enamel after applying the load of 400 mN. The indents and arrays are 50 µm apart with no evident residual overlaps. Scale bar = 20 µm.

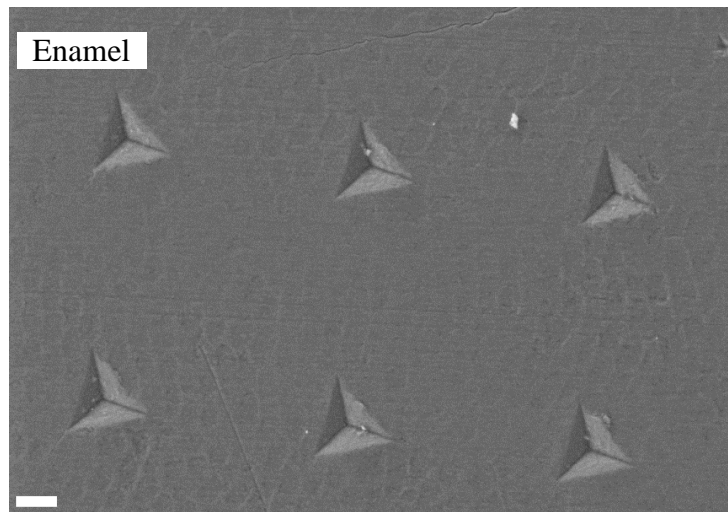


Figure 12-6. Backscattered SEM image of Berkovich indents 50 µm apart in the middle region of tooth enamel. Notably, the applied load of 400 mN did not yield crack. Scale bar = 10 µm.

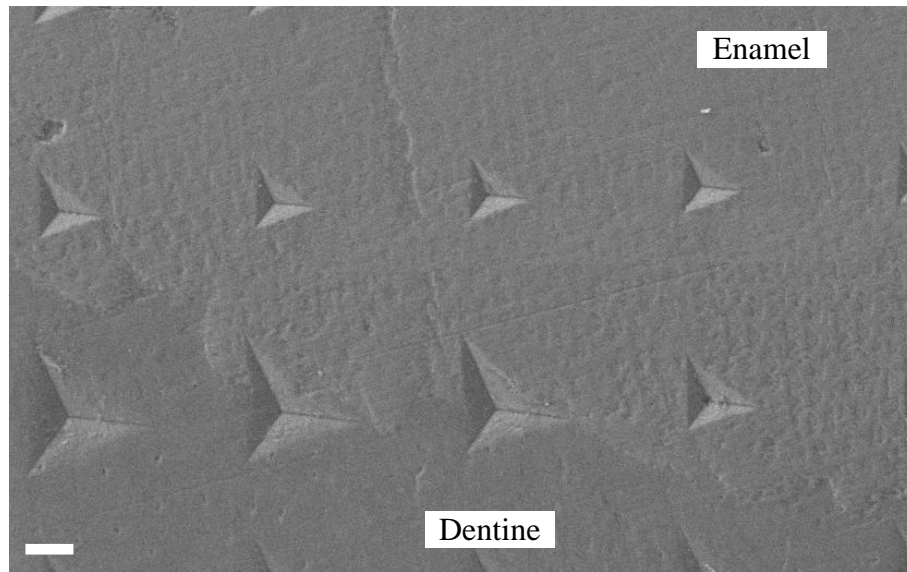


Figure 12-7. Berkovich indents across the enamel-dentine junction. There were no radial cracks initiated from the edges of indents even after 400 mN load across the boundary between hard, brittle enamel and soft, tough dentin. Scale bar = 10 μm .

Appendix E: E and H spatial distribution

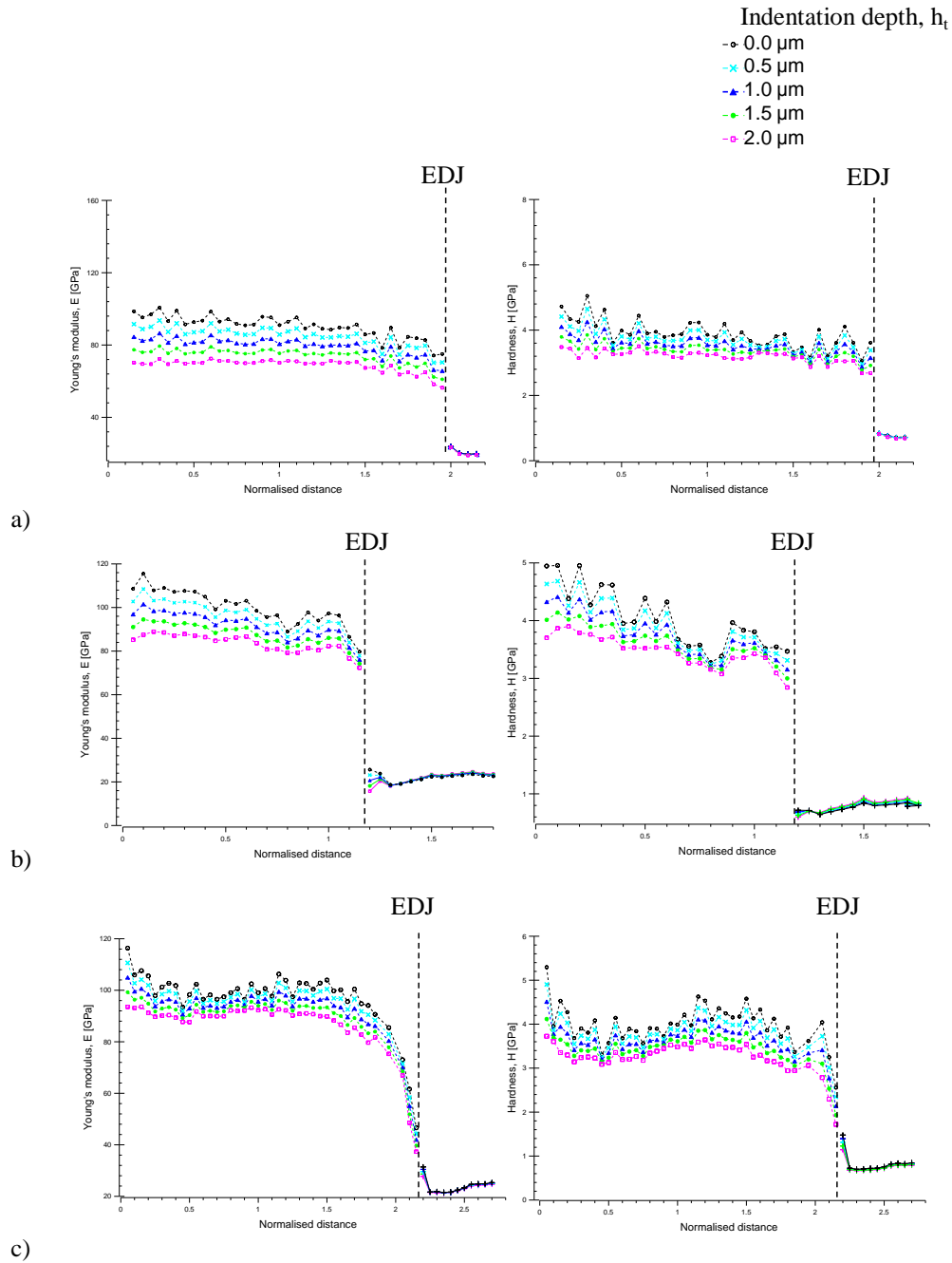


Figure 12-8. Typical distributions of E and H of three healthy molars (a-c) from the enamel occlusal surface (normalised distance = 0) across the enamel-dentine junction (EDJ). The EDJ is indicated by a dashed line in the charts.

Appendix F: E values - conventional methods A and B

Table 12-1. E moduli values comparison between conventional methods A and B.

Young's modulus, E [GPa]	Comparison of conventional method, B to conventional method A				
Depth [μm]	0.00	0.50	1.00	1.50	2.00
Conventional method, B	92.50	78.63	66.55	56.25	47.75
Std. error, std. method B	2.24	3.31	4.20	4.71	4.81
Max	94.73	81.94	70.74	60.97	52.56
Min	90.26	75.32	62.35	51.54	42.93
Conventional method, A	98.60	92.99	87.49	82.12	76.87
Std. error, std. method A	1.95	1.96	2.28	2.67	3.09
Max	100.55	94.94	89.77	84.79	79.97
Min	96.66	91.03	85.21	79.45	73.78
Comparison of means: method B to A in %	-6.19%	-15.44%	-23.94%	-31.50%	-37.89%
Max	-5.78%	-13.70%	-21.20%	-28.10%	-34.27%
Min	-6.62%	-17.25%	-26.82%	-35.13%	-41.81%
Average % - Max (absolute value)	0.41%	1.74%	2.74%	3.40%	3.62%
Min - Average % (absolute value)	0.43%	1.82%	2.88%	3.63%	3.92%
Averaged std. error comparison in % (absolute value)	0.42%	1.78%	2.81%	3.52%	3.77%
Overall average	-22.99%				
Overall std. error	6.30%				

Table 12-2. P-values from t-tests for comparing E values between conventional methods A and B at 0 μm indentation depth.

Depth 0 μm		
t-Test: Two-Sample Assuming Equal Variances	Method B	Method A
Mean	92.495	98.603
Variance	40.077	30.312
P(T<=t) two-tail	0.047	
Note: there is a significant difference between E values		
F-Test Two-Sample for Variances		
P(F<=f) one-tail	0.364	
P(F<=f) two-tail	0.182	

Table 12-3. P-values from t-tests for comparing E values between conventional methods A and B at 0.5 μm indentation depth.

Depth 0.5 μm		
t-Test: Two-Sample Assuming Equal Variances	Method B	Method A
Mean	78.629	92.985
Variance	87.527	38.327
P(T<=t) two-tail	0.002	
Note: there is a significant difference between E values		
F-Test Two-Sample for Variances		
P(F<=f) one-tail	0.144	
P(F<=f) two-tail	0.289	

Table 12-4. P-values from t-tests for comparing E values between conventional methods A and B at 1.0 μm indentation depth.

Depth 1.0 μm		
t-Test: Two-Sample Assuming Equal Variances	Method B	Method A
Mean	66.548	87.491
Variance	140.818	52.169
P(T<=t) two-tail	0.001	
Note: there is a significant difference between E values		
F-Test Two-Sample for Variances		
P(F<=f) one-tail	0.102	
P(F<=f) two-tail	0.204	

Table 12-5. P-values from t-tests for comparing E values between conventional methods A and B at 1.5 μm indentation depth.

Depth 1.5 μm		
t-Test: Two-Sample Assuming Equal Variances	Method B	Method A
Mean	56.254	82.119
Variance	177.651	71.268
P(T<=t) two-tail	0.001	
Note: there is a significant difference between E values		
F-Test Two-Sample for Variances		
P(F<=f) one-tail	0.121	
P(F<=f) two-tail	0.242	

Table 12-6. P-values from t-tests for comparing E values between conventional methods A and B at 2.0 μm indentation depth.

Depth 2.0 μm		
t-Test: Two-Sample Assuming Equal Variances	Method B	Method A
Mean	47.745	76.871
Variance	185.418	95.781
P(T<=t) two-tail	0.001	
Note: there is a significant difference between E values		
F-Test Two-Sample for Variances		
P(F<=f) one-tail	0.198	
P(F<=f) two-tail	0.396	

Appendix G: H values - conventional methods A and B

Table 12-7. H values comparison between conventional methods A and B.

Hardness, H [GPa]	Comparison of conventional method, B to conventional method A				
Depth [μm]	0.00	0.50	1.00	1.50	2.00
Conventional method, B	4.63	4.17	3.79	3.39	3.08
Std. error, std. method B	0.05	0.05	0.08	0.07	0.08
Max	4.68	4.22	3.87	3.46	3.17
Min	4.58	4.12	3.71	3.32	3.00
Conventional method, A	4.64	4.22	3.89	3.65	3.48
Std. error, std. method A	0.08	0.03	0.05	0.07	0.08
Max	4.72	4.25	3.94	3.72	3.56
Min	4.57	4.19	3.84	3.58	3.40
Comparison of means: method B to A in %	-0.26%	-1.11%	-2.61%	-6.94%	-11.48%
Max	-0.78%	-0.67%	-1.95%	-6.81%	-11.12%
Min	0.27%	-1.56%	-3.29%	-7.06%	-11.87%
Average % - Max (absolute value)	-0.52%	0.44%	0.66%	0.12%	0.36%
Min - Average % (absolute value)	-0.54%	0.45%	0.68%	0.13%	0.38%
Averaged std. error comparison in % (absolute value)	-0.53%	0.44%	0.67%	0.13%	0.37%
Overall average	-4.48%				
Overall std. error	2.34%				

Table 12-8. P-values from t-tests employed for comparing H values between conventional methods A and B at the enamel surface (i.e., 0 μm indentation depth).

Depth 0 μm		
t-Test: Two-Sample Assuming Equal Variances	Method B	Method A
Mean	4.629	4.641
Variance	0.021	0.046
P(T<=t) two-tail	0.896	
Note: there is no significant difference between H values		
F-Test Two-Sample for Variances		
P(F<=f) one-tail	0.162	
P(F<=f) two-tail	0.081	

Table 12-9. P-values from t-tests employed for comparing H values between conventional methods A and B at 0.5 μm indentation depth.

Depth 0.5 μm		
t-Test: Two-Sample Assuming Equal Variances	Method B	Method A
Mean	4.173	4.220
Variance	0.020	0.008
P(T \leq t) two-tail	0.446	
Note: there is no significant difference between H values		
F-Test Two-Sample for Variances		
P(F \leq f) one-tail	0.127	
P(F \leq f) two-tail	0.254	

Table 12-10. P-values from t-tests employed for comparing H values between conventional methods A and B at 1.0 μm indentation depth.

Depth 1.0 μm		
t-Test: Two-Sample Assuming Equal Variances	Method B	Method A
Mean	3.791	3.893
Variance	0.047	0.022
P(T \leq t) two-tail	0.291	
Note: there is no significant difference between H values		
F-Test Two-Sample for Variances		
P(F \leq f) one-tail	0.162	
P(F \leq f) two-tail	0.324	

Table 12-11. P-values from t-tests employed for comparing H values between conventional methods A and B at 1.5 μm indentation depth.

Depth 1.5 μm		
t-Test: Two-Sample Assuming Equal Variances	Method B	Method A
Mean	3.394	3.647
Variance	0.039	0.039
P(T \leq t) two-tail	0.023	
Note: there is a significant difference between H values		
F-Test Two-Sample for Variances		
P(F \leq f) one-tail	0.497	
P(F \leq f) two-tail	0.993	

Table 12-12. P-values from t-tests employed for comparing H values between conventional methods A and B at 2 μm indentation depth.

Depth 2.0 μm		
t-Test: Two-Sample Assuming Equal Variances	Method B	Method A
Mean	3.083	3.483
Variance	0.058	0.053
P(T<=t) two-tail	0.004	
Note: there is a significant difference between H values		
F-Test Two-Sample for Variances		
P(F<=f) one-tail	0.456	
P(F<=f) two-tail	0.911	

Appendix H: E values - conventional method A and the new method

Table 12-13. E moduli values comparison between conventional method A and the new method.

Young's modulus, E [GPa]		Comparison of new method to conventional method A			
Depth [μm]	0.00	0.50	1.00	1.50	2.00
New method	114.97	106.27	99.01	93.16	88.75
Std. error, new method	1.41	0.92	0.76	0.79	0.82
Max	116.38	107.19	99.76	93.95	89.57
Min	113.56	105.35	98.25	92.38	87.92
Conventional method, A	98.60	92.99	87.49	82.12	76.87
Std. error, std. method A	1.95	1.96	2.28	2.67	3.09
Max	100.55	94.94	89.77	84.79	79.97
Min	96.66	91.03	85.21	79.45	73.78
Comparison of means: new method to method, A in %	16.60%	14.29%	13.16%	13.45%	15.45%
Max	15.74%	12.90%	11.13%	10.80%	12.01%
Min	17.49%	15.74%	15.30%	16.27%	19.18%
Average % - Max (absolute value)	0.85%	1.39%	2.03%	2.65%	3.44%
Min - Average % (absolute value)	0.89%	1.45%	2.14%	2.82%	3.73%
Average std. error comparison in % (absolute value)	0.87%	1.42%	2.09%	2.73%	3.58%
Overall average	14.59%				
Overall std. error	0.72%				

Table 12-14. P-values from t-tests for comparing E values between conventional method A and the new method at the enamel surface (i.e., 0 μm indentation depth).

Depth 0 μm		
t-Test: Two-Sample Assuming Equal Variances	New method	Method A
Mean	114.968	98.603
Variance	15.907	30.312
P(T<=t) two-tail	8.48E-06	
Note: there is a significant difference between E values		
F-Test Two-Sample for Variances		
P(F<=f) one-tail	0.207	
P(F<=f) two-tail	0.104	

Table 12-15. P-values from t-tests for comparing E values between conventional method A and the new method at 0.5 μm indentation depth.

Depth 0.5 μm		
t-Test: Two-Sample Assuming Unequal Variances	New method	Method A
Mean	106.273	92.985
Variance	6.749	38.327
P(T<=t) two-tail	0.001	
Note: there is a significant difference between E values		
F-Test Two-Sample for Variances		
P(F<=f) one-tail	0.018	
P(F<=f) two-tail	0.036	

Table 12-16. P-values from t-tests for comparing E values between conventional method A and the new method at 1.0 μm indentation depth.

Depth 1.0 μm		
t-Test: Two-Sample Assuming Unequal Variances	New method	Method A
Mean	99.005	87.491
Variance	4.606	52.169
P(T<=t) two-tail	0.003	
Note: there is a significant difference between E values		
F-Test Two-Sample for Variances		
P(F<=f) one-tail	0.002	
P(F<=f) two-tail	0.005	

Table 12-17. P-values from t-tests for comparing E values between conventional method A and the new method at 1.5 μm indentation depth.

Depth 1.5 μm		
t-Test: Two-Sample Assuming Unequal Variances	New method	Method A
Mean	93.163	82.119
Variance	4.940	71.268
P(T<=t) two-tail	0.007	
Note: there is a significant difference between E values		
F-Test Two-Sample for Variances		
P(F<=f) one-tail	0.001	
P(F<=f) two-tail	0.002	

Table 12-18. P-values from t-tests for comparing E values between conventional method A and the new method at 2.0 μm indentation depth.

Depth 2.0 μm		
t-Test: Two-Sample Assuming Unequal Variances	New method	Method A
Mean	88.748	76.871
Variance	5.435	95.781
P(T<=t) two-tail	0.010	
Note: there is a significant difference between E values		
F-Test Two-Sample for Variances		
P(F<=f) one-tail	0.001	
P(F<=f) two-tail	0.001	

Appendix I: H values - conventional method A and the new method

Table 12-19. H values comparison between conventional method A and the new method.

Comparison of new method to conventional method A					
Hardness, H [GPa]					
Depth [μm]	0.00	0.50	1.00	1.50	2.00
New method	5.10	4.48	4.07	3.66	3.47
Std. error, new method	0.13	0.07	0.04	0.05	0.05
Max	5.23	4.55	4.11	3.71	3.52
Min	4.97	4.41	4.03	3.62	3.41
Conventional method, A	4.64	4.22	3.89	3.65	3.48
Std. error, std. method A	0.08	0.03	0.05	0.07	0.08
Max	4.72	4.25	3.94	3.72	3.56
Min	4.57	4.19	3.84	3.58	3.40
Average %	9.85%	6.17%	4.59%	0.46%	-0.51%
Max	10.79%	7.11%	4.29%	-0.11%	-1.28%
Min	8.87%	5.21%	4.90%	1.06%	0.30%
Average % - Max (absolute value)	-0.95%	-0.95%	0.30%	0.57%	0.77%
Min - Average % (absolute value)	-0.98%	-0.96%	0.31%	0.60%	0.81%
Average std. error comparison in % (absolute value)	-0.96%	-0.95%	0.30%	0.59%	0.79%
Overall average	4.11%				
Overall std. error	2.12%				

Table 12-20. P-values from t-tests for comparing H values between conventional method A and the new method at the enamel surface (i.e., 0 μm indentation depth).

Depth 0 μm		
t-Test: Two-Sample Assuming Unequal Variances	New method	Method A
Mean	5.098	4.641
Variance	0.132	0.046
P(T<=t) two-tail	0.011	
Note: there is a significant difference between H values		
F-Test Two-Sample for Variances		
P(F<=f) one-tail	0.021	
P(F<=f) two-tail	0.041	

Table 12-21. P-values from t-tests for comparing H values between conventional method A and the new method at 0.5 μm indentation depth.

Depth 0.5 μm		
t-Test: Two-Sample Assuming Unequal Variances	New method	Method A
Mean	4.481	4.220
Variance	0.044	0.008
P(T<=t) two-tail	0.009	
Note: there is a significant difference between H values		
F-Test Two-Sample for Variances	New method	Method A
P(F<=f) one-tail	0.021	
P(F<=f) two-tail	0.041	

Table 12-22. P-values from t-tests for comparing H values between conventional method A and the new method at 1.0 μm indentation depth.

Depth 1.0 μm		
t-Test: Two-Sample Assuming Equal Variances	New method	Method A
Mean	4.072	3.893
Variance	0.012	0.022
P(T<=t) two-tail	0.016	
Note: there is no significant difference between H values		
F-Test Two-Sample for Variances		
P(F<=f) one-tail	0.240	
P(F<=f) two-tail	0.480	

Table 12-23. P-values from t-tests for comparing H values between conventional method A and the new method at 1.5 μm indentation depth.

Depth 1.5 μm		
t-Test: Two-Sample Assuming Equal Variances	New method	Method A
Mean	3.664	3.647
Variance	0.019	0.039
P(T<=t) two-tail	0.847	
Note: there is no significant difference between H values		
F-Test Two-Sample for Variances		
P(F<=f) one-tail	0.183	
P(F<=f) two-tail	0.366	

Table 12-24. P-values from t-tests for comparing H values between conventional method A and the new method at 2.0 μm indentation depth.

Depth 2.0 μm		
t-Test: Two-Sample Assuming Equal Variances	New method	Method A
Mean	3.465	3.483
Variance	0.023	0.053
P(T<=t) two-tail	0.858	
Note: there is no significant difference between H values		
F-Test Two-Sample for Variances		
P(F<=f) one-tail	0.144	
P(F<=f) two-tail	0.288	

Appendix J: E and H values for wet and dry samples

Table 12-25. E and H values of “enamel sample 1” in dry and wet environments. The overall mean values denote the average of all E values for all indentation depths and regions.

Enamel sample 1					
E values [GPa]	Indentation depth [μm]				
	0.00	0.50	1.00	1.50	2.00
Dry sample					
Mean E [GPa]	100.39	97.11	94.84	92.58	90.31
Standard error of E [GPa]	1.46	0.81	0.64	0.49	0.40
Overall E mean [GPa]	95.04				
Overall E standar error [GPa]	0.79				
Wet sample					
Mean E [GPa]	99.37	96.43	92.48	88.52	84.57
Standard error of E [GPa]	1.01	1.35	1.25	1.16	1.07
Overall E mean [GPa]	92.28				
Overall E standar error [GPa]	1.19				
Dry to wet E ratio	1.01	1.01	1.03	1.05	1.07
Dry to wet E overall ratio	1.03				

H values [GPa]					
Dry sample					
Mean H [GPa]	4.37	4.19	4.02	3.84	3.67
Standard error of H [GPa]	0.03	0.02	0.02	0.03	0.04
Overall mean [GPa]	4.02				
Overall standard error [GPa]	0.05				
Wet sample					
Mean H [GPa]	3.99	3.85	3.72	3.59	3.46
Standard error of H [GPa]	0.17	0.14	0.11	0.08	0.05
Overall H mean [GPa]	3.72				
Overall H standard error [GPa]	0.06				
Dry to wet H ratio	1.10	1.09	1.08	1.07	1.06
Dry to wet H overall ratio	1.08				

Table 12-26. E and H values of “enamel sample 2” in dry and wet environments. The overall mean values denote the average of all E values for all indentation depths and regions.

Enamel sample 2					
	Indentation depth [μm]				
E values [GPa]	0.00	0.50	1.00	1.50	2.00
Dry sample					
Mean E [GPa]	102.46	99.95	97.44	94.93	92.42
Standard error of E [GPa]	1.63	1.23	0.83	0.43	0.12
Overall E mean [GPa]	97.44				
Overall E standard error [GPa]	0.91				
Wet sample					
Mean E [GPa]	97.20	94.88	92.57	91.51	88.71
Standard error of E [GPa]	1.22	1.03	1.02	1.43	1.04
Overall E mean [GPa]	92.64				
Overall E standard error [GPa]	0.81				
Dry to wet E ratio	1.05	1.05	1.05	1.04	1.04
Dry to wet E ratio standard error	1.05				

H values [GPa]					
Dry sample					
Mean H [GPa]	4.53	4.35	4.17	3.99	3.81
Standard error of H [GPa]	0.17	0.14	0.10	0.07	0.04
Overall mean [GPa]	4.17				
Overall standard error [GPa]	0.07				
Wet sample					
Mean H [GPa]	4.27	4.09	3.90	3.72	3.54
Standard error of H [GPa]	0.14	0.11	0.08	0.06	0.04
Overall H mean [GPa]	3.90				
Overall H standard error [GPa]	0.06				
Dry to wet H ratio	1.06	1.06	1.07	1.07	1.08
Dry to wet H overall ratio	1.07				

Appendix K: Indentation depths for occlusal surface and EDJ

Table 12-27. Values of indentation depths measured at the occlusal surface and near the EDJ.

Specimen 1		Specimen2		Specimen 2	
Occlusal surface	EDJ	Occlusal surface	EDJ	Occlusal surface	EDJ
0.78	0.93	0.82	0.91	0.84	0.82
1.28	1.36	1.21	1.28	1.29	1.19
1.56	1.73	1.46	1.55	1.50	1.47
1.77	2.02	1.72	1.78	1.68	1.71
1.97	2.28	1.92	2.05	1.95	1.91
2.31	2.52	2.24	2.22	2.11	2.12
2.64	2.77	2.41	2.39	2.24	2.31
2.79	3.07	2.58	2.55	2.38	2.48
0.88	0.79	0.69	0.85	0.78	0.83
1.24	1.16	1.11	1.23	1.26	1.22
1.49	1.44	1.35	1.53	1.48	1.52
1.70	1.71	1.65	1.76	1.67	1.78
1.92	1.95	1.83	1.99	1.83	2.00
2.15	2.24	2.02	2.18	2.01	2.20
2.58	2.43	2.31	2.37	2.36	2.39
2.74	2.61	2.47	2.53	2.53	2.56
0.81	0.74	0.76	0.80	0.81	0.81
1.16	1.09	1.19	1.20	1.12	1.19
1.60	1.40	1.42	1.46	1.34	1.49
1.79	1.66	1.66	1.69	1.70	1.74
2.11	1.91	1.85	1.90	1.90	1.96
2.32	2.12	2.02	2.09	2.04	2.16
2.52	2.31	2.19	2.27	2.17	2.35
2.79	2.49	2.38	2.44	2.31	2.53
0.84	0.89	0.72	0.80	0.74	0.83
1.16	1.30	1.07	1.17	1.21	1.21
1.46	1.59	1.37	1.45	1.43	1.51
1.69	1.83	1.58	1.69	1.62	1.76
1.89	2.08	1.74	1.92	1.78	2.00
2.10	2.30	1.93	2.09	1.96	2.22
2.57	2.51	2.09	2.26	2.15	2.43
2.72	2.73	2.25	2.42	2.30	2.63
0.82	0.90	0.74	0.80	0.75	0.98
1.18	1.45	1.11	1.17	1.18	1.39
1.68	1.92	1.43	1.46	1.50	1.69
1.96	2.34	1.63	1.70	1.67	1.94
2.16	2.71	1.82	1.91	1.85	2.19
2.35	3.07	2.13	2.24	2.01	2.45
2.53	3.37	2.28	2.39	2.16	2.69
2.70	3.64	2.41	2.53	2.30	2.88
Average:	1.87	1.98	1.69	1.77	1.84

Summary:

Indentation depth difference between occlusal surface and EDJ in %

Specimen 1 0.06

Specimen 2 0.05

Specimen 3 0.08

Overall difference (\pm standard deviation) 6.11 (\pm 1.42)%

Appendix L: Elastic behaviour of tooth enamel

Table 12-28. Resulting values of enamel model in its elastic region.

Variable:		Value	
hm [nm]		50	
hp = d [nm]		1.5	
l [nm]		500	
vm [-]		0.25	
vp [-]		0.45	
Em [GPa]		129	
Ep [GPa]		2	
d [nm]		1.5	
Calculate		Resulting value	
Gp [GPa]	Shear modulus of protein	$G_p = E_p / (2 \cdot (1 + \nu_p))$	0.69
Kp [GPa]	Bulk modulus of protein	$K_p = E_p / (3 \cdot (1 - 2\nu_p))$	6.67
G [GPa]	Shear modulus of mineral-protein comp.	$G = [(h_p + h_m) / h_p] \cdot G_p$	23.68
Φ_m [-]	Volume fraction of mineral	$\Phi = h_m / (h_m + h_p)$	0.97
ρ [-]	Aspect ratio	$\rho = l / h_m$	10.00
E1 reduced [GPa]	Elastic modulus of the composite parallel to c axis	$1/E_1 = 4 \cdot (1 - \Phi) / (G_p \cdot \Phi^2 \cdot \rho^2) + 1 / \Phi \cdot E_m$	102.28
E2 sandwich [GPa]	Elastic modulus of the composite perpend. to c axis. Sandwich model	$1/E_2 = 3h_p / (h_p + h_m) \cdot (4G_p + 3K_p) + 1 / E_m \cdot 3K_p / (4G_p + 3K_p) \cdot (h_m^2 + 4\nu_m h_m h_p + 2h_p^2 - 2\nu_m h_p^2) / h_m \cdot (h_m + h_p)$	93.80
E2 staggered [GPa]			93.79
E1 if alpha not =1, ie. not uniform shear deformation between mineral platelets			
Conditions:			
Gp € <0.05;0.2>			
Gp ≈ Ep/3			
Em/Ep = 1000			
E2 STAGGERED	Elastic modulus of the composite perpend. to c axis. Staggered model	$1/E_2 = 12K_p h_p (h_m + h_p) / \alpha^2 G_p (4G_p + 3K_p) + 1 / E_{sandwich}$	125.22
Factor α		$12K_p h_p (h_m + h_p)$	6180.00
$[(h_p + h_m) \cdot l]^2$		$\alpha^2 l^2 G_p (4G_p + 3K_p)$	6097599168.86
$(h_p(l+d))^2$		c_{26}/c_{27}	0.00
$1 + 4/3(B_{27}/B_{28})$			
l-d			
l+d			
alpha factor			
E1 if alpha is not equal 1			
$(h_p + h_m) / h_m$			1.03
$4h_p h_m / \alpha^2 G_p$			1.11972E-06
			125.2246306

Table 12-29. Mean \pm standard deviation of E values at 5 indents (from one indentation row) measured from the middle region (i.e., a normalised distance of 0.5) used for the calculation of the effective crystal orientation angle, θ as a function of indentation depth, h for specimen 1.

E [GPa]	A	B	C	X1	X2	sqrt(X1)	Sqrt(X2)			Angle	MINUS SD	PLUS SD
95.70	-184.74	280.44	-93.79	0.50	1.02	0.71	1.01	-0.71	-1.01	44.85	0.41	0.44
92.91	-187.53	280.44	-93.79	0.50	0.99	0.71	1.00	-0.71	-1.00	45.28	0.58	0.66
89.70	-190.74	280.44	-93.79	0.51	0.96	0.72	0.98	-0.72	-0.98	45.83	0.39	0.43
88.53	-191.91	280.44	-93.79	0.52	0.94	0.72	0.97	-0.72	-0.97	46.04	0.44	0.49
86.71	-193.73	280.44	-93.79	0.52	0.92	0.72	0.96	-0.72	-0.96	46.40	0.52	0.59
85.59	-194.85	280.44	-93.79	0.53	0.91	0.73	0.95	-0.73	-0.95	46.63	0.55	0.63
85.13	-195.31	280.44	-93.79	0.53	0.91	0.73	0.95	-0.73	-0.95	46.74	0.73	0.87
82.65	-197.79	280.44	-93.79	0.54	0.88	0.74	0.94	-0.74	-0.94	47.32	0.47	0.53
98.58	-181.86	280.44	-93.79	0.49	1.05	0.70	1.03	-0.70	-1.03	44.45	0.55	
96.73	-183.71	280.44	-93.79	0.49	1.03	0.70	1.02	-0.70	-1.02	44.71		
91.98	-188.46	280.44	-93.79	0.51	0.98	0.71	0.99	-0.71	-0.99	45.43		
91.00	-189.44	280.44	-93.79	0.51	0.97	0.71	0.98	-0.71	-0.98	45.60		
89.43	-191.01	280.44	-93.79	0.52	0.95	0.72	0.98	-0.72	-0.98	45.88		
88.31	-192.13	280.44	-93.79	0.52	0.94	0.72	0.97	-0.72	-0.97	46.08		
88.72	-191.72	280.44	-93.79	0.52	0.95	0.72	0.97	-0.72	-0.97	46.01		
84.63	-195.81	280.44	-93.79	0.53	0.90	0.73	0.95	-0.73	-0.95	46.85		
92.82	-187.62	280.44	-93.79	0.51	0.99	0.71	0.99	-0.71	-0.99	45.30		
89.09	-191.35	280.44	-93.79	0.52	0.95	0.72	0.97	-0.72	-0.97	45.94		
87.42	-193.02	280.44	-93.79	0.52	0.93	0.72	0.96	-0.72	-0.96	46.26		
86.06	-194.38	280.44	-93.79	0.53	0.92	0.73	0.96	-0.73	-0.96	46.53		
83.99	-196.45	280.44	-93.79	0.53	0.89	0.73	0.94	-0.73	-0.94	46.99		
82.87	-197.57	280.44	-93.79	0.54	0.88	0.73	0.94	-0.73	-0.94	47.26		
81.54	-198.90	280.44	-93.79	0.55	0.86	0.74	0.93	-0.74	-0.93	47.61		
80.67	-199.77	280.44	-93.79	0.55	0.85	0.74	0.92	-0.74	-0.92	47.85		

P [mN]	E [GPa]	θ°
50.00	95.70 \pm 2.88	44.85 +0.44 -0.41
100.00	92.91 \pm 3.82	45.28 +0.66 -0.58
150.00	89.70 \pm 2.28	45.83 +0.43 -0.39
200.00	88.53 \pm 2.47	46.04 +0.49 -0.44
250.00	86.71 \pm 2.72	46.40 +0.59 -0.52
300.00	85.59 \pm 2.72	46.63 +0.63 -0.55
350.00	85.13 \pm 3.59	46.74 +0.87 -0.73
400.00	82.65 \pm 1.98	47.32 +0.53 -0.47

Table 12-30. Mean \pm standard deviation of E values at 5 indents (from one indentation row) measured from the middle region (i.e., a normalised distance of 0.5) used for the calculation of the effective crystal orientation angle, θ as a function of indentation depth, h for specimen 2.

E [GPa]	A	B	C	X1	X2	sqrt(X1)	Sqrt(X2)			Angle	MINUS SD	PLUS SD
97.54	-182.90	280.44	-93.79	0.49	1.04	0.70	1.02	-0.70	-1.02	44.59	0.26	0.27
95.14	-185.30	280.44	-93.79	0.50	1.01	0.71	1.01	-0.71	-1.01	44.94	0.38	0.41
93.13	-187.31	280.44	-93.79	0.50	0.99	0.71	1.00	-0.71	-1.00	45.25	0.18	0.19
92.29	-188.15	280.44	-93.79	0.51	0.98	0.71	0.99	-0.71	-0.99	45.38	0.13	0.13
92.19	-188.25	280.44	-93.79	0.51	0.98	0.71	0.99	-0.71	-0.99	45.40	0.18	0.19
91.38	-189.06	280.44	-93.79	0.51	0.97	0.71	0.99	-0.71	-0.99	45.53	0.15	0.15
90.36	-190.08	280.44	-93.79	0.51	0.96	0.72	0.98	-0.72	-0.98	45.71	0.16	0.16
89.12	-191.32	280.44	-93.79	0.52	0.95	0.72	0.97	-0.72	-0.97	45.93	0.14	0.14
99.45	-180.99	280.44	-93.79	0.49	1.06	0.70	1.03	-0.70	-1.03	44.33	0.20	
97.78	-182.66	280.44	-93.79	0.49	1.04	0.70	1.02	-0.70	-1.02	44.56		
94.30	-186.14	280.44	-93.79	0.50	1.01	0.71	1.00	-0.71	-1.00	45.06		
93.09	-187.35	280.44	-93.79	0.50	0.99	0.71	1.00	-0.71	-1.00	45.25		
93.31	-187.13	280.44	-93.79	0.50	0.99	0.71	1.00	-0.71	-1.00	45.22		
92.27	-188.17	280.44	-93.79	0.51	0.98	0.71	0.99	-0.71	-0.99	45.39		
91.26	-189.18	280.44	-93.79	0.51	0.97	0.71	0.99	-0.71	-0.99	45.55		
89.88	-190.56	280.44	-93.79	0.51	0.96	0.72	0.98	-0.72	-0.98	45.79		
95.63	-184.81	280.44	-93.79	0.50	1.02	0.71	1.01	-0.71	-1.01	44.86		
92.50	-187.94	280.44	-93.79	0.51	0.99	0.71	0.99	-0.71	-0.99	45.35		
91.96	-188.48	280.44	-93.79	0.51	0.98	0.71	0.99	-0.71	-0.99	45.44		
91.49	-188.95	280.44	-93.79	0.51	0.98	0.71	0.99	-0.71	-0.99	45.52		
91.07	-189.37	280.44	-93.79	0.51	0.97	0.71	0.99	-0.71	-0.99	45.59		
90.49	-189.95	280.44	-93.79	0.51	0.96	0.72	0.98	-0.72	-0.98	45.69		
89.46	-190.98	280.44	-93.79	0.52	0.95	0.72	0.98	-0.72	-0.98	45.87		
88.36	-192.08	280.44	-93.79	0.52	0.94	0.72	0.97	-0.72	-0.97	46.08		

P [mN]	E [GPa]	θ°
50.00	97.54 \pm 1.91	44.59 +0.27 -0.26
100.00	95.14 \pm 2.64	44.94 +0.41 -0.38
150.00	93.13 \pm 1.17	45.25 +0.19 -0.18
200.00	92.29 \pm 0.80	45.38 +0.13 -0.13
250.00	92.19 \pm 1.12	45.40 +0.19 -0.18
300.00	91.38 \pm 0.89	45.53 +0.15 -0.15
350.00	90.36 \pm 0.90	45.71 +0.16 -0.16
400.00	89.12 \pm 0.76	45.55 +0.14 -0.14

Appendix M: E values for tooth enamel during whitening treatment

Table 12-31. E values of tooth enamel during 14 days bleaching treatment.

The Young's modulus [GPa]	Indentation depth [μm]					Overall
AVERAGE	0.00	0.50	1.00	1.50	2.00	-
DAY1: no bleaching	103.94	97.95	91.96	85.97	79.98	91.96
DAY1: no bleaching, SD	1.46	1.62	1.92	2.32	2.77	1.55
The Young's modulus [GPa]	Indentation depth [μm]					Overall
AVERAGE	0.00	0.50	1.00	1.50	2.00	-
DAY 2: 1 day bleaching	105.60	100.23	94.86	89.50	84.13	94.86
DAY 2: 1 day bleaching, SD	2.12	2.00	2.13	2.45	2.91	1.52
The Young's modulus [GPa]	Indentation depth [μm]					Overall
AVERAGE	0.00	0.50	1.00	1.50	2.00	-
DAY 4: 3 days bleaching	104.51	100.28	96.04	91.81	87.58	96.04
DAY 4: 3 days bleaching, SD	2.09	1.94	1.81	1.73	1.69	1.35
The Young's modulus [GPa]	Indentation depth [μm]					Overall
AVERAGE	0.00	0.50	1.00	1.50	2.00	-
DAY 8: 7 days bleaching	104.10	98.87	93.63	88.39	83.16	93.63
DAY 8: 7 days bleaching, SD	1.45	1.50	1.64	1.85	2.11	1.34
The Young's modulus [GPa]	Indentation depth [μm]					Overall
AVERAGE	0.00	0.50	1.00	1.50	2.00	-
DAY 15: 14 days bleaching	104.76	97.84	90.93	84.01	77.10	90.93
DAY 15: 14 days bleaching, SD	2.77	2.23	1.72	1.30	1.06	1.69
The Young's modulus [GPa]	Indentation depth [μm]					Overall
AVERAGE	0.00	0.50	1.00	1.50	2.00	-
DAY 22: 1 week recovery	97.67	92.46	87.26	82.05	76.85	87.26
DAY 22: 1 week recovery, SD	1.97	1.98	2.11	2.34	2.65	1.46
Differences between recovered enamel and unbleached enamel	0.06	0.06	0.05	0.05	0.04	
Mean difference for indentation depth 0 and 1.5 μm	0.05					
Std. deviation for indentation depth 0 and 1.5 μm	0.01					
Differences between recovered enamel and 14 days bleached enamel	0.07	0.05	0.04	0.02	0.00	
Mean difference for indentation depths 0 and 1.5 μm	0.05					
Std. deviation for indentation depth 0 and 1.5 μm	0.02					

Appendix N: H values for tooth enamel during whitening treatment

Table 12-32. H values of human tooth enamel during whitening treatment.

The Young's modulus [GPa]	Indentation depth [μm]					Overall
AVERAGE	0.00	0.50	1.00	1.50	2.00	-
DAY1: no bleaching	4.28	4.04	3.81	3.57	3.33	3.81
DAY1: no bleaching, SD	0.11	0.10	0.09	0.09	0.10	0.07
The Young's modulus [GPa]	Indentation depth [μm]					Overall
AVERAGE	0.00	0.50	1.00	1.50	2.00	-
DAY 2: 1 day bleaching	4.44	4.17	3.91	3.64	3.38	3.91
DAY 2: 1 day bleaching, SD	0.13	0.11	0.09	0.08	0.08	0.07
The Young's modulus [GPa]	Indentation depth [μm]					Overall
AVERAGE	0.00	0.50	1.00	1.50	2.00	-
DAY 4: 3 days bleaching	4.28	4.06	3.83	3.61	3.39	3.83
DAY 4: 3 days bleaching, SD	0.11	0.09	0.07	0.05	0.04	0.07
The Young's modulus [GPa]	Indentation depth [μm]					Overall
AVERAGE	0.00	0.50	1.00	1.50	2.00	-
DAY 8: 7 days bleaching	4.21	4.00	3.79	3.58	3.37	3.79
DAY 8: 7 days bleaching, SD	0.11	0.09	0.08	0.06	0.06	0.06
The Young's modulus [GPa]	Indentation depth [μm]					Overall
AVERAGE	0.00	0.50	1.00	1.50	2.00	-
DAY 15: 14 days bleaching	4.48	4.19	3.91	3.63	3.34	3.91
DAY 15: 14 days bleaching, SD	0.19	0.16	0.14	0.11	0.09	0.09
The Young's modulus [GPa]	Indentation depth [μm]					Overall
AVERAGE	0.00	0.50	1.00	1.50	2.00	-
DAY 22: 1 week recovery	3.57	3.39	3.21	3.02	2.84	3.21
DAY 22: 1 week recovery, SD	0.16	0.14	0.11	0.09	0.09	0.06
Differences between recovered enamel and unbleached enamel	0.17	0.16	0.16	0.15	0.15	
Mean difference for indentation depth 0 and 2.0 μm	0.16					
Std. deviation for indentation depth 0 and 2.0 μm	0.01					
Differences between recovered enamel and 14 days bleached enamel	0.20	0.19	0.18	0.17	0.15	
Mean difference for indentation depths 0 and 2.0 μm	0.18					
Std. deviation for indentation depth 0 and 2.0 μm	0.02					

Appendix O: Stress-strain properties of unbleached and bleached enamel

Table 12-33. Experimental stress-strain values of unbleached enamel in its elastic-plastic region.

Sound enamel		Bleached enamel		Sound enamel		Bleached enamel	
ε [-]	σ [GPa]	ε [-]	σ [GPa]	ε [-]	σ [GPa]	ε [-]	σ [GPa]
0.019399454	3.000284	0.059223	3.065561	0.0245412	2.337557	0.0812725	4.27564
0.0311102	3.706704	0.0822181	3.516573	0.0377288	2.635642	0.0989029	4.480052
0.04271262	3.91787	0.0931121	3.913349	0.0483839	3.272387	0.1112067	4.474267
0.0536758	3.982789	0.1040729	4.117671	0.0573951	3.623638	0.122422	4.631022
0.06310308	4.202327	0.1145439	4.337181	0.0664873	3.972208	0.132067	4.733591
0.07191566	4.443325	0.1252601	4.457236	0.0760109	4.198354	0.1396502	4.827995
0.0804965	4.569816	0.1348045	4.538462	0.0848312	4.373466	0.0571584	3.195386
0.0892307	4.676704	0.0599283	3.04023	0.0935118	4.495286	0.0808415	3.6896
0.0982102	4.732808	0.0801925	3.79926	0.1018295	4.593628	0.0806019	3.905934
0.10706238	4.821146	0.0800093	3.957779	0.1098034	4.705336	0.1005361	4.337238
0.11614644	4.888074	0.097582	4.622631	0.1182665	4.841598	0.1127729	4.470912
0.1253246	4.932003	0.1067439	4.936758	0.1270596	4.948369	0.1226762	4.617051
0.13504702	5.011731	0.1163171	5.052284	0.1351101	5.044605	0.1311447	4.800377
0.018422616	3.243412	0.1266487	5.101793	0.0197676	2.88027	0.1407776	4.749356
0.03057726	3.767115	0.1350119	5.168097	0.0302645	3.715747	0.0571154	3.299853
0.04105142	3.811519	0.0699515	2.647707	0.0394971	4.072058	0.0806714	3.724552
0.05102772	4.301571	0.0840632	3.100658	0.0483724	4.632127	0.0941283	3.893942
0.05994766	4.476565	0.0964375	3.591026	0.0560739	4.958851	0.105148	4.050265
0.06942948	4.674934	0.1053067	4.04662	0.0642702	5.166389	0.1147637	4.317095
0.0781961	4.805948	0.1142865	4.358734	0.0725248	5.328329	0.1269475	4.359878
0.08731156	4.84926	0.1230193	4.595041	0.0809921	5.449015	0.1359423	4.465216
0.09656696	4.923282	0.1314952	4.776445	0.0889294	5.48049	0.0688891	2.694865
0.1057185	4.92413	0.1388236	4.888339	0.097533	5.515971	0.0817537	3.561985
0.1152917	4.97281	0.0750378	2.366586	0.1066886	5.431083	0.0902279	3.874565
0.12482328	4.987825	0.0794039	2.721641	0.1163924	5.420109	0.1001731	4.371619
0.13451774	5.034566	0.0993001	3.344896	0.1258883	5.445055	0.1064091	4.501224
0.02006694	2.961455	0.1052386	3.653895	0.136072	5.418108	0.121331	4.701719
0.03215346	3.484949	0.1194185	4.028411	0.0212989	2.776232	0.1301841	4.873909
0.0426094	3.865534	0.1281556	4.289557	0.0350026	3.20049	0.1388947	4.881745
0.051779	4.080295	0.1363073	4.438586	0.0469761	3.559457	0.0568502	3.323904
0.06119752	4.343865	0.0658001	2.847793	0.0578443	3.588963	0.0776583	4.145315
0.06992356	4.580155	0.0820956	3.533973	0.0683769	3.920414	0.0791435	4.031207
0.07901636	4.705454	0.0940488	3.911186	0.0789051	4.059009	0.098121	4.561542
0.08843042	4.749701	0.1023604	4.221361	0.0890489	4.122633	0.107634	4.872593
0.0971239	4.81629	0.1109882	4.476927	0.0985445	4.223484	0.1176102	4.95472
0.1060809	4.900917	0.1209533	4.728796	0.1076912	4.324986	0.12745	5.049557
0.11469764	4.984396	0.1301139	4.880292	0.117156	4.395565	0.1352076	5.154318
0.12251286	5.064031	0.1374705	4.98615				
0.13055012	5.191578	0.0561785	3.372485				
0.13932958	5.267976	0.0774843	4.157374				

Table 12-34. The best fit modelling values (i.e., $\tau_c = 2.5\%$ of E_2 and $\theta = 50^\circ$) of unbleached enamel in its elastic-plastic region.

Calculated values from elastic model					$\tau = 2.5 \% E_2$ Sound enamel: $\theta = 50$ degrees	
G [GPa]	23.68				strain	stress
E2 for staggered composite [GPa]	93.79				0.000	0.000
$2*\tau(\cos\theta/\sin\theta)$					0.005	0.374
$\tau = 2.5 \% E_2$ [GPa]	2.34				0.007	0.524
Angle θ	E elastic	E plastic	τ 2.5 % * E2	$2*\tau(\cos\theta/\sin\theta)$	0.010	0.749
50.00	74.90	8.21		3.94	0.020	1.498
ELASTIC REGION		PLASTIC REGION		Modelling:	0.030	2.247
ϵ	σ	ϵ	σ	Elastic region: $\sigma = E_{elastic} * \epsilon$	0.040	2.996
0.00	0.00	0.00	4.08	Plastic region: $\sigma = E_{plastic} * \epsilon + 2*\tau(\cos\theta/\sin\theta)$	0.050	3.745
0.01	0.75	0.01	4.16		0.060	4.494
0.02	1.50	0.02	4.24		0.061	4.579
0.03	2.25	0.03	4.32		0.061	4.579
0.04	3.00	0.04	4.41		0.070	4.652
0.05	3.74	0.05	4.49		0.080	4.734
0.06	4.49	0.06	4.57		0.090	4.816
0.07	5.24	0.07	4.65		0.100	4.898
0.08	5.99	0.08	4.73		0.110	4.980
Elastic		Plastic		Critical point Elastic=Plastic	0.120	5.062
Angle	a1	a2	b	b/a1-a2	0.130	5.144
50.00	74.90	8.21	4.08	0.061	0.140	5.227

Table 12-35. The best fit modelling values (i.e., $\tau_c = 2.0\%$ of E_2 and $\theta = 50^\circ$) of unbleached enamel in its elastic-plastic region.

Calculated values from elastic model					$\tau = 2.0\% \cdot E_2$ Sound enamel: $\theta = 50^\circ$ strain stress	
G [GPa]	23.68					
E2 for staggered composite [GPa]	93.79					
$2 \cdot \tau(\cos\theta/\sin\theta)$						
$\tau = 2\% \cdot E_2$ [GPa]	1.88					
Angle θ	E elastic	E plastic	τ	$2 \cdot \tau(\cos\theta/\sin\theta)$		
50.00	74.90	8.21	$2\% \cdot E_2$	3.15	0.000	0.000
					0.005	0.374
					0.007	0.524
					0.010	0.749
ELASTIC REGION		PLASTIC REGION		Modelling:		
ϵ	σ	ϵ	σ	Elastic region: $\sigma = E_{\text{elastic}} \cdot \epsilon$		
0.00	0.00	0.00	3.26		0.020	1.498
0.01	0.00	0.01	3.34		0.030	2.247
0.02	0.00	0.02	3.43	Plastic region: $\sigma = E_{\text{plastic}} \cdot \epsilon + 2 \cdot \tau(\cos\theta/\sin\theta)$	0.040	2.996
0.03	0.00	0.03	3.51		0.047	3.536
0.04	0.00	0.04	3.59		0.047	3.536
0.05	0.00	0.05	3.67		0.050	3.559
0.06	0.00	0.06	3.75		0.060	3.641
0.07	0.00	0.07	3.84		0.070	3.723
0.08	0.00	0.08	3.92		0.080	3.805
					0.090	3.887
					0.100	3.969
					0.110	4.052
Elastic		Plastic		Critical point Elastic=Plastic		
Angle	a1	a2	b	b/a1-a2		
	74.899	8.21299503	3.148114		0.120	4.134
50	049	7	271	0.047	0.130	4.216
					0.140	4.298

Table 12-36. The best fit modelling values (i.e., $\tau_c = 1.5\%$ of E_2 and $\theta = 54^\circ$) of unbleached enamel in its elastic-plastic region.

Calculated values from elastic model					$\tau = 1.5\% \cdot E_2$ Bleached enamel: $\theta = 54$ degrees	
G [GPa]	23.68				strain	stress
E2 for staggered composite [GPa]	93.79				0	0.00
$2 \cdot \tau(\cos\theta/\sin\theta)$						
$\tau = 1.5\% \cdot E_2$ [GPa]	1.41					
Angle θ	E elastic	E plastic	τ	$2 \cdot \tau(\cos\theta/\sin\theta)$		
			1.5% *			
54.00	70.90	20.91	E_2	2.04	0.005	0.35
					0.007	0.50
					0.01	0.71
ELASTIC REGION		PLASTIC REGION		Modelling:		
ε	σ	ε	σ	Elastic region:		
0.00	0.00	0.00	2.04	$\sigma = E_{\text{elastic}} \cdot \varepsilon$	0.02	1.42
0.01	0.71	0.01	2.25		0.03	2.13
0.02	1.42	0.02	2.46	Plastic region:	0.04	2.84
				$\sigma = E_{\text{plastic}} \cdot \varepsilon + 2 \cdot \tau(\cos\theta/\sin\theta)$	0.041	2.899
0.03	2.13	0.03	2.67		0.041	2.899
0.04	2.84	0.04	2.88			
0.05	3.55	0.05	3.09		0.05	3.09
0.06	4.25	0.06	3.30		0.06	3.30
0.07	4.96	0.07	3.51		0.07	3.51
0.08	5.67	0.08	3.72		0.08	3.72
					0.09	3.93
					0.1	4.14
					0.11	4.34
Elastic		Plastic		Critical point Elastic=Plastic		
Angle	a1	a2	b	b/a1-a2		
54	70.90	20.91	2.04	0.041	0.12	4.55
					0.13	4.76
					0.14	4.97